Material Property Characterization of Ultra-High Performance Concrete

U.S. Department of Transportation
Federal Highway Administration

FOREWORD

Advances in the knowledge and understanding of the behaviors of concrete on the microstructural level have led to the development of the next generation of concrete, namely ultra-high performance concrete (UHPC). This report characterizes the material behaviors of one UHPC in terms of accepted concrete testing methodologies. The Federal Highway Administration (FHWA) has been investigating the optimal use of UHPC in highway bridges, and this report presents results from the first phase of this research program. Of primary importance, the results contained herein provide a starting point for bridge owners interested in advancing the state of bridge engineering through the use of extremely high strength and high durability concretes. This report presents both what can be achieved today through the use of a commercially available concrete as well as the types of advancements that can be achieved by reevaluating the traditional components and proportions normally present in cementitious structural materials.

Gary Henderson
Director, Office of Infrastructure
Research and Development

Quality Assurance Statement
The Federal Highway Administration (FHWA) provides high-quality information to serve Government, industry, and the public in a manner that promotes public understanding. Standards and policies are used to ensure and maximize the quality, objectivity, utility, and integrity of its information. FHWA periodically reviews quality issues and adjusts its programs and processes to ensure continuous quality improvement.

Form DOT F 1700.7 (8-72)

1. Report No. FHWA-HRT-06-103	2. Government Accession No.	3. Recipient's Catalog No.
4. Title and Subtitle Material Property Characterization of Ultra-High Performance Concrete		5. Report Date August 2006
		6. Performing Organization Code
7. Author Benjamin A. Graybeal		8. Performing Organization Report No.
9. Performing Organization Name and Address PSI, Inc. 2930 Eskridge Road Fairfax, VA 22031		10. Work Unit No.
		11. Contract or Grant No.
12. Sponsoring Agency Name and Address Office of Infrastructure Research and Development Federal Highway Administration 6300 Georgetown Pike McLean, VA 22101-2296		13. Type of Report and Period Covered Final Report, October 2002–December 2005
		14. Sponsoring Agency Code

15. Supplementary Notes
Additional FHWA Contacts—Joseph Hartmann (Technical Advisor), William Wright (COTR)

16. Abstract
In the past decade significant advances have been made in the field of high performance concretes (HPC). The next generation of concrete, ultra-high performance concrete (UHPC), exhibits exceptional strength and durability characteristics that make it well suited for use in highway bridge structures. This material can exhibit compressive strength of 193 megapascals (MPa) (28 kilopounds per square inch (ksi)), tensile strength of 9.0 MPa (1.3 ksi), significant tensile toughness, elastic modulus of 52.4 gigapascals (GPa) (7,600 ksi), and minimal long-term creep or shrinkage. It can also resist freeze-thaw and scaling conditions with virtually no damage and is nearly impermeable to chloride ions.

This report presents the results from a large suite of material characterization tests that were completed in order to quantify the behaviors of a commercially available UHPC. The characteristics of this UHPC under four different curing regimes were captured. This study focused on strength-based behaviors (e.g., compressive and tensile strength), long-term stability behaviors (e.g., creep and shrinkage), and durability behaviors (e.g., chloride ion penetration and freeze-thaw).

17. Key Words UHPC, ultra-high performance concrete, fiber-reinforced, durability, material characterization, tensile behavior, compressive behavior		18. Distribution Statement No restrictions. This document is available to the public through the National Technical Information Service, Springfield, VA 22161.		
19. Security Classif. (of this report) Unclassified		20. Security Classif. (of this page) Unclassified	21. No of Pages 186	22. Price

SI* (MODERN METRIC) CONVERSION FACTORS

APPROXIMATE CONVERSIONS TO SI UNITS

Symbol	When You Know	Multiply By	To Find	Symbol
LENGTH				
in	inches	25.4	millimeters	mm
ft	feet	0.305	meters	m
yd	yards	0.914	meters	m
mi	miles	1.61	kilometers	km
AREA				
in^2	square inches	645.2	square millimeters	mm^2
ft^2	square feet	0.093	square meters	m^2
yd^2	square yard	0.836	square meters	m^2
ac	acres	0.405	hectares	ha
mi^2	square miles	2.59	square kilometers	km^2
VOLUME				
fl oz	fluid ounces	29.57	milliliters	mL
gal	gallons	3.785	liters	L
ft^3	cubic feet	0.028	cubic meters	m^3
yd^3	cubic yards	0.765	cubic meters	m^3
NOTE: volumes greater than 1000 L shall be shown in m^3				
MASS				
oz	ounces	28.35	grams	g
lb	pounds	0.454	kilograms	kg
T	short tons (2000 lb)	0.907	megagrams (or "metric ton")	Mg (or "t")
TEMPERATURE (exact degrees)				
°F	Fahrenheit	5 (F-32)/9 or (F-32)/1.8	Celsius	°C
ILLUMINATION				
fc	foot-candles	10.76	lux	lx
fl	foot-Lamberts	3.426	candela/m^2	cd/m^2
FORCE and PRESSURE or STRESS				
lbf	poundforce	4.45	newtons	N
lbf/in^2	poundforce per square inch	6.89	kilopascals	kPa

APPROXIMATE CONVERSIONS FROM SI UNITS

Symbol	When You Know	Multiply By	To Find	Symbol
LENGTH				
mm	millimeters	0.039	inches	in
m	meters	3.28	feet	ft
m	meters	1.09	yards	yd
km	kilometers	0.621	miles	mi
AREA				
mm^2	square millimeters	0.0016	square inches	in^2
m^2	square meters	10.764	square feet	ft^2
m^2	square meters	1.195	square yards	yd^2
ha	hectares	2.47	acres	ac
km^2	square kilometers	0.386	square miles	mi^2
VOLUME				
mL	milliliters	0.034	fluid ounces	fl oz
L	liters	0.264	gallons	gal
m^3	cubic meters	35.314	cubic feet	ft^3
m^3	cubic meters	1.307	cubic yards	yd^3
MASS				
g	grams	0.035	ounces	oz
kg	kilograms	2.202	pounds	lb
Mg (or "t")	megagrams (or "metric ton")	1.103	short tons (2000 lb)	T
TEMPERATURE (exact degrees)				
°C	Celsius	1.8C+32	Fahrenheit	°F
ILLUMINATION				
lx	lux	0.0929	foot-candles	fc
cd/m^2	candela/m^2	0.2919	foot-Lamberts	fl
FORCE and PRESSURE or STRESS				
N	newtons	0.225	poundforce	lbf
kPa	kilopascals	0.145	poundforce per square inch	lbf/in^2

*SI is the symbol for the International System of Units. Appropriate rounding should be made to comply with Section 4 of ASTM E380.
(Revised March 2003)

TABLE OF CONTENTS

LIST OF FIGURES

LIST OF TABLES

CHAPTER 1. INTRODUCTION

1.1 INTRODUCTION

Ultra-high performance concrete (UHPC) is a new class of concrete that has been developed in recent decades. When compared with high performance concrete (HPC), UHPC tends to exhibit superior properties such as advanced strength, durability, and long-term stability.

Many researchers around the world have developed concretes that could be classified as UHPC. Although there are differences among types of UHPC, there are also many overall similarities. The Association Française de Génie Civil (AFGC) document *Ultra High Performance Fibre-Reinforced Concretes—Interim Recommendations* indicates that UHPC tends to have the following properties: compressive strength that is greater than 150 megapascals (MPa) (21.7 kilopounds per square inch (ksi)), internal fiber reinforcement to ensure nonbrittle behavior, and a high binder content with special aggregates.[1] Furthermore, UHPC tends to have a very low water content and can achieve sufficient rheological properties through a combination of optimized granular packing and the addition of high-range water reducing admixtures.

Characterization of the material behaviors of UHPC has progressed to such an extent that the full-scale structural use of this concrete is on the horizon. To date, UHPC has been used in the construction of two public highway bridges,[2,3] numerous pedestrian bridges,[4,5] and a wide variety of other projects.[6,7,8] Research and observations to date indicate that UHPC has the potential to expand the use of concrete into new forms that have heretofore been impossible.

This research program focused on determining the behaviors of UHPC because this information is relevant to the highway bridge industry in the United States. Currently, the only UHPC that is commercially available in the United States is Ductal®, a product jointly developed by Lafarge, Bouygues, and Rhodia. Therefore, Ductal was the UHPC product used in this research program.

1.2 OBJECTIVE

The objective of this research is to evaluate the potential use of UHPC in the highway bridge infrastructure by characterizing mechanical- and durability-based material behaviors.

1.3 SUMMARY OF APPROACH

The research included a significant experimental phase and an associated analytical phase. The experimental phase focused on determining the material behaviors of UHPC from the testing of over 1,000 individual specimens, with an emphasis toward determining the compressive and tensile behaviors, the long-term stability, and the durability of UHPC. Many of the material characterization tests were completed according to the American Society for Testing and Materials (ASTM) and the American Association of State Highway and Transportation Officials (AASHTO) standard test procedures; however, in some instances these tests were modified or new tests were devised to accurately capture the relevant behaviors of the concrete. The analytical phase of this research combined, analyzed, and elaborated upon the results from the experimental phase. This work included defining behaviors that can be anticipated to occur in

standardized concrete tests, as well as developing predictor equations for relating basic properties of UHPC.

1.4 OUTLINE OF REPORT

This report is divided into five chapters. Chapters 1 and 2 provide an introduction and relevant background information. Chapter 3 presents the results of the material characterization study. Chapter 4 presents further analysis and discussion of the research, relating results from various aspects of this study to one another and to the practical engineering disposition of this research. Finally, chapter 5 presents the conclusions of this research program.

CHAPTER 2. BACKGROUND AND PREVIOUS WORK

2.1 UHPC CONSTITUENT MATERIALS

The UHPC used in this study is a patented product of a major worldwide concrete manufacturer. The product is a reactive powder concrete that is marketed under the name Ductal. This product has a number of different material compositions depending on the particular application. A typical composition is provided in table 1.

The constituent material proportions were determined, in part, based on an optimization of the granular mixture. This method allows for a finely graded and highly homogeneous concrete matrix. Fine sand, generally between 150 and 600 micrometers (µm), is dimensionally the largest granular material. The next largest particle is cement with an average diameter of approximately 15 µm. Of similar size is the crushed quartz with an average diameter of 10 µm. The smallest particle, the silica fume, has a diameter small enough to fill the interstitial voids between the cement and the crushed quartz particles.

Dimensionally, the largest constituent in the mix is the steel fibers. In this study, the fibers in the mix had a diameter of 0.2 millimeters (mm) (0.008 inch) and a length of 12.7 mm (0.5 inch). Given the relative sizes of the sand and the fibers, the steel fibers are able to reinforce the concrete matrix on the micro level. A further discussion of the properties of the steel fibers is provided in section 2.3.

Table 1. Typical UHPC composition.

Material	Amount (kg/m^3 (lb/yd^3))	Percent by Weight
Portland Cement	712 (1,200)	28.5
Fine Sand	1020 (1,720)	40.8
Silica Fume	231 (390)	9.3
Ground Quartz	211 (355)	8.4
Superplasticizer	30.7 (51.8)	1.2
Accelerator	30.0 (50.5)	1.2
Steel Fibers	156 (263)	6.2
Water	109 (184)	4.4

1 kg/m^3 = 1.686 lb/yd^3
RDM = relative dynamic modulus (see p. 134)

2.2 MANUFACTURER-SUPPLIED UHPC MATERIAL PROPERTIES

As previously discussed, the UHPC used in this study is a proprietary product. The manufacturer has performed significant material property testing and has reported typical characteristics. Table 2 provides some of the material properties relevant to using this material in bridge applications. In general, these properties have not been verified and are provided here solely for completeness.

Table 2. Manufacturer-supplied material characteristics.

Material Characteristic	Range
Compressive Strength (MPa)	180–225
Modulus of Elasticity (GPa)	55–58.5
Flexural Strength (MPa)	40–50
Chloride Ion Diffusion (m^2/s)	1.9×10^{-14}
Carbonation Penetration Depth (mm)	< 0.5
Freeze-Thaw Resistance (RDM)	100%
Salt-Scaling Resistance (kg/m^2)	< 0.012
Entrapped Air Content	2–4%
Post-Cure Shrinkage (microstrain)	0
Creep Coefficient	0.2–0.5
Density (kg/m^3)	2,440–2,550

1 MPa = 145 psi
1 GPa = 145 ksi
1 m^2/s = 1,550 inches^2/s
1 kg/m^2 = 0.205 lb/ft^2
1 kg/m^3 = 1.69 lb/yd^3

2.3 STEEL FIBER MATERIAL PROPERTIES

The steel fibers used in this test program were straight steel wire fibers manufactured by Bekaert Corporation. The fibers have a nominal diameter of 0.2 mm (0.008 inch) and a nominal length of 12.7 mm (0.5 inch). The chemical composition of the fibers is shown in table 3. A thin brass coating is applied to the fibers during the drawing process; therefore, virgin fibers may be gold-colored. This coating disappears during the mixing process and is no longer clearly visible during the casting of the UHPC.

The intended function of these fibers within UHPC requires that the fibers have a very high tensile strength. The manufacturer's specified minimum tensile strength is 2,600 MPa (377 ksi), and tension tests are performed as a means of quality control on the fiber production. The stress-strain behavior as recorded during one of these quality control tests is presented in figure 1. The results from three quality control tests were used to determine an average yield strength of 3,160 MPa (458 ksi) as calculated by the 0.2 percent offset method. The average modulus of elasticity was 205 gigapascals (GPa) (29,800 ksi), and the average ultimate strength was 3,270 MPa (474 ksi). These results clearly show that these high-strength steel wires have little reserve strength or ductility capacity beyond yield.

Table 3. Chemical composition of steel fibers.

Element	Composition (percent)
Carbon	0.69–0.76
Silicon	0.15–0.30
Manganese	0.40–0.60
Phosphorus	≤ 0.025
Sulfur	≤ 0.025
Chromium	≤ 0.08
Aluminum	≤ 0.003

Yield Stress = 3150 MPa
Maximum Stress = 3250 MPa
Modulus of Elasticity = 210 GPa

1 MPa = 145 psi
1 GPa = 145,000 psi
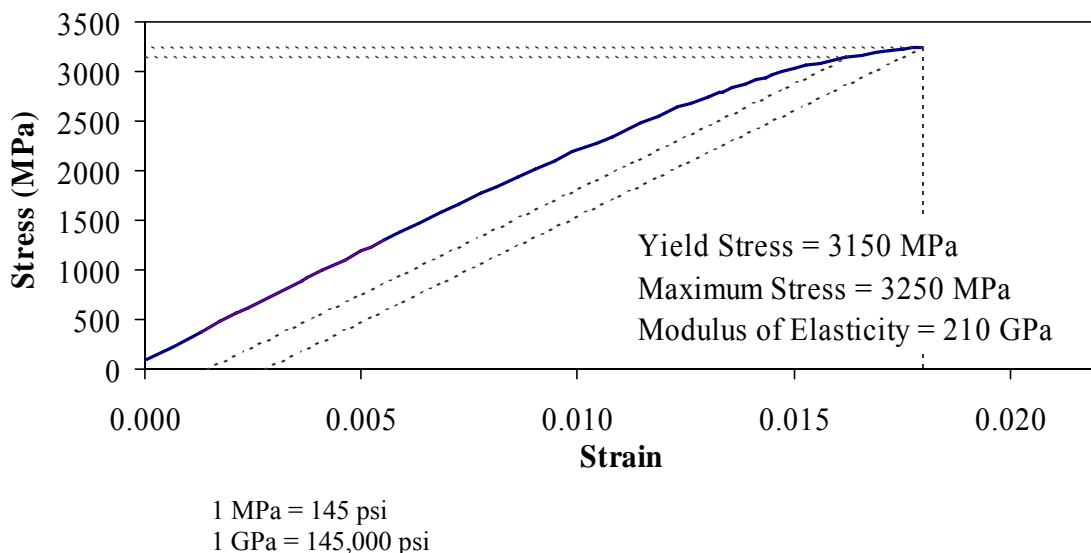
Figure 1. Graph. Sample tensile stress-strain response for steel fiber reinforcement.

2.4 RELEVANT MATERIAL PROPERTY CHARACTERIZATION STUDIES

2.4.1 Fiber Orientation Effect on Mechanical Properties

Stiel, Karihaloo, and Fehling have conducted a research program investigating the effect of fiber orientation on the mechanical properties of UHPC.[9] These researchers focused on a patented UHPC marketed under the name CARDIFRC®. This UHPC is composed of similar constituent materials and in similar proportions to the UHPC investigated in the present study. One primary difference is that CARDIFRC contains two lengths of steel fibers and a total fiber volumetric percentage of 6 percent.

This research program focused on the effect of UHPC flow direction during casting on the compressive and flexural tensile behaviors of the concrete. Fiber reinforcement tends to align

with the direction of flow during casting. This research program investigated the tensile and compressive behaviors of UHPC when loaded parallel to and perpendicular to the direction of flow during casting. The compression tests were performed on 100-mm (4-inch) cubes. The three-point bending flexure tests were performed on 100-mm by 100-mm (4- by 4-inch) prisms with a 500-mm (20-inch) length.

The cube compression tests indicated that preferential fiber alignment has no significant effect on either the compressive strength or the modulus of elasticity of UHPC. However, the three-point flexure tests showed that the peak equivalent flexural strength of the UHPC prisms was decreased by a factor of more than three when the fibers were preferentially aligned perpendicular to the principal flexural tensile forces. This preferential fiber alignment was clearly apparent on failure surfaces of the prisms. These prisms also did not exhibit the traditional postcracking toughness behaviors normally associated with UHPC and frequently exhibited an abrupt load decrease immediately after first cracking. All of these findings point to the importance of understanding the structural loadings that will be carried by a UHPC member and following correct placement techniques when casting UHPC members.

2.4.2 Permeability of Cracked Concrete

Rapoport et al. investigated the permeability of steel fiber-reinforced concrete as compared to normal concrete.[10] The research focused on creating small cracks in 0.5 percent and 1.0 percent steel fiber-reinforced concrete, then determining the permeability of the concrete. The two primary findings of interest from this study are as follows. First, this study confirmed the findings of other researchers that cracks less than 0.1 mm (0.004 inch) wide have little impact on the permeability of normal concrete.[11] Second, this study confirmed that steel fiber reinforcement reduces the total permeability of a strained section of concrete by changing the cracking mechanism from a few large width cracks to many small width cracks. As would be expected, the concrete with the higher volume percentage of fiber reinforcement displayed more distributed cracking and had a lower permeability.

2.4.3 Creep and Shrinkage of UHPC

Recall the very low post-steam treatment creep and shrinkage values presented in table 2. Lafarge, the manufacturer and distributor of the UHPC discussed in this report, has performed significant research focusing on the creep and shrinkage behaviors of this concrete. Some results of this research were presented in Acker wherein the microstructural behaviors leading to creep and shrinkage of UHPC, HPC, and normal concrete are discussed.[12] Additional discussion with further experimental results is presented in Acker.[13]

Acker argues that creep and shrinkage are closely related behaviors that cannot generally be uncoupled and studied separately. He indicates that shrinkage is primarily caused by self-desiccation of the concrete binder resulting in the irreversible collapse of calcium-silicate-hydrate (CSH) sheets. As UHPC contains a very low water-to-cementitious materials ratio, this concrete completely self-desiccates between casting and the conclusion of steam treatment. Thus, UHPC exhibits no post-treatment shrinkage.

6

In regard to creep, Acker restates previous research indicating that the CSH phase is the only constituent in UHPC that exhibits creep. Also, he points out that concrete creep tends to be much more pronounced when it occurs as the concrete is desiccating. Thus, the collapsed CSH microstructure and the lack of internal water both work to reduce UHPC creep.

2.4.4 Abrasion Resistance of HSC via ASTM C944

Horszczaruk studied the abrasion resistance of high-strength fiber-reinforced concrete using the ASTM C944 standard procedure.[14,15] This is the same procedure that was followed in the abrasion tests discussed in section 3.13.4 of the present report. Horszczaruk's study focused on 83 to 100 MPa (12 ksi to 14.5 ksi) compressive strength concretes containing basalt aggregates (2.5 to 12.7 mm (0.1 to 0.5 inch) diameter) and natural river sands (less than 2.5 mm (0.1 inch) diameter). The testing followed ASTM C944, except that the duration of test was increased from 2 to 40 minutes to allow for differentiation between concretes.

The relevant results from this study include the following. The linear best-fit approximation of the concrete mass loss per 2-minute abrading cycle ranged from 0.14 to 0.78 grams (0.005 to 0.027 ounce). Of the 10 concretes tested, six of them ranged from 0.14 to 0.25 grams (0.005 to 0.009 ounce). Horszczaruk also indicates that the rate of mass loss was relatively consistent throughout the abrading, with no clear increased abrasion resistance during the abrading of the smooth exterior face of the concrete.

CHAPTER 3. UHPC MATERIAL CHARACTERIZATION

3.1 RESEARCH PLAN

The stated goal of the UHPC material characterization study is to determine the basic behaviors of UHPC with the intent of using UHPC in highway bridges. Many material behaviors are critical to the successful use of concrete in a highway bridge. These behaviors include strength, durability, and long-term stability. Each of these behaviors will be discussed in depth in this chapter.

The curing treatment applied to concrete—which is always important—is even more important in the case of UHPC. The UHPC studied in this research program is normally steam treated once it has reached sufficient strength to undergo the process. However, steam treatment of UHPC in a controlled environment may not always be feasible or even desirable. For this reason, the focus of the research, which is discussed in this chapter, is on characterizing UHPC that had been treated to one of four curing conditions. The four curing conditions were the standard steam treatment, a delayed version, a lower temperature version of the same steam treatment, and an untreated regime wherein no steaming was conducted. These curing regimes will be described in more detail later in this chapter.

This chapter describes the results of the material characterization study. The chapter begins by introducing specimen nomenclature and test matrix information. Next, the batching, casting, and curing procedures and results are presented. Results from individual tests that focused on specific aspects of UHPC behavior are discussed in the remainder of this chapter.

3.1.1 Batch and Specimen Nomenclature

The material characterization study detailed in this chapter included well over 1,000 individual UHPC specimens. A naming scheme was created to allow for easy, unique identification of each specimen. The large majority of specimens cast for this study were part of the standardized set of batches designed to investigate the behavior of UHPC cured under various curing conditions. The other specimens were cast in extraneous batches that focused on specific behaviors of UHPC, primarily as related to compression testing.

For clarity, the nomenclature discussed here will not be mentioned throughout most of this chapter. In most instances, the presentation and discussion of results can be completed without naming individual specimens. However, in some instances, the naming system has to be used because of the large amount of similar specimens and testing procedures.

The nomenclature used to describe the specimens in the standardized batches is based on a five-digit alphanumeric identifier. A letter that identifies the premix delivery fills the first digit in the identifier. This letter is L, M, or N for the first, second, or third delivery, respectively. The second digit in the identifier is filled by an integer that identifies the curing treatment applied to the specimen. This number ranges from one to four for the steam-treated, untreated, tempered steam-treated, and delayed steam-treated regimes, respectively. The third digit in the identifier is reserved for a letter that identifies the tests performed on that batch of specimens. These letters

and the associated tests will be discussed further in the following section. A two-digit number indicating the particular specimen within the batch occupies the fourth and fifth digits. In the few cases in which a batch was repeated, the second batch was named identically to the first batch, except that the letter A was placed at the end of the identifier for each specimen.

An example of this alphanumeric identification scheme is as follows. The first three digits in the name M1F01 indicate that this specimen was from the second premix delivery that was first steam-treated and then subjected to testing within the general durability batches. The "01" in the fourth and fifth digits indicates that this specimen was a prism subjected to freeze-thaw testing.

A simpler naming scheme was used for the extraneous batches. These batches were named sequentially based on the premix delivery. For example, the 10th batch cast from the L delivery focused on the effect of varying the load rate on compression test results. Thus, the specimens from this batch are identified as L10-xx, with the xx being an integer identifier for each of the cylinders cast. In general, 30 or more cylinders populated these batches, and the associated testing was designed to indicate the effect of some external action on compressive behavior. The primary exception to this rule is batch N06, which focused on the early age shrinkage behavior of UHPC.

3.1.2 Test Matrix

The test matrix devised for the material characterization study was intended to cover a wide range of the basic behaviors of UHPC. The types of tests performed can generally be grouped into three classes. First, strength tests focused on the compressive and tensile behaviors of UHPC at various ages and under various curing conditions. Second, durability tests focused on the durability of UHPC under conditions with standardized aggressors. Finally, stability tests focused on the long-term ability of UHPC to maintain dimensional stability under various loading and environmental conditions.

Table 4 lists the standardized batches that were used throughout this study. The batch letter listed in the first column is the same letter that would reside in the third digit of the alphanumeric identifier in a specimen's name. A simplified description of the batch along with the associated testing is included in the next column. The specimens cast for each particular batch are included in the third column. Finally, the last two columns include the volume of material that was in an individual batch as well as the curing regimes for which each batch was cast. A batch of the size indicated was cast for each curing regime listed. Note that this large table continues across three pages.

Table 5 provides similar information for the extraneous batches that were cast. The only difference between this table and table 4 is that the batches were not cast for each curing regime listed. Because the first column lists individual batches of concrete, the curing regimes listed were applied to some of the specimens in each batch.

Table 4. Batching descriptions with associated specimens and curing regimes.

Batch	Batch Description *Test Completed*	Specimens Cast [†]	Batch Size (m³)	Curing Regimes [‡]
A	Compressive Strength		0.033	1,2,3,4
	Compressive Strength, Stress-Strain	36 *76x152 cylinders*	–	–
	Penetration Resistance	1 *152x152 cylinder*	–	–
B	Cubes/Cylinders Compression		0.025	1,2
	28-day Compressive Strength	6 *76x152 cylinders*	–	–
	28-day Compressive Strength	3 *76x165 cylinders*	–	–
	28-day Compressive Strength	6 *51x102 cylinders*	–	–
	28-day Compressive Strength	5 *102x203 cylinders*	–	–
	28-day Compressive Strength	6 *51 mm cubes*	–	–
	28-day Compressive Strength	5 *100 mm cubes*	–	–
C	Split Tensile		0.027	1,2,3,4
	Split Tensile	12 *102x203 cylinders*	–	–
	28-day Compressive Strength	6 *76x152 cylinders*	–	–
D	Direct Tension		0.028	1,2,3,4
	Direct Tension	12 *102x203 cylinders*	–	–
	Mortar Briquette	18 *briquettes*	–	–
	28-day Compressive Strength	6 *76x152 cylinders*	–	–
E	Prism Flexure		0.031	1,2,3,4
	Prism Flexure	3 *76x102x406 prisms*	–	–
	Prism Flexure	8 *51x51x279 prisms*	–	–
	Prism Flexure	8 *51x51x432 prisms*	–	–
	28-day Compressive Strength	6 *76x152 cylinders*	–	–
P	Fracture/Fatigue of Prisms		0.030	1,2
	Notched Prism Fracture	4 *51x102x457 prisms*	–	–
	Flexural Toughness	5 *51x51x432 prisms*	–	–
	Flexural Fatigue	7 *51x51x432 prisms*	–	–
	28-day Compressive Strength	6 *76x152 cylinders*	–	–

Table 4. Batching descriptions with associated specimens and curing regimes (continued).

Batch	Batch Description / *Test Completed*	Specimens Cast [†]	Batch Size (m³)	Curing Regimes [‡]
F	Durability (Cl⁻ Pen, FT, etc.)		0.028	1,2,3,4
	Rapid Chloride Penetrability	3 *102x76 cylinders*	–	–
	Chloride Penetration	3 *102x76 cylinders*	–	–
	Freeze-Thaw	3 *76x102x406 prisms*	–	–
	Abrasion	3 *152x76 cylinders*	–	–
	ASR	6 *25x25x279 prisms*	–	–
	28-day Compressive Strength	6 *76x152 cylinders*	–	–
Q	Freeze-Thaw Supplemental		0.031	1,2,3,4
	Frequency Response	4 *76x102x406 prisms*	–	–
	28-day Compressive Strength	6 *76x152 cylinders*	–	–
G	Scaling Slabs		0.025	1,2,3,4
	Scaling	2 *76x356x356 slabs*	–	–
	28-day Compressive Strength	6 *76x152 cylinders*	–	–
R	Split Tensile Crack Corrosion		0.030	1,2
	Split Tensile	9 *102x203 cylinders*	–	–
	Split Tensile w/ Ponding	6 *102x203 cylinders*	–	–
	28-day Compressive Strength	6 *76x152 cylinders*	–	–
H	Creep, Shrinkage, Thermal Expansion		0.030	1,2,3,4
	Creep	5 *102x203 cylinders*	–	–
	Shrinkage	3 *76x76x279 prisms*	–	–
	Thermal Expansion	3 *102x203 cylinders*	–	–
	28-day Compressive Strength	6 *76x152 cylinders*	–	–
S	Early Age Sustained Compressive Stress		0.027	1,2
	Compressive Strength	25 *76x152 cylinders*	–	–
	28-day Compressive Strength	8 *76x152 cylinders*	–	–

Table 4. Batching descriptions with associated specimens and curing regimes (continued).

Batch	Batch Description *Test Completed*	Specimens Cast [†]	Batch Size (m^3)	Curing Regimes [‡]
J	Air Content, Fiber Dispersion		0.020	1
	Air Content, Fiber Dispersion	8 *102x203 cylinders*	–	–
	28-day Compressive Strength	6 *76x152 cylinders*	–	–
K [*]	Air Content, Fiber Dispersion		0.020	1
	Air Content, Fiber Dispersion	8 *102x203 cylinders*	–	–
	28-day Compressive Strength	6 *76x152 cylinders*	–	–
M	Heat of Hydration		0.025	1,2
	Heat of Hydration	3 *152x305 cylinders*	–	–
	Heat of Hydration	2 *76x152 cylinders*	–	–
	28-day Compressive Strength	6 *76x152 cylinders*	–	–
N [*]	Heat of Hydration		0.025	1,2
	Heat of Hydration	3 *152x305 cylinders*	–	–
	Heat of Hydration	2 *76x152 cylinders*	–	–
	28-day Compressive Strength	6 *76x152 cylinders*	–	–

[†] Cylinders listed as *diameter x height*. Prisms listed as *depth x width x length* in tested configuration.
[‡] 1 = Steam, 2 = Untreated, 3 = Tempered Steam, 4 = Delayed Steam
[*] Batch mix design did not contain any accelerator.
1 m^3 = 35.315 ft^3

Table 5. Batching descriptions with associated specimens and curing regimes for nonstandardized batches.

Batch	Batch Description	Specimens Cast [†]	Batch Size (m³)	Curing Regimes [‡]
	Test Completed			
L10	Load Rate Effect		0.028	1
	Compressive Strength	24 *76x152 cylinders*	–	–
L12	Fiber Effect on Compression		0.0042	1
	Compressive Strength	3 *76x152 cylinders*	–	–
L21	Long-Term Delayed Steam		0.028	1,2
	Compressive Strength	36 *76x152 cylinders*	–	–
L22	Long-Term Delayed Steam		0.028	1,2
	Compressive Strength	36 *76x152 cylinders*	–	–
L23	Demolding Time Effect		0.030	1,2
	Compressive Strength	36 *76x152 cylinders*	–	–
N06	Early Age Shrinkage		0.0048	1,2
	Shrinkage	2 *76x76x279 prisms*	–	–
	Compressive Strength	2 *76x152 cylinders*	–	–

[†] Cylinders listed as *diameter x height*. Prisms listed as *depth x width x length*.
[‡] 1 = Steam, 2 = Untreated
1 m³ = 35.3 ft³

3.2 BATCHING, CASTING, AND CURING OF UHPC

The first phase of the material characterization study described in this chapter is to determine the properties of fresh UHPC. To achieve consistent results throughout the entire study, a series of specific, standardized procedures were implemented for the creation of the specimens described in the previous section. The casting of these specimens allowed for the mixing, associated testing, and observation of over 50 batches of UHPC.

The UHPC used in this study can be divided into three parts—premix, fibers, and liquids. The premix consists of all of the cementitious, aggregate, and filler materials (described in chapter 2). The premix was batched and blended by the manufacturer and delivered in bulk to the researchers. All of the UHPC testing described in this chapter consists of specimens created from one of the three premix deliveries made to the researchers over the course of 18 months. As described in the previous section, these deliveries were designated as the L, M, and N premixes. For the purpose of this study, all of the premixes are assumed to be identical; however, it is realized that manufacturing processes can vary with time, and the final premix product could show slight variations.

The liquids that were mixed with the UHPC included water, accelerator, and a high-range water-reducing admixture (HRWA). The accelerator used in this study was Rheocrete CNI. The HRWA was Glenium 3000NS.

The fibers included in the UHPC were always nondeformed cylindrical steel fibers that were 12.7 mm (0.5 inch) long and had a 0.2-mm (0.008-inch) diameter. These fibers were included in the mix at a concentration of 2 percent by volume.

The mix proportions used throughout this study included:

- Premix   2,195 kg/m^3 (137.0 lb/ft^3) of concrete.
- Water   109 kg/m^3 (6.81 lb/ft^3) of concrete.
- HRWA   30.8 kg/m^3 (1.92 lb/ft^3) of concrete.
- Accelerator   30.0 kg/m^3 (1.87 lb/ft^3) of concrete.
- Steel Fibers   156 kg/m^3 (9.74 lb/ft^3) of concrete.

These mix proportions were followed for all except three batches. Those three batches followed a slightly different mix design as required by the material property being investigated. In two batches, M1K and M1N, the accelerator was replaced by an additional 28.8 kg/m^3 (1.80 lb/ft^3) of water. In the remaining batch, L12, the fibers were not included in the mix so that compression test behavior in nonreinforced UHPC could be studied.

A 0.057-m^3 (2.0-ft^3) capacity pan mixer was used for nearly all of the UHPC mixing. This 1934 vintage mixer was somewhat underpowered for this application, resulting in extended mix times as compared to mixing UHPC in modern mixers. Regardless, this mixer was able to impart enough energy into the mix to obtain sufficient rheology for the casting of laboratory specimens. A 0.0085-m^3 (0.3-ft^3) mixer was used for the two batches that required only a small volume of material.

Key points in the mixing procedure are shown in figure 2. The mixing procedure for UHPC included the following steps:

- Weigh all constituent materials. Add half of HRWA to water.
- Place premix in mixer pan and mix for 2 minutes.
- Add water (with half of HRWA) to premix slowly over the course of 2 minutes.
- Wait 1 minute, then add remaining HRWA to premix over the course of 30 seconds.
- Wait 1 minute, then add accelerator over the span of 1 minute.
- Continue mixing as the UHPC changes from a dry powder to a thick paste. The time for this process will vary.
- Add fibers to the mix slowly over the course of 2 minutes.
- After the fibers have been added, continue running mixer for 1 minute to ensure that the fibers are well dispersed.

As soon as mixing was completed, the casting of specimens and the measurement of the rheological properties of the UHPC commenced. The rheology of the UHPC was measured via a flow table test similar to that described in ASTM C1437.[16] In the test that was implemented in this study, the mini slump cone is filled, then removed to allow the concrete to flow outward. Once the concrete reaches a steady state, the average diameter is determined by measuring the concrete at three locations. Next, the flow table is dropped 20 times in approximately 20 seconds. Again, the concrete is allowed to settle, and then its average diameter is recorded.

The casting of all UHPC specimens used in this material characterization study was completed within 20 minutes after the completion of mixing. All specimens were cast on a vibrating table and were allowed to remain on the table for approximately 30 seconds after filling. The filling of molds was completed via scoops used to move the UHPC from the mixing pan into the mold. In prisms specimens for flexure tests, the UHPC was always placed in one end of the mold and allowed to flow to the other end to complete the filling. As was discussed in section 2.4.1, the tensile properties of UHPC depend on fiber reinforcement orientation, which is a direct result of casting procedure.

After filling, specimens were removed from the vibrating table and were screeded. Although screeding is not normally recommended for UHPC and is very difficult to complete on a large-scale cast, it was implemented here to make the later preparation of cured specimens easier. After screeding, each specimen had its exposed surface covered in plastic to prevent moisture loss. The specimens then sat undisturbed until final set had occurred.

The demolding of the specimens occurred approximately 24 hours after casting. As will be discussed later in this chapter, this timetable sometimes resulted in the demolding of specimens that were marginally ready and had only very recently achieved set. Demolding of larger specimens that would have needed sufficient strength to support their greater self-weight would not have been possible in all cases on this timetable.

As previously mentioned, four curing regimes were implemented to study UHPC characteristics under different curing conditions. The standard, manufacturer-recommended curing treatment included steaming the UHPC at 90 ºC (194 ºF) and 95 percent relative humidity (RH) for 48 hours.
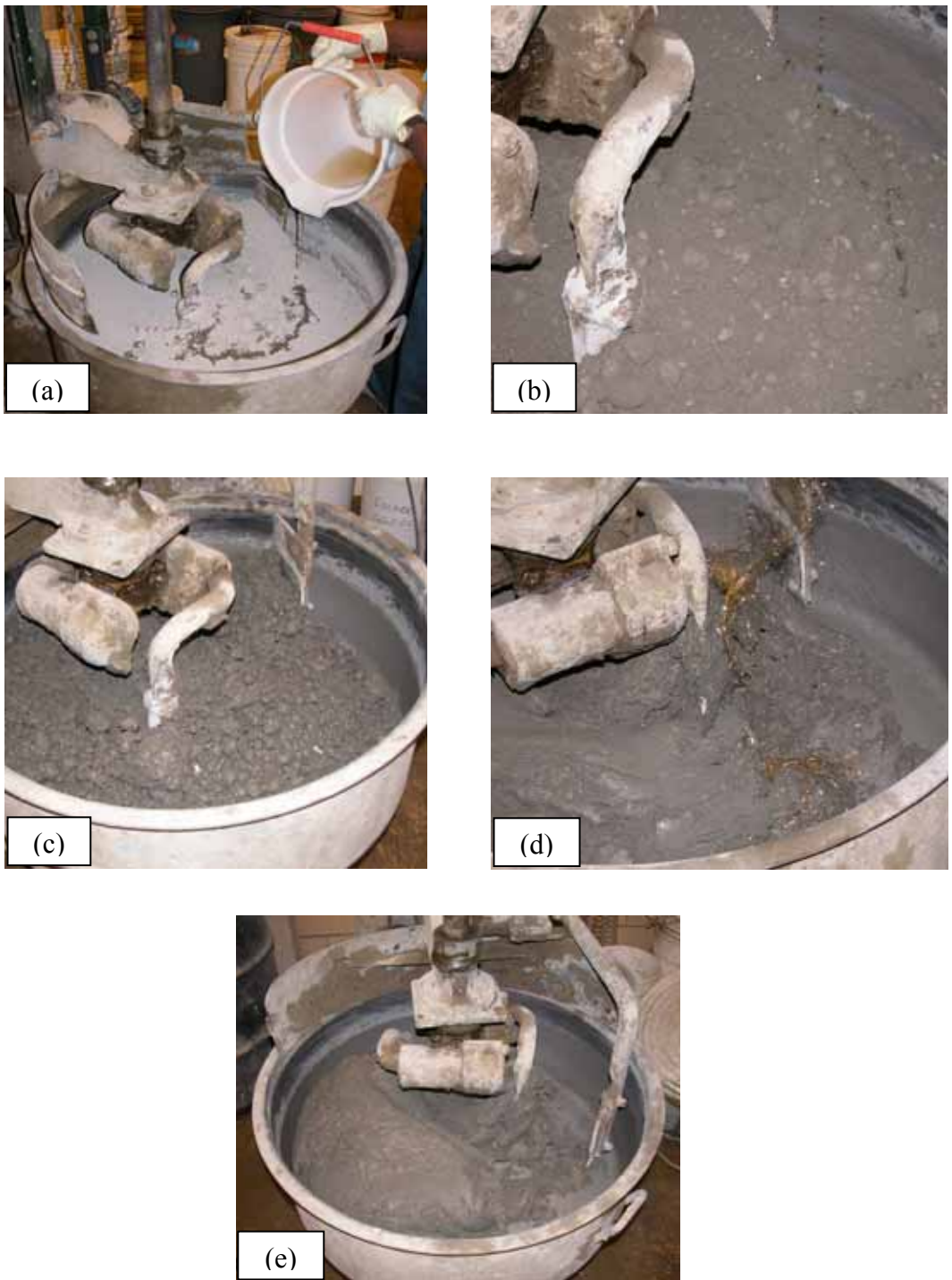
Figure 2. Photos. Mixing of UHPC. (a) Water addition. (b) HRWA addition. (c) Prepaste consistency. (d) Fiber addition. (e) Finished mix.

In practice, this procedure included 2 hours of increasing steam and 2 hours of decreasing steam, leaving 44 total hours of constant steaming at 90 ºC (194 ºF) and 95 percent RH. This treatment was initiated within 4 hours after demolding. This curing condition will henceforth be referred to as steam treatment.

The remaining three regimes include untreated, tempered steam treatment, and delayed steam treatment. The untreated regime allowed the specimens to remain in a standard laboratory environment from demolding until testing. The tempered steam treatment is very similar to the steam treatment, except that the temperature inside the steam chamber was limited to 60 ºC (140 ºF). Finally, the delayed steam treatment is a curing regime wherein the steam treatment described above is followed, but it is not initiated until the 15th day after casting. Until the 15th day, delayed steam specimens are equivalent to untreated specimens. Note that this report also uses the term steam-based treatment, which refers to the collection of specimens that underwent either steam treatment, tempered steam treatment, or delayed steam treatment.

Tables 6 and 7 provide information relating to the casting and curing of each of the batches included in this material characterization study. Table 6 focuses on the primary sets of specimens that were implemented across most curing regimes. These batches were all cast with premix from the M or N deliveries. Table 7 provides the results from other batches cast and primarily focuses on material cast from the L premix delivery.

The tables include a listing of the age of the UHPC premix at the time of casting along with the total mixing time for each batch. Observation of the mixing and casting procedure throughout all the mixes completed in this study indicated that the behavior of the mix changed as the premix aged. This qualitative observation is confirmed by the results as shown in figure 3. The total mixing time for each mix in the M and N premixes is plotted against the premix age at casting. This figure shows a clear trend in which younger premixes could mix within 15 minutes while older mixes could take twice as long. Although not verified, it is likely that these increased times result from the agglomeration of fine particles within the premix as it ages. These mix times are relative and are specifically applicable only to the pan mixer used in this study.

The rheology measures are also listed in tables 6 and 7. The final values ranged from 165 to 210 mm (6.5 to 8.25 inches). This wide range is indicative of large differences in rheology. The UHPC exhibiting the stiffer results was much more difficult to cast and would definitely have been problematic outside of a laboratory setting. Alternatively, a flow measure that was near or above 200 mm (8 inches) was consistent with UHPC that was easy to place.

Figure 4 shows the final rheology values for the M and N premixes. The first castings of the M premix were completed during a time period when the laboratory conditions included very low humidity. For this reason, the results are shown in two series that indicate whether the humidity was low or normal during casting. Very stiff rheology results were obtained for a few mixes just before the rectification of the humidity situation. It is expected that the large diameter of the pan in the pan mixer combined with the low air moisture content worked to sap a small amount of moisture from the UHPC. This moisture loss was sufficient to adversely affect the rheological properties.

Table 6. Batching and casting properties of steam-treated and untreated UHPC.

Batch	Batch Description	Age at Casting	Batch Size (m³)	Mixing Time (min)	Flow (mm)		Demolded (hours)	Curing Regime
					Initial	Final		
N1A	Compressive Strength	4 months	0.032	24.0	170	195	22.5	Steam
N1AxxA	Compressive Strength	5 months	0.027	28.0	170	190	28.0	Steam
M1B	Cubes/Cylinders Compression	6 weeks	0.025	20.0	150	170	26.0	Steam
N1C	Split Tensile	2 weeks	0.027	20.0	165	190	22.0	Steam
M1D	Direct Tension	9 weeks	0.028	22.0	165	190	28.0	Steam
N1E	Prism Flexure	4 weeks	0.031	21.0	170	195	23.0	Steam
M1F	Durability (Cl⁻ Pen, FT, etc.)	4 weeks	0.028	15.0	165	190	26.0	Steam
M1G	Scaling Slabs	4 weeks	0.025	14.0	180	190	26.0	Steam
N1H	Creep and Shrinkage	15 weeks	0.030	23.0	170	195	22.5	Steam
M1J	Air Content, Fiber Dispersion	6 weeks	0.020	21.5	140	165	26.0	Steam
M1JxxA	Air Content, Fiber Dispersion	8 weeks	0.020	23.0	160	190	26.0	Steam
M1K †	Air Content, Fiber Dispersion	7 weeks	0.020	20.0	165	190	72.0	Steam
M1M	Heat of Hydration	6 weeks	0.025	21.5	140	170	26.0	Steam
M1MxxA	Heat of Hydration	7 weeks	0.014	23.5	145	170	26.0	Steam
M1MxxB	Heat of Hydration	8 weeks	0.025	20.0	160	185	26.0	Steam
M1N †	Heat of Hydration	7 weeks	0.025	16.5	185	210	72.0	Steam
M1P	Fracture/Fatigue of Prisms	7 weeks	0.030	20.0	160	190	26.0	Steam
M1Q	Freeze-Thaw Supplemental	12 weeks	0.031	20.0	150	180	29.0	Steam
N2A	Compressive Strength	8 weeks	0.032	22.0	170	200	20.0	Untreated
N2C	Split Tensile	3 weeks	0.027	21.0	180	210	24.0	Untreated
M2D	Direct Tension	9 weeks	0.028	21.0	150	180	26.0	Untreated
N2E	Prism Flexure	3 weeks	0.031	20.0	170	195	24.0	Untreated
M2F	Durability (Cl⁻ Pen, FT, etc.)	5 weeks	0.030	17.5	150	180	26.0	Untreated
M2G	Scaling Slabs	5 weeks	0.025	17.0	160	185	26.0	Untreated
N2H	Creep and Shrinkage	8 weeks	0.030	21.5	165	190	22.0	Untreated
M2P	Fracture/Fatigue of Prisms	12 weeks	0.030	20.0	150	185	29.0	Untreated
M2Q	Freeze-Thaw Supplemental	12 weeks	0.031	19.5	160	190	29.0	Untreated

† Batch mix design did not contain any accelerator.

Table 6. Batching and casting properties of tempered steam and delayed steam-treated UHPC (continued).

Batch	Batch Description	Age at Casting	Batch Size (m³)	Mixing Time (min)	Flow (mm) Initial	Flow (mm) Final	Demolded (hours)	Curing Regime
N3A	Compressive Strength	8 weeks	0.032	20.0	165	190	21	T. Steam
N3C	Split Tensile	3 weeks	0.027	21.0	180	200	23	T. Steam
M3D	Direct Tension	8 weeks	0.028	20.0	165	190	26	T. Steam
N3E	Prism Flexure	5 weeks	0.031	21.0	170	195	25	T. Steam
M3F	Durability (Cl⁻ Pen, FT, etc.)	5 weeks	0.030	15.0	160	185	26	T. Steam
M3G	Scaling Slabs	5 weeks	0.025	14.0	165	185	26	T. Steam
N3H	Creep and Shrinkage	7 weeks	0.030	20.0	165	195	22	T. Steam
M3Q	Freeze-Thaw Supplemental	12 weeks	0.031	19.5	160	190	29	T. Steam
N4A	Compressive Strength	2 weeks	0.032	16.0	165	195	24	D. Steam
N4C	Split Tensile	2 weeks	0.027	20.0	170	200	23	D. Steam
M4D	Direct Tension	7 weeks	0.028	20.0	160	190	26	D. Steam
N4E	Prism Flexure	2 weeks	0.031	20.0	170	200	22	D. Steam
M4F	Durability (Cl⁻ Pen, FT, etc.)	4 weeks	0.028	16.0	170	195	26	D. Steam
M4G	Scaling Slabs	4 weeks	0.025	15.0	165	185	26	D. Steam
N4H	Creep and Shrinkage	7 weeks	0.030	21.0	185	210	23	D. Steam
M4Q	Freeze-Thaw Supplemental	12 weeks	0.031	20.0	150	180	29	D. Steam

$1 \text{ m}^3 = 35.3 \text{ ft}^3$

Table 7. Batching and casting properties of batches cast to complete the study by addressing special issues.

Batch	Batch Description	Age at Casting	Batch Size (m^3)	Mixing Time (min)	Flow (mm) Initial	Flow (mm) Final	Demolded (hours)	Curing Regime
L1B	Cubes/Cylinders Compression	16 months	0.025	26	150	180	48	Steam
L1F	Durability (Cl$^-$ Pen, FT, etc.)	11 months	0.025	20	160	180	41	Steam
L1G	Scaling Slabs	11 months	0.028	23	160	185	44	Steam
L1R	Split Tensile Cracked Corrosion	16 months	0.031	22	165	190	48	Steam
L2B	Cubes/Cylinders Compression	8 months	0.025	34	150	180	114	Untreated
L2F	Durability (Cl$^-$ Pen, FT, etc.)	11 months	0.028	17	145	170	50	Untreated
L2G	Scaling Slabs	11 months	0.025	20	145	170	43	Untreated
L2R	Split Tensile Cracked Corrosion	16 months	0.031	24	170	195	47	Untreated
L2S	Early Age Sustained Compressive Stress	26 months	0.028	23	170	195	–	Steam and Untreated
L03 [†]	Fiber Dispersion	8 months	0.028	19	210	235	139	Untreated
L10	Load Rate Effect	10 months	0.028	27	165	185	47	Steam
L12	Fiber Effect on Compression	11 months	0.0042	18	185	200	42	Steam
L21	Long-Term Delayed Steam	25 months	0.028	22	185	210	44	Steam and Untreated
L22	Long-Term Delayed Steam	25 months	0.028	22	185	200	43	Steam and Untreated
L23	Demolding Time Effect	25 months	0.028	22	165	190	Various	Steam and Untreated
N06	Early Age Shrinkage	5 months	0.0048	23	N/A	N/A	–	Steam and Untreated

[†] Batch mix design did not contain any accelerator.
1 m^3 = 35.3 ft^3
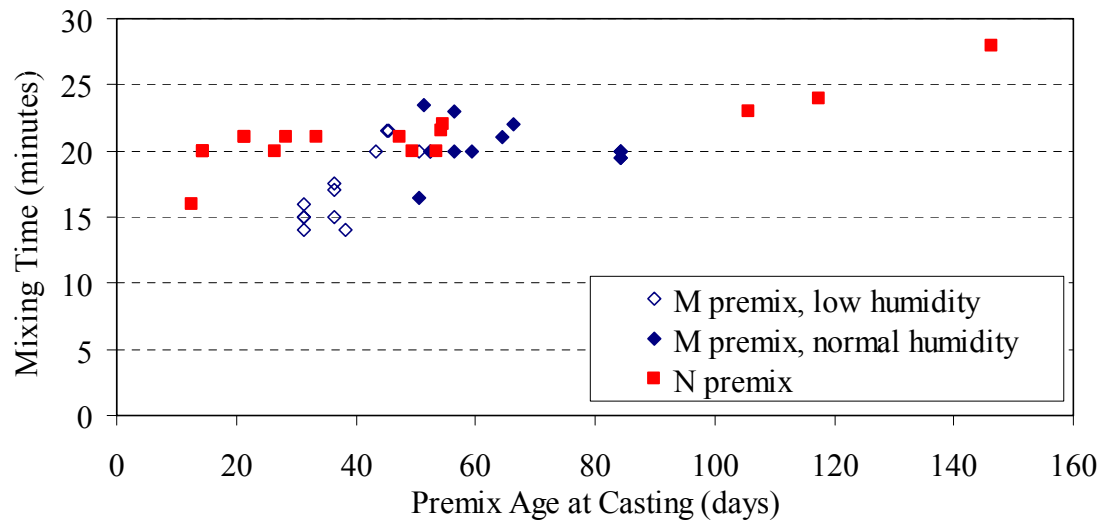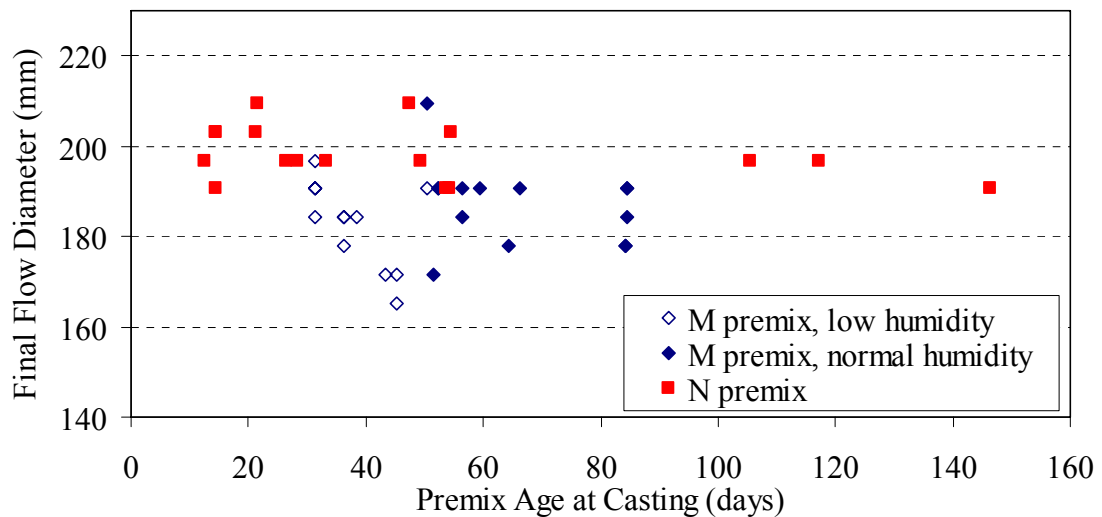
Figure 3. Graph. Mix time as affected by premix age.

1 mm = 0.039 inch

Figure 4. Graph. Final flow diameter as affected by premix age.

3.3 COMPRESSION TESTING

A significant portion of this study focused on the behaviors of molded UHPC cylinders under compressive loading. The compressive tests discussed in this section were all completed nominally according to the ASTM C39 standard test method for cylinders and the ASTM C109 standard test method for cubes.[17,18] Throughout the entire material characterization study, nearly 1,000 compression specimens were tested. Although the load configuration and basic test setup remained constant, various properties were investigated through the use of different data collection techniques and different specimen geometries.

The basic compression test on UHPC was the ASTM C39 test on a 76-mm (3-inch) diameter cylinder. This test was used as a control test throughout the material characterization study to ensure that consistent batching, mixing, and curing of the UHPC had occurred. The 76-mm (3-inch) cylinders were cast on a vibrating table in 152-mm (6-inch)-tall plastic molds. The concrete was scooped into the molds and was not rodded due to the presence of the fibers. Once full, the molds were held on the vibrating table for a few extra seconds before being removed and having their top surfaces screeded. After the molds were set, curing treatments were applied according to each of the four curing regimes.

The preparation of the cylinders for testing was somewhat more involved than that normally used for cylinder testing. The largest difference is that the end planeness of the cylinders was ensured through the use of an end grinder. Figure 5 shows a picture of the end grinding procedure. All cylinders that were projected to have strengths above 83 MPa (12 ksi) were subjected to grinding. UHPC cylinders with strengths under this level were sulfur-capped, as grinding tends to pull out the fibers and create a nonuniform end surface at these lower strengths.

After grinding, the cylinders were measured to verify end planeness and to determine length, diameter, and density. The end planeness was verified through the use of a flat steel plate and a dial gage as shown in figure 5. Sliding the cylinder under the dial gage allowed for determination of the longest and shortest lengths of the cylinder to an accuracy of 0.025 mm (0.001 inch). The out-of-planeness of the cylinder ends could be determined from this information. Each cylinder had to exhibit under 1 degree of out-of-planeness or the ends were reground. Next, the length was measured at four points around the circumference of the cylinder, and the average was calculated. The diameter was then measured at six locations—at the top, middle, and bottom of the cylinder on two perpendicular diameters. The average value was then used to calculate the area of the cylinder. Finally, the mass of the cylinder was determined, and the density was calculated. The entire grinding and measuring procedure was completed after any steam-based treatment was applied to the cylinder or at least 2 weeks after casting for the untreated specimens, unless the testing timetable required otherwise. In this case, a cylinder was prepared for testing within 1 day of performing the test.

The testing of all cylinders was completed in a Forney 4,450-kilonewton (kN) (1,000-kilopound (kip)) capacity compression testing machine. The operator of this hydraulically operated machine uses a needle valve to set and control the loading rate. Aside from some preliminary testing that will be discussed later, the load rate for all cylinder and cube compression tests was set at 1.0 MPa/s (150 pounds per square inch per second (psi/s)). This load rate is higher than the load rates recommended in ASTM C39 and C109. The increased load rate was necessary, as the high

strengths of UHPC would mean that a UHPC cylinder tested at the ASTM C39 load rate might take 15 to 20 minutes to reach failure. A small study, completed to determine if the higher load rate would have any adverse effect on results, indicated that the higher load rate was acceptable. A further discussion of this set of tests is presented subsequently in this chapter.
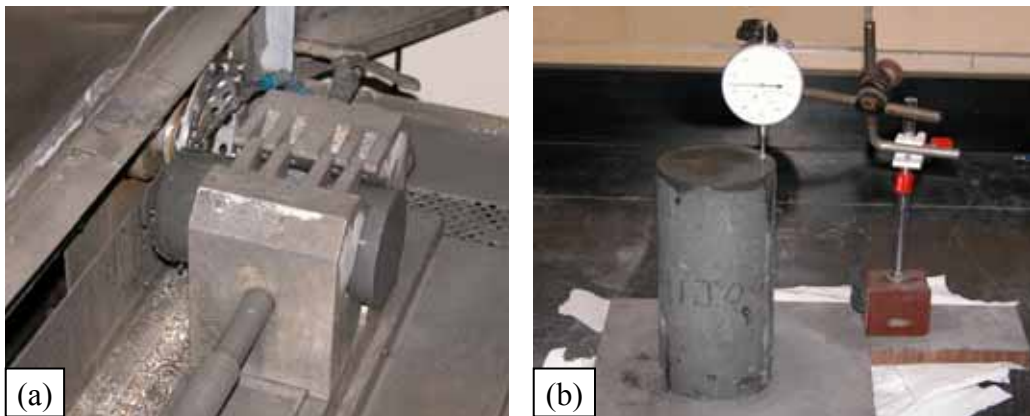
Figure 5. Photos. (a) Grinding and (b) measuring of 76-mm (3-inch) diameter cylinders.

A 165-mm (6.5-inch) diameter spherical bearing was used as the upper loading platen for all cylinder and cube tests. Although this bearing would normally only be used for 102-mm (4-inch) diameter cylinders, it was used for all of the tests because of the high stress levels placed on the bearing by this high-strength concrete. The lower test platen was always either the machine's lower platen or a machined steel plate resting on the machine's platen.

Figure 6 shows a cylinder that is prepared for testing. All specimens were loaded via the hydraulically controlled constant load rate from approximately 22 kN (5 kips) through failure. The cylinders and cubes exhibited very little decrease in stiffness throughout testing, thus the load rate remained relatively constant. Figure 6 also shows a picture of a cylinder after testing. Notice that the cylinder remains intact. This is due to the presence of the fibers as will be discussed more fully later in this chapter.

3.3.1 Strength

The compressive strength results from 44 batches of UHPC are presented in table 8. These results are from the control cylinders cast with each batch from the M and N deliveries of UHPC premix. Control cylinder results from the L delivery are shown in table 9. All tests were performed on the corresponding day that is listed in the table. In general, six cylinders were tested for each batch, and the results were averaged to obtain the result shown in the table.
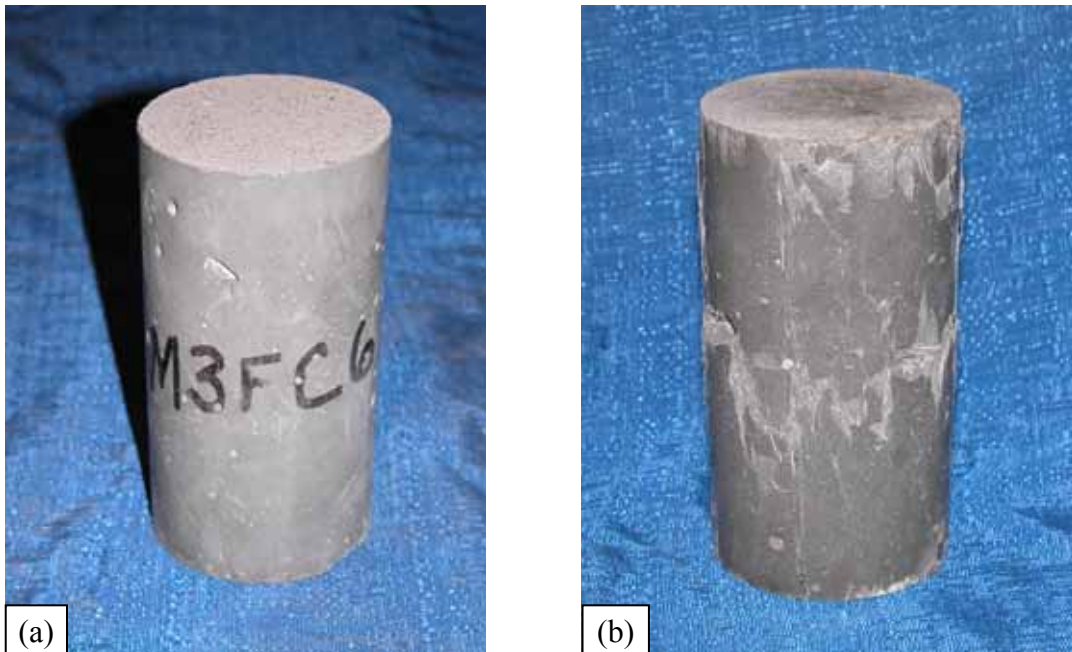
**Figure 6. Photos. 76-mm (3-inch) diameter cylinders (a) before
and (b) after compression testing.**

Based on these tests, the average 28-day compressive strength of UHPC has been determined.
Steam-treated UHPC was found to have a compressive strength of 193 MPa (28.0 ksi) with a
95 percent confidence interval of 191 to 195 MPa (27.7 to 28.3 ksi). Untreated UHPC has a
compressive strength of 126 MPa (18.3 ksi) with a 95 percent confidence interval of
123 to 129 MPa (17.9 to 18.7 ksi). Tempered steam-treated UHPC has a compressive strength of
171 MPa (24.8 ksi) with a 95 percent confidence interval of 168 to 174 MPa (24.3 to 25.3 ksi).
Finally, delayed steam-treated UHPC has a compressive strength of 171 MPa (24.8 ksi) with a
95 percent confidence interval of 168 to 174 MPa (24.3 to 25.3 ksi).

These results, although quite high for concrete, are likely lower than would normally be observed
with this UHPC. Two factors that have been found to clearly influence the compressive strength
are the environment that UHPC is kept in before any steam-based treatment and the steaming
environmental conditions. In this study, the UHPC was demolded as soon as it had sufficient
strength to maintain its geometric integrity. At this age, the UHPC is still rather permeable and is
susceptible to moisture loss and resulting lower strength values. This factor will be discussed in
more depth later in this chapter. Second, the UHPC manufacturer recommends 48 hours of steam
treatment, whereas in this study the UHPC actually received only 44 hours at the steam treatment
level with 2 hours of ramping up and down from room temperature.

Table 8. Control cylinder compressive strength results from the M and N deliveries.

Batch	Curing	Batch Description	Compressive Strength (MPa)			
			Day	No.	Average	St. Dev.
N1A	Steam	Compressive Strength	28	6	181	7.0
N1AxxA	Steam	Compressive Strength	30	6	196	14.3
M1B	Steam	Cubes/Cylinders Compression	29	6	203	4.2
N1C	Steam	Split Tensile	28	6	181	12.1
M1D	Steam	Direct Tension	28	6	168	6.6
N1E	Steam	Prism Flexure	28	6	189	8.6
M1F	Steam	Durability (Cl⁻ Pen, FT, etc.)	28	6	202	11.0
M1G	Steam	Scaling Slabs	28	6	201	10.5
N1H	Steam	Creep and Shrinkage	28	6	188	9.2
M1J	Steam	Air Content, Fiber Dispersion	28	6	191	8.5
M1JxxA	Steam	Air Content, Fiber Dispersion	28	6	177	7.4
M1K	Steam	Air Content, Fiber Dispersion	28	6	188	9.2
M1M	Steam	Heat of Hydration	28	6	194	6.9
M1MxxA	Steam	Heat of Hydration	28	6	191	15.0
M1MxxB	Steam	Heat of Hydration	28	6	197	7.5
M1N	Steam	Heat of Hydration	28	6	195	9.4
M1P	Steam	Fracture/Fatigue of Prisms	28	6	177	17.4
M1Q	Steam	Freeze-Thaw Supplemental	28	4	143	5.0
N2A	Untreated	Compressive Strength	28	6	112	5.0
N2C	Untreated	Split Tensile	28	6	121	4.5
M2D	Untreated	Direct Tension	28	6	106	3.4
N2E	Untreated	Prism Flexure	28	6	121	4.8
M2F	Untreated	Durability (Cl⁻ Pen, FT, etc.)	28	6	131	5.2
M2G	Untreated	Scaling Slabs	28	6	117	3.3
N2H	Untreated	Creep and Shrinkage	28	6	114	3.4
M2P	Untreated	Fracture/Fatigue of Prisms	28	6	107	4.3
M2Q	Untreated	Freeze-Thaw Supplemental	28	4	105	1.4
N3A	T.Steam	Compressive Strength	28	6	154	6.3
N3C	T.Steam	Split Tensile	28	6	168	4.6
M3D	T.Steam	Direct Tension	28	6	174	5.0
N3E	T.Steam	Prism Flexure	28	6	173	4.2
M3F	T.Steam	Durability (Cl⁻ Pen, FT, etc.)	28	6	183	8.3
M3G	T.Steam	Scaling Slabs	28	6	170	9.4
N3H	T.Steam	Creep and Shrinkage	28	5	177	2.1
M3Q	T.Steam	Freeze-Thaw Supplemental	28	5	149	5.0
N4A	D.Steam	Compressive Strength	30	6	173	7.2
N4C	D.Steam	Split Tensile	28	6	170	6.1
M4D	D.Steam	Direct Tension	28	6	158	11.9
N4E	D.Steam	Prism Flexure	28	5	172	4.3
M4F	D.Steam	Durability (Cl⁻ Pen, FT, etc.)	28	6	179	7.4
M4G	D.Steam	Scaling Slabs	28	6	179	7.2
N4H	D.Steam	Creep and Shrinkage	28	5	168	8.3
M4Q	D.Steam	Freeze-Thaw Supplemental	28	5	123	6.4
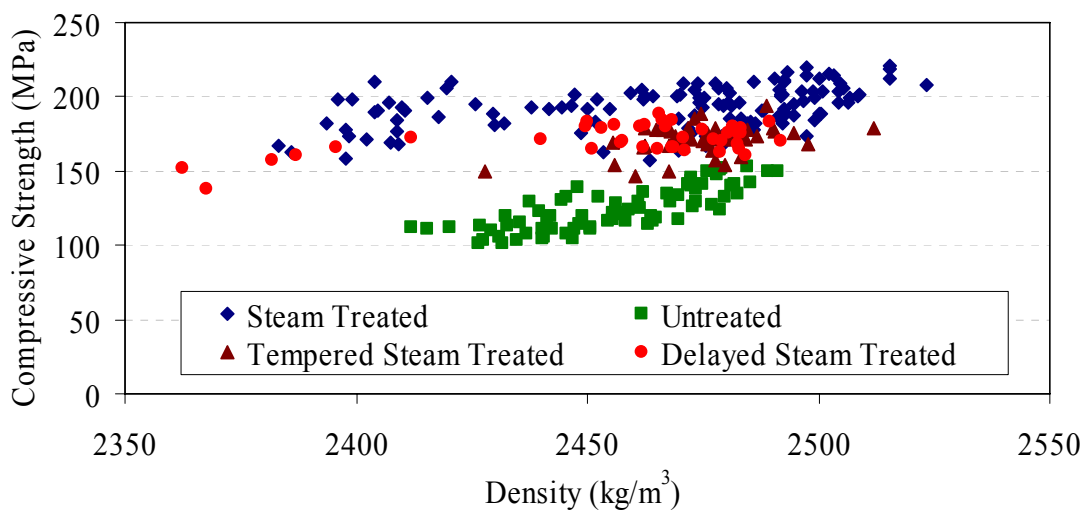
1 MPa = 145 psi

Table 9. Control cylinder compressive strength results from the L delivery.

Batch	Curing	Batch Description	Compressive Strength (MPa)			
			Day	No.	Average	St. Dev.
L1B	Steam	Cubes/Cylinders Compression	28	6	210	7.0
L2B	Untreated	Cubes/Cylinders Compression	28	8	149	3.8
L1R	Steam	Split Tensile Ponding	28	6	206	5.2
L2R	Untreated	Split Tensile Ponding	28	6	142	4.1
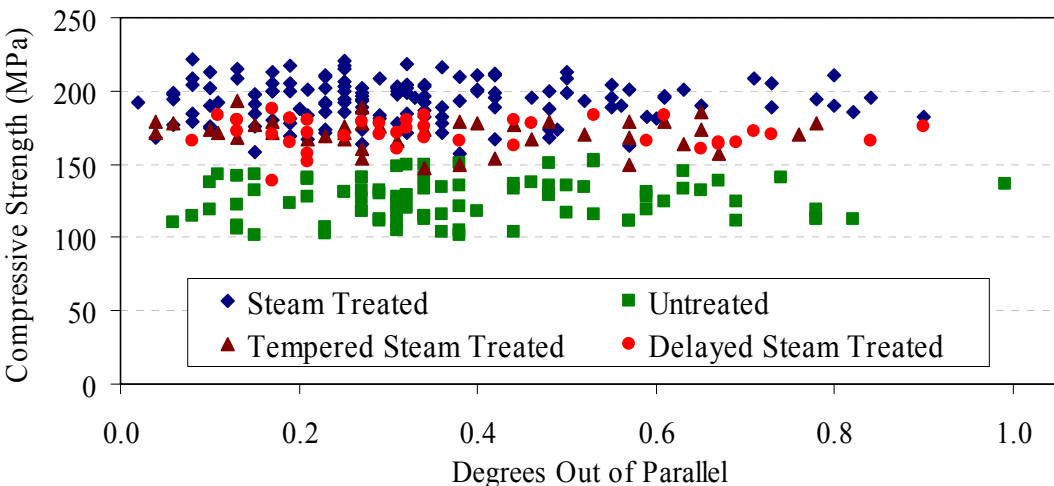
1 MPa = 145 psi

The results from the individual compression tests listed in table 8 are shown in figures 7 and 8 relative to density and cylinder end planeness, respectively. The density results show that this concrete ranges from 2,400 to 2,500 kg/m^3 (150 to 156 lb/ft^3). An estimate of 2,480 kg/m^3 (155 lb/ft^3) is reasonable regardless of the type of curing treatment applied. Also, within each curing regime there seems to be a slight increase in compressive strength as the density increases. The cylinder end planeness results show that the out-of-planeness of the cylinders had little impact on the compressive strength. The spherical bearing used in these tests clearly was able to accommodate for these differences in planeness.

1 MPa = 145 psi
1 kg/m3 = 1.69 lb/yd^3

Figure 7. Graph. Compressive strength and density of control cylinders.

Figure 8. Graph. Compressive strength and cylinder end planeness of control cylinders.

1 MPa = 145 psi

3.3.2 Strength, Modulus of Elasticity, and Strain Capacity With Time

The age-dependent compressive behavior of UHPC was investigated through a series of compression tests completed from 1 day to 8 weeks after casting. This testing provided results related to strength, modulus of elasticity, and compressive strain capacity both before and after the application of any curing treatment.

These tests were also completed in the 4,450-kN (1,000-kip) Forney test machine following the same procedures discussed previously. However, in these tests, a deformation measuring device was attached to each cylinder to capture the axial movement. These tests were completed nominally in accordance with ASTM C469 with one exception: A number of the allowances made by this test method for the collection of data via simplified systems were bypassed in favor of more robust methodologies.[19]

The test setup included the specially designed axial deformation measuring device shown in figure 9. The two parallel rings are both rigidly attached to the cylinder with a 51-mm (2-inch) gage length between attachment points. The upper ring holds three linear variable displacement transducers (LVDTs) whose ends bear on the lower ring. Thus, the axial deformation of the cylinder can be measured accurately from initiation of loading through failure. The load and the output from the three LVDTs were digitally recorded at approximately 4 hertz (Hz) throughout the test.

The testing of each cylinder was completed in a single constant load application from start to failure. This procedure runs counter to the standard procedure presented in ASTM C469 but is consistent with both ASTM C39 and the alternate loading procedure presented in ASTM C469. It is expected that the normal ASTM C469 procedure was designed to allow for assurance of seating by repeatedly loading and unloading the cylinder and to allow for removal of the deformation measuring apparatus by stopping the test well before reaching failure. In this test program, proper seating of the cylinder could be assured by monitoring the load-deformation

28

response during the test. Removal of the deformation measuring device was not necessary, as a loose-fitting plastic sleeve was sufficient to stop any UHPC chips from damaging the LVDTs during cylinder failure.

As previously mentioned, the preparation of specimens for tests at early ages was completed within 1 day prior to the test. Also, cylinders with projected strengths below 83 MPa (12 ksi) were sulfur capped instead of ground.
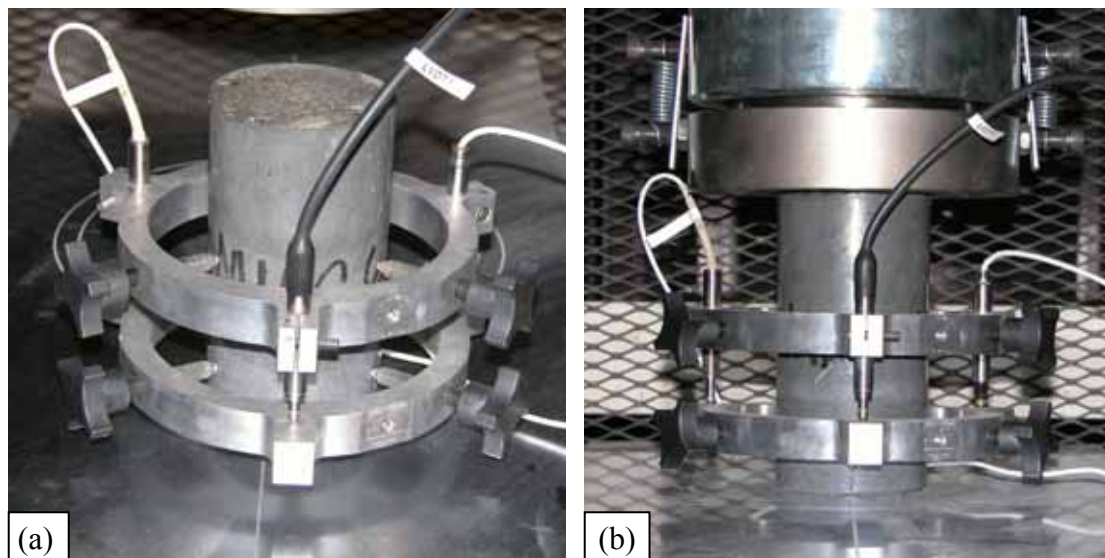
Figure 9. Photos. Modulus ring attachment (a) before and (b) during testing.

Selected results from these tests are compiled in figures 10 through 14. These figures show one stress-strain curve for each of the ages at which compression responses were collected. Note that a replicate (N1AxxA) was completed for the steam-treated portion of the testing as the compressive strength results from the initial set (N1A) were somewhat below the anticipated value. Unfortunately, the replicate compressive strength results were also somewhat lower than anticipated.

The stress-strain responses obtained from these tests will be the focus of the remainder of this section as well as the next section. In a qualitative sense, note the change in the overall shape of the curves in figures 10 through 14. At 1, 2, or even 3 days after casting if no steam-based curing is applied, the UHPC exhibits a ductile stress-strain response. The rounded curve and the steady decrease after peak stress illustrate that the UHPC can sustain some load-carrying capacity through large deformations without brittle failure. The overall behavior changed dramatically after the steam-based treatment. In this case, the UHPC exhibits more of a brittle response wherein the attainment of the peak compressive load results in a rapid, uncontrolled decrease in load-carrying capacity. As the curing progresses or as the steam-based treatment becomes more acute, the brittle nature of the compressive failure response also becomes more acute.
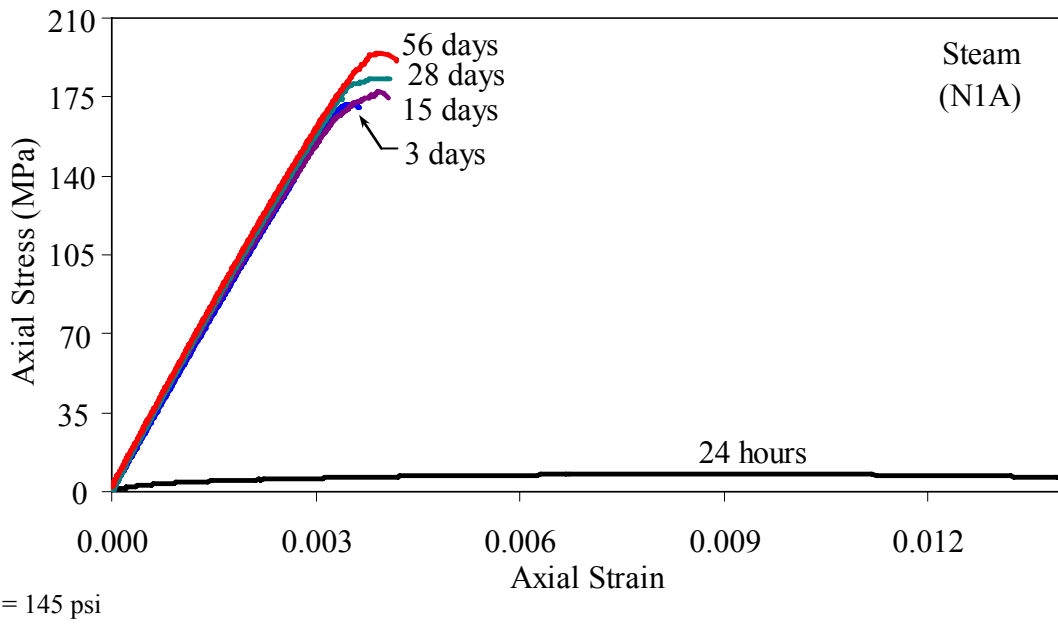
Figure 10. Graph. Selected stress-strain responses for steam-treated UHPC (N1A).

1 MPa = 145 psi
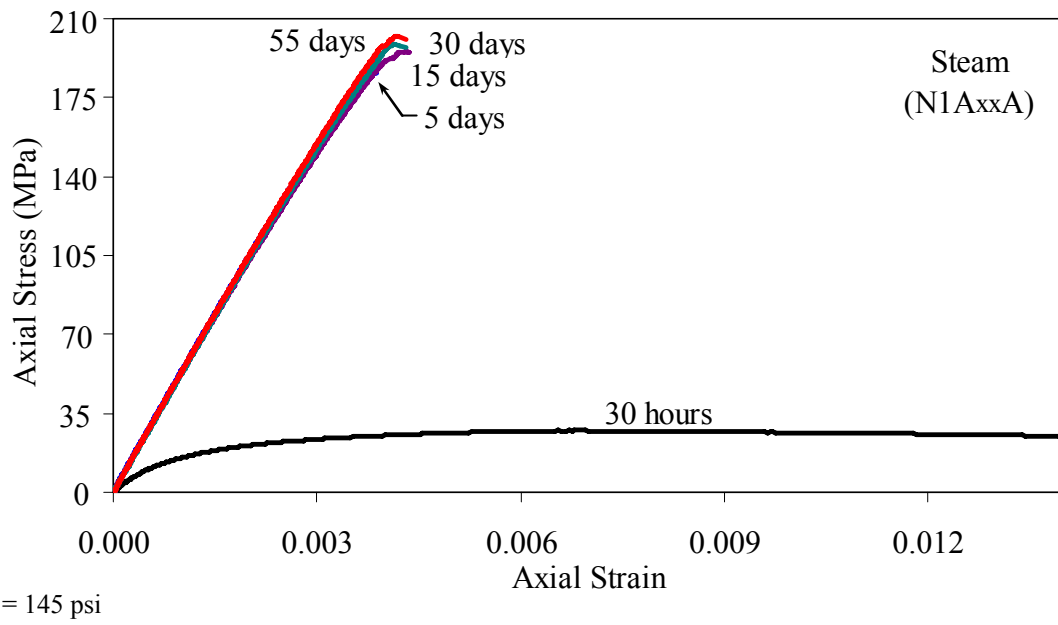
Figure 11. Graph. Selected stress-strain responses for steam-treated UHPC (N1AxxA).

1 MPa = 145 psi
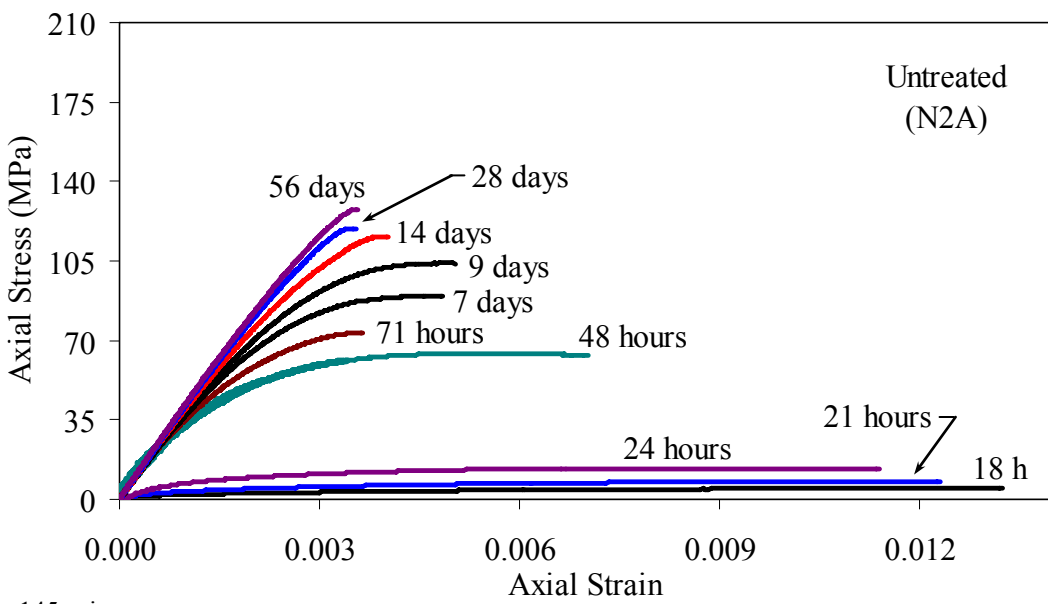
Figure 12. Graph. Selected stress-strain responses for untreated UHPC.

1 MPa = 145 psi
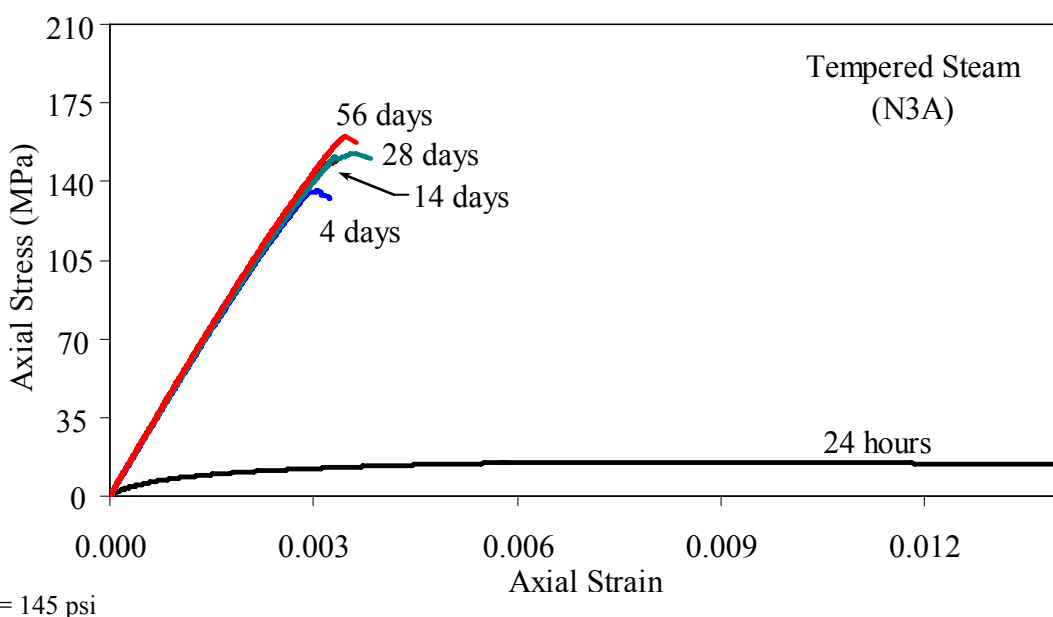
Figure 13. Graph. Selected stress-strain responses for tempered steam-treated UHPC.

1 MPa = 145 psi

31
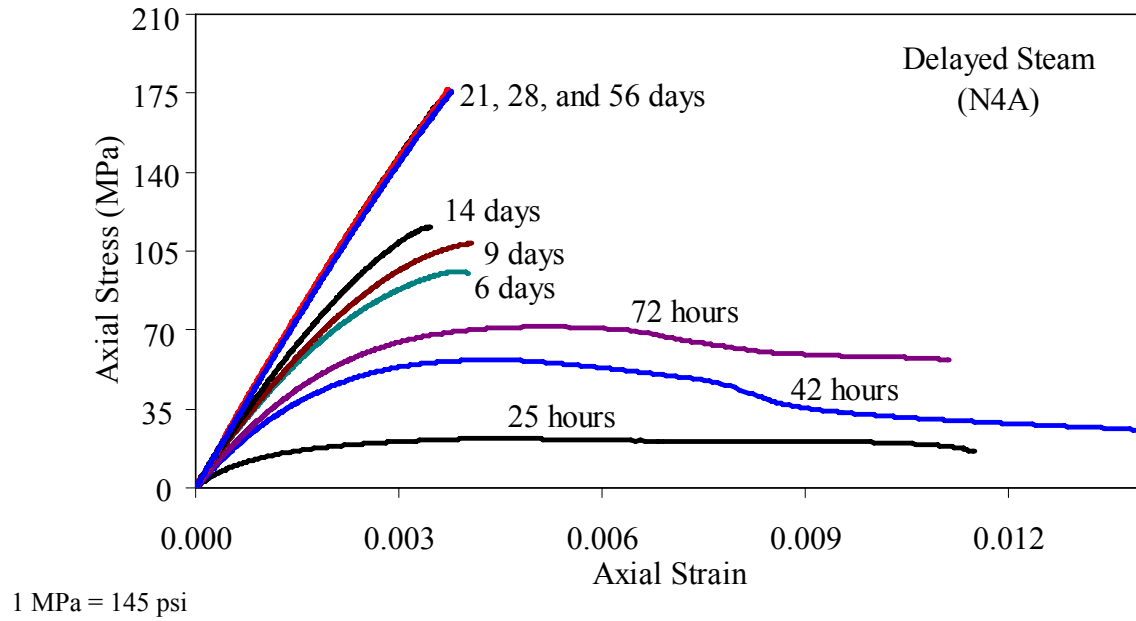
Figure 14. Graph. Selected stress-strain responses for delayed steam-treated UHPC.
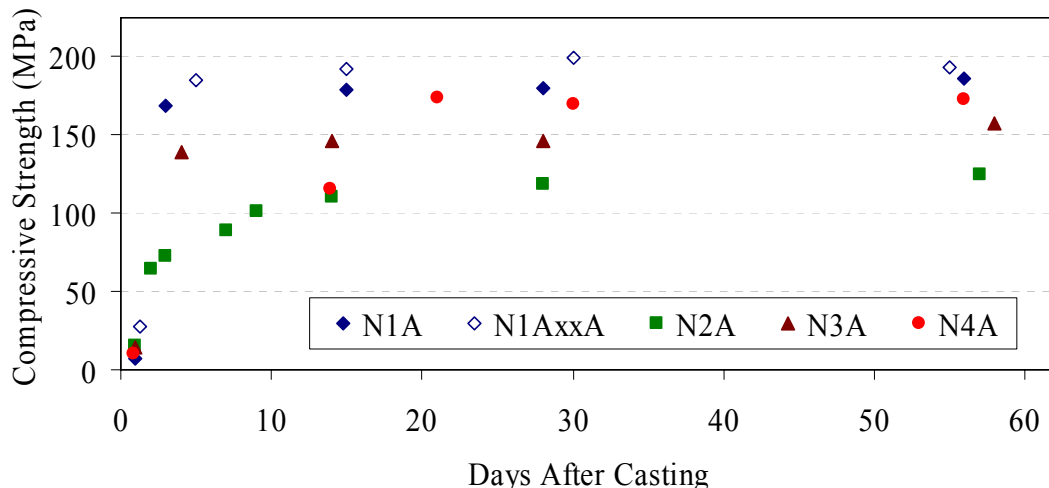
Figure 15 shows the strength results for five sets of specimens. The results presented in the figure are also shown in table 10 along with standard deviation values and the numbers of cylinders tested. In a similar fashion, figure 16 shows the modulus of elasticity results for the five sets of specimens. The modulus of elasticity was calculated based on the average LVDT-based deformation measurements and the load reading. A best-fit linear approximation of the stress-strain results from 10 to 30 percent of the compressive strength of each individual cylinder was used. Again, table 10 presents further information relating to these results.

Additional modulus of elasticity tests were also completed on spare cylinders from various batches of UHPC cast for this research program. These tests were completed following the same procedures discussed above and were all completed at 1 month of age. In general, between 20 and 30 cylinders were tested at this age for each curing regime. The overall modulus of elasticity results include a stiffness of 52.8 GPa (7,650 ksi) for steam-treated, 42.8 GPa (6,200 ksi) for untreated, 51.0 GPa (7,400 ksi) for tempered steam-treated, and 50.3 GPa (7,300 ksi) for delayed steam-treated UHPC.

Finally, the axial strain carried by each cylinder at peak compressive loading was also determined based on the load-deformation results from each cylinder. This strain value was calculated as the average deformation exhibited by the cylinder over the 51-mm (2-inch) gage length of the deformation measuring system. These results are presented in figure 17 and table 10. The additional modulus of elasticity tests discussed above also provided extra information related to strain at peak stress. The overall strain at peak stress results include 0.0041 for steam-treated, 0.0035 for untreated, 0.0035 for tempered steam-treated, and 0.0039 for delayed steam-treated UHPC.
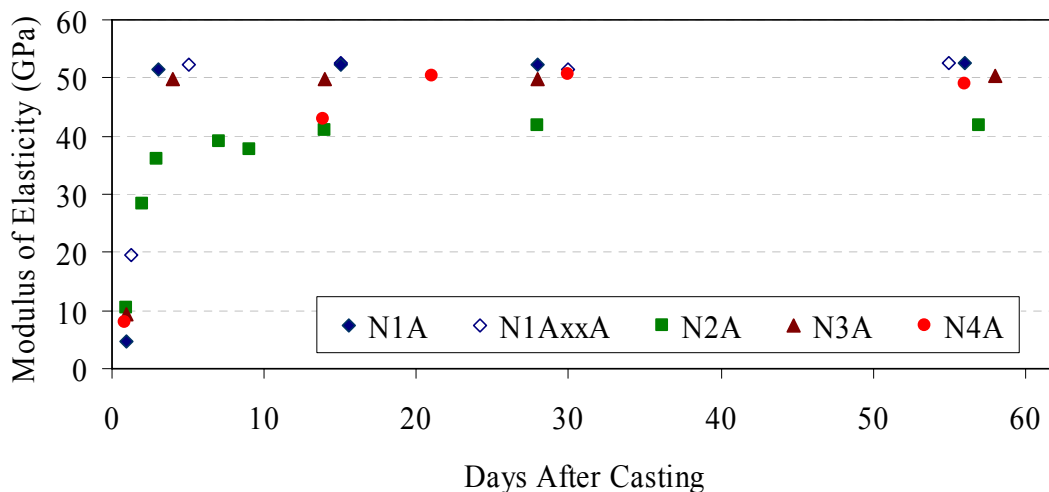
The results presented thus far in this section illustrate three primary findings. First, after steam or delayed steam treatment, the UHPC is stabilized. In terms of strength, stiffness, and strain at

peak load, the UHPC shows very little change after a steam-based treatment has been applied. Second, untreated UHPC continues to gain strength for at least 8 weeks after casting, but its increase in stiffness and decrease in strain at peak load seem to be curtailed at 1 month. Finally, UHPC gains strength and stiffness very quickly at early ages, while also becoming much less ductile with a large decrease in strain at peak load. Specifically, the compressive strength and stiffness after 24 hours are around 10 MPa and 10.3 GPa (1.5 ksi and 1,500 ksi), respectively. After 3 days, however, these values have increased to over 69 MPa and 34.5 GPa (10 ksi and 5,000 ksi), respectively, without any curing treatment.

1 MPa = 145 psi

Figure 15. Graph. Compressive strength gain from casting up to 8 weeks of age.

1 GPa = 145,000 psi

Figure 16. Graph. Modulus of elasticity gain from casting up to 8 weeks of age.
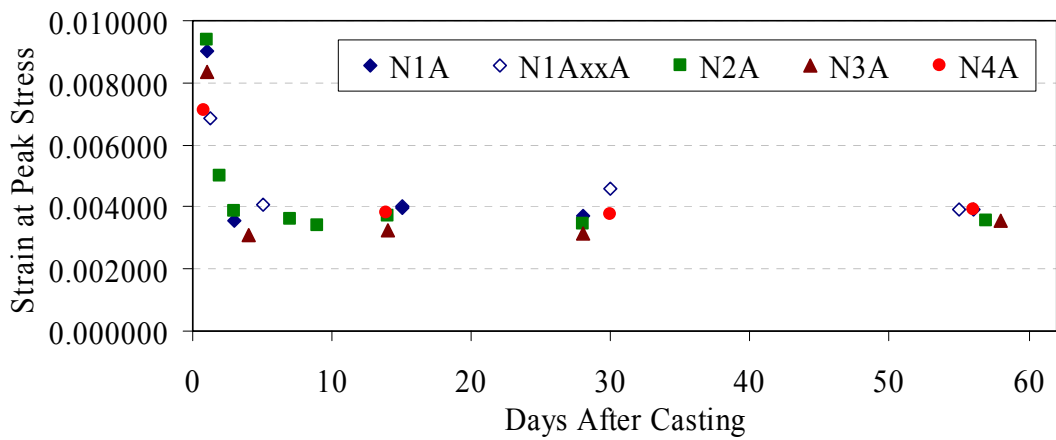
Figure 17. Graph. Strain at peak compressive stress from casting up to 8 weeks of age.

Table 10. Strength, modulus of elasticity, and strain at peak stress results at various ages after casting.

Test Age (days)	Compressive Strength (MPa)			Modulus of Elasticity (GPa)			Strain at Peak Stress		
	No.	Ave.	St. Dev.	No.	Ave.	St. Dev.	No.	Ave.	St. Dev.
Steam (N1A)									
1.0	6	7.6	0.6	6	4.6	1.0	6	0.009020	0.001740
3	6	169	4.0	6	51.5	1.5	1	0.003580	–
15	6	179	4.8	6	52.2	1.4	1	0.003970	–
28	6	180	3.4	6	52.3	1.0	2	0.003740	0.000080
56	6	186	5.7	5	52.5	1.3	2	0.003900	0.000080
Steam (N1AxxA)									
1.3	5	27	2.5	5	19.4	1.9	5	0.006830	0.000840
5	5	185	6.3	5	52.4	0.8	4	0.004080	0.000470
15	6	193	5.2	6	52.5	1.1	4	0.004020	0.000250
30	6	199	6.7	6	51.4	1.2	4	0.004580	0.000300
55	6	194	8.3	6	52.5	0.7	4	0.003920	0.000300
Untreated (N2A)									
1.0	3	15	1.4	3	10.5	2.2	3	0.009360	0.001930
2.0	2	65	0.7	2	28.3	0.5	3	0.005020	0.000530
3	2	73	0.6	2	36.0	0.3	3	0.003850	0.000340
7	3	89	0.6	3	39.0	0.8	3	0.003620	0.000800
9	2	101	4.1	2	37.6	0.8	3	0.003400	0.001640
14	6	110	4.2	6	41.2	1.2	6	0.003710	0.000590
28	6	119	3.7	6	41.9	1.1	4	0.003430	0.000130
57	6	125	4.8	6	42.0	1.0	3	0.003570	0.000240

1 MPa = 145 psi
1 GPa = 145,000 psi

Table 10. Strength, modulus of elasticity, and strain at peak stress results at various ages after casting (continued).

Test Age (days)	Compressive Strength (MPa)			Modulus of Elasticity (GPa)			Strain at Peak Stress		
	No.	Ave.	St. Dev.	No.	Ave.	St. Dev.	No.	Ave.	St. Dev.
Tempered Steam (N3A)									
1.0	6	14	1.2	6	9.3	1.8	6	0.008380	0.001430
4	6	139	4.0	4	49.9	0.9	2	0.003100	0.000200
14	6	146	6.8	6	49.7	0.7	3	0.003260	0.000080
28	6	147	5.4	6	49.9	1.1	1	0.003150	–
58	6	157	5.2	6	50.4	0.9	3	0.003550	0.000220
Delayed Steam (N4A)									
0.8	2	9.7	0.4	2	7.9	3.6	3	0.007120	0.003600
14	4	115	2.8	4	42.9	1.7	3	0.003810	0.000280
21	6	174	4.4	5	50.3	1.0	0	–	–
30	6	170	4.8	6	50.7	0.7	1	0.003760	–
56	6	172	4.5	6	49.1	1.5	3	0.003890	0.000150

1 MPa = 145 psi
1 GPa = 145,000 psi

3.3.3 Linearity of UHPC Compressive Response

It is normally assumed that concrete begins to develop internal microcracking and exhibit an associated reduction in stiffness at high stresses. The stress level varies depending on the composition of the concrete. The linearity of the compressive stress-strain response of UHPC was investigated through the elastic modulus testing results that were described in the previous section.

Two methods are used to describe the linearity of the compressive stress-strain response of concrete. The first is the secant modulus. The secant modulus, E_0, is defined as the compressive strength of the concrete divided by the strain at the peak strength. The second method involves determining the proportion of the strength at which the observed stress is some percentage below the elastic modulus predicted stress. Figure 18 shows an example of both of these linearity descriptors in conjunction with an untreated UHPC cylinder tested at 57 days after casting. Both of these linearity descriptors relate to the elastic modulus, also known as the tangent modulus, which was defined previously as being the linear best-fit approximation of the stress-strain response between 10 and 30 percent of the compressive strength.

1 MPa = 145 psi
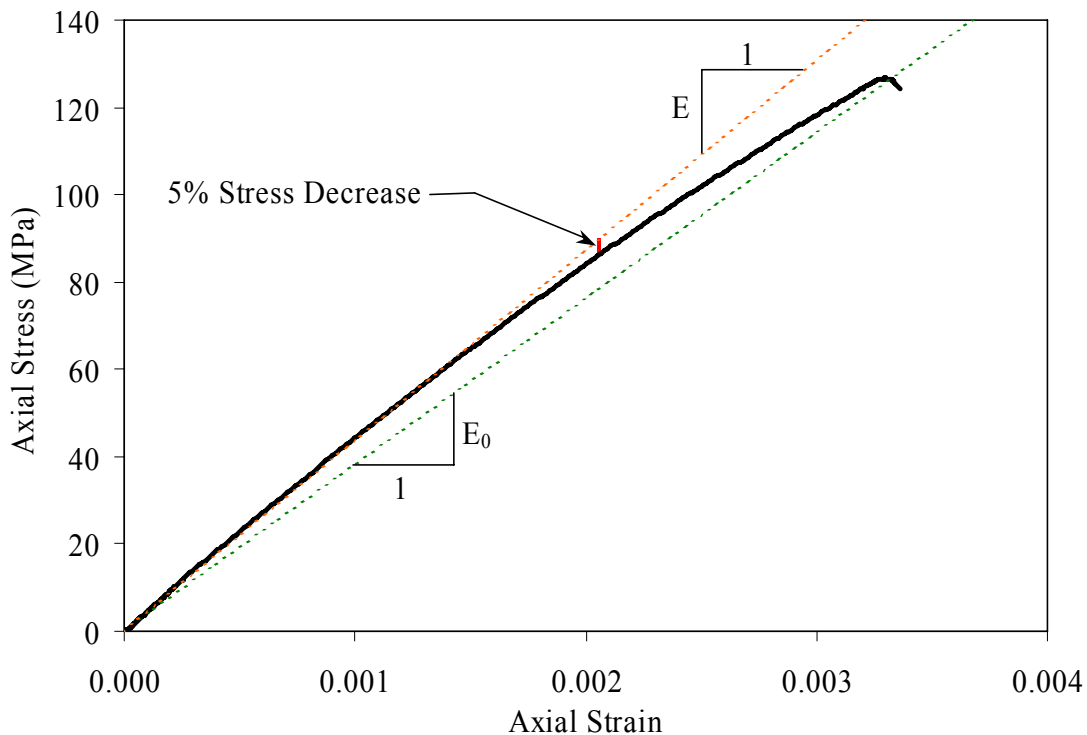
Figure 18. Graph. Sample untreated stress-strain curve with linearity descriptors.

The linearity to peak strength results, as defined by the secant modulus, are presented in table 11 and figures 19 and 20. The secant modulus shows very similar qualitative behaviors compared with the elastic modulus behaviors described in the previous section. More importantly, the ratio

of the tangent to secant modulus values illustrates how the UHPC behavior changes as curing progresses. At 1 day after casting this ratio ranges from 5 to 7, but by 3 days it is under 2 even without any supplemental curing. The ratio tends to stabilize around 1.1 for the steam-based specimens and around 1.2 for the untreated specimens. For reference, this value is normally approximately 4 for normal weight 7 MPa (1,000 psi) compressive strength concrete and approximately 1.3 for 70 MPa (10 ksi) compressive strength concrete.[20]

The linearity results—in terms of the stress at which the stress will have dropped some percentage from the linear elastic expected value—are presented in table 11 and figures 21 and 22. The research program focused on stress drops of 1, 3, and 5 percent. The results from the 1 percent drop are highly dependent on the predefined range for calculation of the elastic modulus and as such are of less interest. The results from the 5 percent drop clearly show that UHPC exhibits nearly linear behavior up to high stress levels. Figure 22 shows that the cylinders that underwent steam-based treatment reach between 80 and 90 percent of their compressive strength before diverging 5 percent from linear elastic behavior. The untreated cylinders seem to be asymptotically approaching the same type of response by 8 weeks after casting, having reached 70 percent of their compressive strength before diverging 5 percent from the linear elastic behavior.

Table 11. Compressive stress-strain response linearity at various ages after casting.
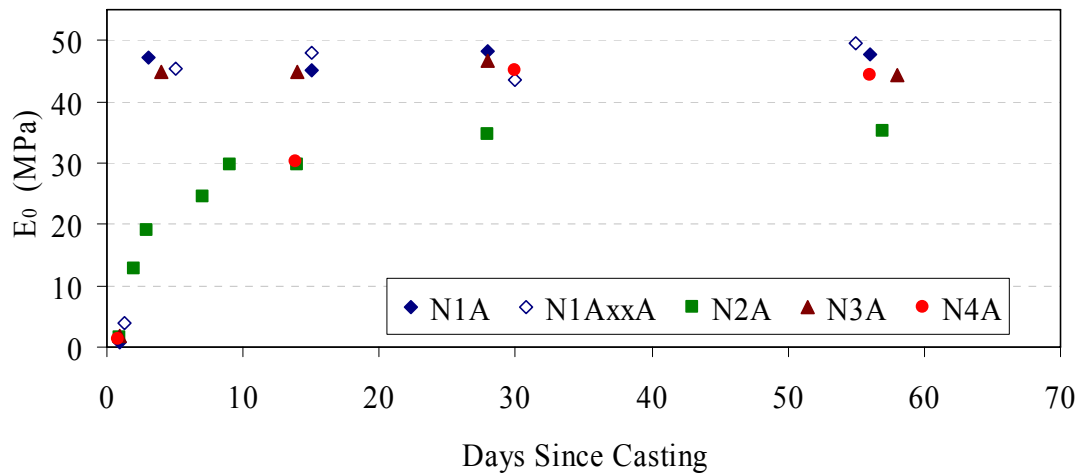
Test Age (days)	Compressive Strength (MPa)	Strain at Peak Stress	E / E_0	No.	Linearity (1%)		Linearity (3%)		Linearity (5%)	
					Strain	Stress (MPa)	Strain	Stress (MPa)	Strain	Stress (MPa)
Steam (N1A)										
1.0	7.6	0.009020	5.53	6	0.000440	1.9	0.000490	2.1	0.000530	2.2
3	169	0.003580	1.09	6	0.001540	79	0.002520	126	0.003070	150
15	179	0.003970	1.16	6	0.001470	76	0.002620	132	0.003380	166
28	180	0.003740	1.08	6	0.001570	81	0.002570	130	0.003290	164
56	186	0.003900	1.10	5	0.001610	83	0.002670	137	0.003360	168
Steam (N1AxxA)										
1.3	27	0.006830	4.90	5	0.000340	6.5	0.000420	7.6	0.000470	8.3
5	185	0.004080	1.16	5	0.001730	90	0.002790	141	0.003400	169
15	193	0.004020	1.09	6	0.001830	95	0.002890	147	0.003440	172
30	199	0.004580	1.18	5	0.001930	99	0.002960	149	0.003620	177
55	194	0.003920	1.06	6	0.001870	97	0.002960	151	0.003700	184
Untreated (N2A)										
1.0	15	0.009360	6.49	2	0.000330	3.0	0.000380	3.8	0.000410	4.1
2.0	65	0.005020	2.20	0	–	–	–	–	–	–
3	73	0.003850	1.90	2	0.000590	21	0.000740	26	0.000870	30
7	89	0.003620	1.59	3	0.000680	26	0.000930	35	0.001140	42
9	101	0.003400	1.26	2	0.000920	34	0.001250	46	0.001520	54
14	110	0.003710	1.39	6	0.000860	34	0.001200	48	0.001490	58
28	119	0.003430	1.21	6	0.001040	43	0.001530	62	0.001930	77
57	125	0.003570	1.20	6	0.001180	49	0.001760	72	0.002220	88

1 MPa = 145 psi

Table 11. Compressive stress-strain response linearity at various ages after casting (continued).
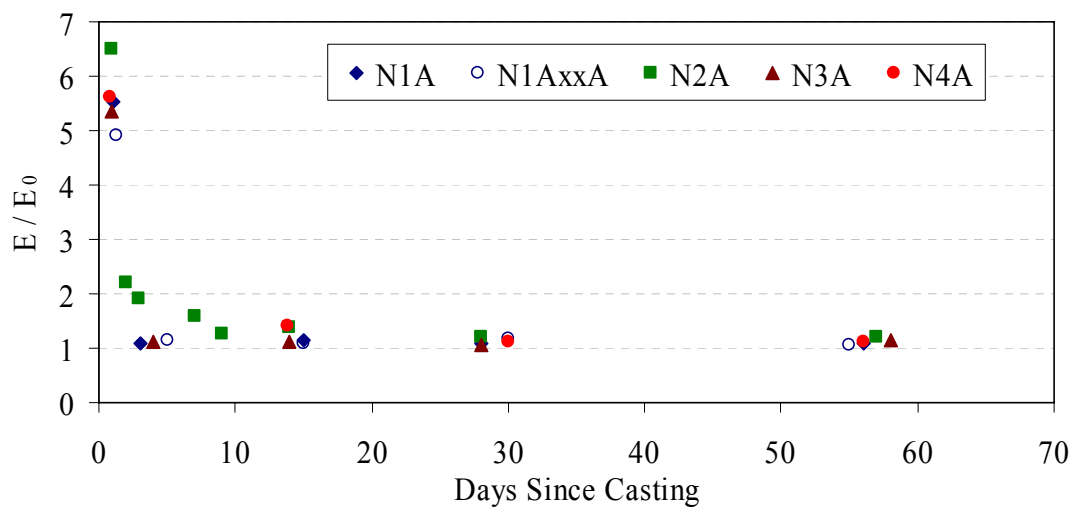
Test Age (days)	Compressive Strength (MPa)	Strain at Peak Stress	E / E_0	No.	Linearity (1%)		Linearity (3%)		Linearity (5%)	
					Strain	Stress (MPa)	Strain	Stress (MPa)	Strain	Stress (MPa)
Tempered Steam (N3A)										
1.0	14	0.008380	5.34	6	0.000390	3.5	0.000460	4.1	0.000520	4.6
4	139	0.003100	1.11	4	0.001310	65	0.001940	94	0.002400	114
14	146	0.003260	1.11	6	0.001380	68	0.002110	102	0.002630	124
28	147	0.003150	1.07	6	0.001180	58	0.002070	100	0.002580	123
58	157	0.003550	1.14	6	0.001360	68	0.002150	105	0.002710	130
Delayed Steam (N4A)										
0.8	9.7	0.007120	5.61	1	0.000480	2.5	0.000550	2.8	0.000380	2.3
14	115	0.003810	1.42	4	0.000870	37	0.001190	49	0.001480	60
21	174	–	–	5	0.001490	74	0.002250	110	0.002900	139
30	170	0.003760	1.13	6	0.001630	82	0.002420	119	0.003000	145
56	172	0.003890	1.11	6	0.001700	83	0.002630	125	0.003280	153

1 MPa = 145 psi

Figure 19. Graph. Secant modulus from casting up to 8 weeks of age.

1 MPa = 145 psi

Figure 20. Graph. Ratio of elastic to secant modulus from casting up to 8 weeks of age.

1 MPa = 145 psi
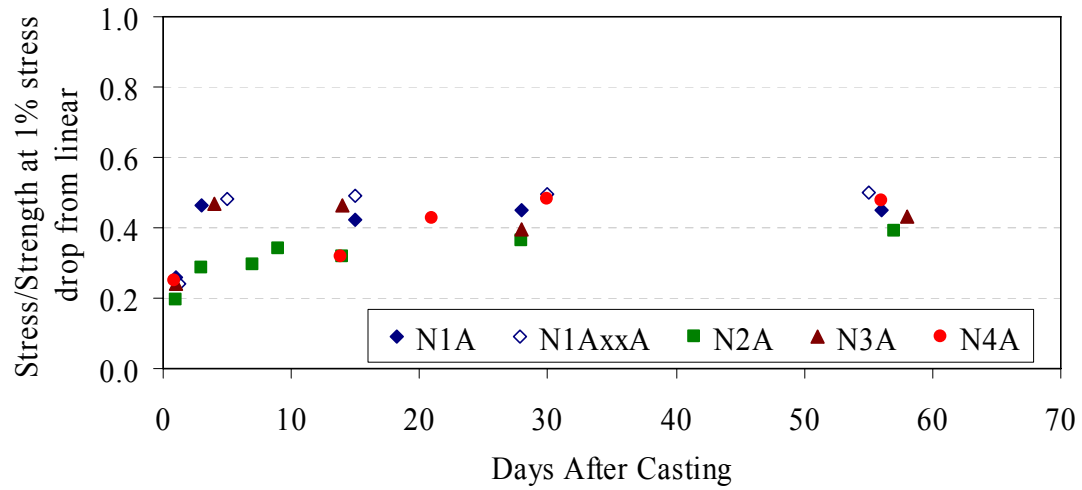
Figure 21. Graph. Compressive stress to strength ratio at 1 percent stress drop from linear elastic.
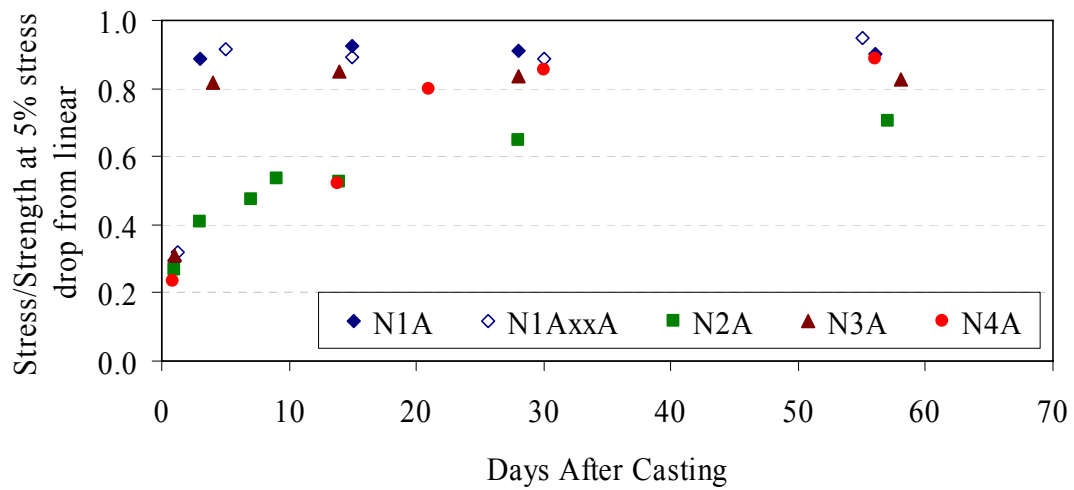
Figure 22. Graph. Compressive stress to strength ratio at 5 percent stress drop from linear elastic.

3.3.4 Compression Specimen Geometry

In the United States, the cylinder is the standard concrete compression test specimen. Conversely, the cube is the standard specimen in parts of Europe. It is generally accepted that with normal strength concrete the cube will result in a higher compressive strength due to its shorter aspect ratio and the proportionally larger lateral confinement provided by the machine platens.

A series of tests were completed to determine the effect of various specimen geometries on the compressive strength of UHPC. Compression tests were completed according to ASTM C39 on 51-, 76-, and 102-mm (2-, 3-, and 4-inch) diameter cylinders with cast lengths of twice their diameters. ASTM C39 compression tests were also performed on overlength 76-mm (3-inch) diameter cylinders that had a cast length of 165 mm (6.5 inches). Cube compression tests were completed according to ASTM C109 on 51- and 100-mm (2- and 4-inch) cubes. Figure 23 shows the range of sizes and geometries of the specimens tested. Figure 24 shows the cylinder and cube specimens in the compression testing machine. All specimens were tested in a hydraulically actuated 4,450 kN (1,000 kip) Forney test machine with a load rate equivalent to 1.0 MPa/s (150 psi/s).

The test program described above was repeated three times. Each time, the set of cylinder and cube specimens was cast from a single batch. Two of the batches were steam treated while the third batch was untreated. Table 12 provides the results from the compression tests. The 76-mm (3-inch) diameter cylinder—used as the control specimen throughout the entire study—was also the control specimen for this series of tests.

Figure 23. Photo. Compression cubes and cylinders including (clockwise from upper left) 102-mm (4-inch), 76-mm (3-inch) overlength, 76-mm (3-inch), and 51-mm (2-inch) diameter cylinders and 51-mm (2-inch) and 100-mm (4-inch) cubes.
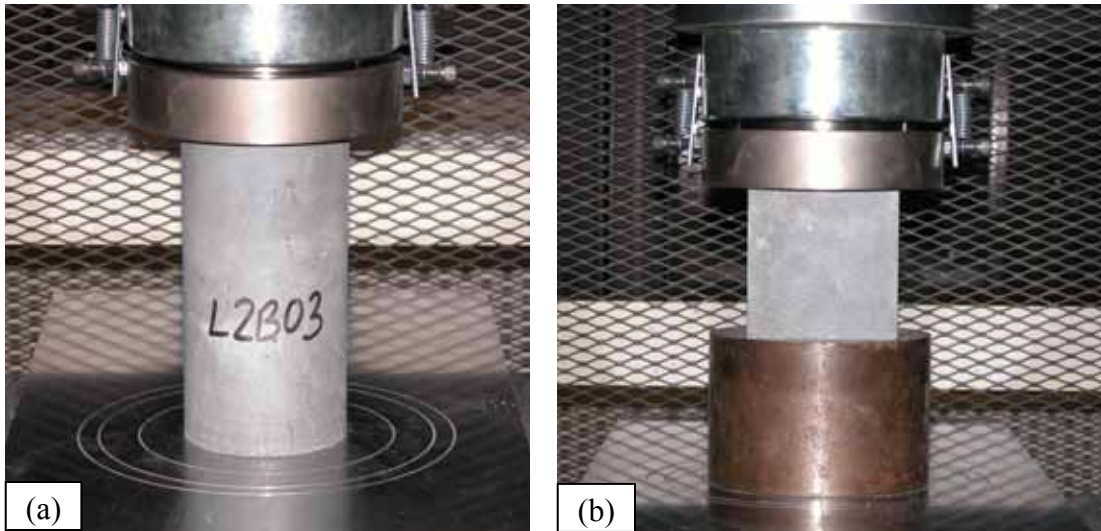
Figure 24. Photos. (a) Cylinder and (b) cube compression testing.

The combined results from the three sets of tests indicate that the compressive strength of UHPC can be measured, relatively accurately, through various sizes of cubes and cylinders. Results were never more than 8 percent removed from the control cylinder result. The cubes tended to exhibit slightly higher strengths on the order of 5 percent. In addition, the 51-mm (2-inch) diameter cylinders tended to exhibit slightly lower strengths. The smaller cubes and cylinders tended to exhibit larger standard deviations. Conversely, the large specimens tended to exhibit smaller standard deviations. These results were expected because heterogeneities in the concrete would likely remain in a uniform size range but would be proportionally larger in smaller specimens.

3.3.5 Demolding Age Effect on Compressive Strength

Throughout this test program, control cylinder compressive strengths were sometimes below the anticipated value. As previously mentioned, the mix design, constituent materials, and mixing procedure were always the same. For this reason, the deviations in strength were troubling. Two observations were made during the early stages of the test program: (1) the set time of the UHPC sometimes varied and (2) in general, the older the premix, the longer the set time. Regardless of these observations, the cylinders were nearly always demolded at approximately 24 hours after casting. This delayed setting sometimes resulted in the cylinders barely having enough strength to remain intact throughout the demolding process.

After the bulk of the test program was complete, an additional batch was added to the test program. This batch included two sets of 76-mm (3-inch) diameter cylinders that were demolded at various ages after casting. One of the sets was then steam treated while the other was untreated. The earliest that any cylinders could be stripped was determined to be 28 hours after casting because of the advanced age of the premix by this point in the test program. The other cylinders were stripped at 47 and 55 hours after casting. Otherwise, the cylinders in each set were treated identically up through compression testing at 28 days.

Table 12. Cylinder and cube compressive strength results.

Specimen	No.	Compressive Strength (MPa)		% Difference From Control
		Average	St. Dev.	
Steam (M1B)				
76-mm Cylinder [†]	6	203	4.2	–
102-mm Cylinder	5	202	6.3	−0.3
Overlength 76-mm Cylinder	3	188	8.9	−7.5
51-mm Cylinder	6	203	6.9	0.3
100-mm Cube	5	201	12.1	−1.2
51-mm Cube	6	214	11.7	5.8
Steam (L1B)				
76-mm Cylinder [†]	6	210	7.0	–
102-mm Cylinder	5	215	5.4	2.2
Overlength 76-mm Cylinder	3	194	8.2	−7.5
51-mm Cylinder	6	200	12.3	−5.0
100-mm Cube	5	220	5.0	4.6
51-mm Cube	6	220	10.8	4.6
Untreated (L2B)				
76-mm Cylinder [†]	8	149	3.8	–
102-mm Cylinder	5	154	2.1	3.7
Overlength 76-mm Cylinder	3	150	1.5	1.1
51-mm Cylinder	6	140	14.8	−5.9
100-mm Cube	3	161	2.9	8.0
51-mm Cube	6	158	8.8	6.1

1 MPa = 145 psi
1 mm = 0.039 inch

Table 13 presents the results from this set of compression tests. These results clearly indicate that the age of the UHPC at stripping has a major impact on the compressive strength. The cylinders that were stripped as soon as their integrity allowed had a 25 to 30 percent lower compressive strength at 28 days compared with the cylinders that were stripped approximately 20 hours later. Once the cylinder has gained sufficient integrity to support itself, the primary role of the cylinder mold is to retain moisture within the cylinder. The loss of that moisture barrier clearly resulted in a decrease in the moisture that was available for hydration and a resulting decrease in compressive strength.

Table 13. Demolding age effect on 28-day compressive strength results.

Specimen Group	No.	Compressive Strength (MPa)	
		Average	St. Dev.
Steam			
Stripped at 28 hours after casting	6	143	8.6
Stripped at 47 hours after casting	6	203	5.9
Stripped at 55 hours after casting	6	208	13.0
Untreated			
Stripped at 28 hours after casting	6	99	3.4
Stripped at 47 hours after casting	6	129	3.5
Stripped at 55 hours after casting	6	136	5.2

1 MPa = 145 psi

3.3.6 Long-Term Delayed Steam Effect on Compressive Strength

Although the delayed steam-curing regime was designed to mimic the postponed steam curing of UHPC, it is anticipated that longer delays prior to steam treatment could occur. For this reason, two batches of UHPC were cast to focus on the compressive strength level that UHPC can attain if the steam treatment is significantly delayed. Each of these batches included 36 cylinders, half of which were untreated and half of which had a steam treatment applied at a time distant from casting. The steam treatment was the same as the standard steam treatment except for the start date. The steam treatment always started 6 days before the date of the compression testing.

Table 14 presents the results of these tests. The first batch, L21, was tested at 8, 12, and 16 weeks after casting. The second batch, L22, was tested at 8, 20, and 32 weeks after casting. In both cases, the untreated cylinders and the cylinders that underwent the long-term, delayed steam treatment showed consistent compressive strengths over the months of testing. The diminishing impact of the steam treatment, delayed from 1 day to 2 weeks after casting, does not seem to continue indefinitely. By 2 months, the impact seems to have leveled off such that steaming at this time is as effective as steaming at up to 32 weeks after casting. Additionally, it is important to note that the application of the steam treatment increased the compressive strength by 30 percent, regardless of when it was applied.

3.3.7 Fiber Effect on Compression Failure

The steel fiber reinforcement included in UHPC provides a number of advantages, most notably in terms of tensile structural behavior. Normally, a compression test on high-strength concrete would result in a very brittle, dramatic failure. As noted earlier in the discussion of UHPC compression behavior, the UHPC that is reinforced with steel fibers does not exhibit explosive failures during compression tests. Recalling figure 6, a compression test on steam-treated UHPC would likely result in a rapid load drop, but the cylinder would remain intact.

Table 14. Long-term delayed steam effect on compressive strength.

Batch	Curing	Steam Days	Test Day	No.	Compressive Strength (MPa)	
					Average	St. Dev.
L21	Untreated	–	56 days	6	142	3.9
	Untreated	–	84 days	6	138	4.6
	Untreated	–	112 days	6	134	2.3
	Steam	50 to 52	56 days	6	181	7.2
	Steam	78 to 80	84 days	6	174	4.1
	Steam	106 to 108	112 days	6	178	5.1
L22	Untreated	–	56 days	6	130	2.4
	Untreated	–	140 days	6	128	5.7
	Untreated	–	224 days	6	131	6.1
	Steam	50 to 52	56 days	6	173	6.3
	Steam	134 to 136	140 days	6	167	8.6
	Steam	218 to 220	224 days	7	171	4.8

1 MPa = 145 psi

A few UHPC cylinders were cast according to the normal mix design and procedures except that the steel fiber reinforcement was not added. Thus, the high compressive strength abilities of the UHPC matrix are present, but the restraining and confining effects of the fibers are absent. The test results from these cylinders indicated a dramatic change in the compression failure behavior.

Figure 25 shows four still pictures of the failure of one of these cylinders. These pictures were captured from a digital video recording. The video was captured at a rate of 30 frames per second, thus the smallest increment of time over which to observe changes in behavior is 1/30 second. The failure of this cylinder occurred when small chips of UHPC began to fly off the top and bottom of the cylinder at its intersection with the platens. This chipping continued for a few seconds until a larger chip exited the top of the cylinder just 1/6 second before failure. The cylinder then rapidly and dramatically failed: Over the course of 1/30 second, the intact cylinder shattered into many small pieces of UHPC.

Although this experiment was not controlled with fiber-reinforced and nonreinforced UHPC tested in parallel, the compressive strength results are still of interest. The cylinders tested averaged 200 MPa (29 ksi), with the cylinder shown in the video reaching 214 MPa (31 ksi). Note that these strengths correspond to loads of approximately 890 kN (200 kips); therefore, the Forney 4,450-kN (1,000-kip) capacity testing machine was only at 20 percent of its capacity and would not have held an inordinately high level of strain energy before failure.

(a)

(b)

(c)

(d)
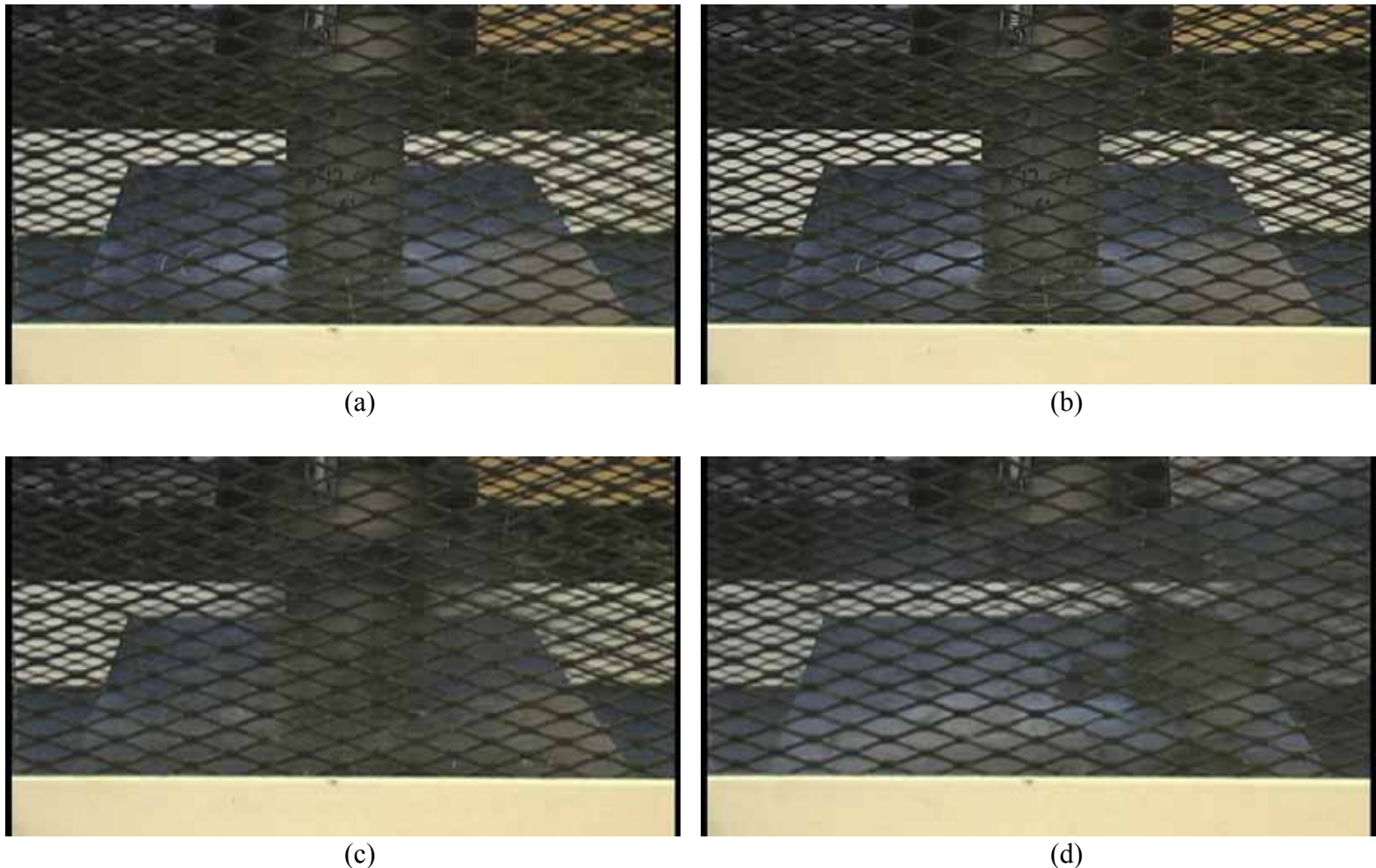
Figure 25. Photos. Compression failure of a steam-treated UHPC cylinder containing no fiber reinforcement (a) 1/6 second before failure, (b) 1/30 second before failure, (c) at failure, and (d) 1/10 second after failure.

48

3.3.8 Load Rate Effect on Compression Testing Results

The compression testing discussed so far in section 3.3 was all completed with a load rate of 1.0 MPa/s (150 psi/s) during the initial elastic portion of the stress-strain response. As previously mentioned, this load rate is outside the bounds recommended by the ASTM C39 test method. Before initiating the compression testing portion of the UHPC material characterization work, a set of UHPC cylinders was cast with the focus being on the effect of various load rates on standard compression testing results.

It is normally accepted that higher load rates will result in higher compression strength and modulus of elasticity results. For this reason, using the ASTM C39 load rate of 0.24 ±0.10 MPa/s (35 ±15 psi/s) is recommended for any standardized compression testing of concrete. However, the high strength results expected from UHPC mean that a single compression test on a concrete cylinder could take 15 to 20 minutes or more. This objectionably long time for a single data point led to the testing discussed below.

Twenty-four cylinders with a 76-mm (3-inch) diameter were cast within a single batch of UHPC for this testing. The cylinders were all cast and steam treated according to normal procedures. The cylinders were then divided into four groups, each of which was tested at a different load rate ranging from 0.24 to 1.7 MPa/s (35 to 250 psi/s). Within each group of six cylinders, three were tested in compression according to ASTM C39. The remaining three were tested according to ASTM C469, including multiple unloads/reloads, before being tested according to ASTM C39. This testing differed from the previously discussed modulus testing, because the axial deformations were measured via a standard compressometer as described in the test method, and data on Poisson's ratio were also collected.

Table 15 presents the results of these tests. The results do not clearly indicate a change in behavior caused by the increasing load rate. For this particular batch, the compressive strength remained around 200 MPa (29 ksi), the modulus of elasticity remained around 56.5 GPa (8,200 ksi), and Poisson's ratio was quite consistent at 0.19. These results indicate that an increase in the load rate would not be detrimental. From a practical standpoint, a compression test run at 1.0 MPa/s (150 psi/s) can be completed within 5 minutes on a steam-treated cylinder and more quickly on lower strengths of UHPC. For these reasons, a load rate of 1.0 MPa/s (150 psi/s) was chosen for all of the UHPC compression testing.

Table 15. Load rate effect on compression testing results.

Load Rate (MPa/s)	Compressive Strength (MPa)			Modulus of Elasticity (GPa)			Poisson's Ratio		
	No.	Ave.	St. Dev.	No.	Ave.	St. Dev.	No.	Ave.	St. Dev.
0.24	6	194	11.2	3	55.8	2.1	3	0.195	0.018
0.34	6	201	6.9	3	57.9	1.5	3	0.193	0.011
1.0	6	201	6.8	3	56.9	1.8	3	0.199	0.007
1.7	6	201	3.3	3	55.2	1.0	3	0.184	0.011

1 MPa/s = 150 psi/s, 1 GPa = 145,000 psi, 1 MPa = 145 psi

3.4 TENSION TESTING

Four types of tension tests were implemented in this research program to experimentally determine the tensile properties of UHPC. These tests included flexural testing of prismatic sections, split tensile testing of cylinders, axial tensile testing of mortar briquettes, and axial tensile testing of cylinders. The following sections discuss the test procedures and the test results.

3.4.1 Flexural Prism

The ASTM C1018 Standard Test Method for Flexural Toughness and First-Crack Strength of Fiber-Reinforced Concrete (Using a Beam With Third-Point Loading) was one test used to determine the tensile properties of UHPC.[21] This test involves the four-point flexural loading of small-scale concrete prisms. During the test, the load on and the deflection of the prism are monitored. These data are then used to determine the cracking strength and postcracking toughness response of the concrete.

This test method requires specialized equipment in order to correctly load the specimen and accurately monitor the response. First, the test setup requires that the deflection measuring system must measure "net values exclusive of any extraneous effects due to seating or twisting of the specimen on its supports or deformation of the support system." Second, the loading of the prism must be completed through a "testing arrangement where specimen net midspan deflection is used to control the rate of increase of deflection using a closed-loop, servo-controlled testing system."

To meet these requirements, a specialized test setup was devised. In this setup, a yoke similar to that shown in figure 2 of ASTM C1018 was used to measure the midspan deflections. LVDTs were attached to the yoke on each side of the specimen at midspan, and the yoke was attached to the specimen at mid-depth over the support points. The LVDTs bore on a plate that was epoxied to the compression face and extended to hang over the sides of the prism. Figure 26 shows two examples of the deflection measurement setup for this four-point bending test.

The loading control of the test was accomplished by completing the test in an MTS® load frame. The control signal for the MTS was the midspan net deflection of the specimen as captured by the LVDTs. The signals from the two LVDTs were electronically averaged, then submitted to the MTS control panel. In this way, the deflection rate of the prism was accurately and consistently maintained at the correct level. This loading technique also limited the amount of potential energy stored in the load frame that could be transmitted into the concrete prism during the temporary stiffness loss associated with cracking.

The loading apparatus used to test the prisms was reconfigurable to allow for testing of multiple sizes of prisms. The rollers and their support blocks are movable to allow for lower support spans from 152 to 406 mm (6 to 16 inches) and upper loading spans from 51 to 152 mm (2 to 6 inches). As shown in figure 26, the two upper load points and the two lower support points are steel rollers that impart no axial restraint on the prism. Torsional effects caused by misalignment between the planes of the prism faces and the rollers were overcome by placing individual shims between each roller and its bearing block. The bearing blocks under the rollers

are supported by 152-mm (6-inch) deep solid steel beams that are connected to the heads of the MTS machine. These deep steel beams reduce flexibility in the loading apparatus, thus allowing for easier and more refined control of the test during cracking of the prism.

The ASTM C1018 test was performed on prisms from all four curing regimes. The casting and curing of the prisms was completed following normal procedures. During casting of each prism, special care was taken to ensure that the UHPC flowed from one end of the prism to the other, thus ensuring a fiber distribution and alignment system that was similar to that which would occur in the large-scale casting of a beam or plate type flexural member.
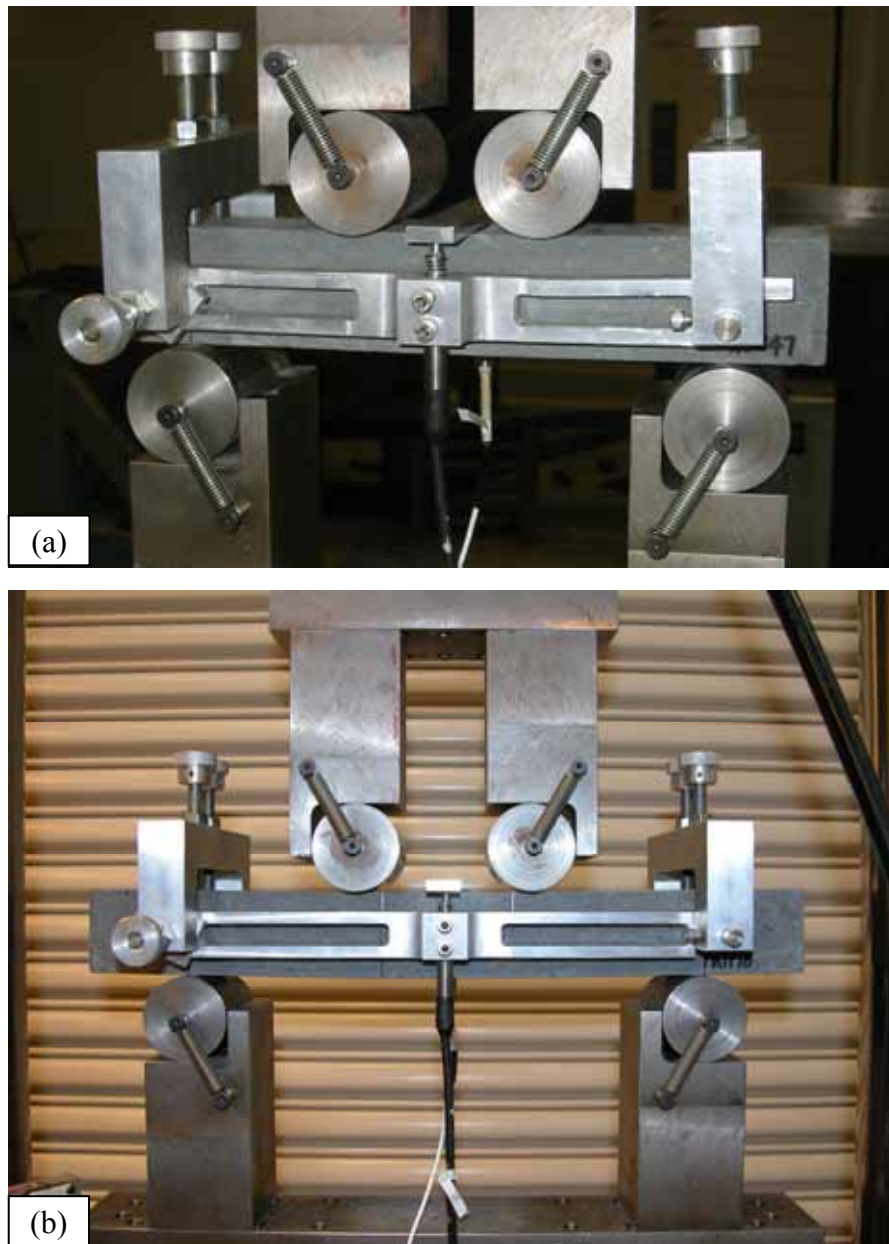
Figure 26. Photos. Prism flexural test setup for (a) a 229-mm (9-inch) span and (b) a 305-mm (12-inch) span.
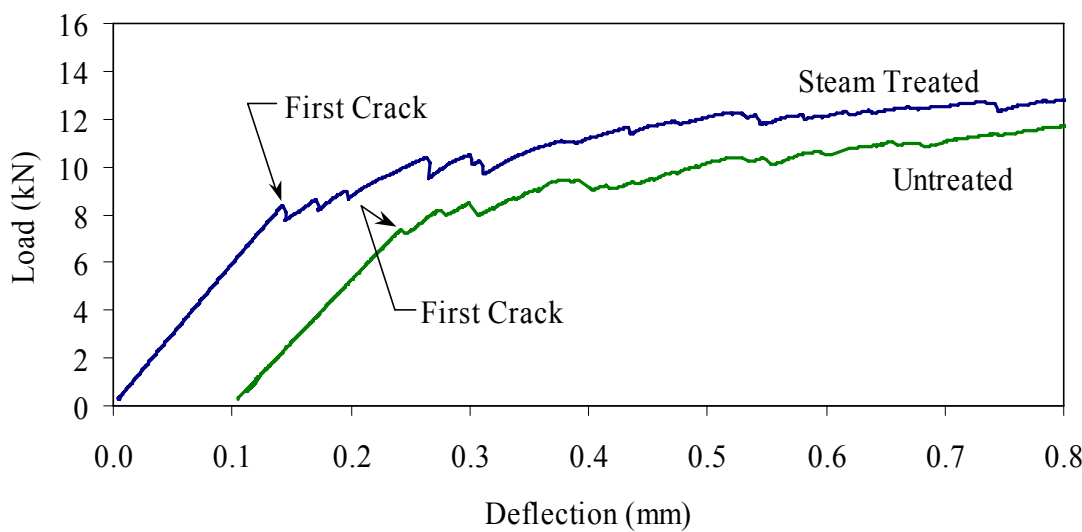
The test specification recommends a preferred standard size of molded specimen of 356 by 102 by 102 mm (14 by 4 by 4 inches), resulting in a third-point loading configuration with a 305-mm (12-inch) lower span. This specimen size was not used for a number of reasons. First, this depth of prism is on the high end of the likely thickness of UHPC plate members subject to flexural forces. Second, a shear span-to-prism depth ratio equal to one, as recommended by the specification, will create a stress field and deflection response in the prism that is substantially both flexural and shear. A larger shear span-to-prism depth ratio would much more accurately represent the flexural response of UHPC. Finally, the specification indicates that the prism cross-sectional dimensions must only be at least three times the length of a fiber. This requirement can easily be met by smaller cross-sectional sizes.

The test program included two prism cross sections and a total of four loading configurations. The cross sections investigated were 51- by 51-mm (2- by 2-inch) prisms and 76-mm (3-inch) deep by 102-mm (4-inch) wide prisms. The 51- by 51-mm (2- by 2-inch) prisms were cast in lengths of 279 mm (11 inches) and 432 mm (17 inches). The 76- by 102-mm (3- by 4-inch) prisms were cast 406 mm (16 inches) long. Four loading configurations were used to test the 51- by 51-mm (2- by 2-inch) prisms. These included third-point loading on 152-, 229-, and 305-mm (6-, 9-, and 12-inch) lower spans, as well as loading on a 381-mm (15-inch) lower span with 76 mm (3 inches) between the upper load points. The third-point loading with a 305-mm (12-inch) lower span was also used for the 76- by 102-mm (3- by 4-inch) cross section prisms. These various cross sections and loading configurations allow for the comparison of observed tensile behaviors, because the 51- by 51-mm (2- by 2-inch) prism on a 152-mm (6-inch) span is a scaled model of the ASTM C1018 recommended prism. Other test setups provide more realistic representations of flexural tensile material behaviors.

The following procedure was used to complete the test:

1. The prism was centered in the load frame with the screeded face of the prism oriented toward the front and the vertical molded faces placed as the compression and tension faces.
2. The load was manually increased to approximately 220 newtons (N) (50 lb).
3. The setup was checked to ensure that all rollers were bearing on the prism.
4. The LVDTs were then set in place, and control of the machine was transferred to the averaging circuit attached to the LVDTs.
5. The MTS MicroProfiler™ was then used to apply a constant deflection rate to the prism.
6. The deflection rate was set so that the expected first crack deflection would occur approximately 1 minute into the test. This rate varied depending on the prism cross section and loading configuration.
7. The test was stopped after a deflection of at least 16 times the cracking deflection was reached.
8. The collection of the data for the test was completed through an analog data acquisition system. It was set to record data at 10 Hz until well after first cracking of the prism had clearly occurred.
9. The record rate was then manually decreased to 4 Hz for the remainder of the test. The time, load, deflection from both LVDTs, and electronic circuit averaged deflection values were all recorded.
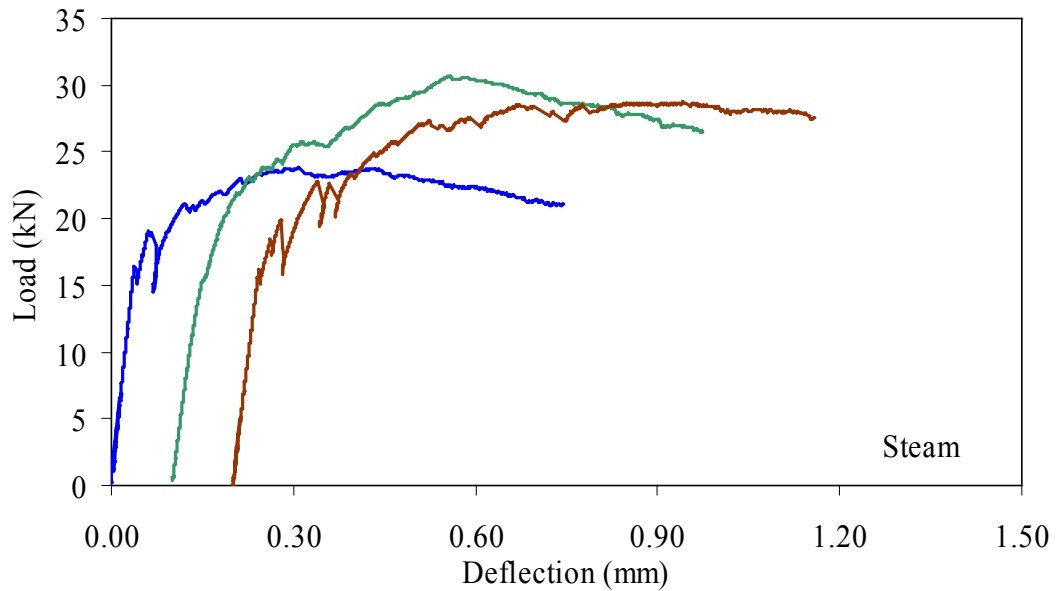
The strength and toughness results and analysis presented in the next two sections are highly dependent on the correct identification of first cracking in each prism test. Plain concrete and fiber-reinforced concrete may begin to behave nonlinearly due primarily to internal microcracking before the first overall cracking of the prism; therefore, determining first cracking can be somewhat subjective. The behavior of UHPC is such that the first cracking is tensile stress cracking on the bottom flange of the prism. Thus, first cracking—recorded by the data acquisition system and physically observed on the specimen—is usually quite clear. Figure 27 shows the early parts of load-deflection response curves for both a steam and an untreated prism. This figure shows that the prism response is linear until first cracking when a clearly defined decrease in load-carrying capacity occurs. Soon thereafter the load again begins to increase. The sawtooth pattern visible in the response is indicative of additional individual cracks forming throughout the highly stressed tension face of the prism.

1 kN = 0.225 kip, 1 mm = 0.039 inch
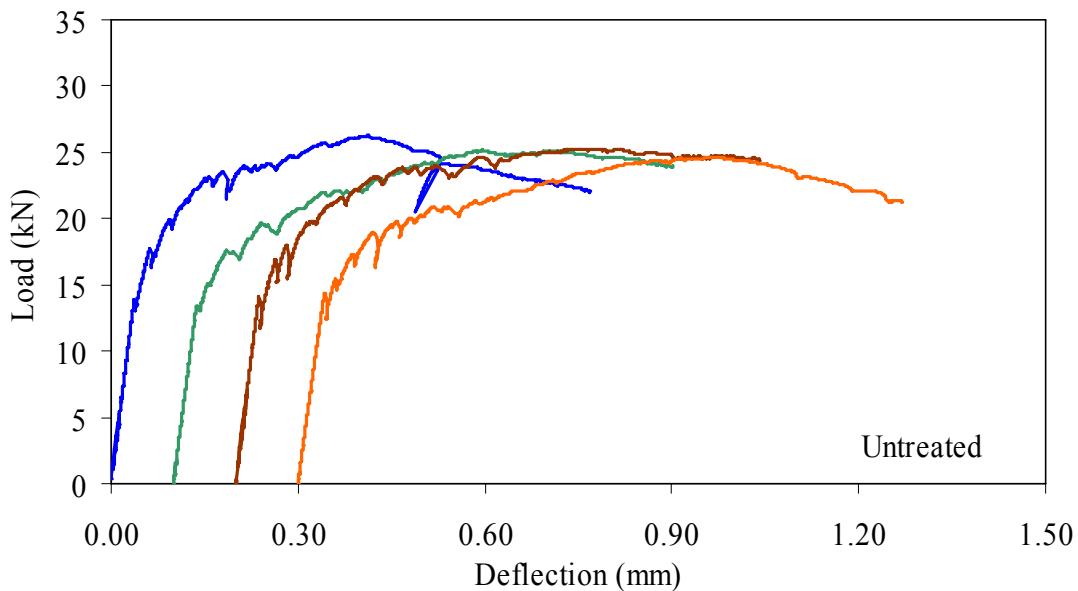
Figure 27. Graph. Examples of first crack shown on load-deflection response curves.

A total of 76 prisms were tested over the five loading/cross section configurations. Seventy-one prisms were tested successfully out of this group. The load-deflection results are presented in figures 28 through 47. Figures 28 through 31 present the results from the scaled standard ASTM C1018 test on 51- by 51-mm (2- by 2-inch) prisms with third-point loading over a 152-mm (6-inch) span. Figures 32 through 35 present the results from the 76- by 102-mm (3- by 4-inch) prisms tested with third-point loading over a 305-mm (12-inch) span. Figures 36 through 39 and 40 through 43 present the results from 51- by 51-mm (2- by 2-inch) prisms tested with third-point loading on 229-mm (9-inch) and 305-mm (12-inch) spans, respectively. Finally, figures 44 through 47 present the results from the 51- by 51-mm (2- by 2-inch) prisms tested over a 381-mm (15-inch) span with 76 mm (3 inches) between the load points. Sequential results in each set have been offset by 0.1 mm (0.004 inch) to allow for clear presentation. The curing regime applied to each set of prisms is listed in the lower right corner of each set of results.
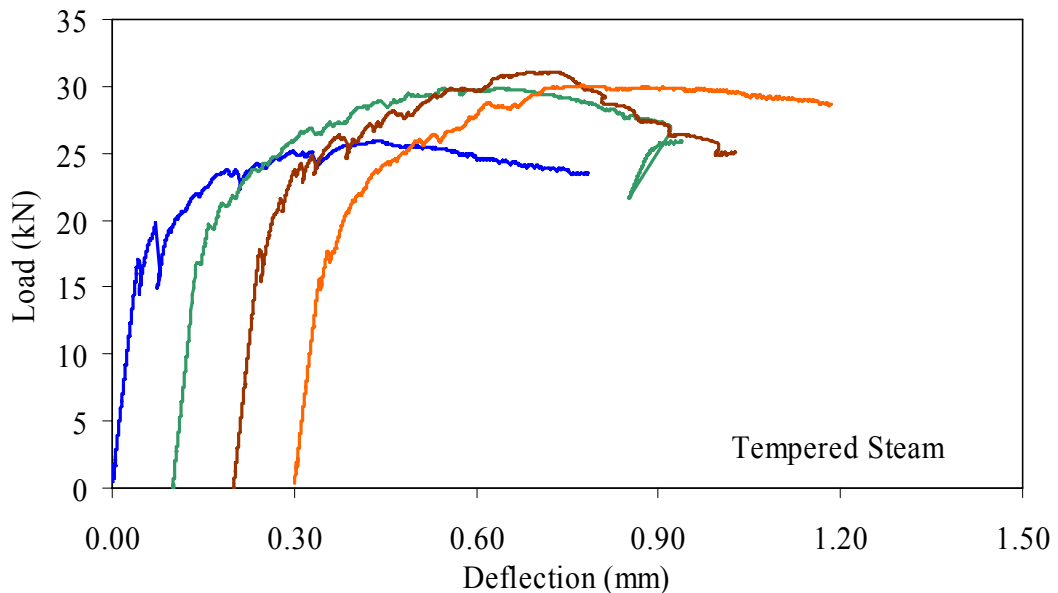
1 kN = 0.225 kip, 1 mm = 0.039 inch

Figure 28. Graph. ASTM C1018 load-deflection response results for steam-treated 51- by 51-mm (2- by 2-inch) prisms over a 152-mm (6-inch) span with third-point loading.
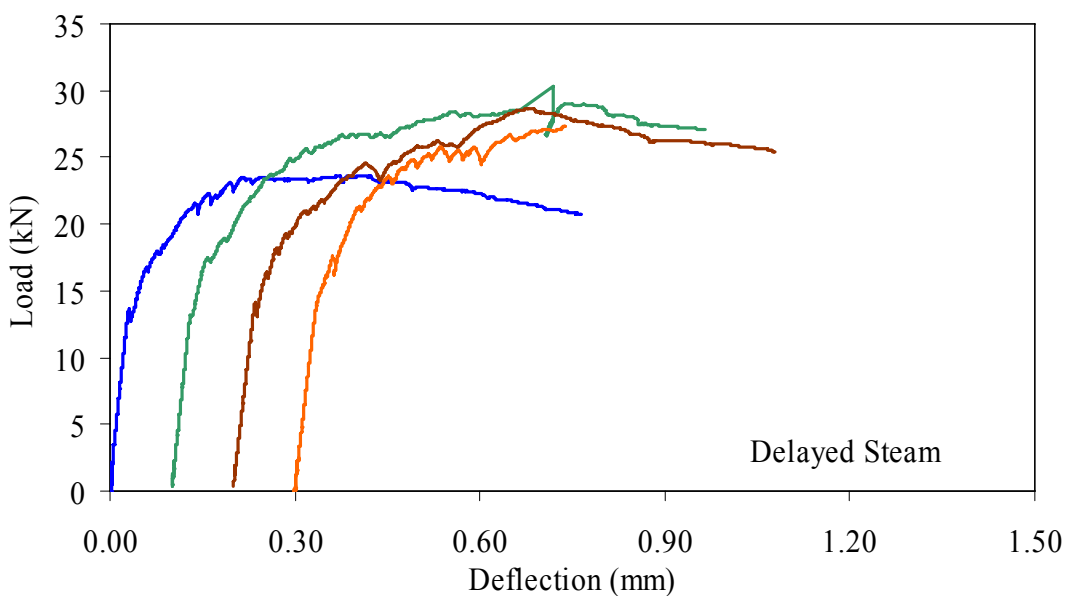
1 kN = 0.225 kip, 1 mm = 0.039 inch

Figure 29. Graph. ASTM C1018 load-deflection response results for untreated 51- by 51-mm (2- by 2-inch) prisms over a 152-mm (6-inch) span with third-point loading.

1 kN = 0.225 kip, 1 mm = 0.039 inch

Figure 30. Graph. ASTM C1018 load-deflection response results for tempered steam-treated 51- by 51-mm (2- by 2-inch) prisms over a 152-mm (6-inch) span with third-point loading.

1 kN = 0.225 kip, 1 mm = 0.039 inch

Figure 31. Graph. ASTM C1018 load-deflection response results for delayed steam-treated 51- by 51-mm (2- by 2-inch) prisms over a 152-mm (6-inch) span with third-point loading.

1 kN = 0.225 kip, 1 mm = 0.039 inch
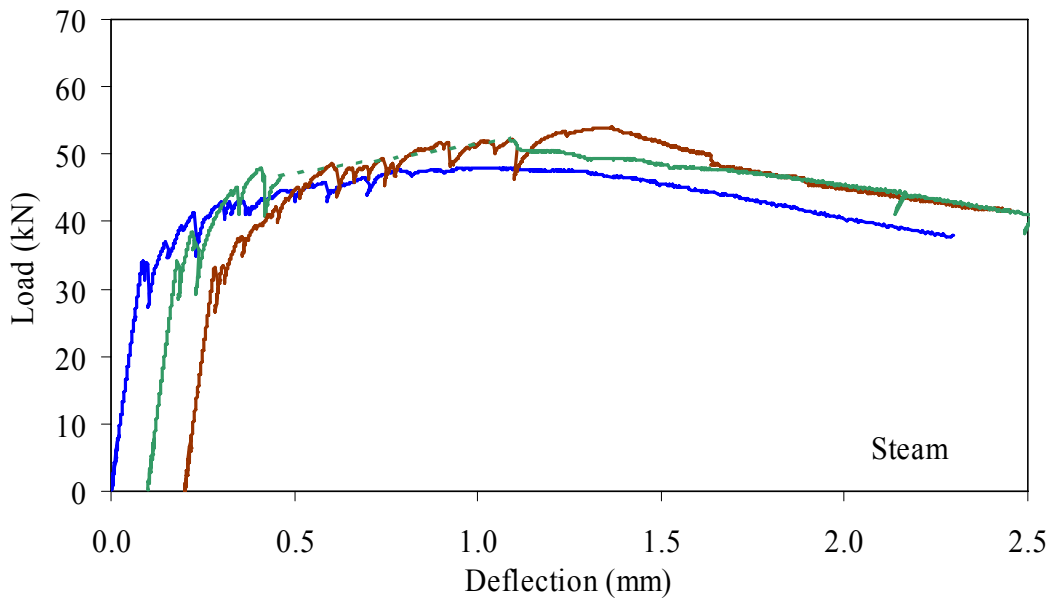
Figure 32. Graph. ASTM C1018 load-deflection response results for steam-treated 76- by 102-mm (3- by 4-inch) prisms over a 305-mm (12-inch) span with third-point loading.

1 kN = 0.225 kip, 1 mm = 0.039 inch
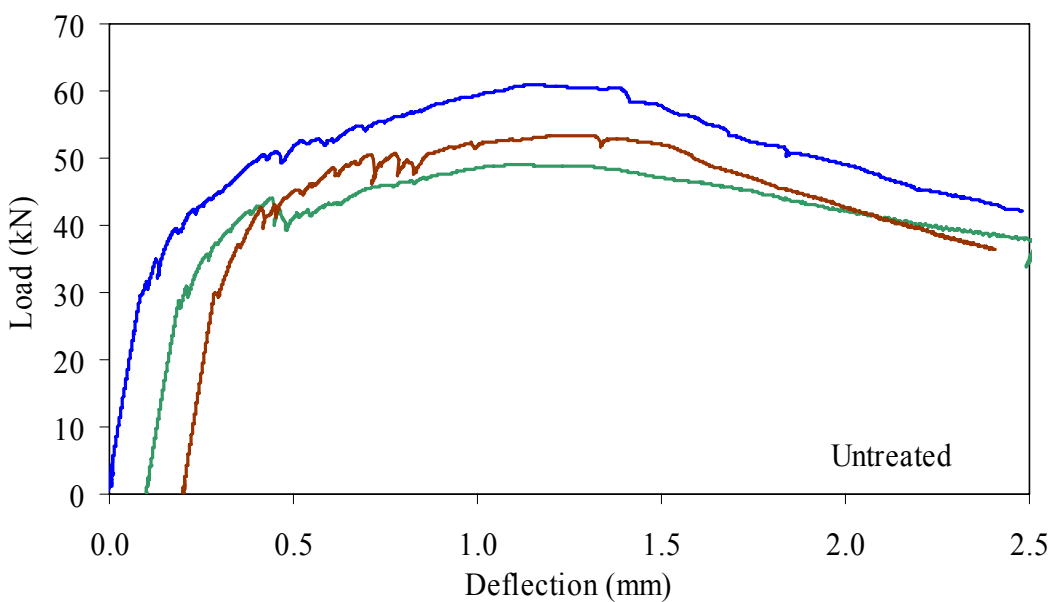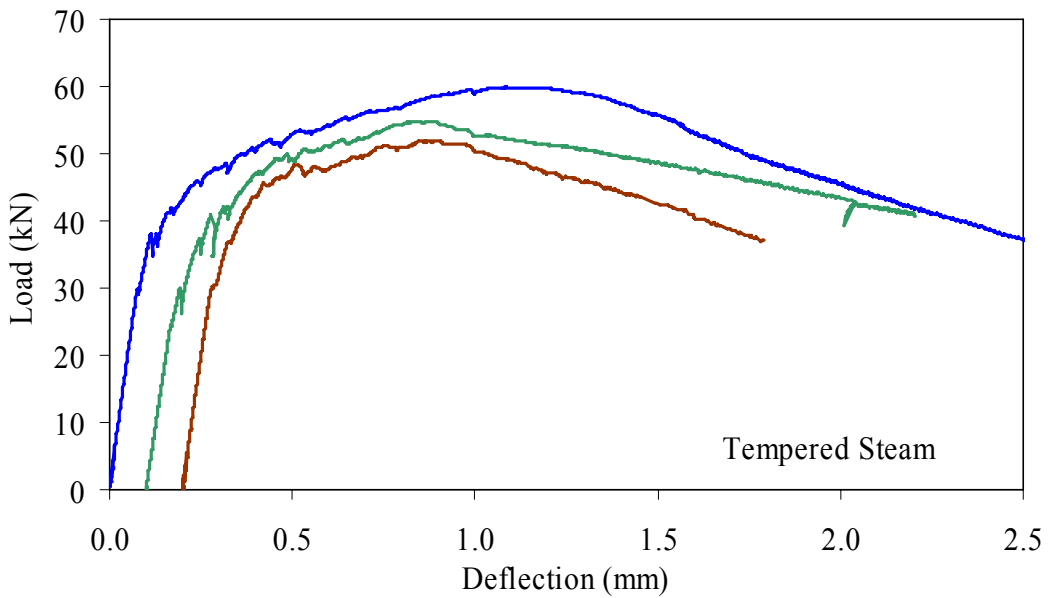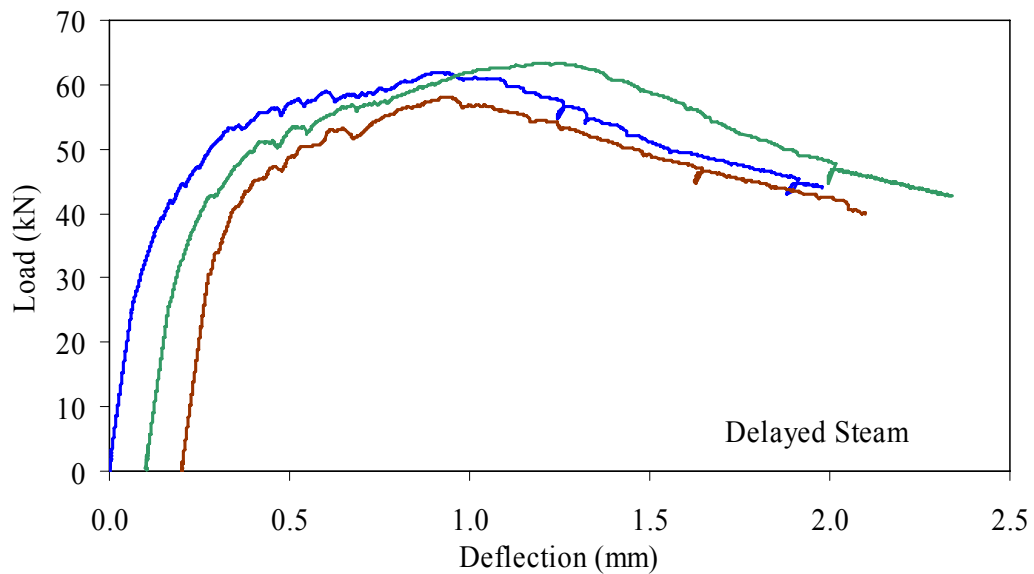
Figure 33. Graph. ASTM C1018 load-deflection response results for untreated 76- by 102-mm (3- by 4-inch) prisms over a 305-mm (12-inch) span with third-point loading.

56
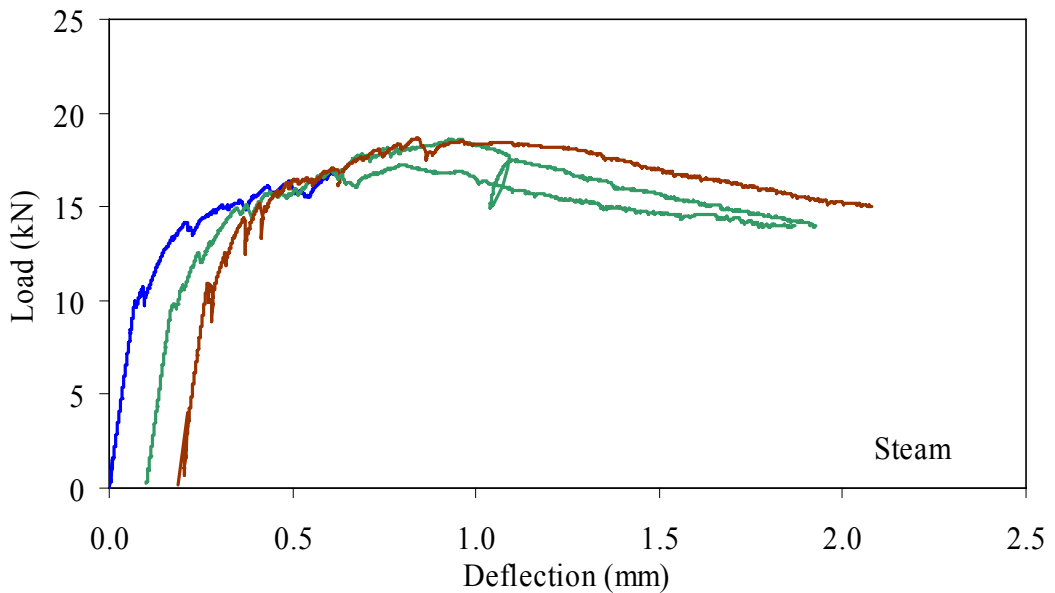
1 kN = 0.225 kip, 1 mm = 0.039 inch

Figure 34. Graph. ASTM C1018 load-deflection response results for tempered steam-treated 76- by 102-mm (3- by 4-inch) prisms over a 305-mm (12-inch) span with third-point loading.
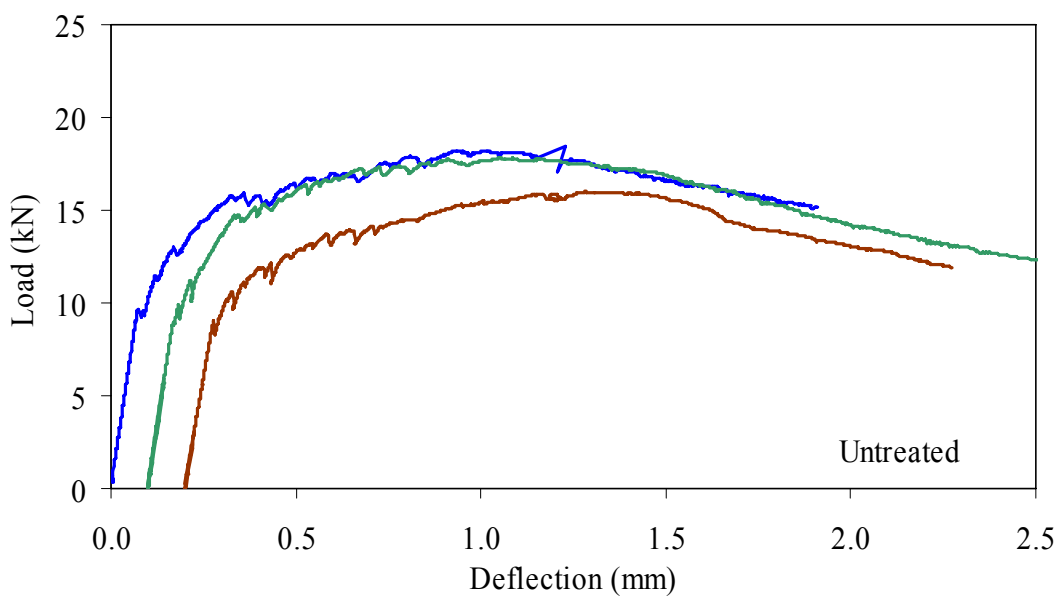
1 kN = 0.225 kip, 1 mm = 0.039 inch

Figure 35. Graph. ASTM C1018 load-deflection response results for delayed steam-treated 76- by 102-mm (3- by 4-inch) prisms over a 305-mm (12-inch) span with third-point loading.
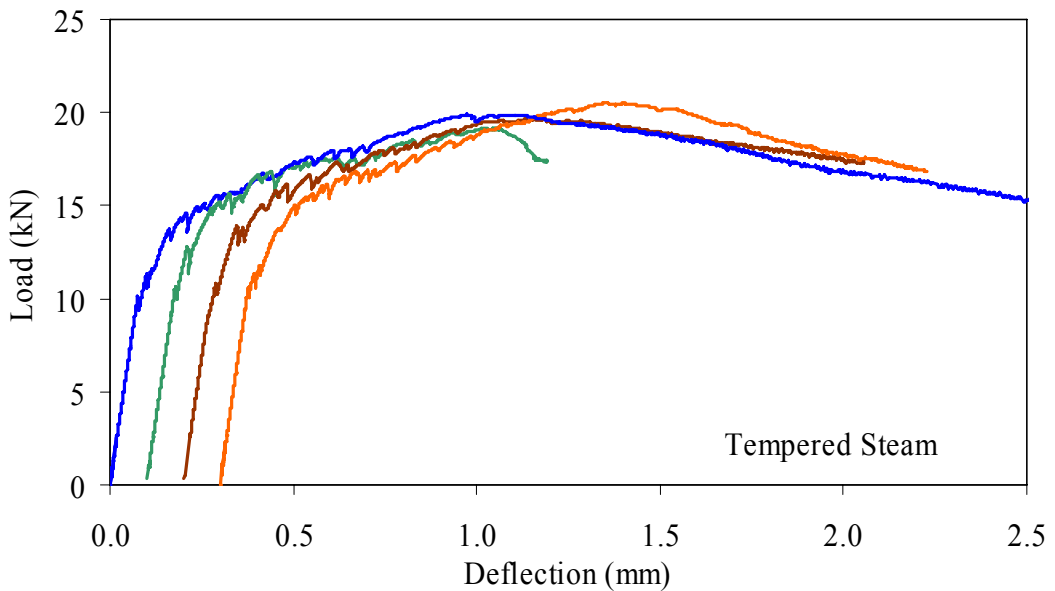
1 kN = 0.225 kip, 1 mm = 0.039 inch

Figure 36. Graph. ASTM C1018 load-deflection response results for steam-treated 51- by 51-mm (2- by 2-inch) prisms over a 229-mm (9-inch) span with third-point loading.
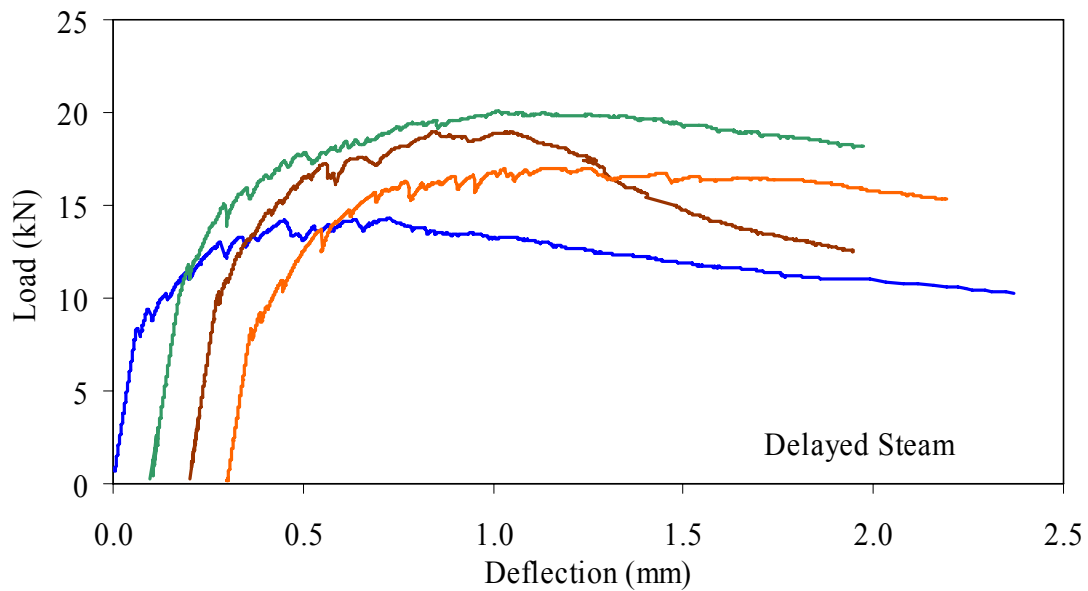
1 kN = 0.225 kip, 1 mm = 0.039 inch

Figure 37. Graph. ASTM C1018 load-deflection response results for untreated 51- by 51-mm (2- by 2-inch) prisms over a 229-mm (9-inch) span with third-point loading.
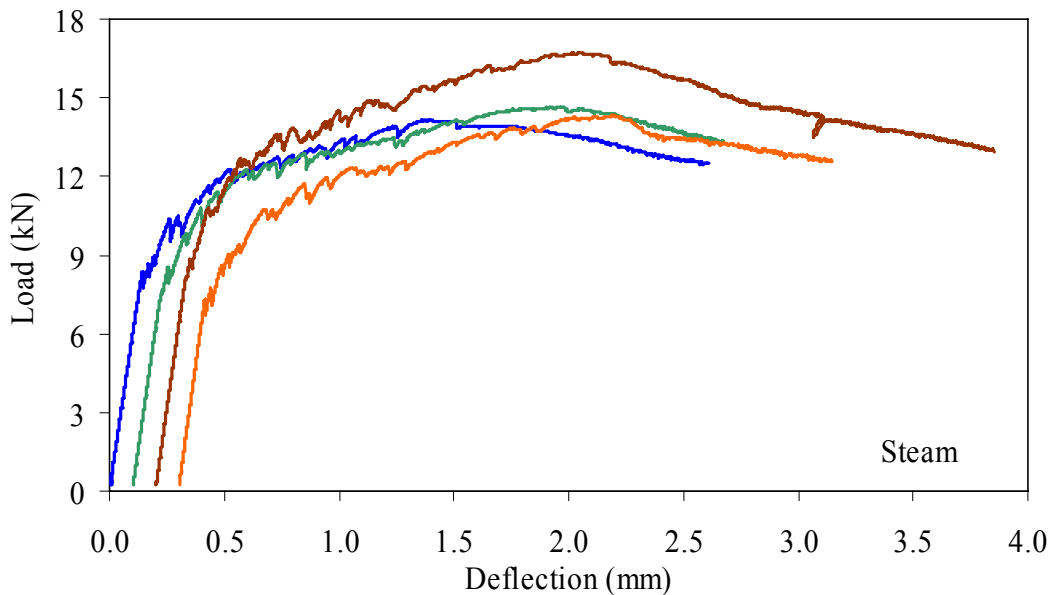
1 kN = 0.225 kip, 1 mm = 0.039 inch

Figure 38. Graph. ASTM C1018 load-deflection response results for tempered steam-treated 51- by 51-mm (2- by 2-inch) prisms over a 229-mm (9-inch) span with third-point loading.
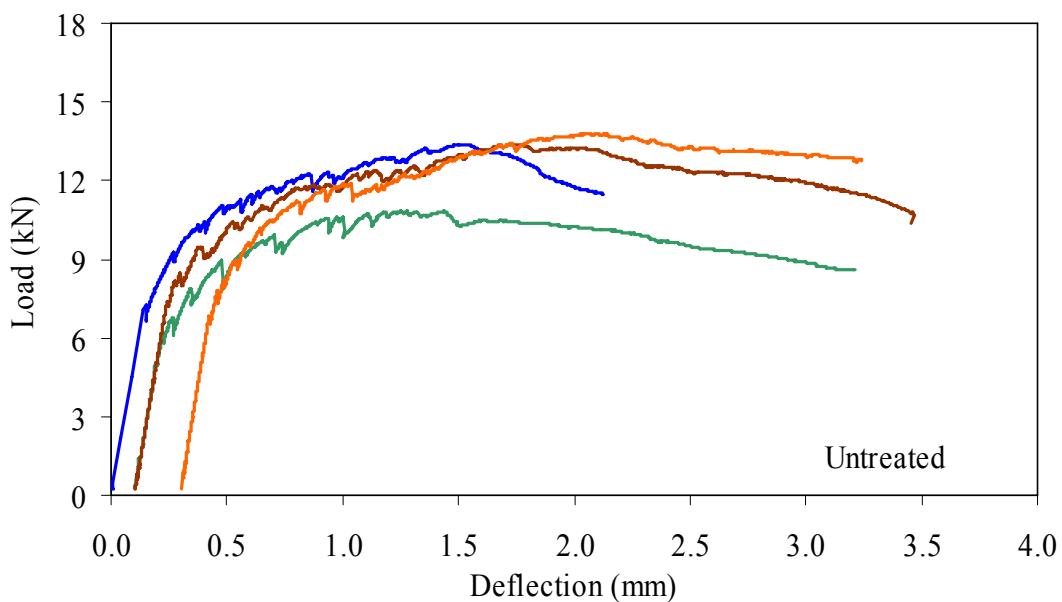
1 kN = 0.225 kip, 1 mm = 0.039 inch

Figure 39. Graph. ASTM C1018 load-deflection response results for delayed steam-treated 51- by 51-mm (2- by 2-inch) prisms over a 229-mm (9-inch) span with third-point loading.
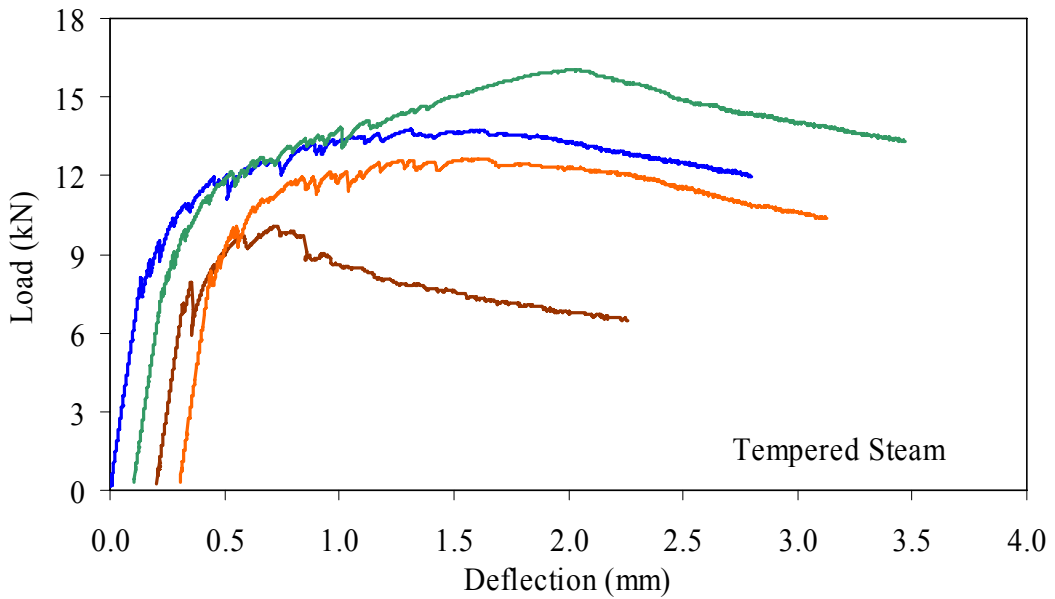
1 kN = 0.225 kip, 1 mm = 0.039 inch

Figure 40. Graph. ASTM C1018 load-deflection response results for steam-treated 51- by 51-mm (2- by 2-inch) prisms over a 305-mm (12-inch) span with third-point loading.
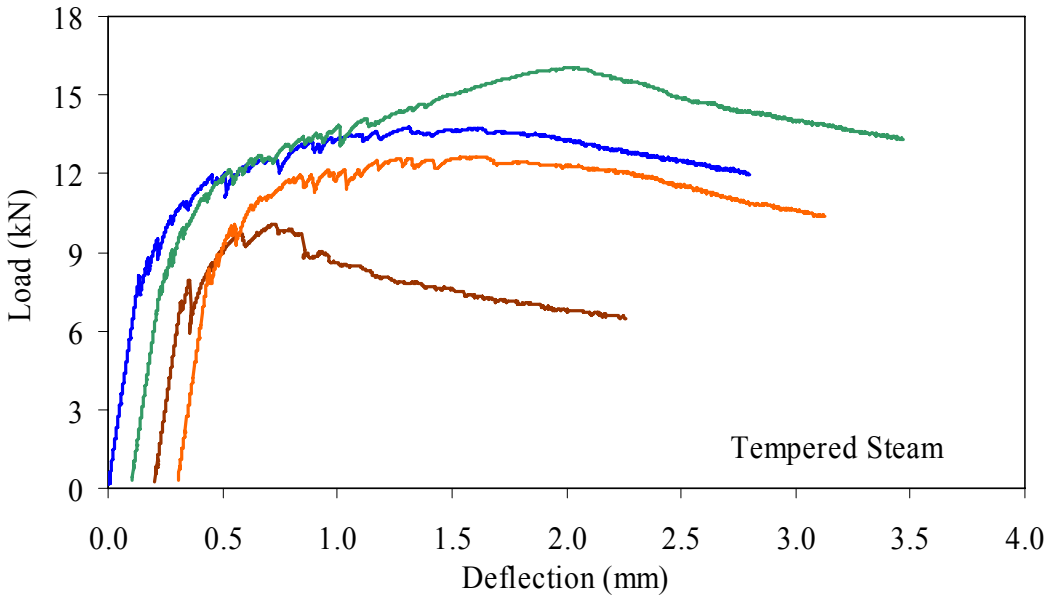
1 kN = 0.225 kip, 1 mm = 0.039 inch

Figure 41. Graph. ASTM C1018 load-deflection response results for untreated 51- by 51-mm (2- by 2-inch) prisms over a 305-mm (12-inch) span with third-point loading.
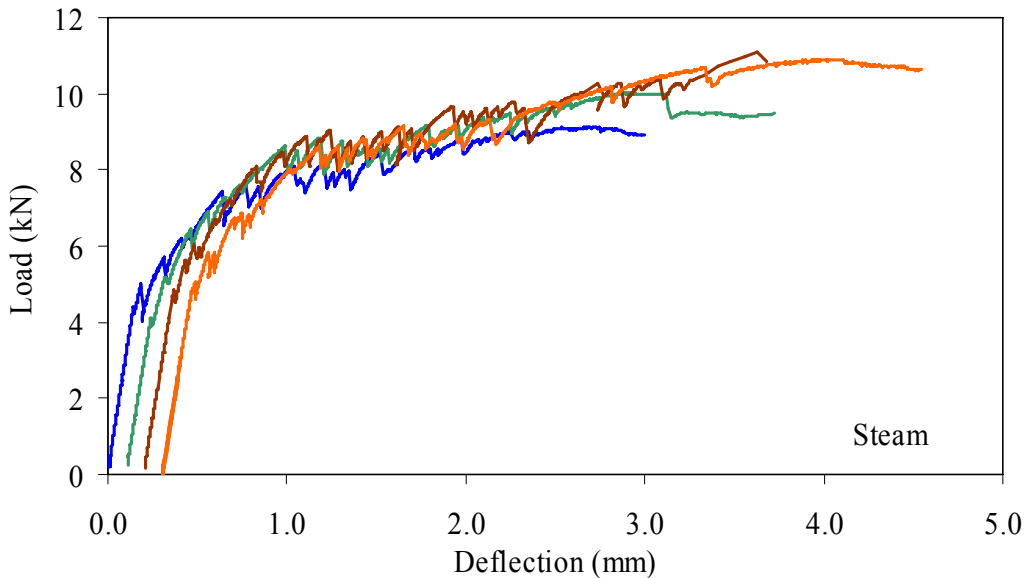
1 kN = 0.225 kip, 1 mm = 0.039 inch

Figure 42. Graph. ASTM C1018 load-deflection response results for tempered steam-treated 51- by 51-mm (2- by 2-inch) prisms over a 305-mm (12-inch) span with third-point loading.
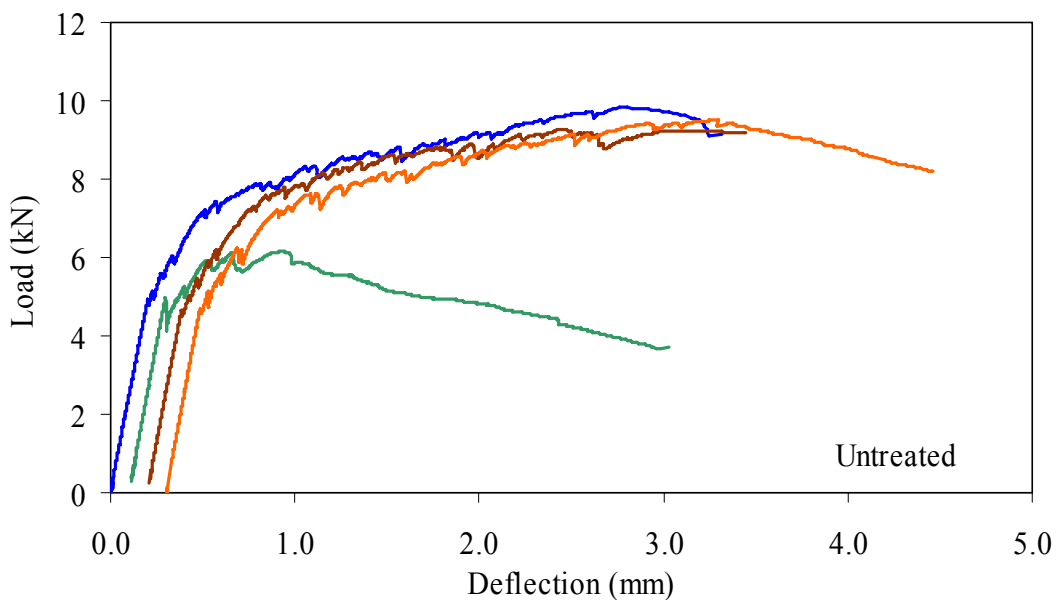
1 kN = 0.225 kip, 1 mm = 0.039 inch

Figure 43. Graph. ASTM C1018 load-deflection response results for delayed steam-treated 51- by 51-mm (2- by 2-inch) prisms over a 305-mm (12-inch) span with third-point loading.
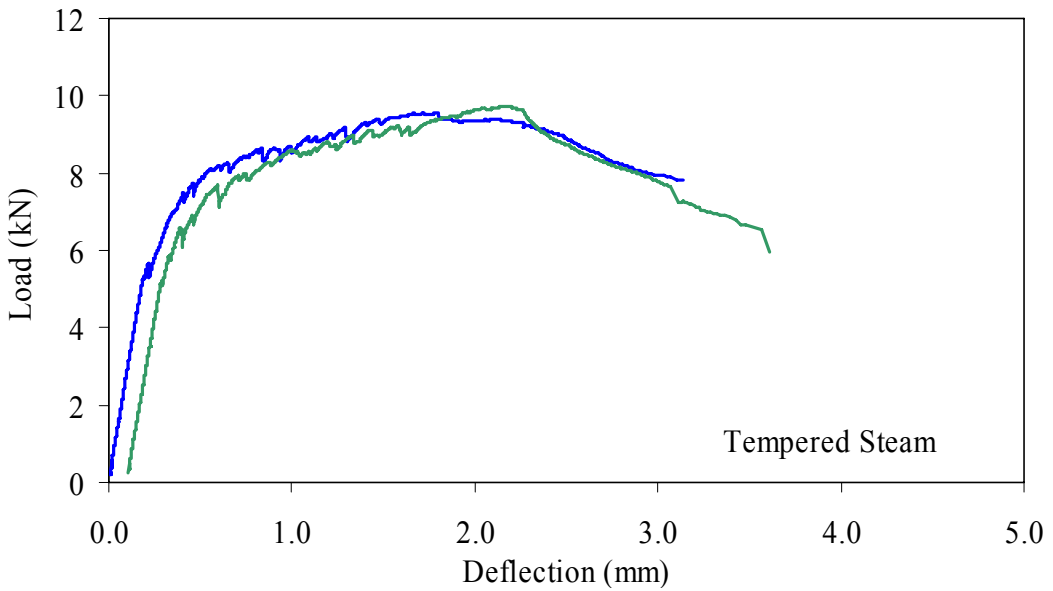
kN = 0.225 kip, 1 mm = 0.039 inch

Figure 44. Graph. ASTM C1018 load-deflection response results for steam-treated 51- by 51-mm (2- by 2-inch) prisms over a 381-mm (15-inch) span with 76 mm (3 inches) between loads.
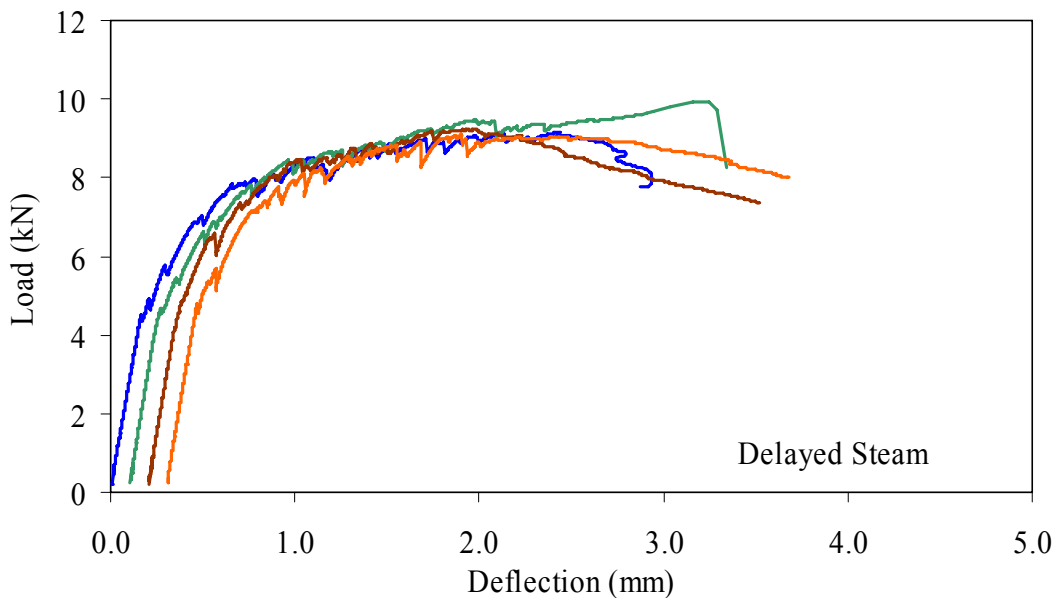
1 kN = 0.225 kip, 1 mm = 0.039 inch

Figure 45. Graph. ASTM C1018 load-deflection response results for untreated 51- by 51-mm (2- by 2-inch) prisms over a 381-mm (15-inch) span with 76 mm (3 inches) between loads.

62

1 kN = 0.225 kip, 1 mm = 0.039 inch

Figure 46. Graph. ASTM C1018 load-deflection response results for tempered steam-treated 51- by 51-mm (2- by 2-inch) prisms over a 381-mm (15-inch) span with 76 mm (3 inches) between loads.

1 kN = 0.225 kip
1 mm = 0.039 inch

Figure 47. Graph. ASTM C1018 load-deflection response results for delayed steam-treated 51- by 51-mm (2- by 2-inch) prisms over a 381-mm (15-inch) span with 76 mm (3 inches) between loads.

3.4.1.1 Strength

The procedure implemented for the ASTM C1018 prism flexure tests allowed for accurate recording of the flexural behavior of UHPC from initial elastic behavior, through tensile cracking, to tensile fiber pullout. The strength-based results from these tests are presented in table 16. The table provides the averaged results from the prisms in each set. The first and most important result from these tests is behavior at first cracking of the UHPC matrix. As previously discussed, the first crack is an indication of the tensile cracking strength of UHPC. The load, strength, and deflection at first cracking are all listed in the table. The first crack strength is based on the equation in figure 48, which is referenced in ASTM C1018, provided in ASTM C78, and based on mechanics of materials principles assuming pure bending.[22] In the equation, $f_{ct,flexure}$ is the flexural tensile cracking strength, P is the total load applied to the prism, l is the span, b is the width of the prism, and d is the depth. The variable η equals 1.0 for third-point loading and 1.2 for the loading configuration with a 381-mm (15-inch) span and 76 mm (3 inches) between load points. This factor accounts for the difference in the bending moment at midspan on the prism under the differing loading configurations.

$$f_{ct,flexure} = \eta \frac{Pl}{bd^2}$$

Figure 48. Equation. Flexural cracking strength of a concrete prism.

It has been widely observed that the actual tensile cracking strength of concrete, f_{ct}, is overestimated by the tensile cracking strength results of a small-scale flexural test, $f_{ct,flexure}$. Carpinteri and Chiaia summarized extensive amounts of previous research on this topic.[23] They indicated that the overestimation is usually caused by depth and strain gradient effects on the flexural cross section. Chanvillard and Rigaud indicate that the concrete ahead of the crack front tends to microcrack, thus reducing stress concentrations.[24] They performed research on the UHPC that is the subject of this report. Their results indicated that the overestimation of the tensile strength is caused by the fiber reinforcement.

Various correction factors have been suggested to account for this overestimation. The Association Française de Génie Civil (AFGC) *Interim Recommendations for Ultra High Performance Fibre-Reinforced Concretes* recommends the equation in figure 49, which varies depending on the depth of the cross section in millimeters, d, as compared to a reference depth, d_0, of 100 mm (4 inches).[1] Note that this empirical equation is based on experimental data, but it has been verified for UHPC by Chanvillard and Rigaud.[24] The first crack tensile strength results as modified by this correction factor are provided in table 16.

Table 16 also includes results related to the average peak load carried by each set of prisms. The peak load values tended to be between 170 and 200 percent of the cracking load values. The equivalent flexural strength corresponding with the peak load is listed. This strength is based on the equation in figure 48 and substitutes the peak load for the cracking load. This calculation is presented purely for comparative purposes, as this equivalent flexural strength has no physical meaning. At peak loading, the UHPC prism is exhibiting extensive cracking, and its midspan neutral axis no longer resides at mid-depth. Thus, the assumptions of pure bending on a uniform, elastic cross section, which are inherent in this equation, are not met.

$$f_{ct} = f_{ct,flexure} \left(\frac{2.0 \left(\dfrac{d}{d_0} \right)^{0.7}}{1 + 2.0 \left(\dfrac{d}{d_0} \right)^{0.7}} \right)$$

Figure 49. Equation. AFGC correction factor for concrete prism flexural strength.

Finally, this table includes the average effective modulus of elasticity of each set of prisms. The equation in figure 50 provides the relationship between the centerline deflection of a simply supported beam with two point loads and the cross-sectional and material properties of the beam. This equation accounts for both the flexural and shear responses in the beam. In this equation, Δ_{cl} is the centerline deflection, P is the total load applied to the prism, L is the span, a is the shear span, E is the modulus of elasticity, and I is the moment of inertia. In the shear term, A' is the effective shear area (i.e., 80 percent of the cross-sectional area for a prism) and G is the shear modulus. To calculate the shear modulus, it is assumed that the Poisson's ratio of UHPC is 0.18. Manipulation of this equation shows that the modulus of elasticity can be calculated based on the elastic slope of the load-deflection curve and a constant term representing the load configuration and beam cross section.

$$\Delta_{cl} = \frac{Pa}{48EI}(3L^2 - 4a^2) + \frac{Pa}{2GA'}$$

Figure 50. Equation. Centerline deflection of a simply supported prismatic beam.
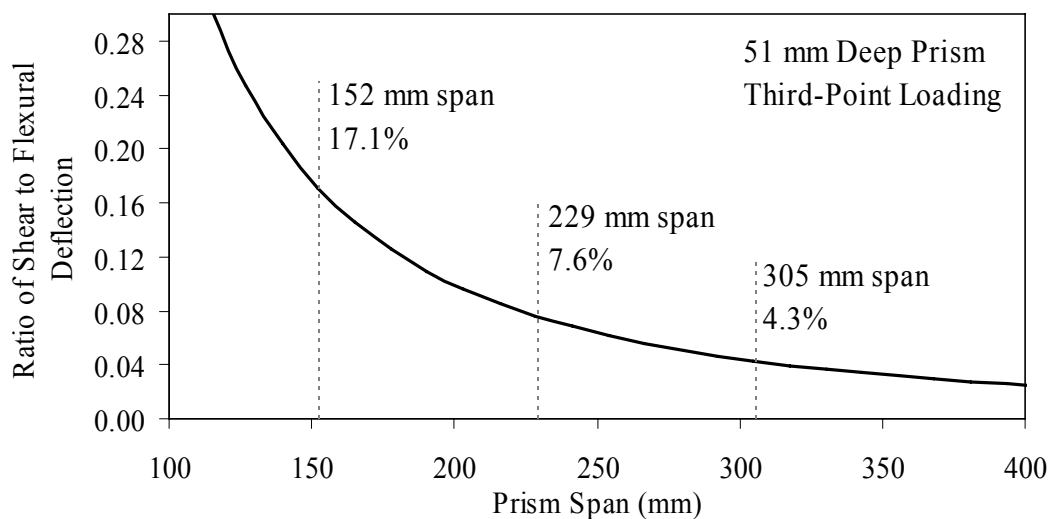
The load-deflection responses presented previously were analyzed to determine the average elastic response between 20 and 50 percent of the load at first cracking. These stiffness values, which are dependent on the test setup, were then used in conjunction with the equation in figure 50 to determine the effective modulus of elasticity. The effective modulus results tend to be higher than those based on the compression tests presented earlier in this chapter. The exception to this tendency is in the prisms where lower modulus values were observed with a span-to-depth ratio of 3.

The lower modulus value in the smaller span-to-depth ratio prisms is likely due to the effects of local disturbed regions near the load application points. With this short span and these close load points, nearly the entire prism could be considered to be locally disturbed, including deformations that could add to the flexure and shear deformations. Any additional deformation would result in a lower calculated effective modulus of elasticity.

Prism flexure testing of five different loading configurations for each curing regime was intended to identify the benefits and detriments of varying the prism span and cross section. From a qualitative standpoint, the easiest completion was of the 229-mm (9-inch) and 305-mm (12-inch) span tests on the 51- by 51-mm (2- by 2-inch) cross section. The behavior of the prisms in these loading configurations was observed to be more consistent than in other configurations. Also in these configurations, the moderate elastic load-displacement response decreased the difficulty encountered with the stiffer and more flexible configurations in the test setups.

Quantitatively, the results from the 229-, 305-, and 381-mm (9-, 12-, and 15-inch) spans for the 51- by 51-mm (2- by 2-inch) cross section prisms were most consistent.

Also, it must be mentioned that the basic intent of the ASTM C1018 test seems to be to create a state of pure bending in a concrete prism to allow for quantification of the tensile properties. As the span-to-depth ratio of the beam decreases, the proportion of the behavior that is shear based increases. Figure 51 shows the ratio of the shear to flexural deflection of a 51-mm (2-inch)-deep prism. This prism was assumed to be loaded at its third points, and it has a shear modulus equal to 61 percent of its elastic modulus based on a Poisson's ratio of 0.18. With a span-to-depth ratio of 3, the shear deflections are 17.1 percent of the flexural deflections, thus the assumption of flexural behavior is questionable. As the span increases toward 305 mm (12 inches), the assumption of flexural behavior becomes much more reasonable. In the longer spans, the state of stress on the cross section in the constant moment region is primarily composed of stresses normal to the face of the cross section. However, the same does not hold true for the shorter spans and the more influential shear forces.

1 mm = 0.039 inch

Figure 51. Graph. Ratio of shear to flexural deflection for a third-point loaded prism.

Table 16. ASTM C1018 strength results.

	Prism Cross Section and Setup[*]	No.	First Crack Deflection (mm)	First Crack Strength[†] (MPa)	Corrected First Crack Strength[‡] (MPa)	Modulus of Elasticity[§] (GPa)	Peak Load Deflection (mm)	Peak Load Equivalent Strength[†] (MPa)
Steam	51x51, 152, 51	3	0.044	18.6	10.3	51.1	0.503	32.3
	76x102, 305, 102	3	0.083	17.5	10.9	60.5	1.055	26.5
	51x51, 229, 76	3	0.069	17.7	9.9	59.8	0.761	31.7
	51x51, 305, 102	4	0.117	16.7	9.2	58.9	1.858	35.4
	51x51, 381, 76	4	0.156	15.9	8.8	59.0	3.174	35.9
Untreated	51x51, 152, 51	4	0.039	16.2	9.0	47.7	0.532	29.4
	76x102, 305, 102	3	0.092	15.6	9.7	49.8	1.083	28.1
	51x51, 229, 76	3	0.074	15.9	8.8	52.3	1.088	30.3
	51x51, 305, 102	4	0.134	15.9	8.8	49.3	1.528	29.9
	51x51, 381, 76	4	0.193	16.8	9.3	50.7	2.216	30.3
Tempered Steam	51x51, 152, 51	4	0.041	19.6	10.8	54.0	0.486	34.0
	76x102, 305, 102	3	0.075	14.6	9.1	56.4	0.855	28.8
	51x51, 229, 76	4	0.076	17.7	9.9	55.5	0.990	34.5
	51x51, 305, 102	4	0.131	18.2	10.1	56.3	1.265	30.5
	51x51, 381, 76	2	0.185	18.2	10.1	56.1	1.933	33.6
Delayed Steam	51x51, 152, 51	4	0.040	17.2	9.6	56.1	0.486	32.0
	76x102, 305, 102	3	0.107	17.7	11.0	58.4	0.918	31.6
	51x51, 229, 76	4	0.069	16.1	9.0	55.6	0.779	30.7
	51x51, 305, 102	4	0.138	16.9	9.4	55.8	1.721	34.3
	51x51, 381, 76	4	0.167	16.1	8.9	56.1	2.240	32.6

* Prism depth x width, span length, distance between upper load points

† Calculated using equation in figure 48, which assumes pure bending on a uniform, elastic, uncracked cross section

‡ Calculated using equation in figure 49

§ Calculated using equation in figure 50, which allows for bending and shear on a uniform, elastic, uncracked cross section

1 MPa = 145 psi, 1 GPa = 145,000 psi, 1 mm = 0.039 inch

3.4.1.2 Toughness

Within concrete materials characterization testing, toughness is a term that provides some indication of the concrete's energy absorption capability. Usually, toughness is quantified in terms of the area under a load-deflection response curve. Toughness values are specific to the testing procedure implemented.

The ASTM C1018 test method presents one means of determining the toughness of fiber-reinforced concrete. The test results are analyzed in terms of the area under the load-deflection curve up to specific deflection levels. The toughness results are then normalized by dividing the total area under the curve up to the specified deflection by the area under the curve up to the deflection at first cracking.

ASTM C1018 defines a set of toughness indices in terms of the behavior that might be expected from a material that exhibits an elastic-plastic, flexural, load-deflection response. (Although not clearly stated in the test method, note that this reference response does not correspond to the response that would be observed for a material that exhibits elastic-plastic uniaxial stress-strain behavior.) Table 17 is reproduced from the appendix of the test method. The table provides basic information relating to the calculation of toughness indices and the expected results from various materials. Additional indices can be created in a similar fashion. Results for I_{30} and I_{40} are also presented in the following discussion.

Table 17. Definition of toughness indices (from ASTM C1018 FIG. X1.1).

Index Designation	Deflection Criterion[*]	Values of Toughness Indices		
		Plain Concrete	Elastic-Plastic Material[†]	Observed Range for Fibrous Concrete
I_5	3.0δ	1.0	5.0	1 to 6
I_{10}	5.5δ	1.0	10.0	1 to 12
I_{20}	10.5δ	1.0	20.0	1 to 25

* δ is the deflection at first cracking.
† This refers to a material that exhibits an elastic-plastic flexural response.

Table 18 presents the toughness results for the sets of prismatic flexural tests. The information layout in the table is similar to table 16. Note that some results are missing for I_{40}. In addition, some other results for I_{40} are from fewer than the total number of prisms listed. This is due to some prisms exhibiting fiber pullout and subsequent failure prior to reaching 20.5 times the cracking deflection. Figures 52 through 55 graphically present the toughness results from the four curing regimes. All of these results show increasing toughness through I_{40}.

Table 18. ASTM C1018 toughness results.

	Prism Cross Section and Setup[*]	No.	First Crack Deflection (mm)	First Crack Strength[†] (MPa)	Toughness Index					Residual Strength Index			
					I_5	I_{10}	I_{20}	I_{30}	I_{40}	$R_{5,10}$	$R_{10,20}$	$R_{20,30}$	$R_{30,40}$
Steam	51x51, 152, 51	3	0.044	10.3	5.6	12.5	28.3	44.2	62.8	138	158	159	172
	76x102, 305, 102	3	0.083	10.9	5.3	11.8	25.9	40.6	54.4	129	141	147	138
	51x51, 229, 76	3	0.069	9.9	5.6	12.7	28.7	45.3	60.6	143	160	166	153
	51x51, 305, 102	4	0.117	9.2	6.2	14.4	32.8	53.0	77.4	165	183	202	218
	51x51, 381, 76	4	0.156	8.8	5.8	13.9	32.0	51.6	72.6	162	180	197	210
Untreated	51x51, 152, 51	4	0.039	9.0	5.7	12.9	29.0	46.3	63.0	144	161	173	167
	76x102, 305, 102	3	0.092	9.7	5.7	12.8	28.5	45.0	59.9	142	158	165	148
	51x51, 229, 76	3	0.074	8.8	5.7	13.1	29.5	46.8	64.2	147	165	173	174
	51x51, 305, 102	4	0.134	8.8	5.6	12.8	28.8	48.3	65.5	143	160	179	171
	51x51, 381, 76	4	0.193	9.3	5.8	13.1	28.7	50.1	67.6	147	156	189	186
Tempered Steam	51x51, 152, 51	4	0.041	10.8	5.8	12.9	28.2	44.2	65.5	141	153	160	176
	76x102, 305, 102	3	0.075	9.1	6.1	14.1	31.9	53.7	73.0	161	178	201	193
	51x51, 229, 76	4	0.076	9.9	6.0	13.8	31.1	50.8	69.6	155	173	194	188
	51x51, 305, 102	4	0.131	10.1	5.8	13.0	28.0	43.1	–	144	150	151	–
	51x51, 381, 76	2	0.185	10.1	6.1	13.9	31.1	47.6	–	156	172	165	–
Delayed Steam	51x51, 152, 51	4	0.040	9.6	5.5	12.6	28.5	43.2	63.7	143	159	157	169
	76x102, 305, 102	3	0.107	11.0	5.5	12.4	27.6	46.7	61.0	138	151	167	143
	51x51, 229, 76	4	0.069	9.0	5.8	13.5	30.9	48.9	65.6	153	175	180	167
	51x51, 305, 102	4	0.138	9.4	5.8	13.4	30.3	48.3	61.7	152	169	180	146
	51x51, 381, 76	4	0.167	8.9	6.0	14.1	32.2	50.8	74.6	162	181	186	193

* Prism depth x width, span length, distance between upper load points
† Corrected tensile cracking strength based on the equation in figure 49
1 mm = 0.039 inch, 1 MPa = 145 psi

69
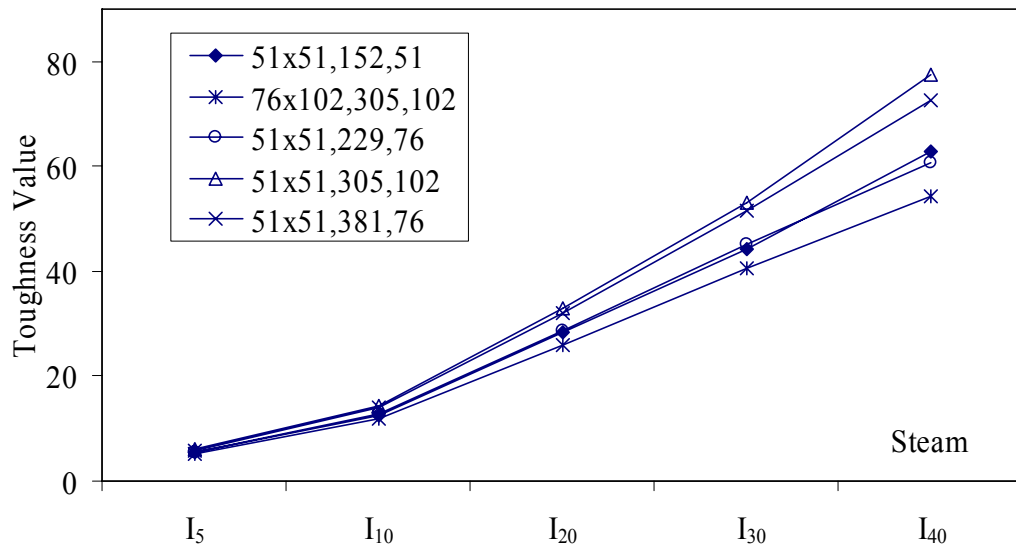
Figure 52. Graph. ASTM C1018 toughness results for steam-treated UHPC prisms.
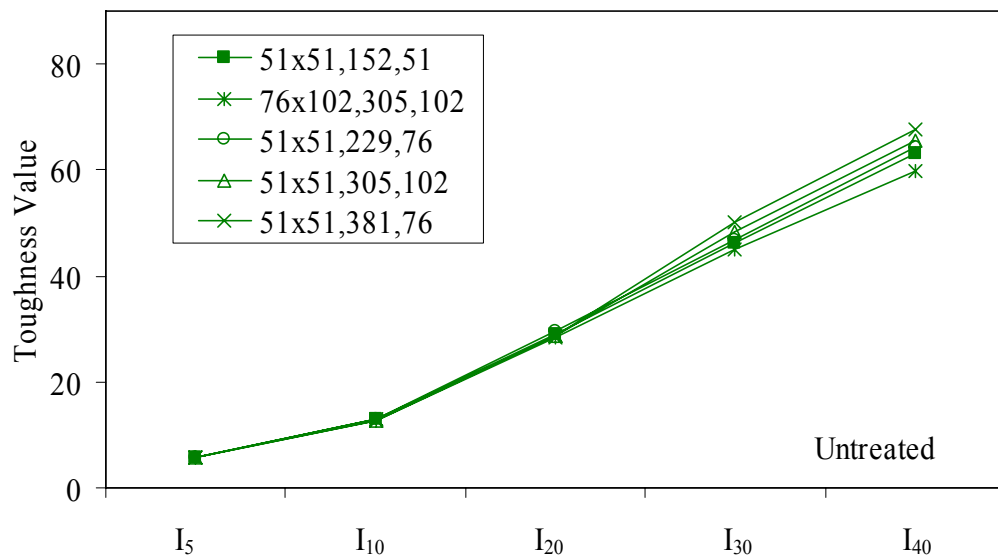
Figure 53. Graph. ASTM C1018 toughness results for untreated UHPC prisms.

70
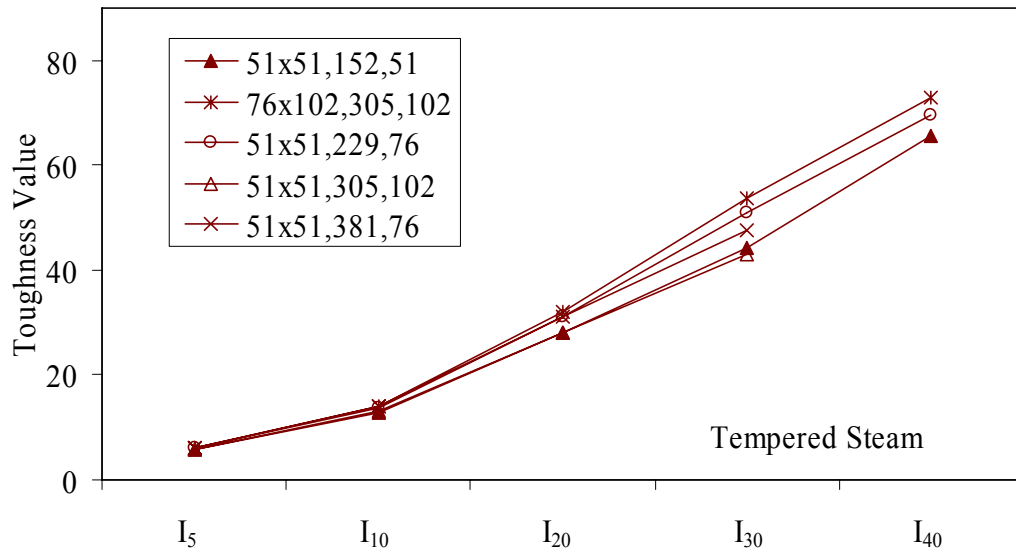
Figure 54. Graph. ASTM C1018 toughness results for tempered steam-treated UHPC prisms.
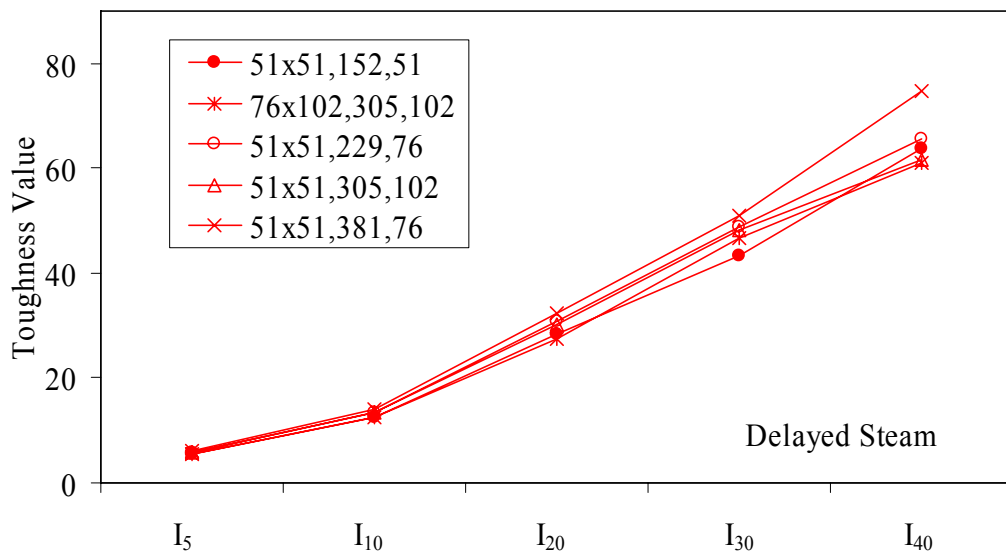
Figure 55. Graph. ASTM C1018 toughness results for delayed steam-treated UHPC prisms.

71
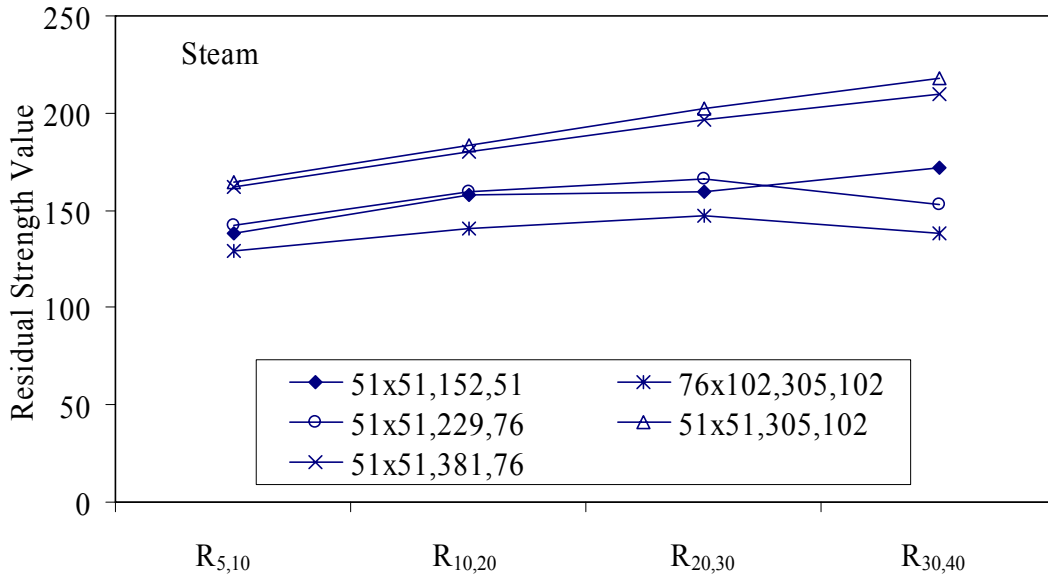
Figure 56. Graph. ASTM C1018 residual strength results for steam-treated prisms.
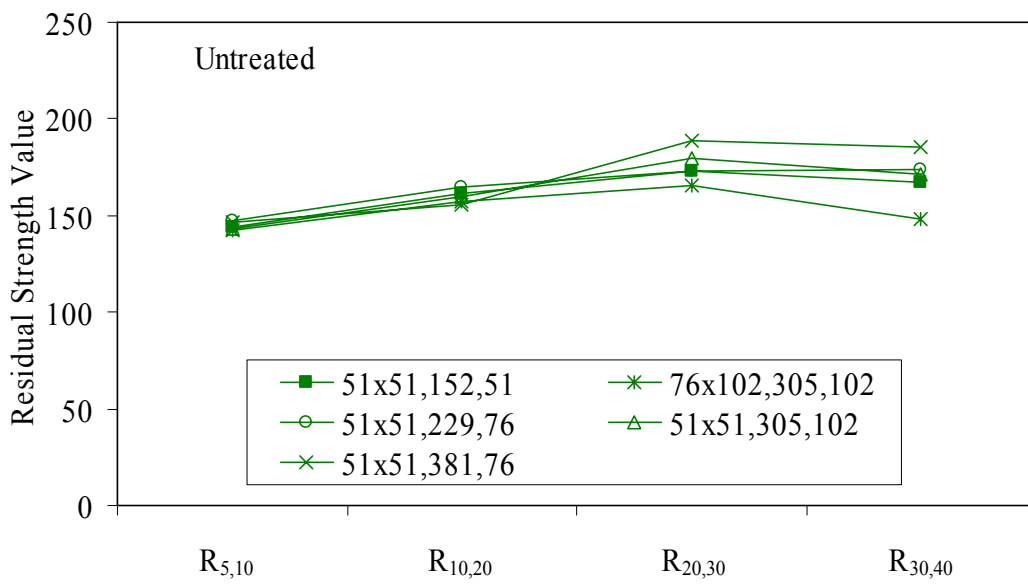
Figure 57. Graph. ASTM C1018 residual strength results for untreated prisms.
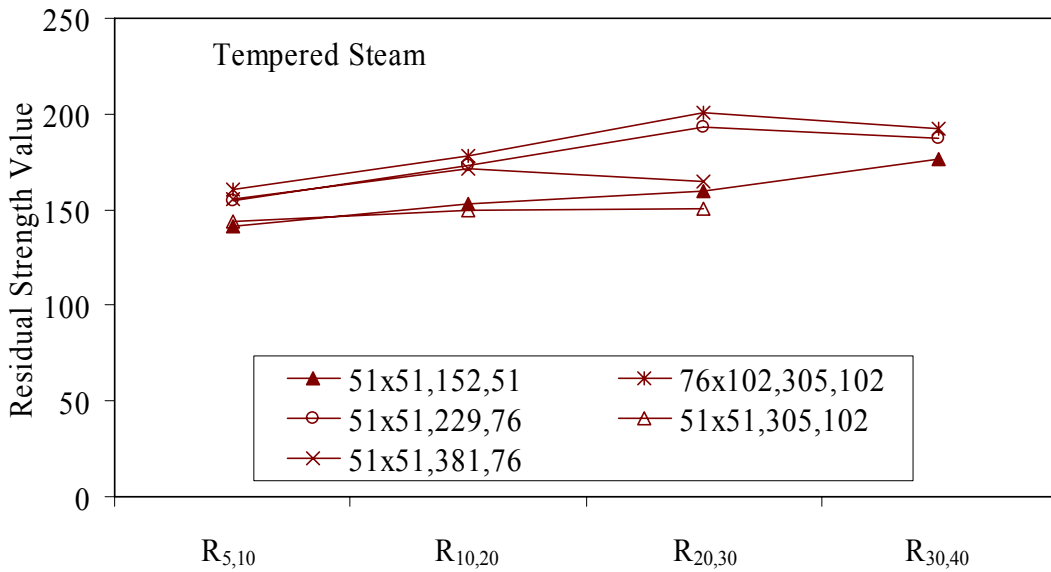
Figure 58. Graph. ASTM C1018 residual strength results for tempered steam-treated prisms.
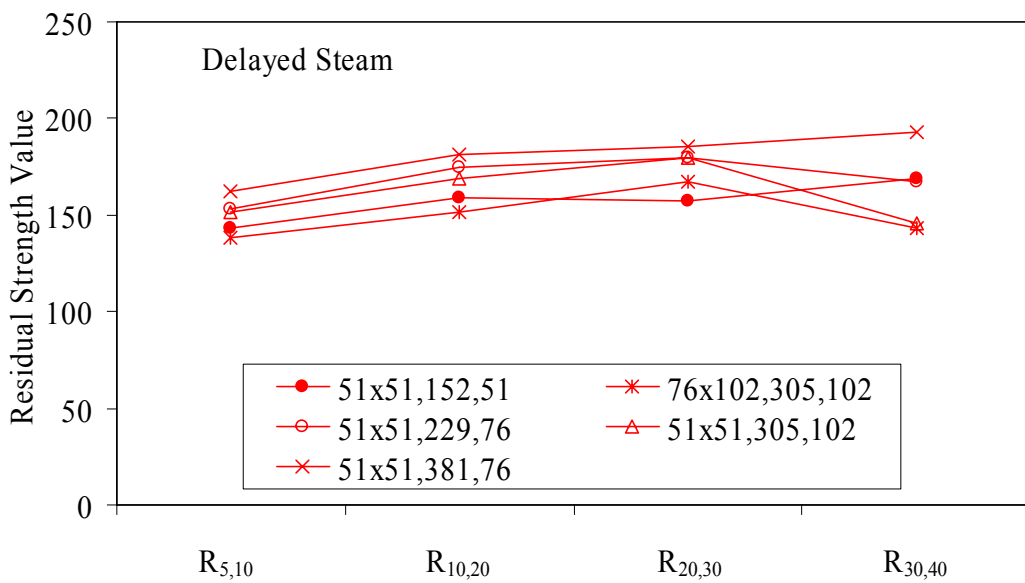
Figure 59. Graph. ASTM C1018 residual strength results for delayed steam-treated prisms.

73

Residual strength factors also are presented in table 18. These values are calculated by subtracting one toughness index from a subsequent index then multiplying the result by a normalizing factor related to the idealized elastic-plastic, flexural response. Regardless of the toughness indices chosen, the residual strength factor for the idealized elastic-plastic, flexural material will equal 100. For example, the residual strength factor, $R_{10,20}$, equals $10(I_{20}-I_{10})$.

The toughness exhibited by the UHPC is quite impressive, regardless of the curing regime or test configuration. The results all tend to be at the upper end or above the ASTM C1018 predicted range for toughness of fiber-reinforced concrete. The UHPC also exhibits residual strength values that tend to increase at least through I_{30}, and these values through this deflection level are all above the 100 reference level for elastic-plastic flexural behavior. Figures 56 through 59 provide a graphical representation of the residual strength factors.

3.4.2 Split Cylinder

The tensile strength of UHPC was also measured through the ASTM C496 *Standard Test Method for Splitting Tensile Strength of Cylindrical Concrete Specimens.*[25] This test, often referred to as the split-cylinder test, indirectly measures the tensile strength of concrete by compressing a cylinder through a line load applied along its length. This test can be completed in a standard concrete compression testing machine, with only one special requirement: the hinged bearing that loads the specimen.

This load configuration creates a lateral tensile stress in the cylinder across the vertical plane of loading. A relatively uniform tensile stress field is created over the middle 75 percent of the cylinder's diameter along the plane of loading, and the maximum tensile stress occurs at the center of the cylinder. ASTM C496 indicates that the maximum tensile stress can be calculated based on the equation in figure 60. In this equation, P is the load applied to the cylinder, l and d are the length and diameter, and f_θ is the tensile stress.

$$f_\theta = \frac{2P}{\pi l d}$$

Figure 60. Equation. Tensile stress in an ASTM C496 split-cylinder test.

The split-cylinder test does not determine the uniaxial tensile cracking strength of concrete. The loading configuration used in this test actually creates a biaxial stress state inside the cylinder that has been described many times.[26,27] For the purposes of this report, it is sufficient to indicate that the vertical compressive stress in the center of the cylinder is approximately three times the lateral tensile stress.

This test is normally completed on standard concrete that does not contain fiber reinforcement. As such, the tensile strength results are normally clear. The cylinder will fail when its tensile strength is reached; therefore, the peak load carried by the cylinder can be used to determine the splitting tensile strength through the equation in figure 60. Fiber-reinforced concrete, and in particular UHPC, tends to behave differently. In these concretes, the initiation of cracking signifies the beginning of a new phase in the material's behavior, but does not signify failure of the material. With UHPC in particular, the load will continue to increase after cracking, and the

cracks that form during cracking will be so small that identification without microscopic investigation may not be possible.

A supplemental feature was added to the ASTM 496 test because the cracking strength is the material property of interest. As the UHPC cylinder cracks, the measured length of the lateral diameter of the cylinder will show a marked increase. A lateral expansion measuring apparatus was devised and is shown in figure 61. This spring-loaded device clamps across the cylinder and measures the lateral expansion of the cylinder from load initiation through failure. The small lateral compressive force exerted by the apparatus on the specimen (less than 0.02 MPa (2 psi)) is considered negligible. Two LVDTs located near the front and back of the cylinder electronically capture the displacements, which are sent to a data acquisition system along with the load. This lateral expansion measuring apparatus is similar to a device used by Nanni in work that he completed on fiber-reinforced concrete.[28]

The typical load versus lateral displacement response for a UHPC cylinder is presented in figure 62. The curve shown is the average of the results from the two LVDTs. The lateral deflection behavior is basically linear until the UHPC cracks. At cracking, a discontinuity occurs in the displacement response while the load level remains relatively constant. The total jump in displacement is usually less than 0.025 mm (0.001 inch) and could be nonexistent in a specimen that has not undergone a steam-based treatment. After cracking, a clear change occurs in the slope of the response curve. The load then continues to increase at a decreasing rate until the peak load is reached.

Normal UHPC mix design and casting procedures were used for this series of tests. Twelve 4-inch diameter cylinders were cast for each curing regime. The screeded end of the cylinder was ground prior to testing, and the length of each cylinder was approximately 200 mm (7.9 inches). The cylinders were tested in groups of four at three different ages for each curing regime. The steam, untreated, and tempered steam regimes were tested at 5, 14, and 28 days after casting. The delayed steam regime was tested at 14, 21, and 28 days after casting. At 14 days, the delayed steam specimen results are more comparable to the untreated specimens than to the other delayed steam treated specimens, because the steam treatment did not occur until days 15 through 17.

The initial load rate for these tests was set at 3.4 MPa/min (500 psi/min) of tensile stress according to the equation in figure 60. The rate was set above the ASTM specified rate of 0.7 to 1.4 MPa/min (100 to 200 psi/min) because of three reasons: (1) the higher tensile cracking strength of the UHPC, (2) the significant displacement that must be traversed before the peak load is reached, and (3) the reluctance to change the load rate after test initiation. Preliminary testing on UHPC prior to the initiation of these tests indicated that this increased load rate should not cause significant changes in material behaviors.

Figure 63 presents the average tensile cracking results from the split-cylinder tests. As previously mentioned, cracking is defined to occur when an abrupt or semiabrupt change in specimen lateral stiffness occurs. The number of days after casting is indicated in parentheses after the curing regime's name. The figure shows both the average stress and the ±1 standard deviation from the average.
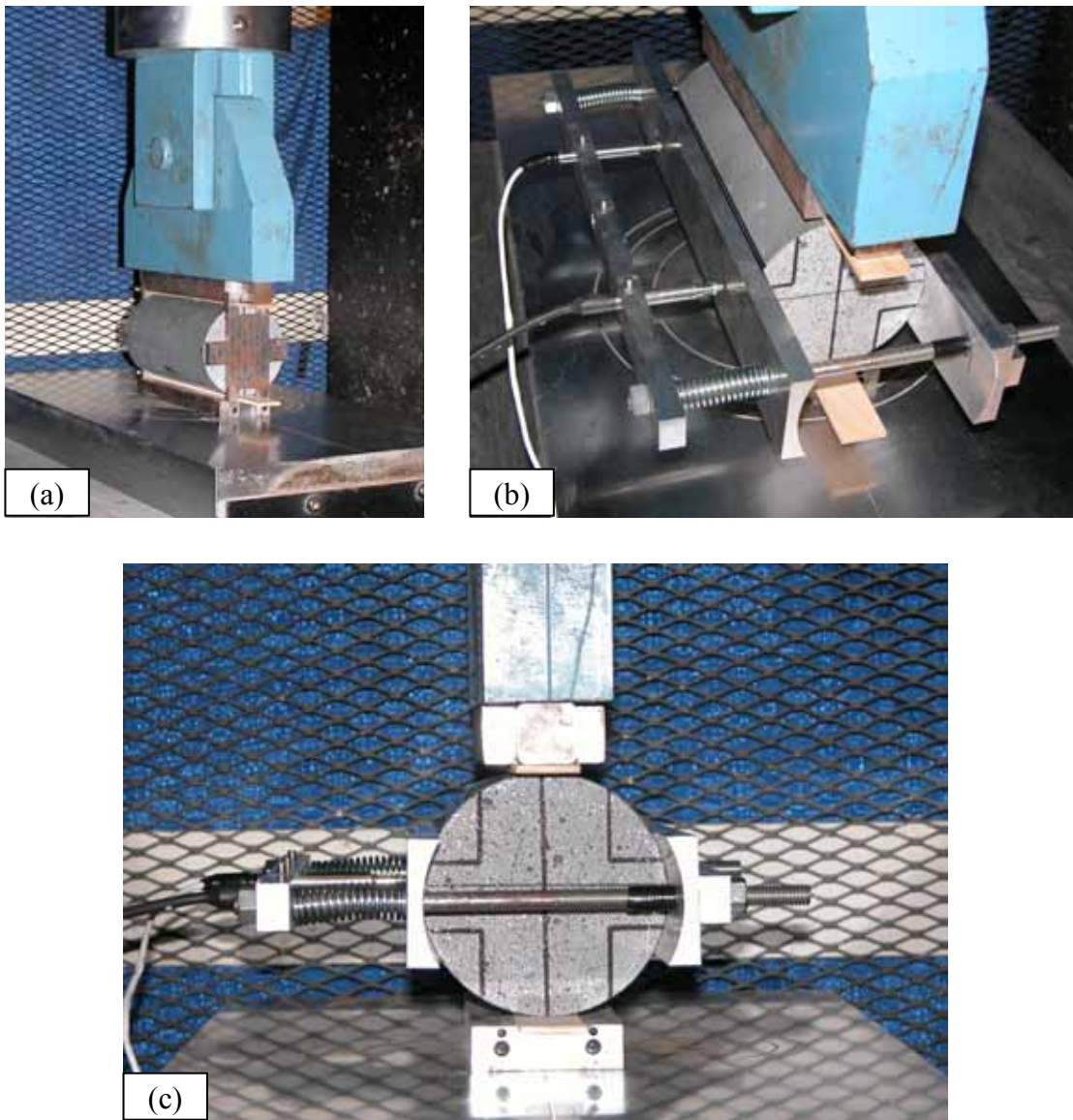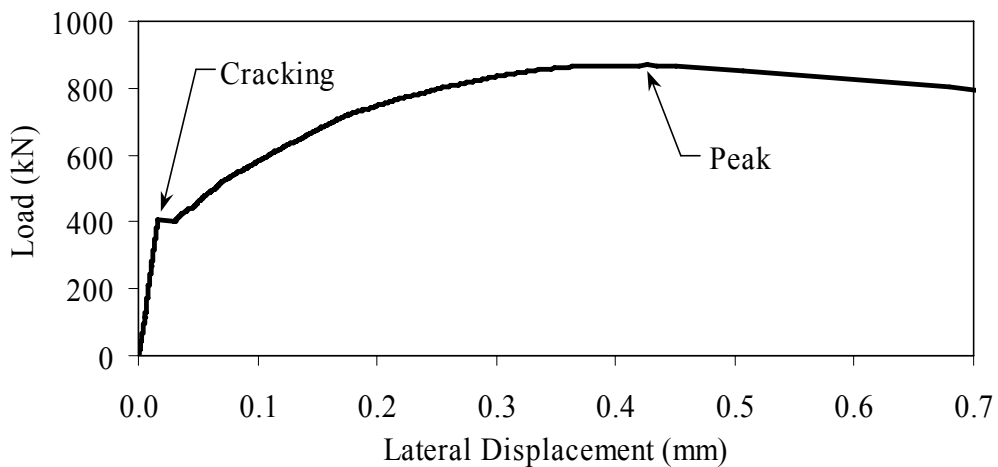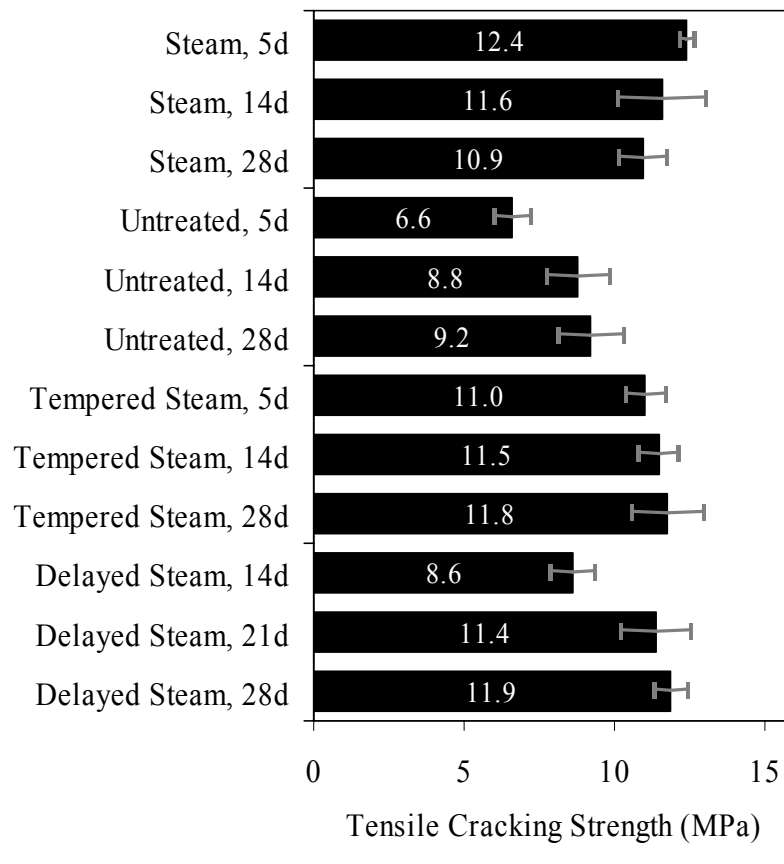
Figure 61. Photos. Split-cylinder tensile test including (a) standard test setup, (b) lateral expansion measuring apparatus, and (c) UHPC cylinder during test.

All of the groups that underwent a steam-based curing regime exhibited a split-cylinder tensile cracking strength of between 11.0 and 12.4 MPa (1.6 and 1.8 ksi). The untreated group exhibited decidedly lower strength values, along with a clear increase in strength over time. At 5 days, the untreated group had a tensile cracking strength of 6.9 MPa (1.0 ksi), and by 28 days this strength had increased to over 9.0 MPa (1.3 ksi).

1 kN = 0.225 kip
1 mm = 0.039 inch

Figure 62. Graph. Typical response for a UHPC cylinder during the ASTM C496 test.
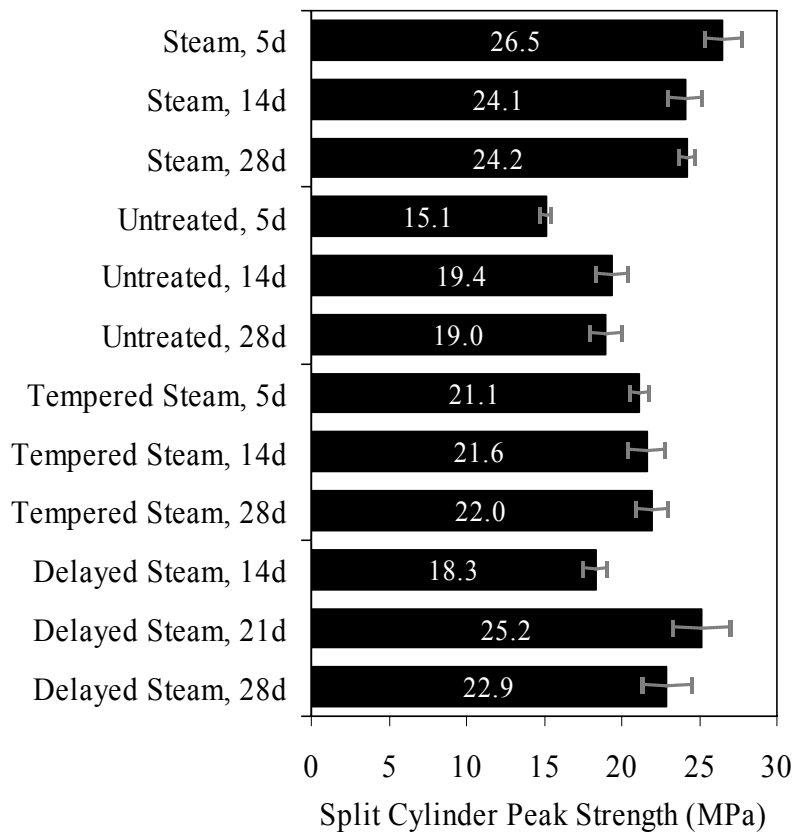
1 MPa = 145 psi

Figure 63. Chart. Average tensile cracking results from the ASTM C496 test.

The split-cylinder loading configuration causes vertical compressive stress and lateral tensile stress in the cylinder. This biaxial stress state has a definite effect on the postcracking behavior. The vertical compressive stresses that are parallel to any cracks cause the fiber reinforcement bridging the cracks to carry higher loads prior to pulling out of the UHPC matrix. For this reason, results derived from the peak load carried by a cylinder and passed through the equation in figure 60 are not accurate general representations of the tensile strength of UHPC.

However, these peak load results may be useful for comparing fiber pullout behavior following different curing treatments. These variations in peak load results may be useful in determining whether curing was properly applied to a UHPC specimen. The average peak stress carried by these groups of specimens is presented in figure 64. This stress is calculated based on both the peak load reached and the equation in figure 60. The results show that fibers in untreated cylinders pull out earlier under this stress state, and the cylinder as a whole can only carry an equivalent stress of around 19.3 MPa (2.8 ksi). The steam treatment in the tempered steam regime enhances the behavior such that 21.4 MPa (3.1 ksi) of equivalent stress can be carried. The steam and delayed steam regimes carried the largest peak loads with average equivalent stresses of around 24.1 MPa (3.5 ksi).

1 MPa = 145 psi

Figure 64. Chart. Average split cylinder peak strength from the ASTM C496 test.

Frequently, the tensile strength of concrete is discussed as a percentage of the compressive strength. The results from the split cylinder tests have been normalized by the 28-day compressive strength of their control cylinders and are presented in table 19. Only the post-curing treatment results are presented, because only the 28-day compressive strengths are known for these particular batches of UHPC. The cracking stress tends to be between 5 and 7 percent of the compressive strength. The equivalent peak stress carried by the cylinders is higher, with values ranging from 12 to 16 percent.

The cracking behavior must be monitored for the ASTM C496 test to provide useful results in terms of tensile cracking strength. The lateral expansion measuring apparatus (described above) allowed for quantification of this cracking behavior. Monitoring of the cracking behavior may also be possible in certain instances via audible observations. Table 20 presents the first crack parameters for each group of specimens. Aural monitoring throughout the test allowed the load at first cracking to be estimated in nearly all of the cylinders that had undergone a steam-based curing treatment. As discussed previously, the data collection during the test allowed for a specific determination of the load at first crack. The size of the first crack was also estimated based on the instantaneous lateral expansion of the cylinder at first cracking. The values presented in the table are the crack size (measured by the front or back LVDT, whichever displayed a larger instantaneous increase). These results provide a clear sense of the width of UHPC tensile stress cracks when they first occur as well as the type of instrumentation that is required to monitor or capture this behavior.

Table 19. Split tensile strength normalized by 28-day compressive strength.

Group	28-day Compression Strength (ksi)	Normalized by 28-day Compressive Strength	
		ASTM C496 Cracking Stress	ASTM C496 Peak Stress
Steam (5)	181	0.051	0.148
Steam (14)	181	0.064	0.132
Steam (28)	181	0.060	0.134
Untreated (28)	121	0.076	0.161
Tempered Steam (5)	168	0.066	0.125
Tempered Steam (14)	168	0.068	0.127
Tempered Steam (28)	168	0.070	0.133
Delayed Steam (21)	170	0.067	0.147
Delayed Steam (28)	170	0.070	0.133

1 ksi = 6.895 MPa

Table 20. First-crack parameters determined by instantaneous lateral expansion of cylinder and aural observations.

Group	Sound (Audible/Inaudible)	First Crack Size (mm)		
		Average	Minimum	Maximum
Steam (5)	Audible	0.0211	0.0170	0.0249
Steam (14)	Audible	0.0221	0.0127	0.0290
Steam (28)	Audible	0.0236	0.0157	0.0391
Untreated (5)	Inaudible	0.0079	0.0038	0.0122
Untreated (14)	Inaudible	0.0091	0.0000	0.0216
Untreated (28)	Inaudible	0.0180	0.0071	0.0277
Tempered Steam (5)	Audible	0.0206	0.0163	0.0257
Tempered Steam (14)	Audible	0.0178	0.0084	0.0371
Tempered Steam (28)	Audible	0.0193	0.0150	0.0279
Delayed Steam (14)	Inaudible	0.0147	0.0066	0.0216
Delayed Steam (21)	Audible	0.0180	0.0086	0.0236
Delayed Steam (28)	Audible	0.0084	0.0008	0.0185

1 mm = 0.039 inch

3.4.3 Mortar Briquette

Another means of concrete tensile strength determination is the briquette tension test. This test method, described in AASHTO T132, normally involves the direct tension testing of a small briquette cast from cement mortar.[29] The dogbone-shaped briquette is 76 mm (3 inches) long, 25 mm (1 inch) thick, and has a 645-mm^2 (1-inch^2) cross section at midlength. Special self-aligning grips allow for passive gripping of the specimen in the test machine and ensure uniform loading.

The standard UHPC mix was used, including the steel fibers, in this test program. The casting of the briquettes is assumed to have caused some preferential alignment of the fibers because the minimum cross section of the briquette is only 645 mm^2 (1 inch^2). This preferential alignment would be expected to be parallel to the walls of the mold; therefore, the fiber percentage aligned across the anticipated failure plane would be higher than normal.

The normal UHPC mix design and casting procedures were used. Eighteen briquettes were cast for each of the four curing regimes: three sets of six briquettes that were tested at 28, 56, and 84 days after casting. Figure 65 shows both the grips that were used to test the briquettes as well as a briquette in the grips.

The testing was completed in a 98-kN (22-kip) capacity MTS testing machine. The tests were controlled based on the displacement of the crosshead of the testing machine to enable the observation of the post-peak load-displacement response. AASHTO T132 recommends loading the briquettes at 2.7 kN/min (600 lb/min). This portion of the test method was modified, and the tests were conducted at a displacement rate of 0.025 mm/s (0.001 inch/s). Given the stiffness of the load carrying apparatus between the crossheads, this displacement rate equates to

approximately 4.0 kN/min (900 lb/min) throughout the initial elastic loading portion of each briquette's response.
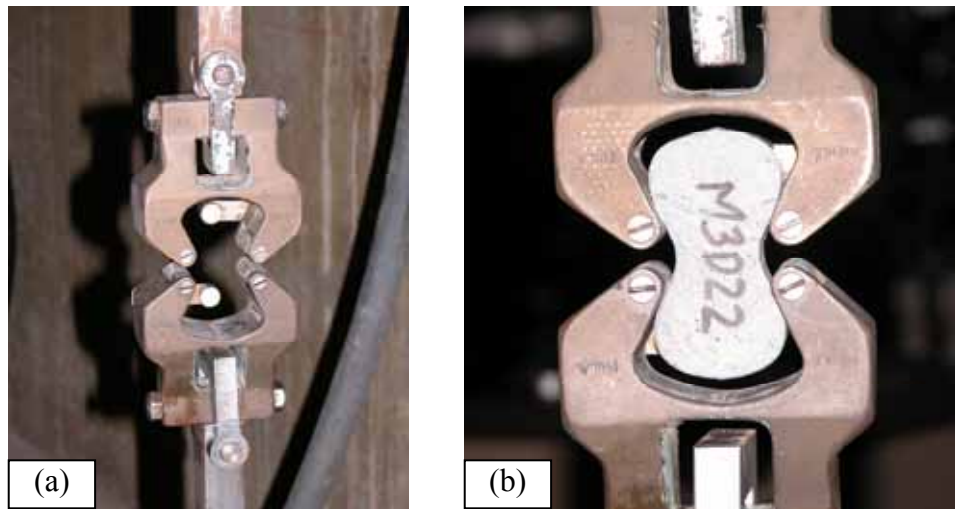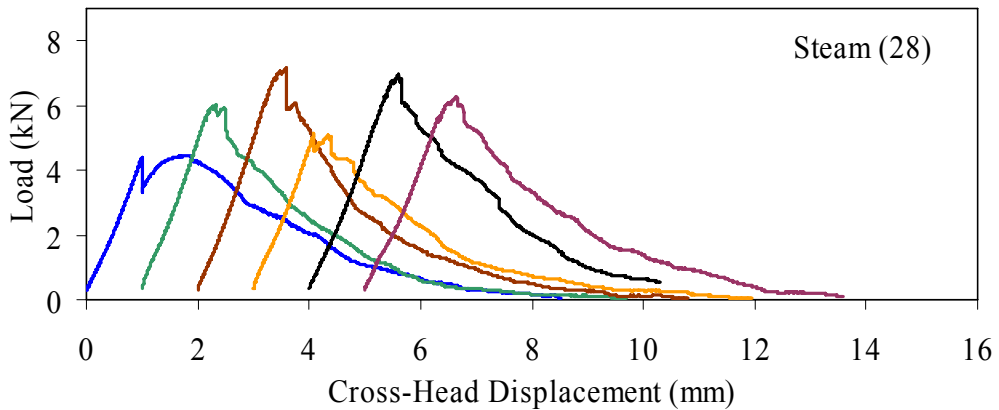
Figure 65. Photos. AASHTO T132 setup including (a) test grips and (b) specimen.
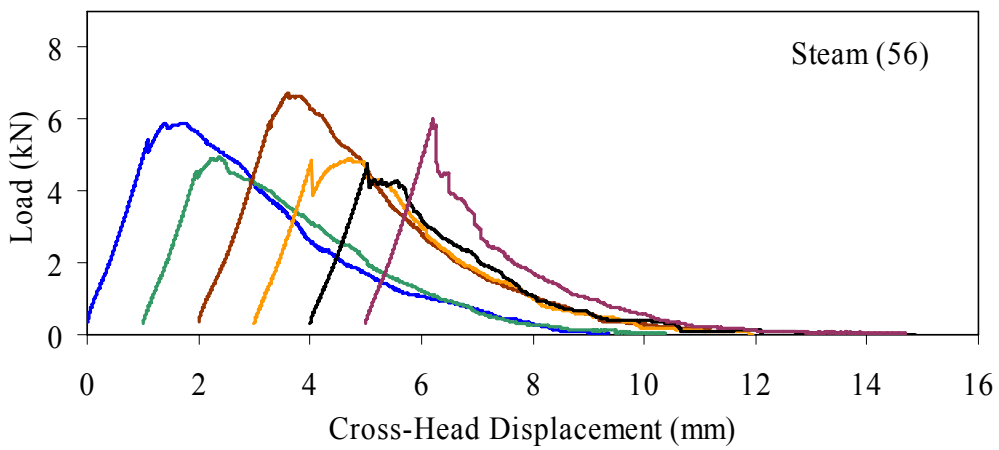
Figures 66 through 77 present the results from the 18 tests for each curing regime. Six replicates are included in each plot, with the results shifted by 1 mm (0.039 inch) to allow for clarity. The curing regime and age (in days) at testing are included in the upper right corner of each plot. These results show that the UHPC behaved linear-elastically up to first cracking. After cracking, a slight decrease in load usually occurred followed by a load increase to a level near or above the cracking load. All of the results show a significant amount of postcracking load-carrying capacity. A more detailed discussion of these test results that focuses on strength and toughness is included in the following two sections.

Similar to all batches of UHPC cast for this research program, compression tests on 7.62-cm (3-inch) diameter control cylinders were completed. The results from the control cylinders for the four batches associated with the briquette testing indicate that three of these batches exhibited strengths below the average values. The steam-treated and untreated batches showed compressive strengths 15 percent below the overall test program average, and the delayed steam-treated batch was 8 percent below the average. These results should be kept in mind as the results in the remainder of this section are discussed.
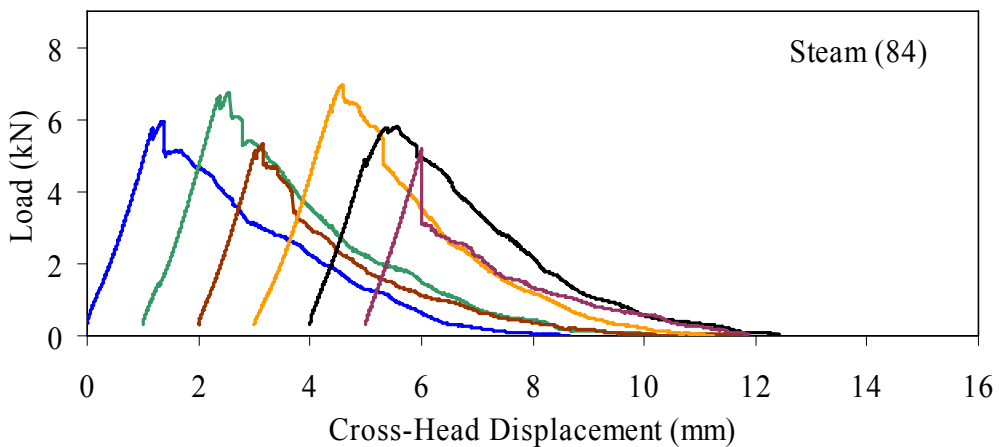
1 kN = 0.225 kıp, 1 mm = 0.039 ınch

Figure 66. Graph. Load-displacement response for steam-treated briquettes (28 days).
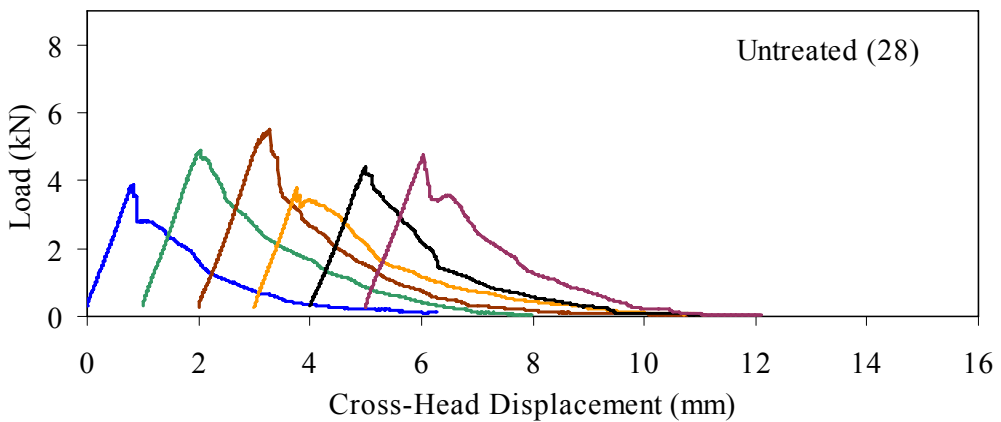
1 kN = 0.225 kip, 1 mm = 0.039 inch

Figure 67. Graph. Load-displacement response for steam-treated briquettes (56 days).
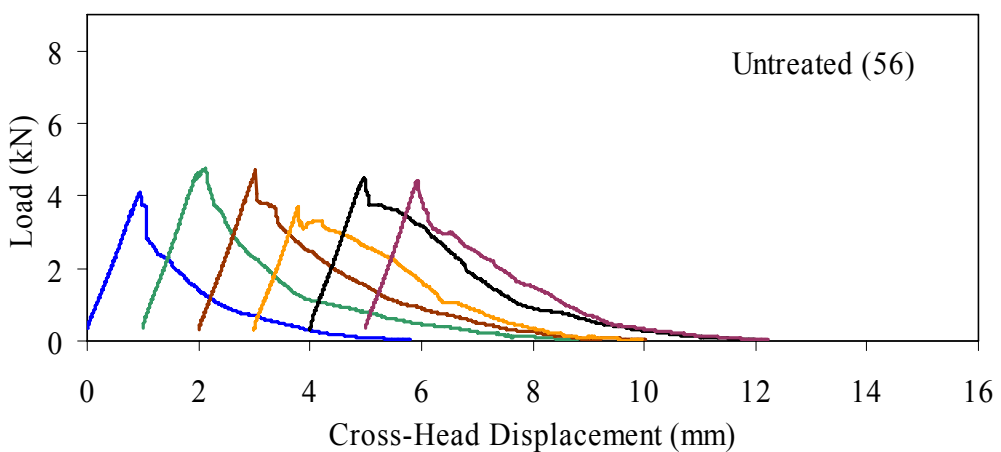
1 kN = 0.225 kip, 1 mm = 0.039 inch

Figure 68. Graph. Load-displacement response for steam-treated briquettes (84 days).
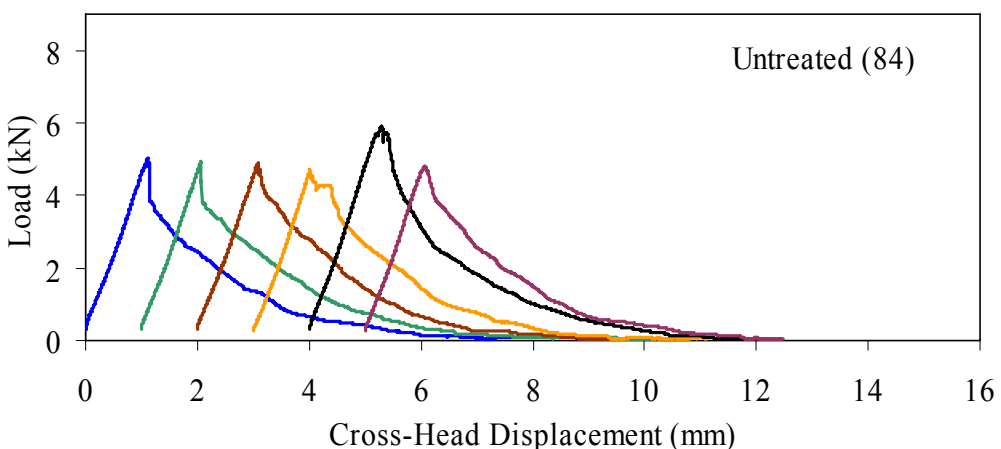
1 kN = 0.225 kip, 1 mm = 0.039 inch

Figure 69. Graph. Load-displacement response for untreated briquettes (28 days).
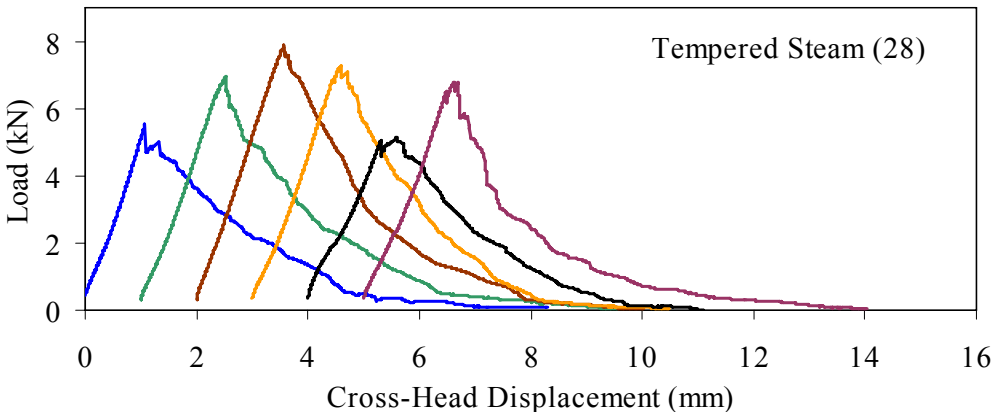
1 kN = 0.225 kip, 1 mm = 0.039 inch

Figure 70. Graph. Load-displacement response for untreated briquettes (56 days).
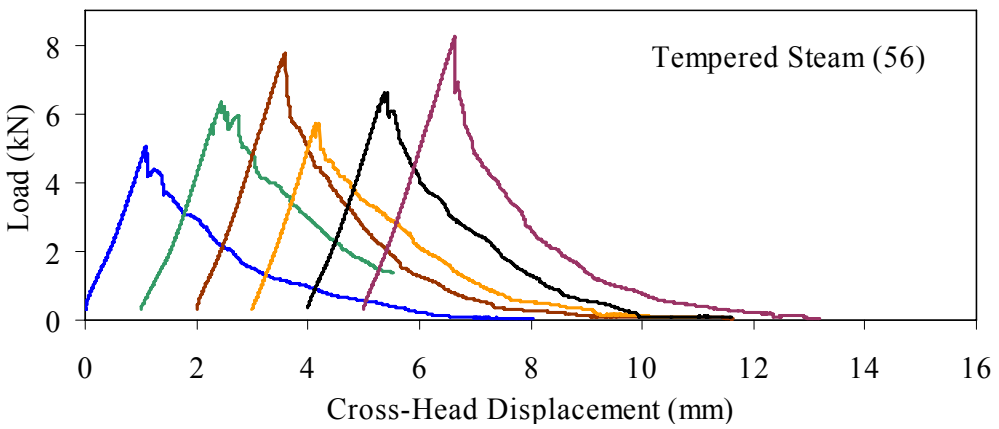
1 kN = 0.225 kip, 1 mm = 0.039 inch

Figure 71. Graph. Load-displacement response for untreated briquettes (84 days).
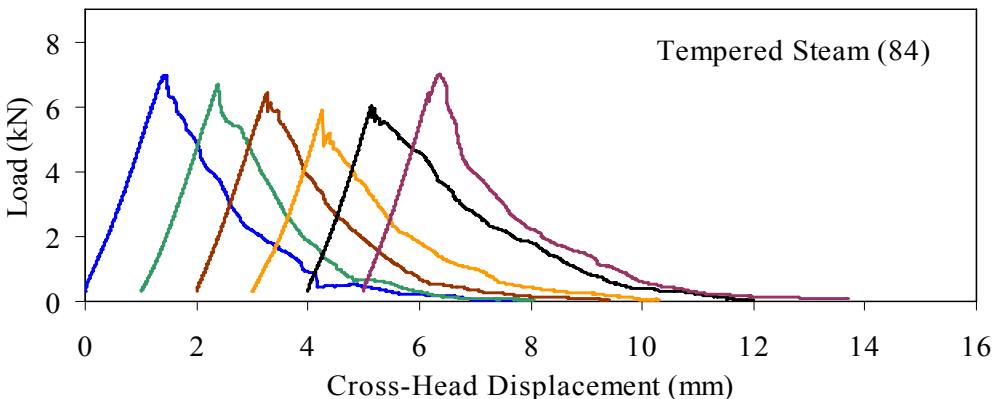
1 kN = 0.225 kip, 1 mm = 0.039 inch

Figure 72. Graph. Load-displacement for tempered steam-treated briquettes (28 days).

1 kN = 0.225 kip, 1 mm = 0.039 inch

Figure 73. Graph. Load-displacement for tempered steam-treated briquettes (56 days).

1 kN = 0.225 kip, 1 mm = 0.039 inch

Figure 74. Graph. Load-displacement for tempered steam-treated briquettes (84 days).
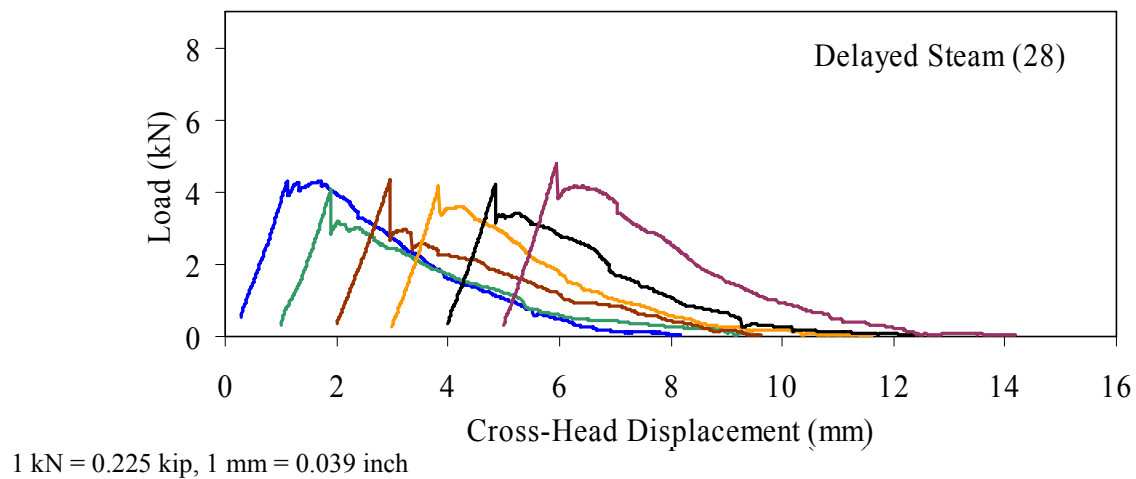
Figure 75. Graph. Load-displacement for delayed steam-treated briquettes (28 days).

1 kN = 0.225 kip, 1 mm = 0.039 inch
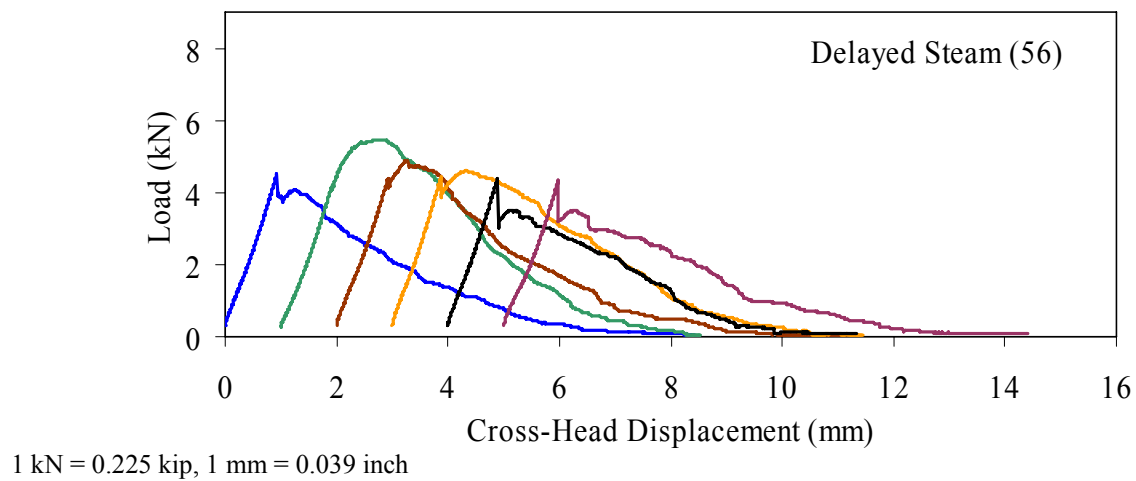
Figure 76. Graph. Load-displacement for delayed steam-treated briquettes (56 days).

1 kN = 0.225 kip, 1 mm = 0.039 inch
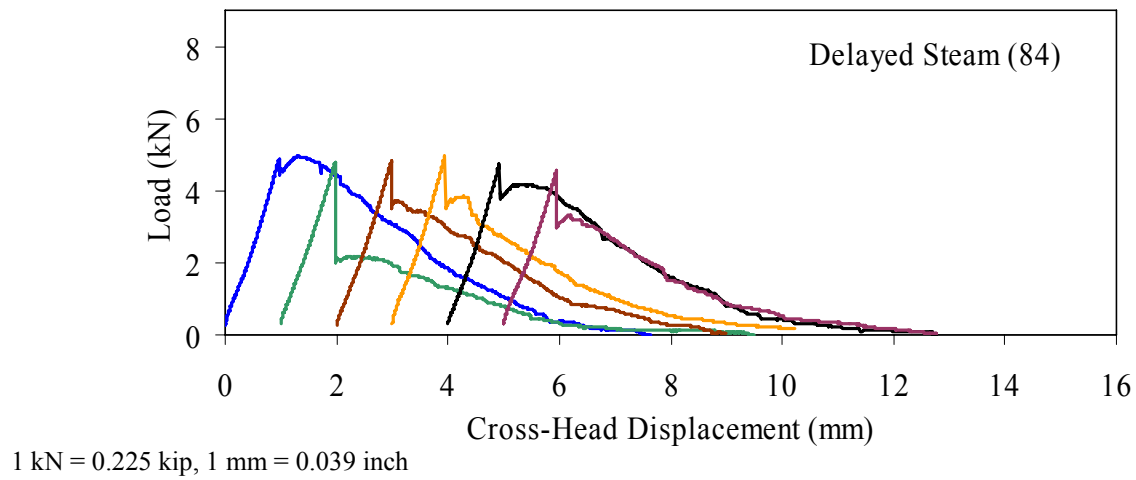
Figure 77. Graph. Load-displacement for delayed steam-treated briquettes (84 days).

3.4.3.1 Strength

The tensile cracking strength results are presented in figure 78. First cracking was defined as a discontinuity in the load-displacement curve caused by an instantaneous decrease in load. The results from the six replicates in each group have been averaged, and the average value is shown on the bar in the chart. The standard deviation within the results for each group is provided by the error bar, which indicates a ±1 standard deviation.

1 MPa = 145 psi
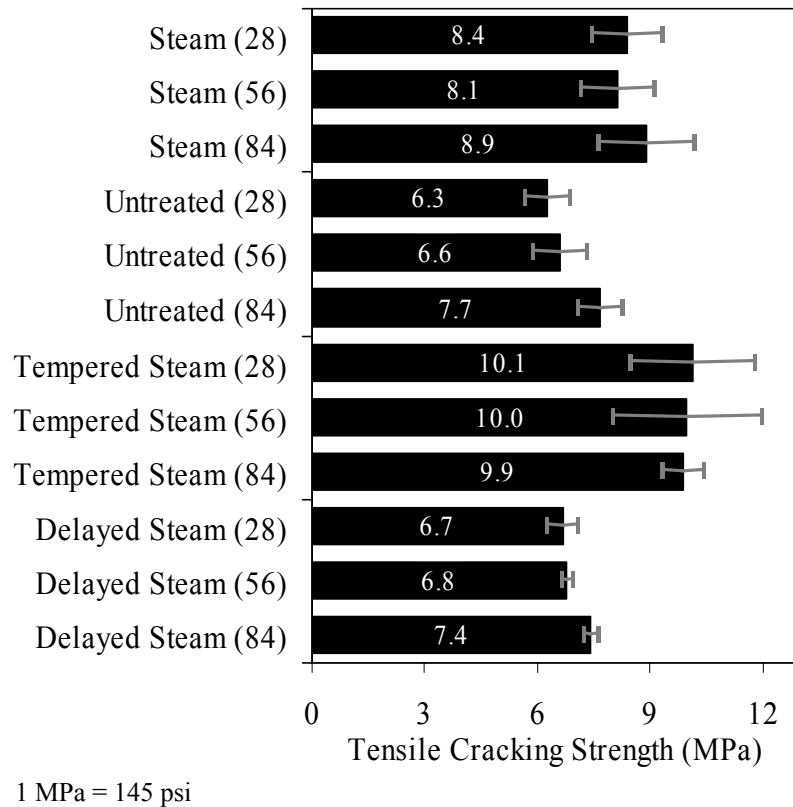
Figure 78. Chart. Tensile cracking strength of UHPC briquettes.

The UHPC that underwent the steam-based curing treatment showed consistent strength levels from 1 to 3 months after casting. The steam-treated UHPC tensile cracking strength is approximately 8.3 MPa (1.2 ksi), while the tempered steam-treated UHPC is 9.7 MPa (1.4 ksi). The delayed steam-treated UHPC shows a lower value of around 1.0 ksi. The untreated UHPC shows a steady increase in strength between the first and third months, with the cracking tensile strength increasing 20 percent to 7.6 MPa (1.1 ksi) by 3 months. Again, recall that the compressive strength results for three of these curing regimes were lower than anticipated, thus the tensile strength results were likely affected as well.

The postcracking strength results are presented in figure 79, which has the same format as figure 78. The postcracking peak strength was defined as the highest load level reached after the tensile cracking load decreased. These results show significantly more scatter than the tensile cracking results. Of most importance, these results show that the postcracking load-carrying

86

capacity is very similar to the precracking capacity. The fiber-reinforced nature of the UHPC matrix allows the fibers bridging a crack to carry a similar load level after cracking as the cement-based matrix did before cracking.

3.4.3.2 Toughness

The toughness exhibited by UHPC after cracking is of utmost importance if the UHPC will carry tensile forces after cracking. The UHPC needs to maintain load-carrying capacity as multiple cracking occurs and as individual cracks widen. As discussed in section 3.4.3.1, one means of measuring toughness is to calculate the area under the load-displacement curve. Frequently, the area under the curve after cracking is compared with the precracking area. Using this means of comparison, normal concrete would have a toughness of nearly zero with no postcracking load-carrying capacity. On the other hand, an elastic-plastic material such as mild steel would exhibit a high post-yield toughness result.

1 MPa = 145 psi
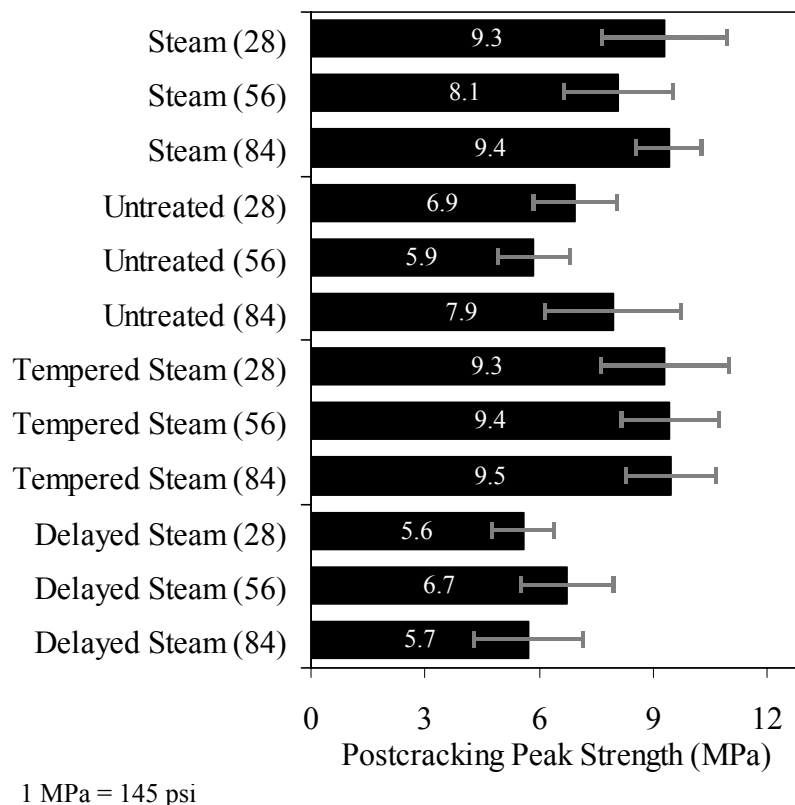
Figure 79. Chart. Postcracking peak strength of UHPC briquettes.

To compare toughness results from one test program to another, the means of measuring the displacement must accurately measure the actual displacement of the concrete in question. Given the nature of the AASHTO T132 test, measuring only the displacement of the UHPC briquette is not possible. Thus, the results presented here include the overall displacement of the loading system. A quantitative comparison of the areas contained under the load-displacement curves

from this test program to other test programs is not possible. However, a quantitative comparison within this test program and qualitative external comparisons are definitely warranted.

Figure 80 presents the average calculated areas under the load-displacement curves after cracking for the 12 groups of briquettes tested. The area calculation includes the entire area under the curve from cracking until the load level dropped to 890 N (200 lb), which is equivalent to a stress of 1.38 MPa (200 psi) on the original minimum cross section. These results show a much larger scatter, but the average results are relatively consistent within each curing regime. The larger area results in the steam-treated regime as compared with the tempered steam-treated regime are quite instructive. Recall that the tempered steam briquettes in figures 72 through 74 show higher tensile strengths but that the shape of the postcracking portion of the curve exhibits a more rapid decrease in load capacity. The steam-treated regime clearly exhibits the best postcracking behavior, with almost twice the area as compared with the untreated briquettes. The tempered steam and delayed steam-treated regimes both show approximately 75 percent of the postcrack area as compared with the steam-treated regime.

1 MPa = 145 psi
1 N-m = 0.74 kip-ft
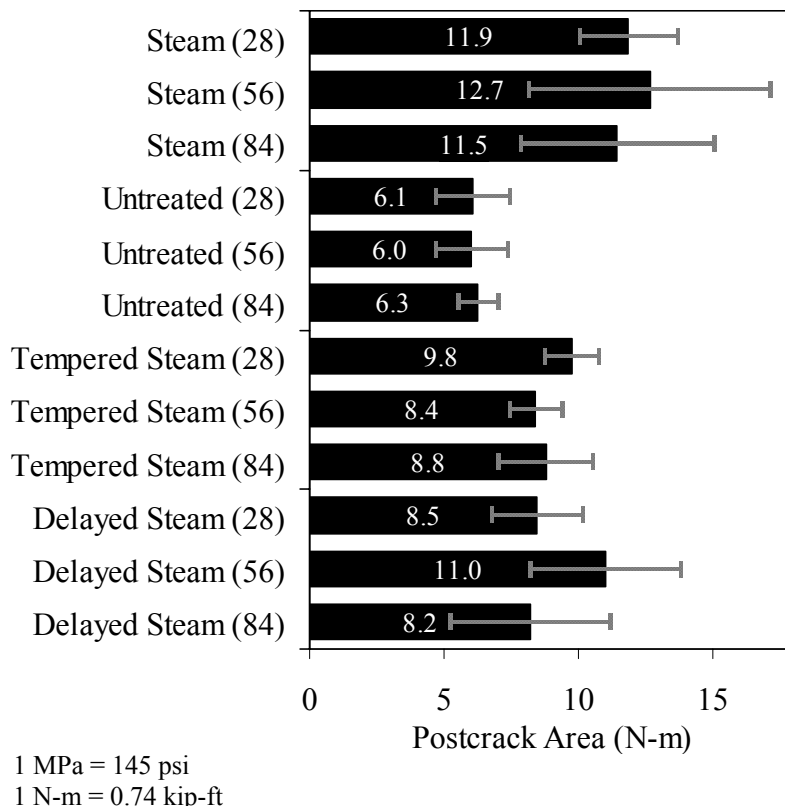
Figure 80. Chart. Area under the load-displacement response curve after cracking.

For completeness, figure 81 presents the results for the ratio of the postcracking area to the precracking area under the load-deflection curve. As previously mentioned, this ratio is the standard means of measuring the toughness of a semibrittle material like fiber-reinforced concrete. The area under the curve before cracking is based on the linear elastic portion of the load-displacement response, thus eliminating the seating behaviors that occur early in each test.

These results seem to indicate that the tempered steam briquettes displayed the poorest toughness results while the delayed steam- and steam-treated briquettes had the best results. However, these results are an artifact of the higher cracking strength exhibited by the tempered steam briquettes and not by their low postcracking toughness.

1 MPa = 145 psi
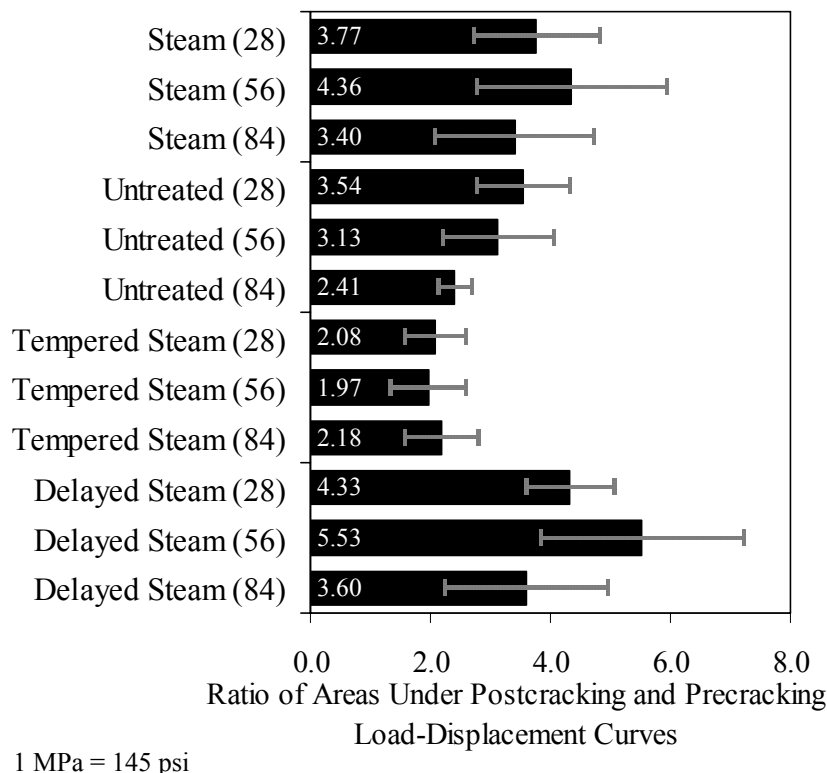
**Figure 81. Chart. Ratio of postcracking to precracking areas
under the load-displacement curve.**

The postcracking behavior of UHPC is dependent primarily on the steel fibers and their attachment to the UHPC matrix. Clearly, a reduction in the number of fibers in the UHPC mix eventually must lead to a decrease in the sustained tensile load capacity after cracking. The curing treatment applied to the UHPC could likely have affected the bond between the fibers and the matrix.

Considering these two points, the failed specimens from the briquette tension tests were evaluated. A significant portion of the briquettes in 9 of the 12 briquette test groups were studied to determine the number of fibers that intersected the failure plane. The fibers extending from each of the failure surfaces in each briquette were counted. The totals are shown in table 21. These results are then compared with the postcrack area under the load-displacement curve to determine what portion of the area could be attributed to each fiber. Obviously, this calculation glosses over many qualifying factors that would cause different fibers to carry different loads (i.e., fiber orientation relative to crack, fibers extension on either side of crack). However, this calculation is instructive in providing some results related to the effect of curing and fiber percentages.

89

Table 21. Fiber influence on postcracking behavior.

Group	No. Samples	Fibers Crossing Failure Plane		Postcrack Area per Fiber (N-m/fiber)	
		Average	Standard Deviation	Average	Standard Deviation
Steam (56)	6	337	47	0.038	0.015
Steam (84)	5	276	46	0.040	0.011
Untreated (28)	5	370	45	0.017	0.003
Untreated (56)	6	356	42	0.017	0.005
Untreated (84)	6	329	77	0.019	0.003
Tempered Steam (56)	3	384	30	0.024	0.003
Tempered Steam (84)	6	321	35	0.028	0.009
Delayed Steam (56)	6	179	63	0.064	0.018
Delayed Steam (84)	6	149	19	0.054	0.014

1 N-m = 0.74 kip-ft

Aside from the delayed steam regime, these results indicate that the curing treatment seems to affect the ability of fibers to bond to the UHPC matrix. All of these groups contained similar numbers of fibers crossing the failure plane, but show three distinct levels of postcrack area per fiber. The steam-treated regime exhibits more than twice the toughness as the untreated regime on a per-fiber basis. Additionally, the delayed steam treatment results show that these briquettes had distinctly fewer fibers crossing the failure plane. Although this result probably could not explain the lower precracking tensile strength of these specimens, it definitely could explain the lower-than-expected postcracking peak strength.

3.4.4 Direct Tension

The fourth tension test used to quantify the material behaviors of UHPC was a direct-tension test. Unlike the flexural or split-cylinder tests, a direct-tension test applies a uniaxial tensile stress onto the concrete and monitors tensile behaviors as tensile strains are increased. In this test program, 102-mm (4-inch) diameter concrete cylinders were subjected to a uniaxial tensile load applied through the flat-end surfaces of each cylinder.

Direct-tension tests are rarely performed on concrete due to the difficulties inherent in this test method. Among other things, direct-tension tests generally require complicated test setups because of the tensile gripping of the concrete and the custom equipment required for the loading and data collection. However, many researchers have investigated this topic and have attempted to develop reliable and repeatable means of testing the tensile stress-strain properties of concrete. (See references 30 through 45.) The direct-tension test setup and procedures used in this research program are an agglomeration of these testing techniques and rely most heavily on USBR 4914 *Procedure for Direct Tensile Strength, Static Modulus of Elasticity, and Poisson's Ratio of Cylindrical Concrete Specimens in Tension*[42] and RILEM TC 162-TDF *Uniaxial Tension Test for Steel Fibre Reinforced Concrete.*[39]

Concrete cylinders that had a 102-mm (4-inch) diameter and a 203-mm (8-inch) length were cast for the direct-tension tests. These cylinders were cast following the normal casting and curing

procedures detailed in section 3.2. Six cylinders were prepared for each curing regime. Note that no special attention was given toward achieving the proper distribution and orientation of the fiber reinforcement within the cylinder, thus it is expected that the fibers were not necessarily randomly distributed and oriented within the cylinder. This topic will be discussed in further detail later in this section. The direct tension tests were completed between 2 and 4 months after casting. Finally, these cylinders were cast from the same four batches of UHPC as the mortar briquettes discussed in section 3.4.3. To reiterate the discussion presented in this section, three of these four batches of cylinders exhibited somewhat low compressive strengths, which indicates that the tensile behaviors could be diminished as well.

Two loading configurations were used in this test program, each for half of the cylinders from each curing regime. In the first configuration, the cylinders were tested as cast. In the second configuration, the cylinders were circumferentially notched to create a plane of reduced cross-sectional area and thus higher stresses per applied load. The notch was created by milling a parabolic-shaped groove into the surface of the cylinder. This groove was 6.4 mm (0.25 inch) deep, thus resulting in a reduced cylinder diameter of 89 mm (3.5 inches). The total height of the groove was 12.7 mm (0.5 inch). Figure 82(a) shows a notched cylinder, while figure 82(b) shows an unnotched cylinder ready for testing.

These tests were completed in a 445-kN (100-kip) capacity MTS testing machine. The axial displacement rate of a portion of the cylinder was used as the control signal. This displacement rate was captured through three LVDTs mounted on a testing apparatus similar to the one that was discussed in section 3.3.2 and shown in figure 82(b). The signal from these LVDTs was electronically averaged and then was sent to the MTS controller. The unnotched cylinders used a 102-mm (4-inch) gage length centered on the specimen, and the notched cylinders used a 38-mm (1.5-inch) gage length centered over the notch. All cylinders were tested with a displacement rate of approximately 0.005 mm/min (0.0002 inch/min), which is the rate recommended in the RILEM test procedure.

Before testing, the cylinders had their ends ground and checked for planeness. The testing machine heads and the ends of the specimen were then lightly sandblasted. A high-strength, high-modulus, rapid-setting epoxy was then applied to the testing machine heads as the cylinder was placed in the machine. A compressive load of approximately 22 kN (5 kip) was then applied to the specimen until the epoxy had cured. Note that the epoxy required at least 8 hours of cure time; thus, testing was completed on a daily cycle.

The test setup and procedures discussed above were implemented in order to capture the full tensile stress-strain behavior of UHPC. Unfortunately, no behaviors after initial tensile cracking could be reliably observed and monitored. The MTS controller temporarily lost control of the cylinder during the brittle initiation of the first tensile crack. When control was regained, the cylinder had undergone some tensile fiber pullout across the crack, and the critical portion of the UHPC tensile behavior just after tensile cracking had been bypassed. This uncontrolled behavior was probably caused by a lack of sensitivity of the MTS control system due to its larger-than-necessary load capacity. However, accurate postcracking results could probably not have been obtained anyway, because failure surfaces have indicated that the fiber distribution and orientation within the cylinders was not sufficiently random.
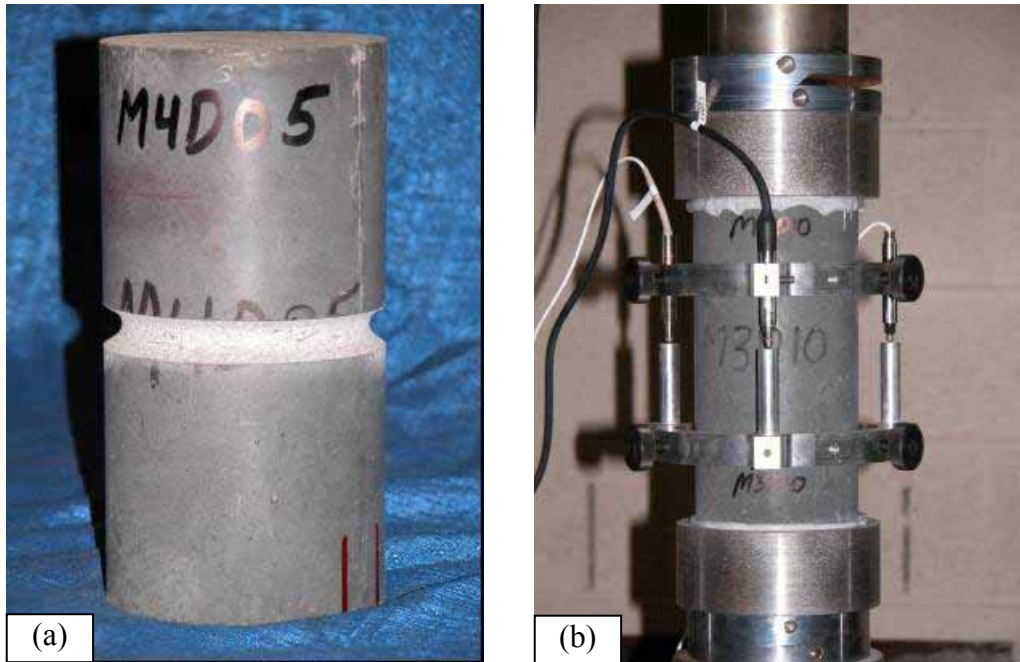
Figure 82. Photos. (a) Notched cylinder and (b) testing of an unnotched cylinder.

For these reasons, the test results presented in this section focus only on the tensile cracking strength and on the modulus of elasticity of the UHPC. Table 22 provides the results from the six cylinders in each curing regime. The table indicates which specimens were notched, the location of the first tensile crack, the tensile cracking strength, and the modulus of elasticity. The modulus of elasticity was determined based on the displacement readings across the 102-mm (4-inch) gage length between the applied stresses of 2.5 MPa (360 psi) compressive and 2.5 MPa (360 psi) tensile. Recall that the cylinders were initially compressed as the epoxy cured; thus, continuous data were recorded during the test over this transition from compressive to tensile behavior.

The table indicates that 11 of the 12 notched specimens failed within the notch. Aside from possible local stress concentrations caused by the notch, it is anticipated that these results accurately represent the tensile cracking strength of the UHPC. For the purposes of this research, local stress concentration effects are ignored, and these tensile cracking strengths are viewed to be accurate representations of pure tensile behavior. Only half of the unnotched cylinders failed remotely from the bearings; therefore, the unnotched specimen results are more limited. It is expected that the specimens that failed within 25.4 mm (1 inch) of the bearing had their strengths reduced by local bearing effects.

Table 22. Direct tension test results.

Specimen	Notched	Cracking Location	Cracking Strength (MPa)	Modulus of Elasticity (GPa)
Steam				
M1D00	Yes	Notch	10.8	N/A
M1D01	Yes	Notch	10.3	N/A
M1D02	Yes	Notch	12.1	N/A
M1D10	No	Within 25 mm of bearing	10.4 [†]	51.9
M1D11	No	Center of specimen	9.9	50.5
M1D12	No	Within 25 mm of bearing	9.4 [†]	53.3
Untreated				
M2D00	Yes	Notch	5.7	N/A
M2D01	Yes	Notch	5.9 [‡]	N/A
M2D02	Yes	Notch	6.5 [‡]	N/A
M2D10	No	Within 25 mm of bearing	6.3 [†]	46.4
M2D11	No	Within 25 mm of bearing	6.6 [†]	47.9
M2D12	No	Within 25 mm of bearing	7.0 [†]	47.9
Tempered Steam				
M3D00	Yes	Notch	7.2	N/A
M3D01	Yes	Notch	8.9	N/A
M3D02	Yes	Notch	7.5	N/A
M3D10	No	Center of specimen	7.8	52.1
M3D11	No	Center of specimen	9.4	52.9
M3D12	No	Center of specimen	9.6	51.2
Delayed Steam				
M4D00	Yes	Unnotched section	8.2 [*]	N/A
M4D01	Yes	Notch	11.5	N/A
M4D02	Yes	Notch	10.9	N/A
M4D10	No	Within 25 mm of bearing	3.5 [†]	50.9
M4D11	No	Center of specimen	9.1 [†]	53.9
M4D12	No	Center of specimen	10.4	51.4

[†] Cracking strength results may have been influenced by crack location.
[‡] Minimum cracking strength value due to difficulty with test apparatus leading to poor data resolution.
[*] Cracking did not occur in the notch that had a peak tensile stress of 10.7 MPa.
1 MPa = 145 psi, 1 GPa = 145,038 psi, 1 mm = 0.039 inch

The limited total data set available from the direct tension tests precludes the presentation of definitive conclusions. However, the results do provide a range in which tensile cracking of UHPC can be anticipated. For steam-treated UHPC, tensile cracking likely occurs between 9.7 and 11.0 MPa (1.4 and 1.6 ksi). For untreated UHPC, the range is from 5.5 to 6.9 MPa

(0.8 to 1.0 ksi). For tempered steam specimens, the range was from 7.6 to 9.0 MPa (1.1 to 1.3 ksi). For delayed steam specimens, the range was from 9.0 to 11.0 MPa (1.3 to 1.6 ksi).

The modulus of elasticity results are not affected by cracking or other localized behaviors. For this reason, three results are available for each curing regime. The steam-treated UHPC modulus of elasticity averaged 51.7 GPa (7,500 ksi). The untreated UHPC averaged 47.6 GPa (6,900 ksi). The tempered steam and the delayed steam-treated UHPC specimens both averaged 52.1 GPa (7,550 ksi). Aside from the steam-treated results, these results are somewhat higher than those presented in section 3.3 that were obtained from purely compressive testing of cylinders.

Finally, the linearity of the tensile stress-strain response from minimal compressive load through tensile cracking was studied. The same stress-strain responses recorded from the testing of the unnotched cylinders that were used for the modulus of elasticity determination were also used to determine the nonlinearity of the response as cracking was approached. Overall, the results indicate that UHPC, regardless of the curing regime, exhibits very linear behavior up through tensile cracking. The theoretical linear-elastic stress-strain response based on the calculated modulus of elasticity was used to determine the actual stress deviation (reduction) at any level of tensile strain. The decrease from the linear-elastic predicted level was less than 0.14 MPa (20 psi) for 10 of the cylinders and was less than 0.21 MPa (30 psi) for the remaining 2 specimens.

3.5 FRACTURE TESTING

Understanding the cracking processes that occur when UHPC is stressed beyond its tensile strength is of great importance. Experience with UHPC structures has indicated that individual cracks tend to grow rapidly to a significant length, but that the width of any such crack is very small. However, this experience is based on structural testing of UHPC members with loading configurations that were not intended to create and to propagate stable cracks.

A series of tests were completed on UHPC prisms to determine some of the basic behaviors of individual cracks. These tests focused on loading a prenotched prism in 3-point bending, with the load being incremented based on the opening at the mouth of the crack. The tests were loosely based on a portion of ASTM E1820 *Standard Test Method for Measurement of Fracture Toughness.*[46]

The prisms and test setup conformed to the ASTM test method for the single-edge beam test discussed in Annex A1 of the specification. The prism had a height of 102 mm (4 inches), a width of 51 mm (2 inches), and a span of 406 mm (16 inches). The only deviation from the ASTM test method was in the size and shape of the notch cut into the prism to act as the crack initiation point. In these tests, the crack was cut into the tension flange to a distance of approximately 25 mm (1 inch). The crack was cut with a 4.75-mm (3/16-inch) thick diamond-tipped saw blade. The crack's tip had a rounded profile and was not sharpened through fatigue cycling or by any other means.

Four prisms were cast for both the steam-treated and untreated curing regimes. These prisms were part of the M1P and M2P batches discussed in section 3.1. The casting of these prisms followed normal procedures except that they were cast upside-down from the orientation in

which they would be tested. These prisms were cast in special steel molds that allowed for partial enclosure of the top of the prism at the ends. Therefore, the only nonmolded surface on the finished prism was the center of the bottom or tension flange in the finished specimen.

These tests were completed in a 98-kN (22-kip) capacity, MTS-controlled load frame. The tests were controlled based on the crack mouth opening displacement (CMOD). The CMOD was measured via a 12.7-mm (0.5-inch) full-range-capacity clip gage that was attached to knife edges epoxied to the bottom flange on either side of the starter notch. The entire test-loading protocol was preprogrammed into the MTS Microprofiler. The testing included an initial CMOD rate of approximately 0.013 mm/min (0.0005 inch/min), as well as a postcracking rate 2.5 and 5.0 times larger. The protocol included periodic unloadings set to occur at predefined CMOD values. Unfortunately, for unknown reasons these unloadings frequently did not occur as planned. Tests were stopped after 2.5 mm (0.1 inch) of CMOD. Figure 83 shows one of the prisms undergoing this fracture test.

Figure 83. Photo. Test setup for 102- by 51-mm (4- by 2-inch) notched prisms loaded on a 406-mm (16-inch) span.

Two methods were used to monitor the crack extension during the test. The primary method involved using an optical microscope to view the fracture process zone just ahead of the tip of the crack. This microscope had a field of view of 2.5 mm (0.1 inch), which allowed the crack tip to be located with relative ease. As the test progressed, alcohol was used as a volatile penetrant to help indicate the extent of cracking. The crack extension measurements were all taken from the bottom of the prism.

The second method used to monitor crack extension involved a crack propagation resistance gage. Figure 84 shows one of these gages during a test as a crack is traversing the grid. The resistance across the gage changes as more of the lines are broken due to crack extension. This method of crack monitoring was used on two prisms from each of the steam-treated and untreated curing regimes.

Figure 84. Photo. Resistance foil gage to monitor crack propagation.

Figures 85 and 86 show photographs of crack propagation on two prisms. Alcohol was used to help indicate the locations of the cracks in both figures. Some important findings observed throughout these tests are illustrated in the figures. First, a single crack formed initially in each prism because the starter notch had sufficient depth. The crack then extended up through the prism as shown in figure 85(a). However, the fibers binding the initial crack together soon allowed for a redistribution of stresses resulting in the formation of other cracks that ran parallel to the first crack. Second, the cracks tended to extend very close to the compression flange. Figure 85(b) shows a crack extending to within 3.8 mm (0.15 inch) of the compression flange.

The load and crack extension results in terms of the CMOD for each specimen are presented in figures 87 through 94. In each figure, (a) shows the overall response of the prism with the load versus CMOD behavior plotted with regard to the left y-axis and the crack extension versus CMOD behavior plotted with regard to the right y-axis. In each figure, (b) shows the initial behavior and first cracking of the UHPC prisms. Additionally, this plot shows the geometric construction used to determine when first cracking occurred.

The ASTM E1820 specification defines cracking for materials that exhibit both stable and unstable first cracking. The data collected from these eight prisms indicate stable cracking behavior occurred with no clear evidence of a pop-in in any specimen. Thus, first cracking is defined by creating a linear best-fit line to the initial elastic portion of the load-CMOD response, then decreasing the slope of this line by 5 percent. The intersection of the new line with the original data is defined as the load and CMOD at first cracking.

Part (b) of the referenced figures shows the required construction and the values at first cracking. Note that the initial load-CMOD response between 1.3 and 2.6 kN (300 and 600 lb) was used to define the elastic portion of the behavior, because it was beyond any initial seating-based nonlinearities and was before the initiation of cracking-based nonlinearities.

The original intent of these tests had been to determine the fracture toughness, K_{Ic}, of steam-treated and untreated UHPC according to ASTM E1820. Unfortunately, the calculations

96

associated with this specification indicate that the test as performed did not meet the standards of a qualified and size-independent K_{Ic} test.
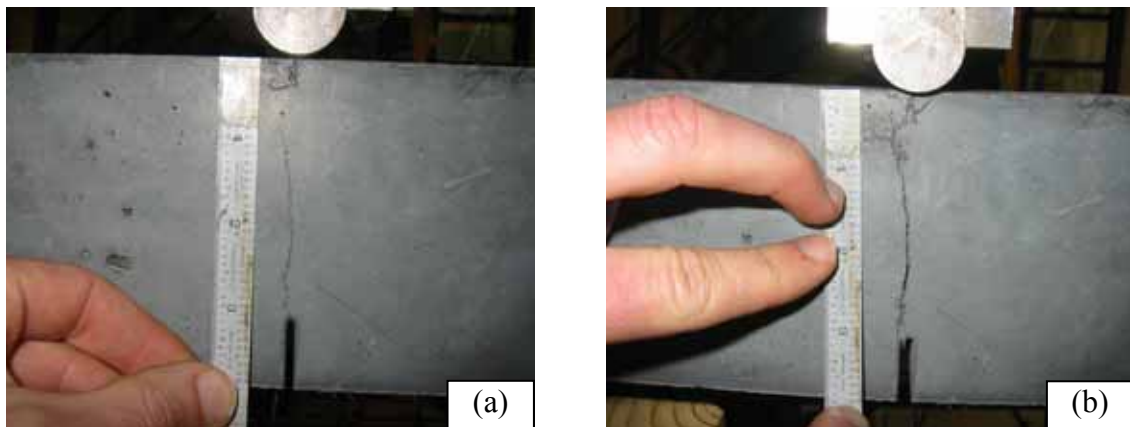
Figure 85. Photos. Prism M1P00 after (a) 86 mm (3.6 inches) and (b) 98 mm (3.8 inches) of crack extension.
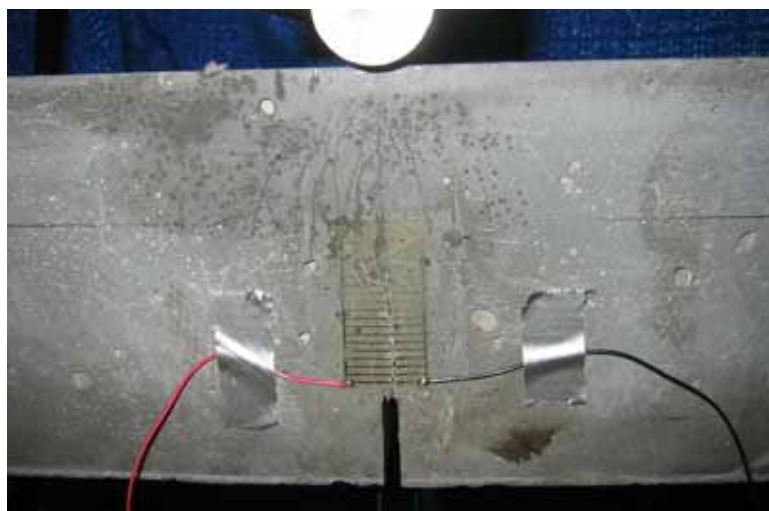
Figure 86. Photo. Prism M2P03 after 93 mm (3.63 inches) of crack extension.

1 kN = 0.225 kip
1 mm = 0.039 inch

(a) Overall response including periodic unloadings.

1 kN = 0.225 kip
1 mm = 0.039 inch

(b) Initial response including elastic stiffness and 95 percent of elastic stiffness curves.
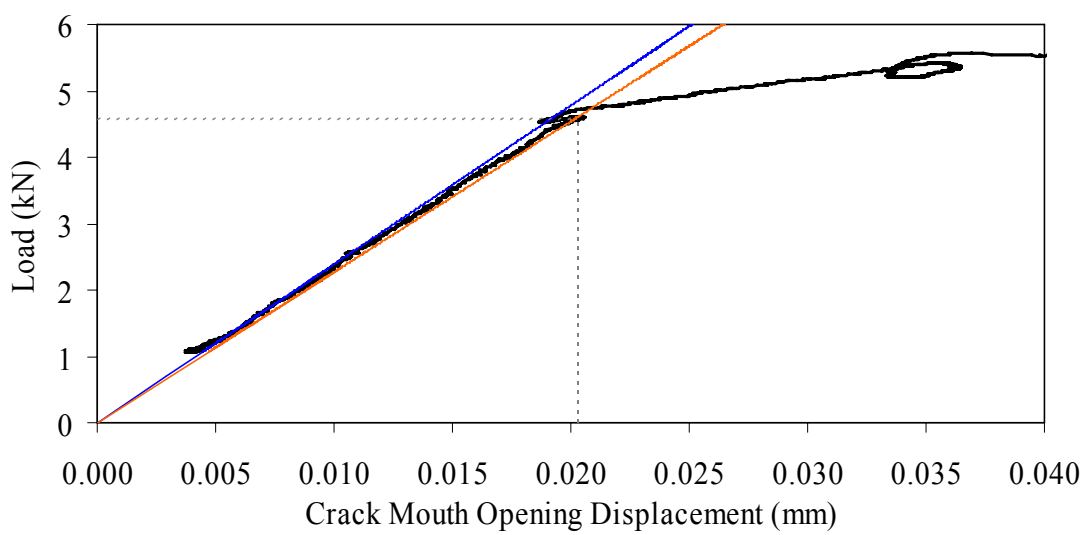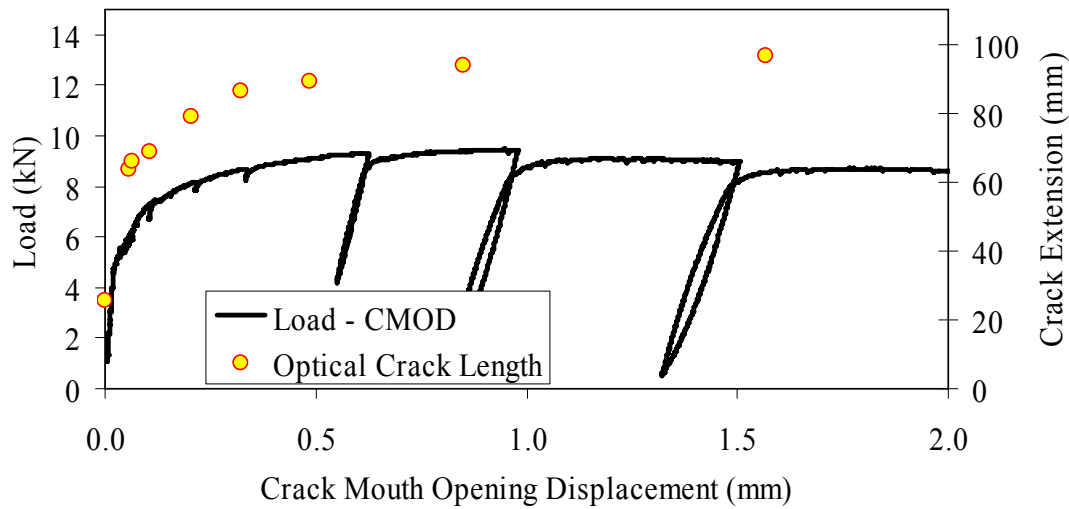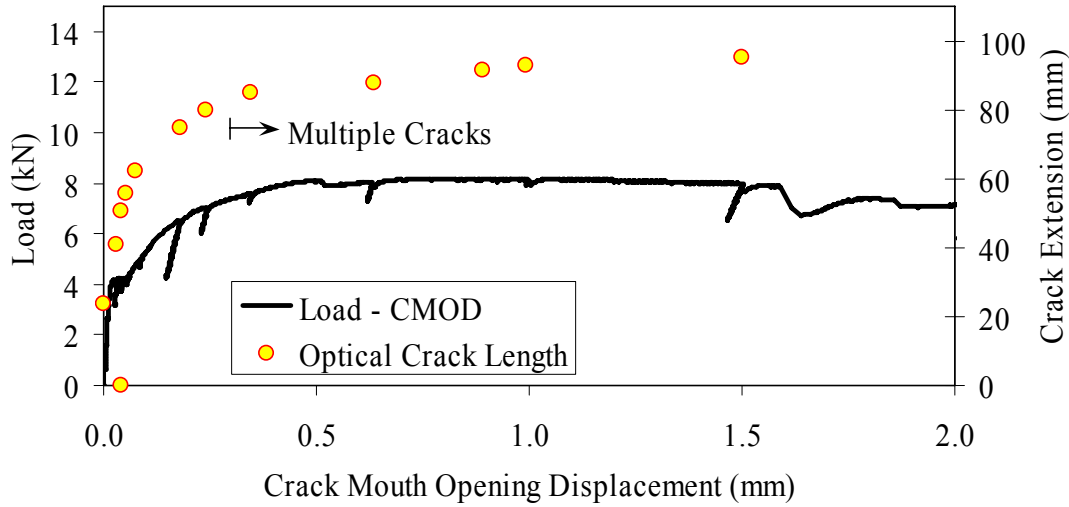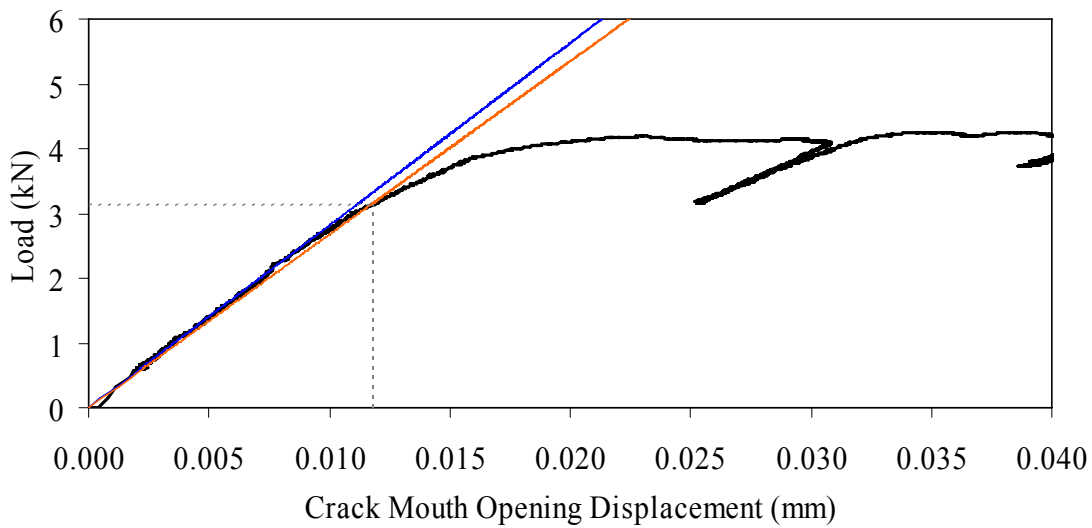
Figure 87. Graph. Load-CMOD response for steam-treated prism M1P00.
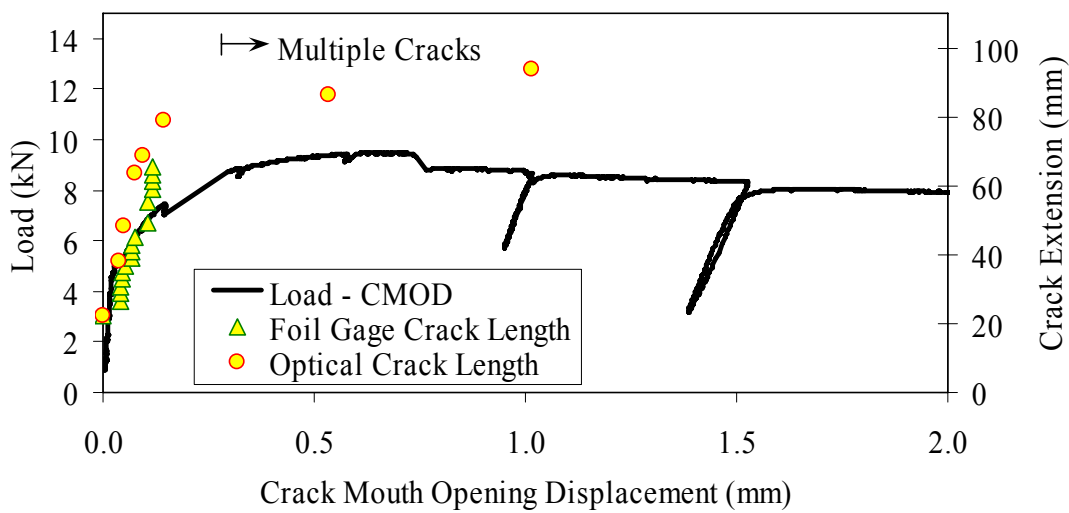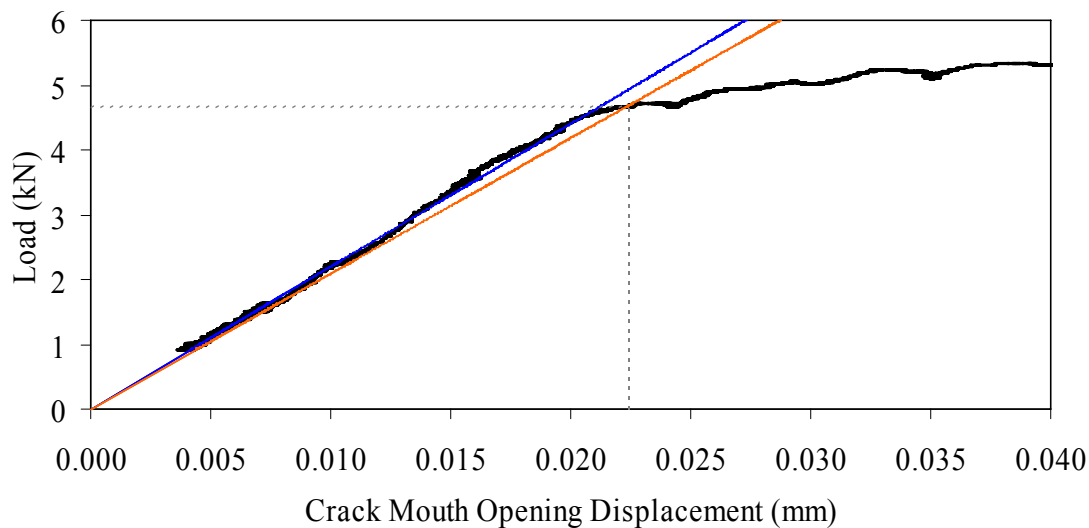
1 kN = 0.225 kip
1 mm = 0.039 inch

(a) Overall response including periodic unloadings.

1 kN = 0.225 kip
1 mm = 0.039 inch

(b) Initial response including elastic stiffness and 95 percent of elastic stiffness curves.

Figure 88. Graph. Load-CMOD response for steam-treated prism M1P01.
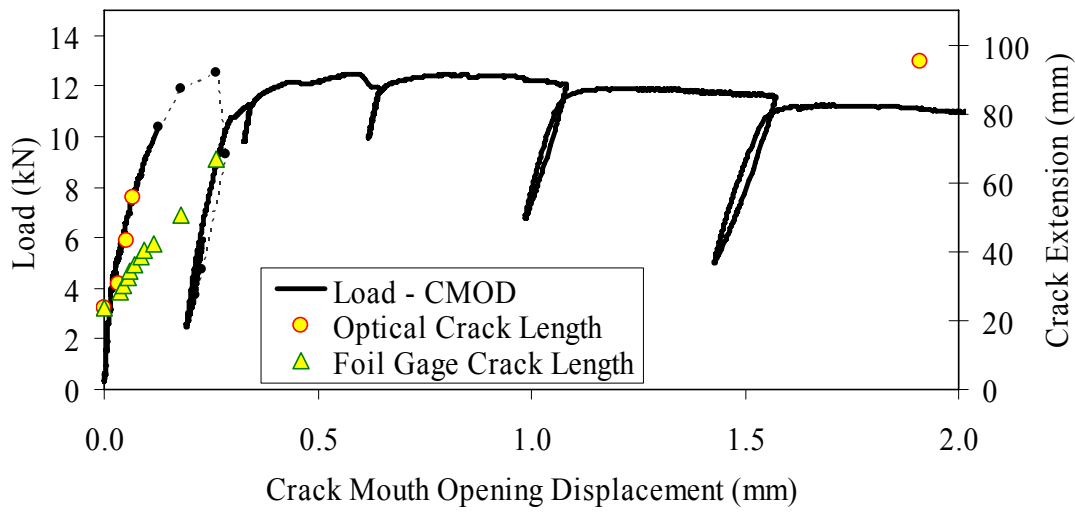
99

1 kN = 0.225 kip
1 mm = 0.039 inch

(a) Overall response including periodic unloadings and crack length from tension flange.

1 kN = 0.225 kip
1 mm = 0.039 inch
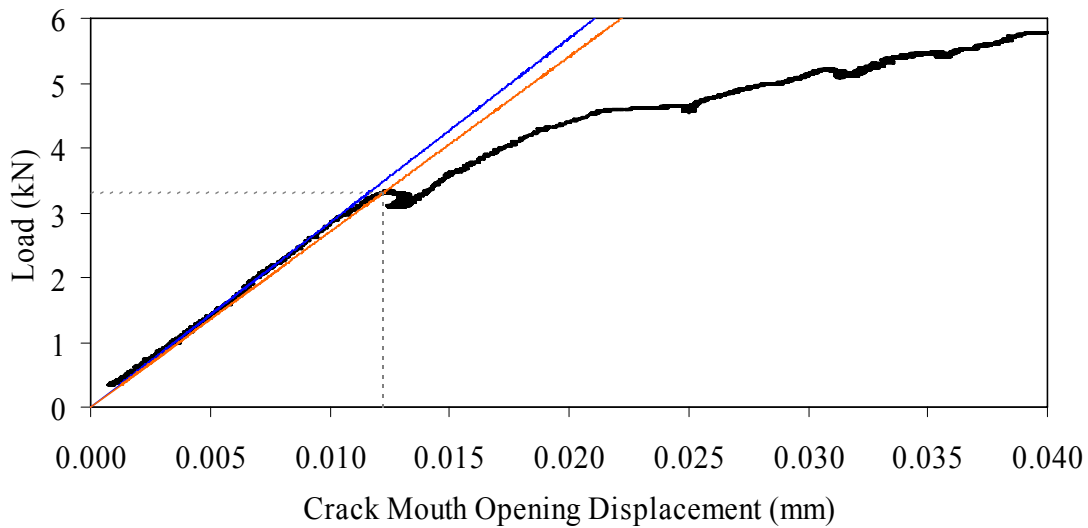
(b) Initial response including elastic stiffness and 95 percent of elastic stiffness curves.

Figure 89. Graph. Load-CMOD response for steam-treated prism M1P02.

1 kN = 0.225 kip
1 mm = 0.039 inch
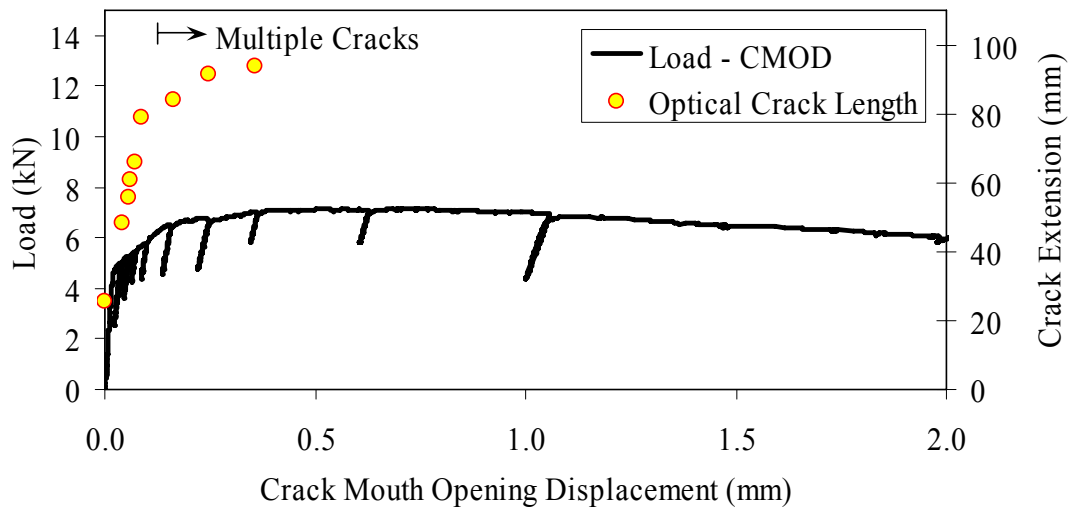
(a) Overall response including periodic unloadings and crack length from tension flange.
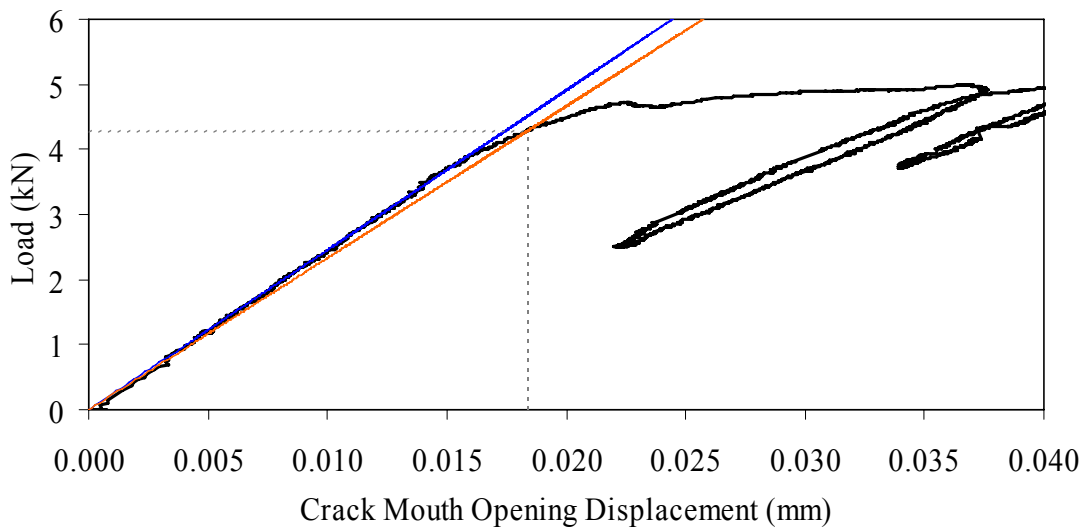
1 kN = 0.225 kip
1 mm = 0.039 inch

(b) Initial response including elastic stiffness and 95 percent of elastic stiffness curves.

Figure 90. Graph. Load-CMOD response for steam-treated prism M1P03.
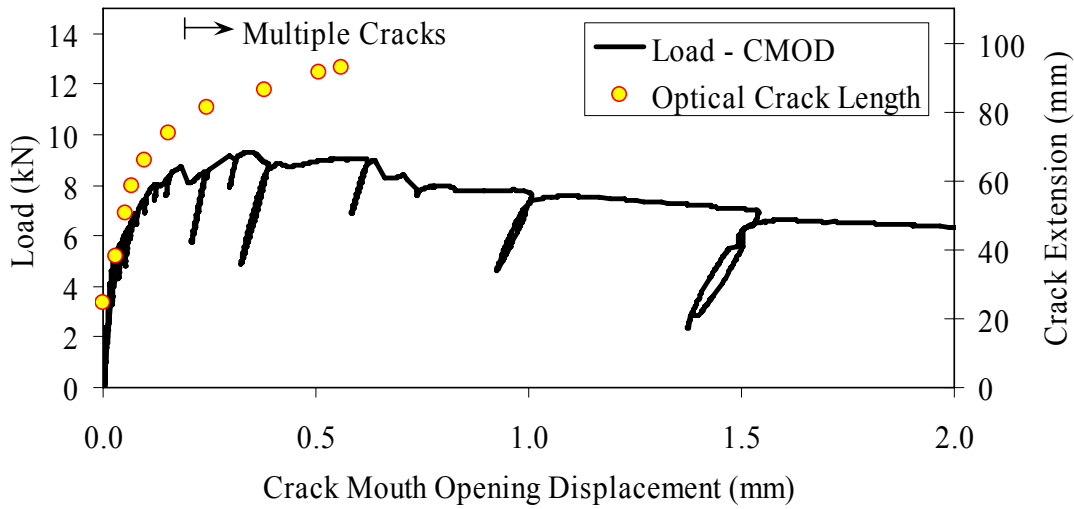
(a) Overall response including periodic unloadings.
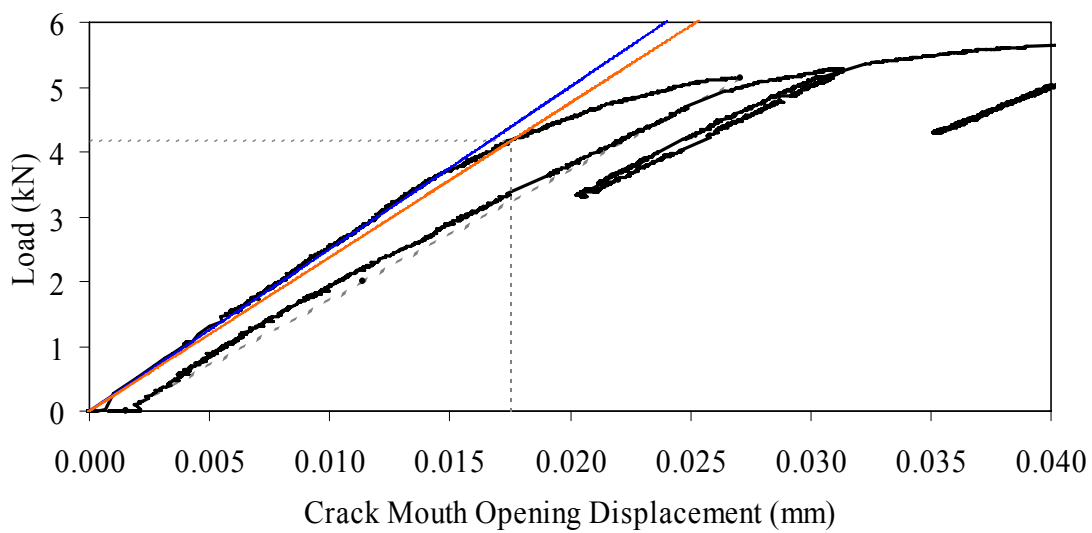
1 kN = 0.225 kip
1 mm = 0.039 inch

1 kN = 0.225 kip
1 mm = 0.039 inch

(b) Initial response including elastic stiffness and 95 percent of elastic stiffness curves.

Figure 91. Graph. Load-CMOD response for untreated prism M2P00.

1 kN = 0.225 kip
1 mm = 0.039 inch
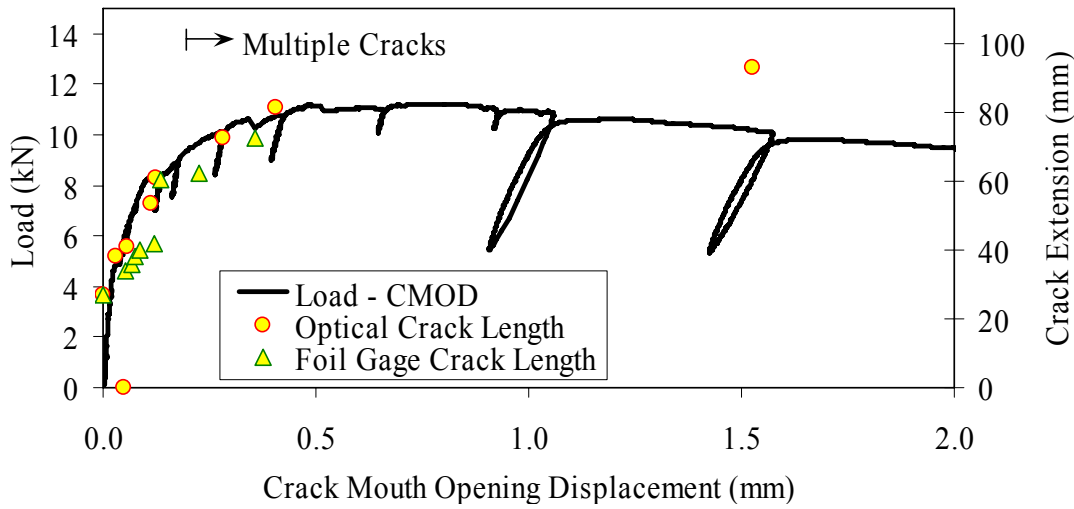
(a) Overall response including periodic unloadings.

1 kN = 0.225 kip
1 mm = 0.039 inch
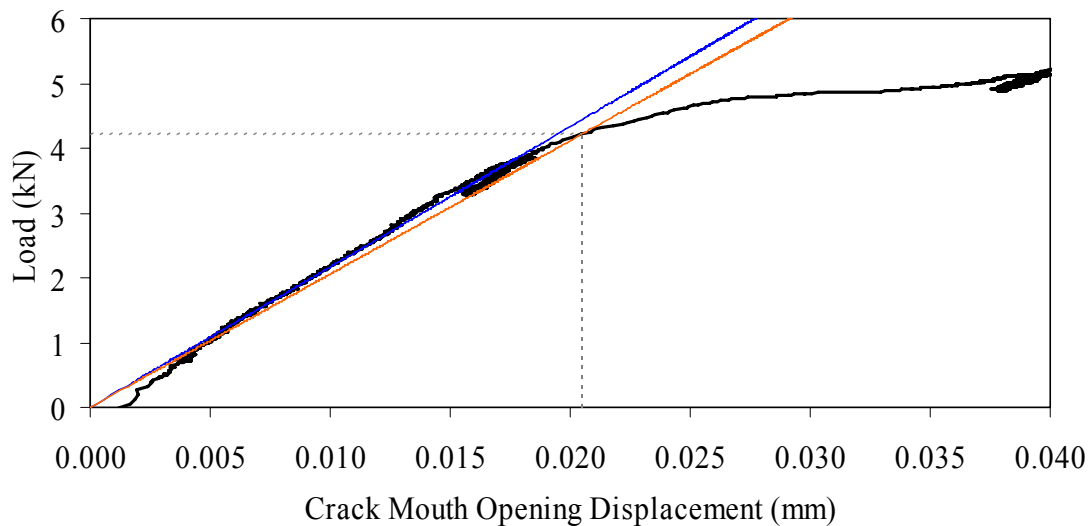
(b) Initial response including elastic stiffness and 95 percent of elastic stiffness curves.

Figure 92. Graph. Load-CMOD response for untreated prism M2P01.

1 kN = 0.225 kip
1 mm = 0.039 inch
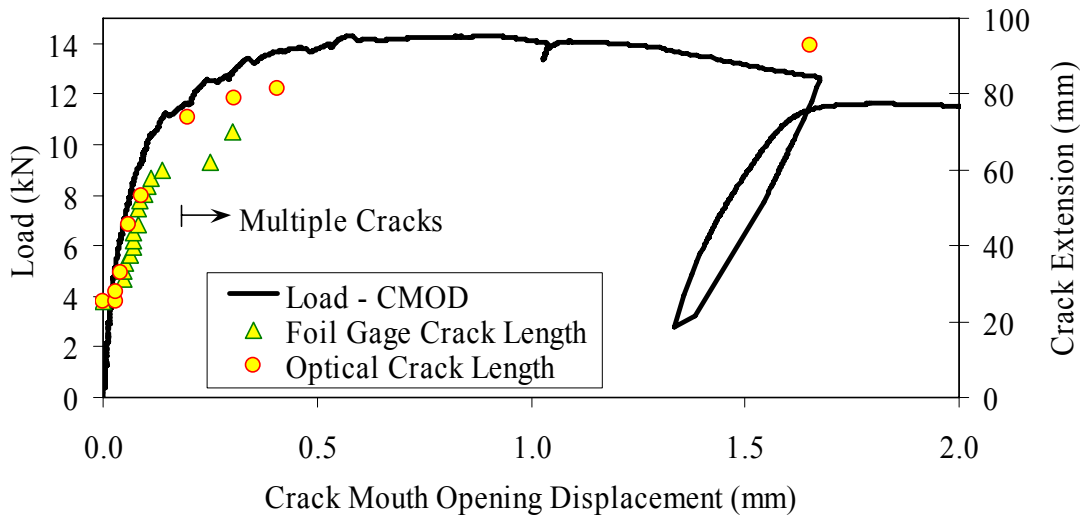
(a) Overall response including periodic unloadings and crack length from tension flange.

1 kN = 0.225 kip
1 mm = 0.039 inch
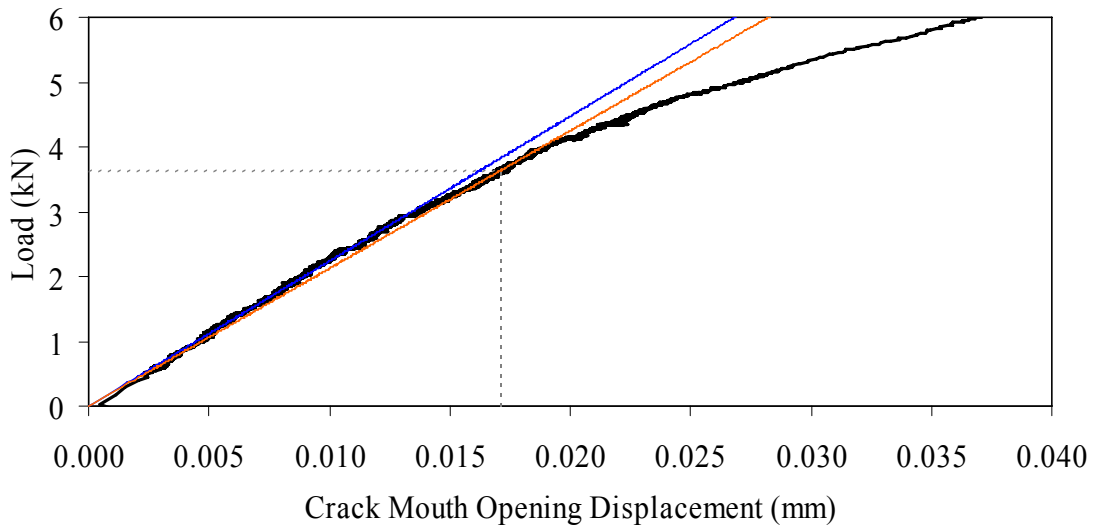
(b) Initial response including elastic stiffness and 95 percent of elastic stiffness curves.

Figure 93. Graph. Load-CMOD response for untreated prism M2P02.

1 kN = 0.225 kip
1 mm = 0.039 inch

(a) Overall response including periodic unloadings and crack length from tension flange.

1 kN = 0.225 kip
1 mm = 0.039 inch

(b) Initial response including elastic stiffness and 95 percent of elastic stiffness curves.

Figure 94. Graph. Load-CMOD response for untreated prism M2P03.

3.6 PENETRATION RESISTANCE TESTING

Penetration resistance testing was completed on early age UHPC to determine the times of initial and final setting. The testing was completed nominally in accordance with the AASHTO T197 standard test method.[47] The primary difference between the T197 test procedure and the one undertaken was that the UHPC was used as cast and was not sieved to obtain a mortar sample. The lack of coarse aggregate and the ease with which a penetration probe could be inserted into fresh UHPC allowed for this change in test procedure.

The T197 penetration resistance test is performed by forcing a flat-headed probe into a sample of fresh concrete. The surface area of the probe and the force required to insert it are used to determine the penetration resistance in psi. Initial setting is defined as when the concrete reaches a penetration resistance of 3.4 MPa (500 psi). Final setting is defined as when the concrete reaches a penetration resistance of 27.6 MPa (4,000 psi). The probe sizes range from 645 mm^2 to 16 mm^2 (1 $inch^2$ to 0.025 $inch^2$). Preliminary testing indicated that the smallest probe could be used to provide consistent results in both the initial and final setting ranges. Additionally, the use of a single probe size eliminates one source of error within the results. For these reasons, the smallest probe was used exclusively in this study.

The penetration testing was performed in conjunction with the compression stress-strain response testing described in section 3.3.2. The requirements of these tests along with the delayed set times inherent in UHPC made the collection of penetration resistance data troublesome. In general, UHPC tends to exhibit virtually no setting for at least 12 hours. Sometime thereafter, the concrete will begin to set and will then quickly reach both initial and final set. This timetable led to the collection of partial penetration resistance results from four different batches of concrete.

Table 23 provides the penetration resistance results. The table indicates the batch from which the penetration resistance specimens came and the subsequent curing action which was applied to all other specimens in that batch. However, it must be reiterated that no curing actions were performed on any of the penetration resistance specimens. These results show that the initial set for this particular UHPC mix design, cast and maintained under laboratory conditions, occurred around 15 hours. The final set occurred a few hours later at approximately 17 hours after casting.

Table 23. Penetration resistance results.

Subsequent Curing Regime	Batch Name	Initial Set (hours)	Final Set (hours)
Steam	N1A	15.25	18 to 20
Untreated	N2A	less than 14.5	16
Tempered Steam	N3A	less than 15	15.75
Delayed Steam	N4A	between 9.5 and 17.5	between 9.5 and 17.5

3.7 SHRINKAGE TESTING

3.7.1 Long-Term Shrinkage Testing

Long-term shrinkage testing of the unrestrained, hardened UHPC was completed according to ASTM C157.[48] Three prisms, 76 mm by 76 mm by 280 mm (3 inches by 3 inches by 11 inches), were cast for each curing regime. Gage studs were cast into the end of each prism so that the length change could be measured according to ASTM C490.[49] After casting, the prisms were kept in a laboratory environment until demolding, which occurred at approximately 22.5 hours. Table 24 shows the demolding time for each curing regime.

Table 24. Long-term shrinkage.

Curing Regime	Premix Age at Casting (days)	Demolding Time (hours)	Ultimate Shrinkage (microstrain)
Steam	105	22.5	766
Untreated	55	22.0	555
Tempered Steam	50	22.0	620
Delayed Steam	47	23.0	657

Each prism had its initial length reading recorded within 30 minutes after demolding. The time of this initial reading was set by the demolding time as shown in table 24 and was not precisely 24 hours as recommend by the specification. The reading also did not capture some of the early age shrinkage of the UHPC, which will be discussed in the following section. All prisms were stored and measured in a temperature and humidity controlled room per the specification except for the duration of any steam-based treatment.

Measurements of the changes in length were recorded on a daily, then weekly, then monthly basis for 1 year. A special emphasis was placed on recording a measurement both before and after any curing treatment was applied to any prism. Figure 95 shows the results of these tests up to 250 days after demolding. After that time, very little change was observed in the recorded values.

Figure 95 also provides best-fit approximations of the shrinkage behavior. The approximating equation, shown in figure 96, is a modification of the equation recommended in ACI 209R-92, where it is recommended that A equal 35.[50] In the research, s_t is the shrinkage at a given time, t is the time in days, s_{ult} is the ultimate shrinkage that the concrete will undergo, and A is a variable defining the shape of the curve.

Figure 95 shows that the prisms that underwent steam or delayed steam treatment exhibited no discernible post-treatment shrinkage. This result corroborates Acker's shrinkage behavior theory presented in chapter 2.[12] In comparison, the untreated and tempered steam-treated prisms show continued shrinkage past 4 months of age. Even so, all the prisms reached at least 95 percent of their ultimate shrinkage by 2 months after demolding. For comparison, the ACI 209R-92

recommended equation indicated that a normal concrete might have reached 60 percent of its ultimate shrinkage at this age.
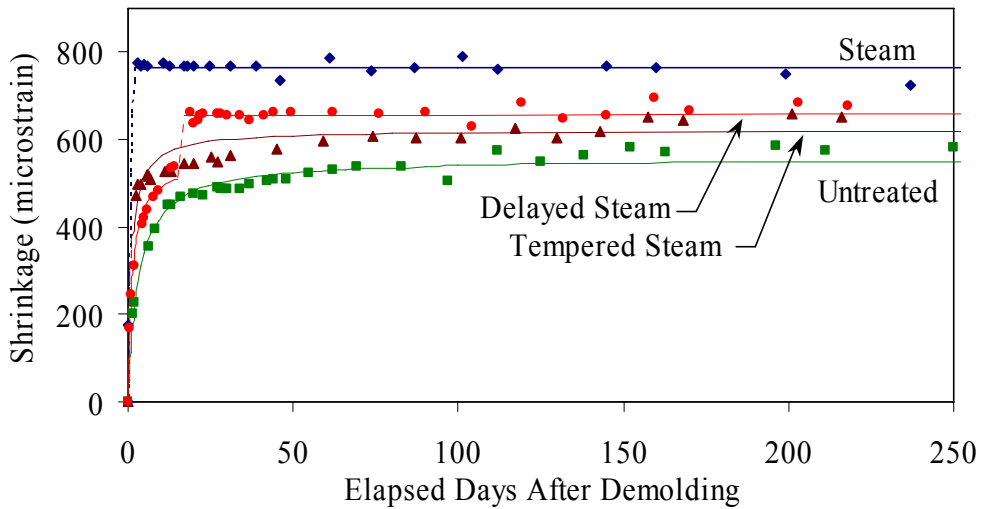
Figure 95. Graph. Long-term shrinkage results.

$$s_t = \frac{t}{A+t} s_{ult}$$

Figure 96. Equation. Shrinkage as a function of time after casting.

3.7.2 Early Age Shrinkage Testing

The results presented in section 3.7.1 show that this concrete can exhibit large, unrestrained shrinkage strains regardless of the curing applied. More importantly, the shrinkage exhibited tends to occur much earlier in the overall behavior than would normally be expected. For these reasons, the ASTM C157 specification and its requirement that the concrete needs to have set prior to the recording of the initial measurement seems ill-suited for determining the full, unrestrained shrinkage behavior of this concrete.

To quantify this early age shrinkage behavior, a test was devised to measure the unrestrained shrinkage of a prism starting at casting. An embedded strain measuring device (Geokon 4202 Vibrating Wire Strain Gage) was cast into the center of a prism. This type of gage, shown in figure 97, measures strain by monitoring the resonant frequency of a wire tensioned between two end blocks that are embedded in the concrete. Aside from the gage embedment, the mixing, casting, and demolding procedures were the same as the ones followed for the long-term shrinkage prisms discussed above. Vibrating wire gages were embedded into one prism that was receiving the steam treatment and into another prism that was subjected to the untreated curing regime. The gages monitored the shrinkage for the first 17 days after casting. After demolding, standard ASTM C490 length change measurements were also recorded for verification purposes.

Figure 97. Photo. Embeddable vibrating wire gage.

Figure 98 shows the unrestrained shrinkage results from these embedded strain gages. The premix for this particular batch was over 150 days old, thus the initial setting was slower and the prisms were demolded at 28 hours. The steam-treated prism was steamed from hours 29 to 77 as shown in the figure, while the untreated prism was maintained in a laboratory environment.
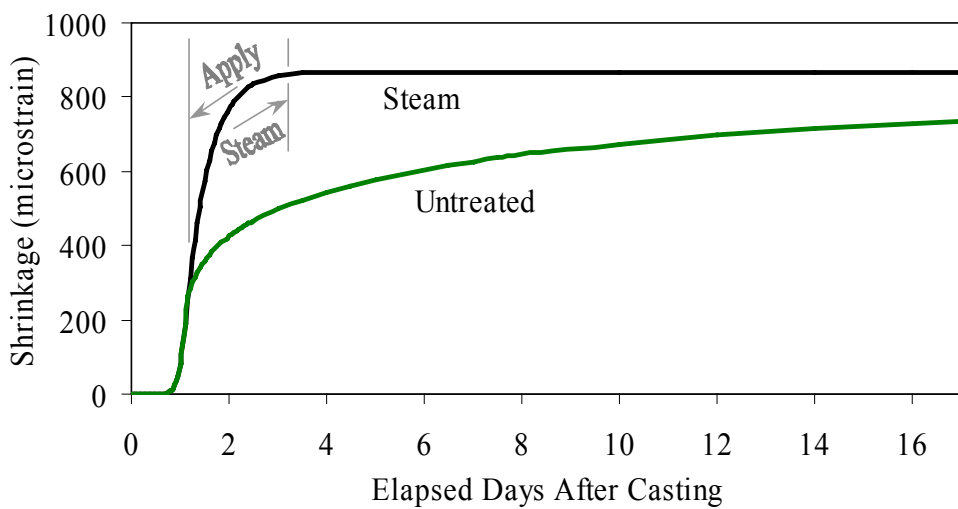
Figure 98. Graph. Early age shrinkage.

The figure shows that this concrete exhibits rapidly occurring, large-value, early age shrinkage. The steam-treated prism reached a total of 850 microstrain, and the untreated prism was continuing to exhibit some shrinkage beyond the 790 microstrain recorded at 40 days after casting. Of greater interest is the rate at which the shrinkage occurs. Table 25 provides shrinkage rates in microstrain per hour that were obtained at discrete times during the early age of these two prisms. In particular, note that the shrinkage rate is over 60 microstrain per hour at 1.18 days, which is just after the prisms are demolded. This high rate of shrinkage soon drops off, but in total over 400 microstrain of shrinkage occurred in the untreated prism in the 24 hours following the 20-hour mark when shrinkage started to occur. For reference, concrete usually has a tensile cracking strain of between 150 and 250 microstrain.

3.8 CREEP TESTING

3.8.1 Long-Term Creep Testing

The long-term compressive creep testing of the UHPC was conducted according to ASTM C512.[51] Four cylinders, 102 mm (4 inches) in diameter by 204 mm (8 inches) long, were cast for each curing regime for these tests. Two additional half-height cylinders were cast for each curing regime to act as loading blocks. All cylinders had their ends ground to within 0.5 degree of parallel. The testing was completed using hydraulically actuated load frames in a room that was controlled for temperature and humidity. No attempt was made to retard moisture gain or loss from the cylinders either prior to or during the test.

Table 25. Early age shrinkage rate.

Elapsed Time Since Casting (days)	Steam Treated Shrinkage Rate (microstrain per hour)	Untreated Shrinkage Rate (microstrain per hour)
0.0	0.0	0.0
0.8	0.0	0.0
1.0	20	20
1.1	36	36
1.2	64	64
1.3	–*	18
1.5	34*	3.5
1.7	11*	3.5
2.0	6.5*	2.9
2.5	2.8*	2.4
3.0	1.2*	0.8
3.5	0.0	0.7
4.5	0.2	1.9
6.0	0.1	1.3
8.0	0.0	0.8
10.0	0.0	0.5

* Prism was undergoing Steam treatment

The four cylinders for each curing regime were instrumented with Whittemore points before being stacked into a load frame. The Whittemore points were attached to each cylinder at three locations around the circumference with a 152-mm (6-inch) nominal gage length. Measurement of the points was completed before loading, immediately after loading, and periodically for 1 year. Figure 99 shows creep cylinders in the load frame as well as the method used to measure the Whittemore points.

The creep testing was initiated for each curing regime after the curing treatment was applied. For the steam and tempered steam cylinders, the creep loading was initiated 4 days after casting. Loading was initiated 21 days after casting for the delayed steam cylinders and 28 days after

casting for the untreated cylinders. The load level applied to each set of cylinders was 77 MPa (11.2 ksi), which is 40 percent of 193 MPa (28 ksi), the anticipated compressive strength of a steam-treated cylinder.
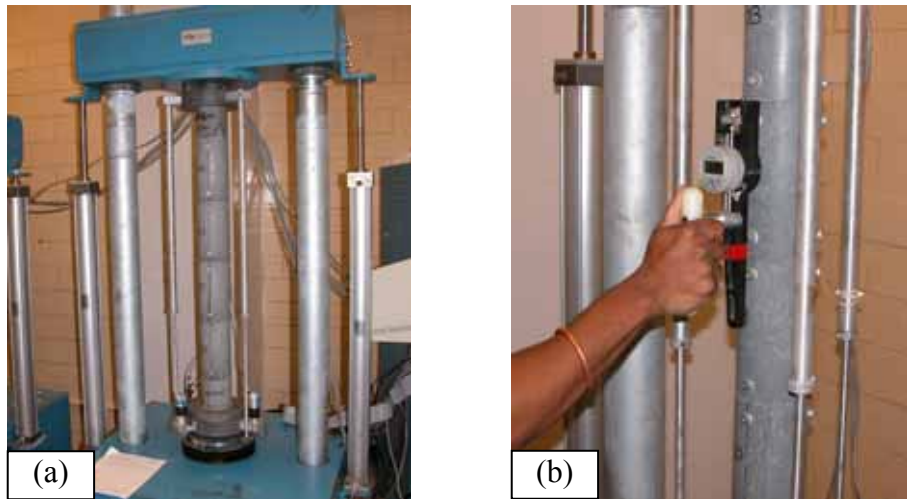
Figure 99. Photos. (a) Creep cylinders in load frame and (b) measurement of creep.

Table 26 provides the creep testing results for the four curing regimes. The 28-day average compressive strength is also shown. Note that in all cases the load applied was in excess of the ASTM recommended load. The initial elastic strain was mechanically measured on the cylinders. The final creep strain is the estimated long-term value that the strain in the cylinders asymptotically approached. Intermediate creep strain values were calculated by subtracting the long-term shrinkage and the initial elastic strain from the overall measured strain. A best-fit approximation, discussed below, allowed for the determination of the final asymptotic value.

Note that the subtraction of the long-term shrinkage from the recorded creep strain assumes that creep and shrinkage are uncoupled behaviors. However, research has indicated that these behaviors are dependent on one another in UHPC.[12] In this research, the shrinkage strain was subtracted from the creep strain for two reasons. First, some of the measured creep strain was necessarily due to shrinkage. Second, the overall shrinkage strains were small or nonexistent, thus the total error introduced was minimal. If the shrinkage strain were not subtracted from the creep strain for the untreated and tempered steam-treated specimens, the creep coefficients would have been less than 10 percent higher.

Table 26. Long-term creep results.

Curing Regime	Control Strength (MPa)	Stress / Strength	Initial Elastic Strain (με)	Final Creep Strain (με)	C_{cu}	δ_{cu} (με/MPa)
Steam	188	0.41	1500	440	0.29	5.7
Untreated	114	0.67	2057	1600	0.78	21.2
Tempered Steam	177	0.43	1670	1100	0.66	14.2
Delayed Steam	168	0.46	1580	485	0.31	6.4

1 MPa = 145 psi

The creep coefficient, C_{cu}, is defined as the final asymptotic amount of additional creep strain that occurs over time divided by the initial elastic strain that occurs when load is first applied. The specific creep, δ_{cu}, is defined as the creep coefficient divided by the elastic modulus of the concrete. For reference, creep coefficients for concrete are normally in the range of 1.5 to 3.0, and specific creep values normally range from 35 to 145 microstrain per MPa.

Recall the discussion in section 2.4.3 regarding the creep and shrinkage of UHPC. The results presented here correlate well with that discussion in that steam and delayed steam-treated UHPC exhibit extremely low creep coefficients, while the tempered steam-treated and untreated UHPC exhibits higher creep coefficients. Specifically, note that the delayed and tempered steam specimens had similar compressive strengths and load levels, but that the tempered steam exhibited more than twice as much creep strain. The more severe steam treatments should cause more rapid and more complete self-desiccation of the UHPC, thus leading to less creep of the concrete.

A plot of the creep data acquired during the year of testing is shown in figure 100. The creep strain shown is the additional strain observed after the initial loading of the cylinders. The data presented are the average results from the four cylinders in each curing regime. The figure also includes best-fit approximations for each dataset. The best-fit curves are based on the equation shown in figure 101, wherein t is the time in days since load initiation, ε_{ct} is the creep strain at that time, and A and B are variables that define the shape of the curve. This equation is loosely based on a creep equation suggested by Branson.[52]

3.8.2 Early Age High-Stress Creep Testing

A test program was initiated to investigate the dimensional stability of UHPC that was subjected to compression loading early in its strength gain. This test program was designed to answer questions related to the delay required prior to stressing a prestressed UHPC girder. Although the rapid-strength gain of UHPC is beneficial with regard to the stressing of a girder, it is important to know what portion of that strength gain is actually useable.

Short-term creep tests were conducted on UHPC cylinders that were of moderate compressive strength. Two strength levels were investigated: 59 and 86 MPa (8.5 and 12.5 ksi). Within one batch of UHPC, 102-mm (4-inch) diameter cylinders were cast for creep tests and 76-mm

(3-inch) diameter cylinders were cast to determine the concurrent compressive strength of the UHPC. The specimen preparation procedures for the creep cylinders mimicked the procedures that were followed for the ASTM C39 compression tests that were previously discussed, including sulfur capping of the cylinder ends due to the relatively low compressive strengths.
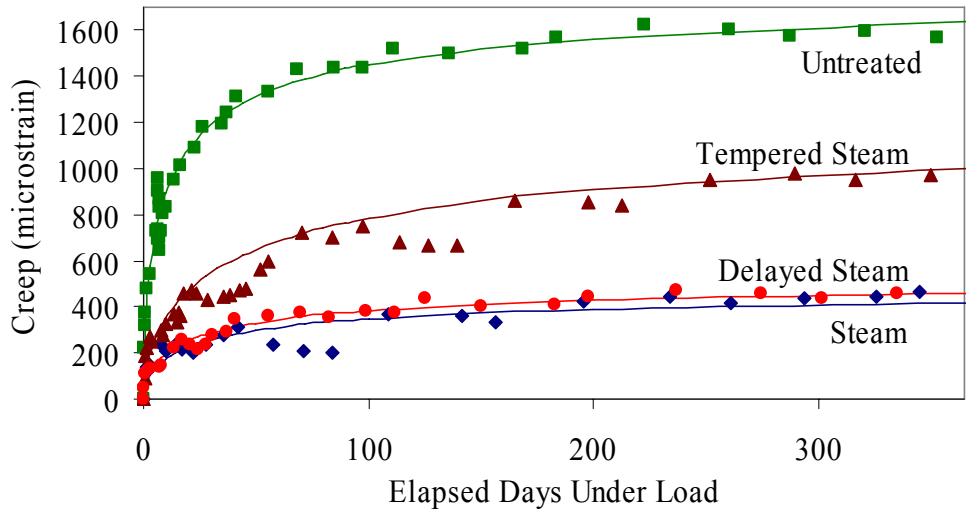
Figure 100. Graph. Long-term creep results.

$$\varepsilon_{ct} = \frac{t^{0.6}}{A + t^{0.6}} B$$

Figure 101. Equation. Creep as a function of time after loading.

The creep testing was completed in a 445-kN (100-kip) capacity MTS testing machine. Each cylinder rested one end on a flat steel bearing and was loaded through the other end by a spherical bearing. Each cylinder was loaded at a computer-controlled constant load rate of 1.0 MPa/s (150 psi/s) until the desired compressive load level was reached. This load level was then maintained for 30 minutes, after which the load was removed at 1.0 MPa/s (150 psi/s). The deformation of the cylinder was monitored throughout the test via three LVDTs that were mounted on two parallel rings attached to the cylinders. This deformation measurement system was the same as the one used in the elastic modulus testing (previously discussed in section 3.3.2). A photograph of the test setup is provided in figure 102.

The early age creep results are presented in table 27. The table provides the cylinder identifier, the compressive test at the time of creep testing based on concurrently tested 76-mm (3-inch) diameter cylinders, and the stress level maintained during the creep test. The stress levels tested ranged from 60 percent of the compressive strength to just over 90 percent.
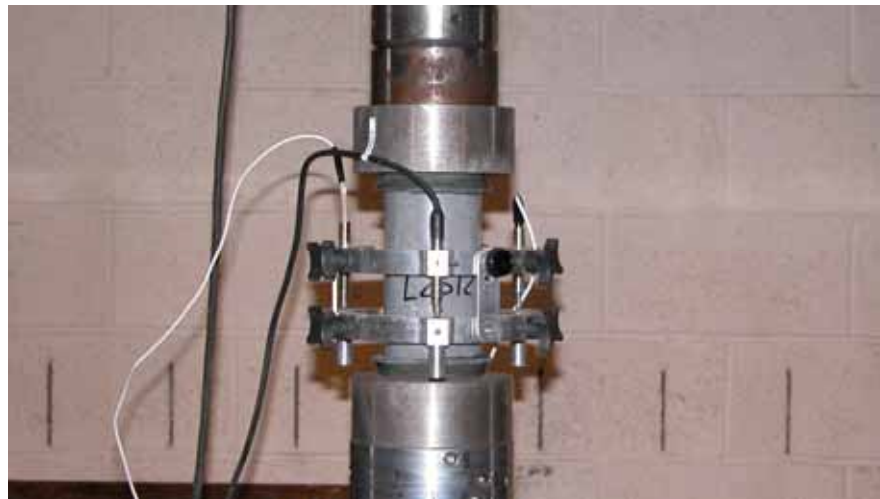
Figure 102. Photo. Short-term creep test setup.

Table 27. Early age creep results.

Cylinder Identifier	Compressive Strength (MPa)	Applied Stress (MPa)	Stress / Strength	$C_{c\text{-}30}$
55 to 65 MPa Compressive Strength				
A1	65	39	0.60	0.42
A2	59	44	0.75	0.66
A3	64	54	0.84	0.79
A4	55	49	0.88	0.80
83 to 90 MPa Compressive Strength				
B1	86	52	0.60	0.32
B2	84	61	0.72	0.39
B3	84	65	0.77	0.44
B4	84	70	0.83	0.52
B5	88	75	0.85	0.85
Failed Under Load				
A5	66	59	0.91	N/A
B6	84	77	0.92	N/A

1 MPa = 145 psi

Table 27 lists the 30-minute creep coefficient, $C_{c\text{-}30}$, for each of the cylinders that was able to carry the load through the end of the test. This creep coefficient is similar to the standard creep coefficient, except that here it equals the amount of additional creep strain that occurred during the 30 minutes divided by the initial elastic strain when the constant load level was reached. The two cylinders loaded to stress levels above 90 percent of the compressive strength both failed, and thus no value of $C_{c\text{-}30}$ is listed.

Figures 103 and 104 show plots of the results of these tests. The observed strain values have been normalized on the strain when the constant stress level is first reached. In this way, the effect of stress level on early age creep is clearly visible. At both strength levels, stressing to above 85 percent causes twice the creep strain to occur, and stressing above 90 percent caused failure. Even stressing to only 60 percent caused a significant amount of creep strain to accumulate in a short time.
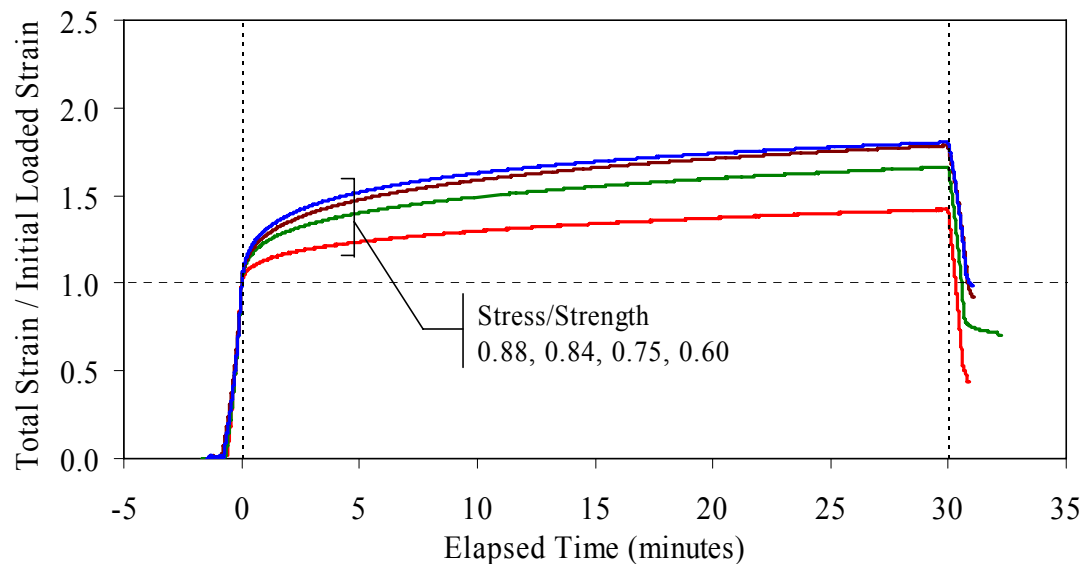
Figure 103. Graph. Early age creep behavior of 55 to 65 MPa (8.0 to 9.5 ksi) UHPC.
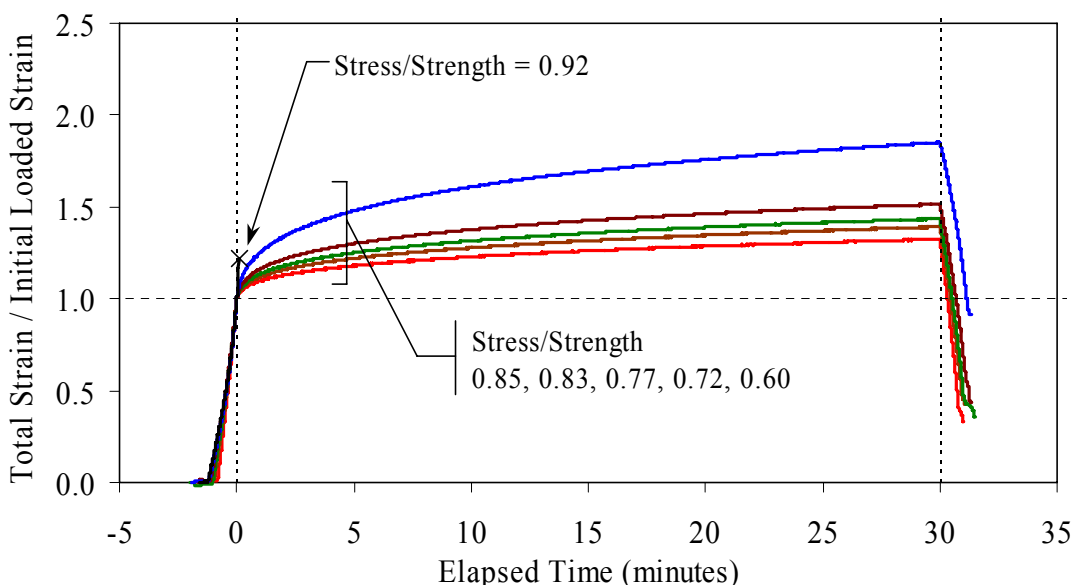
Figure 104. Graph. Early age creep behavior of 86 MPa (12.5 ksi) UHPC.

115

3.9 COEFFICIENT OF THERMAL EXPANSION

The coefficient of thermal expansion of UHPC was measured through the use of the provisional AASHTO test specification, TP60-00.[53] The test method determines the coefficient of thermal expansion (CTE) by measuring the length change of a concrete cylinder in a variable temperature water bath. Three 102-mm (4-inch) diameter UHPC cylinders from each of the four curing regimes were tested.

Normally, the degree of water saturation of a concrete will influence its CTE. To counteract this fact, the test method requires that the concrete needs to be in a saturated condition before testing. In the current testing of UHPC, the saturation of the cylinders before testing was considered to be detrimental to the final results for two reasons. First, one of the primary variables in the overall test program is the curing condition of the UHPC at the time of testing. Saturating the UHPC would change the condition of the UHPC by introducing more water into the matrix, which could then react with unhydrated cement. Second, because saturation of the UHPC is problematic due to its low permeability, determining when a specific degree of saturation was reached would be difficult. Thus, the exterior surfaces of the cylinders, aside from the bearing points of the supports and LVDT, were sealed with epoxy before testing.

The testing of the 12 cylinders was completed after they had undergone their complete curing treatment. All the cylinders were at least 2 months old. The untreated cylinders were the oldest at 4.5 months at the time of testing.

The results from the CTE testing are shown in table 28. In general, the CTE of UHPC is around 15×10^{-6} mm/mm/°Celsius (C) (8.3×10^{-6} inch/inch/°Fahrenheit (F)). This value is somewhat higher than the normally expected value for concrete of around 10×10^{-6} mm/mm/°C (5.6×10^{-6} inch/inch/°F). However, recall that UHPC contains both high cement content and no coarse aggregate. Hydrated Portland cement paste has been reported to have a CTE of between 11×10^{-6} and 16×10^{-6} mm/mm/°C (6.1×10^{-6} and 8.9×10^{-6} inch/inch/°F), and aggregates tend to exhibit lower CTE values.[54]

Table 28. Coefficient of thermal expansion results.

Curing Regime	Coefficient of Thermal Expansion			
	Results ($\times 10^{-6}$ mm/mm/°C)	No.	Average ($\times 10^{-6}$ mm/mm/°C)	Standard Deviation ($\times 10^{-6}$ mm/mm/°C)
Steam	15.3, 15.7, 15.8	3	15.6	0.3
Untreated	14.4, 14.6, 15.1	3	14.7	0.4
Tempered Steam	15.0, 15.5, 15.8	3	15.4	0.4
Delayed Steam	15.0, 15.2, 15.5	3	15.2	0.3

1 mm/mm/°C = 1.8 inches/inches/°F

3.10 HEAT OF HYDRATION

The amount of heat that UHPC generates during initial curing is of interest for two reasons: (1) it can be used as an indicator of other behaviors and (2) it could cause detrimental behaviors if not accounted for in the design. Time-temperature data were gathered for 15.24-cm (6-inch) diameter cylinders during the first few days after casting. This testing was completed on two UHPC mixes. The first mix was the standard UHPC mix that has been discussed throughout this report. The second mix included a slight modification of the mix design in that no accelerator was added. Specifically, 30.0 kg/m^3 (1.87 lb/ft^3) of Rheocrete CNI was eliminated from the mix, and an extra 32.0 kg/m^3 (2.00 lb/ft^3) of water was added.

The time-temperature results were collected for cylinders in three environments. Figure 105 shows the heat that was generated by cylinders in a normal laboratory environment. These results indicate that the accelerator can have a significant effect on set time, but that the overall level of heat generation is not significantly different. Figure 106 shows the heat that was generated by cylinders that were kept in a normal laboratory environment until setting began, after which the steam treatment was applied. Again, the accelerator's primary impact seems to be in the rate of setting and not in the peak heat generated. Note that the steam treatment of the accelerated mix was started earlier in the setting behavior, thus impacting the comparative level of the peak temperatures recorded.

°F = 1.8 (°C) + 32
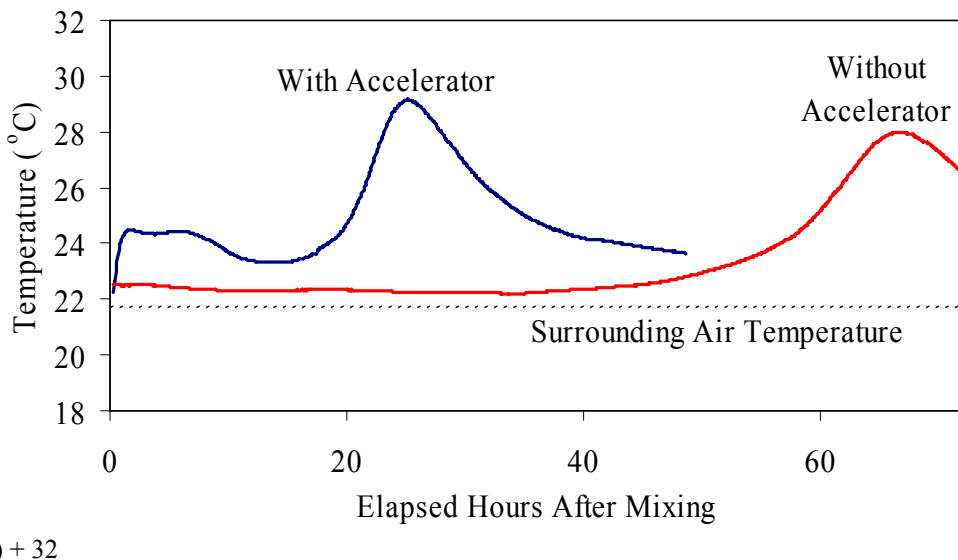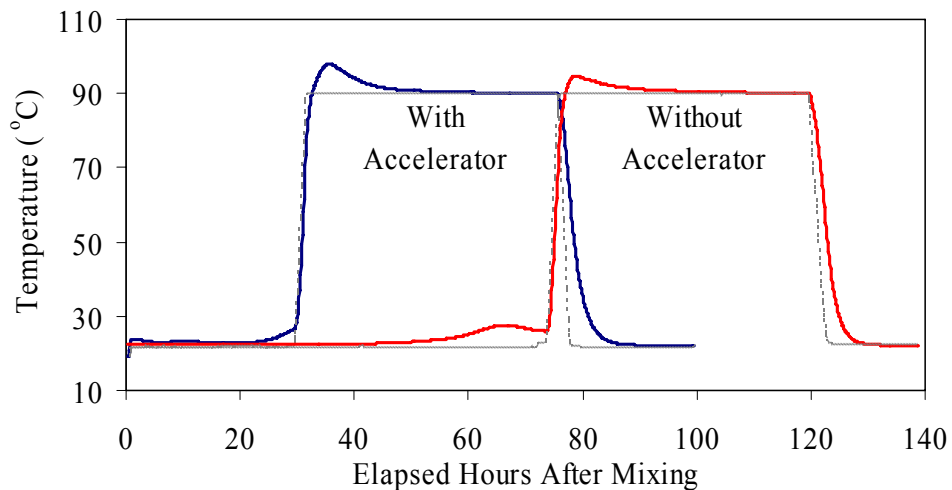
**Figure 105. Graph. Heat generated in 152-mm (6-inch) diameter
cylinders during initial curing.**
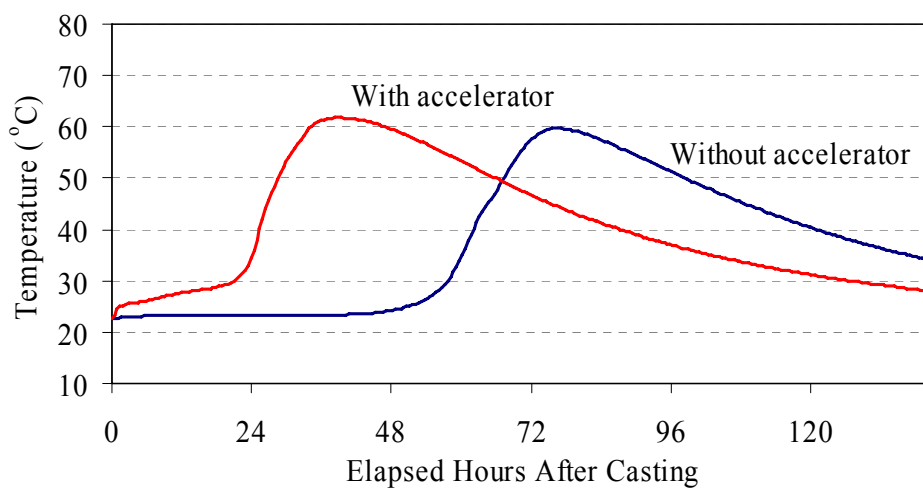
The difficulty with the previously discussed methods of measuring the heat generated by the UHPC is that local conditions within a laboratory environment can vary. Air currents that aid in the dissipation of heat can have a significant impact on final results. To address this issue, time-temperature data were also collected using a well-insulated calorimeter. For these tests, each 152-mm (6-inch) diameter cylinder was placed in a Quadrel iQdrum[TM] heat signature calorimeter and monitored for 6 days. The results are shown in Figure 107. Through the use of the

calorimeter, the effect of the accelerator becomes very clear. The accelerator causes a slow temperature rise to occur before setting and caused setting to begin over 1 day earlier. Heat was generated more quickly during setting, but the peak temperature reached by the cylinder was only 3 ℃ (5.4 ℉) higher than in the unaccelerated mix. Note that these relative changes between mix designs are instructive; however, the actual time-temperature and setting behaviors of any UHPC mix will depend on many other factors as well (i.e., age of premix, precise environmental conditions, quantity of accelerator).

°F = 1.8 (°C) + 32

Figure 106. Graph. Heat generated in 152-mm (6-inch) diameter cylinders from casting through steaming.

°F = 1.8 (°C) + 32

Figure 107. Graph. Heat signature for 152-mm (6-inch) diameter cylinders in a well-insulated calorimeter.

118

3.11 AIR VOID ANALYSIS

An air void analysis was completed on the UHPC. The modified point-count method of ASTM C457 was used to determine the air void structure.[55] The variables investigated in this testing included the effect of the analysis location within individual cast cylinders, the effect of the time a cylinder was held on a vibrating table after casting, the effect of mix stiffness, and the effect of using an accelerator in the mix design.

The casting procedure was as follows. The UHPC was mixed as usual, following the normal mix design and procedure, except that an unaccelerated mix (as described in section 3.2) was included. The UHPC was then cast into 152-mm (4-inch) diameter plastic cylinder molds. The filling of the molds differed from the usual procedure in that some of the molds were filled without using the vibrating table while others were filled on the vibrating table and were then held in place on the table for a specific length of time. After casting, the cylinders were screeded, covered in plastic, and left in a laboratory environment to set.

The preparation and testing of the cylinders for the air void structure analysis was as follows. After setting, the cylinders were cut in half lengthwise. One of the two halves was then polished using up to 800-grit sandpaper. Each cylinder's half was then divided into a top and bottom section on its flat face. Modified point-count measurements were then completed on each of these sections. Because this UHPC did not contain any coarse aggregate, the fibers were counted as coarse aggregate within the data collection procedure. In total, each air void data collection set covered an area of 6,770 mm^2 (10.5 inches^2) and traversed a length of 1,270 mm (50 inches) while counting 1,429 points.

The results from these tests are presented in table 29. The results are grouped into sets for each of the three mixes tested. For reference, the stiff mix has a flow table reading of 165 mm (6.5 inches) after 20 impacts, and the normal flow mixes both have readings of 190 mm (7.5 inches) after 20 impacts. Each pair of rows shown with a common vibrating table time is the top and bottom results from the same cylinder half.

Although some slight differences were observed in various groupings of specimens, the limited sample set makes drawing specific conclusions difficult. In general, the air content across the range of mixes and specimen locations was approximately 6.5 percent. The bottom of the cylinders tended to have slightly more air, likely due to air in the top of the cylinders being removed by vibration. The cylinders that were held on the vibrating table for 300 seconds after filling also tended to have a decrease in air content. The stiffer mix tended to have slightly less air than the more flowable mix, and the results of the accelerated and unaccelerated mixes had no clear differences.

3.12 STEEL FIBER DISPERSION TESTING

Dispersion of fibers throughout UHPC is a necessary part of achieving many of its material properties. In this section, a simple set of tests is described in which the dispersion of fiber throughout UHPC cylinders was measured. This batch of UHPC, L03, exhibited a relatively fluid rheology with a flow table result after 20 impacts of 235 mm (9.25 inches).
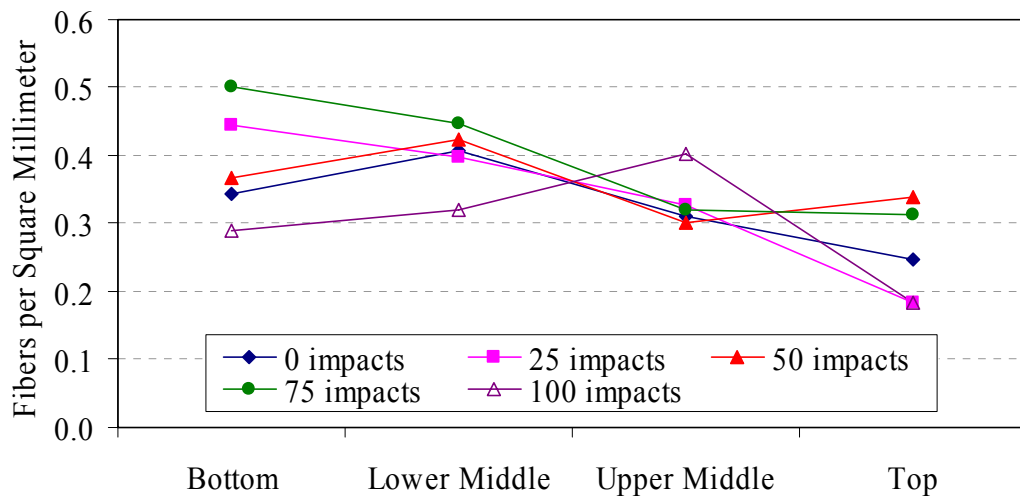
Table 29. Air void analysis results.

Vibration Table Time (seconds)	Location	Air (%)	Paste (%)	Fine Agg. (%)	Fiber (%)	Voids Counted	Mean Chord Length (mm)	Voids per mm	Specific Surface (mm²/mm³)	Spacing Factor (mm)
Stiff Mix w/ Accelerator (M1J)										
0	Top	5.7	47.2	43.3	3.8	249	0.29	0.20	13.8	0.43
0	Bottom	6.2	51.2	38.8	3.8	267	0.29	0.21	13.7	0.43
Fill + 20	Top	5.5	36.4	55.1	3.0	274	0.26	0.22	15.6	0.33
Fill + 20	Bottom	6.9	30.7	59.5	3.0	257	0.34	0.20	11.8	0.38
Fill + 60	Top	6.7	43.2	47.0	3.0	289	0.29	0.23	13.5	0.38
Fill + 60	Bottom	7.4	42.4	47.2	3.0	287	0.33	0.22	12.2	0.41
Fill + 300	Top	6.5	31.5	59.8	2.2	233	0.36	0.19	11.3	0.41
Fill + 300	Bottom	4.7	25.1	66.3	3.9	221	0.27	0.17	14.8	0.33
Normal Flow Mix w/ Accelerator (M1JxxA)										
0	Top	6.2	43.7	48.0	2.1	282	0.28	0.22	14.3	0.38
0	Bottom	7.1	44.7	46.9	1.3	302	0.30	0.24	13.3	0.38
Fill + 20	Top	6.4	45.8	46.5	1.4	291	0.28	0.23	14.4	0.38
Fill + 20	Bottom	7.6	44.0	46.9	1.5	385	0.25	0.30	15.9	0.30
Fill + 60	Top	7.8	29.9	60.8	2.0	349	0.28	0.28	14.1	0.28
Fill + 60	Bottom	9.2	27.6	61.1	2.1	375	0.31	0.30	12.9	0.23
Fill + 300	Top	6.9	42.2	49.3	1.5	234	0.38	0.19	10.6	0.48
Fill + 300	Bottom	6.1	41.5	50.9	1.5	218	0.36	0.17	11.3	0.48
Normal Flow Mix w/o Accelerator (M1K)										
0	Top	6.3	49.0	41.1	3.6	281	0.28	0.22	14.1	0.41
0	Bottom	7.3	48.1	41.9	2.7	251	0.37	0.20	10.9	0.48
Fill + 20	Top	6.7	43.0	47.9	2.4	244	0.35	0.19	11.5	0.46
Fill + 20	Bottom	4.8	39.2	51.8	4.2	207	0.30	0.16	13.5	0.43
Fill + 60	Top	7.5	49.5	39.7	3.3	233	0.41	0.19	9.8	0.53
Fill + 60	Bottom	7.2	49.6	39.7	3.4	285	0.32	0.22	12.4	0.43
Fill + 300	Top	3.2	44.0	50.5	2.2	107	0.38	0.08	10.5	0.69
Fill + 300	Bottom	4.6	42.8	50.0	2.6	151	0.39	0.12	10.3	0.56

1 mm = 0.039 inch, 1 mm²/mm³ = 25.4 inches²/inches³

The 76-mm (3-inch) diameter cylinders for these tests were cast without the use of a vibrating table, and some of the cylinders were then impacted on an ASTM C230 flow table.[56] After the cylinders had gained sufficient strength, they were cut in half along their length. Four 645-mm^2 (1-inch^2) areas were then marked on the flat face of the cylinders. The delineated areas were located in a line along the length of the cylinder at a 12.7-mm (0.5-inch) spacing. The fibers contained within each area were then counted.

Five cylinders were tested according to this procedure. Each of these cylinders underwent a different number of impacts on the flow table, ranging from 0 to 100. The fiber counting results are presented in figure 108. The results seem to indicate that more fibers tend to be located toward the bottom of each cylinder. Whether this result is caused by the impacts administered on the flow table or is an artifact of the method used to pour the UHPC into the cylinder molds is not clear.

1 mm^2 = 0.002 inch^2

Figure 108. Graph. Fiber dispersion analysis results for cylinders impacted on an ASTM C230 flow table.

Of greater importance is the wide range of fiber concentrations evident throughout the five cylinders. Figure 109 shows the four areas measured on the cylinder that underwent 25 impacts. One green dot has been placed on the head of each individual fiber. Clearly, casting technique is very important if equal dispersion of fibers throughout the mix is desired.

3.13 DURABILITY TESTING

A series of durability tests were conducted to determine the resistance of UHPC to various environmental aggressors. These tests included measurement of the chloride ion penetrability, scaling and freeze-thaw resistance, abrasion resistance, and alkali-silica reaction susceptibility. The results are detailed throughout this section.

(a)	(b)	(c)	(d)
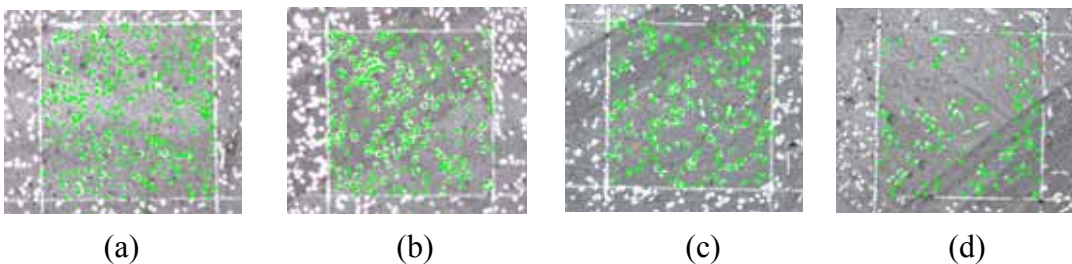
Figure 109. Photos. Fiber dispersion analysis photographs for a 645-mm^2 (1-inch^2) area in the (a) bottom, (b) lower middle, (c) upper middle, and (d) top of a cast cylinder.
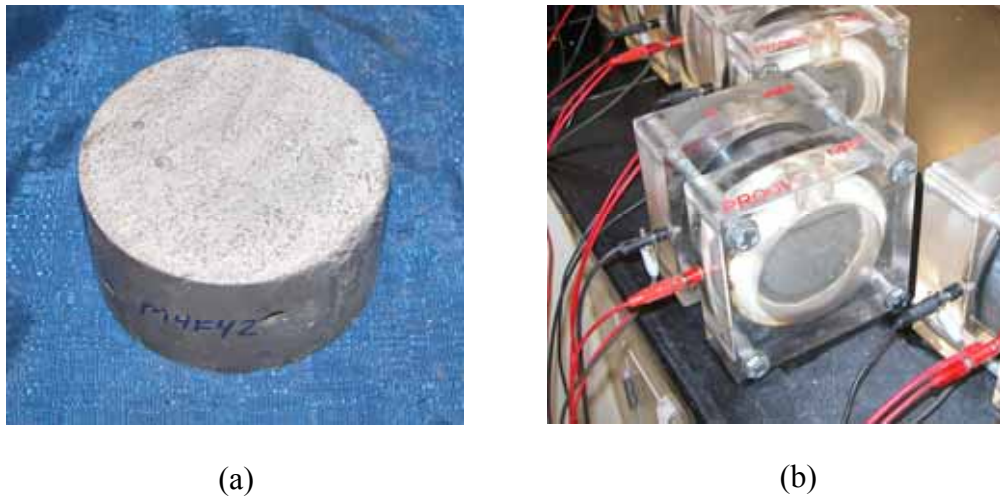
3.13.1 Rapid Chloride Ion Penetrability Testing

The ability of concrete to resist ingress of chloride ions can result in a significantly more durable concrete. The ASTM C1202 test for the Electrical Indication of Concrete's Ability to Resist Chloride Ion Penetration.[57] frequently referred to as the rapid chloride ion penetrability test, was conducted on specimens from the four UHPC curing regimes. This test approximates the resistance that a concrete may exhibit to chloride ion penetration by measuring the amount of electrical current that passes through a 51-mm (2-inch) thick slice of concrete over 6 hours. A 60-volt direct current (DC) potential is applied across the slice of a 102-mm (4-inch) diameter cylinder, while a sodium chloride solution is applied to one side of the slice, and a sodium hydroxide solution is applied to the other side.

Figure 110 shows a cylinder slice before being tested and while a test is in progress. The cylinders were cast and cured following normal procedures. For these tests, each cylinder was cast in a 102-mm (4-inch) diameter mold that was filled to 76 mm (3 inches). After both demolding and the application of any curing treatment, the cylinders were cut to length, and both ends of the cylinder were then ground to create a uniform finish. The outside circumference of each cylinder was sealed with epoxy. The standard amount of steel fiber reinforcement was included in all cylinders. The short, discontinuous nature of the steel fibers in the UHPC matrix allowed for this test to be completed without shortening the circuit or generating significant heat in the ponded fluids.

Results from these tests are presented in table 30. Three tests were performed for each curing regime at 28 days after casting. An additional three tests were performed on the untreated and tempered steam-treated regimes at 56 days, because these regimes had exhibited slightly higher results during the first tests.

Aside from the untreated tests from 28 days, all of the results are in the negligible range as defined by ASTM C1202. Also, the untreated and tempered steam-treated regimes exhibited significant reductions in charge passed between 28 and 56 days. Figure 111 shows averaged results for current versus time from three sets of cylinders. For reference, if 0.003 amps of current were passed through the concrete for the duration of the test, then the total charge passed would be 65 coulombs.

<center>(a)   (b)</center>

Figure 110. Photos. (a) Cylinder and (b) setup for rapid chloride ion penetrability test.

Table 30. Rapid chloride ion penetrability results.

Curing Regime	Age (days)	No.	Coulombs Passed		Chloride Ion Penetrability
			Average	Standard Deviation	
Steam	28	3	18	1	Negligible
Untreated	28	2	360	2	Very Low
Untreated	56	3	76	18	Negligible
Tempered Steam	28	3	39	1	Negligible
Tempered Steam	56	3	26	4	Negligible
Delayed Steam	28	3	18	5	Negligible

3.13.2 Chloride Penetration

In conjunction with the chloride ion tests described in section 3.13.1, standard chloride ion penetration testing was conducted according to the AASHTO T259 specification.[58] This test, often referred to as the chloride ponding test, entails ponding a 3-percent sodium chloride solution on the surface of the concrete for 90 days. After 90 days, the level of migration of chloride ions into the concrete is determined.

This test was conducted on three specimens from each of the curing regimes. The specimens were cast in 102-mm (4-inch) diameter steel cylinder molds that were filled at least 76 mm (3 inches) full during casting. After both demolding and the application of any curing treatment, the circumferential surface of each cylinder was coated in epoxy. A section of rubber hose was then slid over the cast face end of the cylinder and affixed with a hose clamp. Finally, 28 days after casting, the sodium chloride solution ponded on the cylinder face. Note that the solution was ponded on the steel mold cast face of the cylinder to replicate the UHPC surface that would have been achieved in a precast concrete production facility.

<center>123</center>
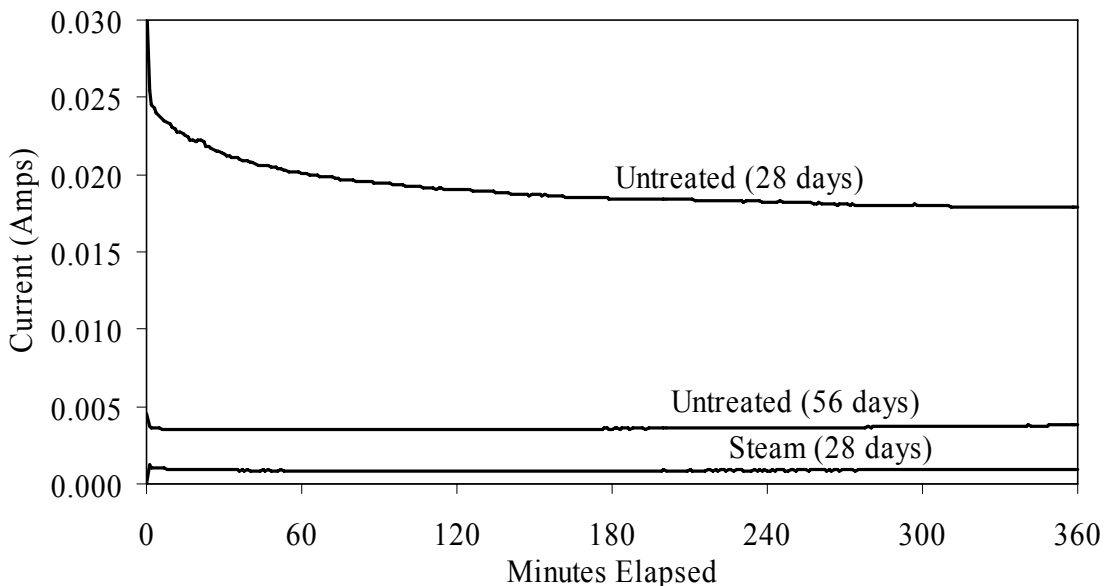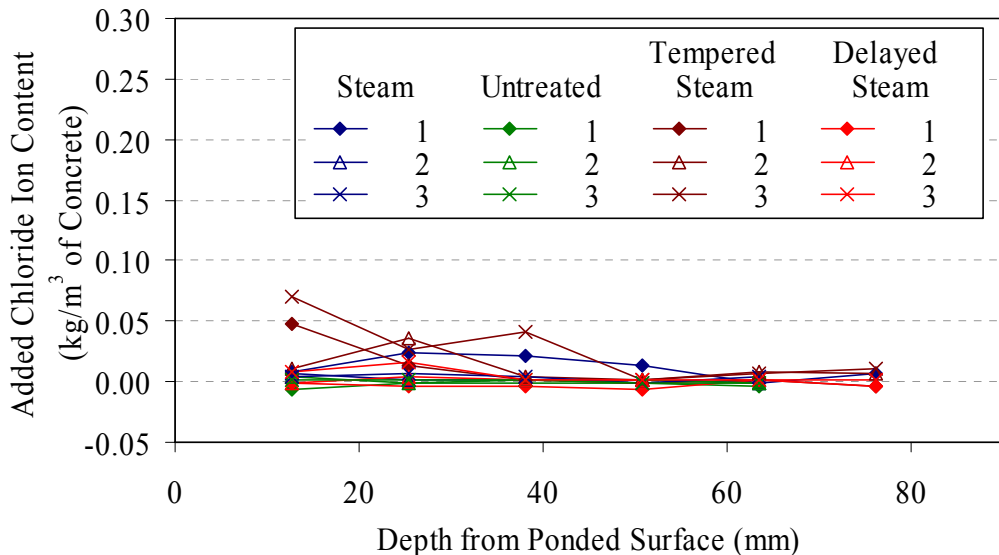
Figure 111. Graph. Average current passed versus time results for three sets of cylinders.

The AASHTO T260 standard test method was used to sample and test the concrete following the ponding.[59] Samples were taken from each cylinder at depths of 13, 25, 38, 51, 64, and 76 mm (0.5, 1.0, 1.5, 2.0, 2.5, and 3.0 inches) from the ponded surface. The samples were obtained by using a drill press with a 6.3-mm (¼-inch) masonry bit to drill into the side of the cylinder at the correct depth. Approximately 15 grams of the pulverized concrete were captured at each specified depth. The steel fiber shavings were then magnetically removed from each sample of the concrete powder. Thus, at least 10 grams of powder were available for the chloride ion testing.

The chloride ion testing was conducted according to Procedure A, Section 5.2: Procedure for Total Chloride Ion Content. The chlorides were unlikely to penetrate any significant distance into the concrete because of the penetrability of this concrete. This allowed a large collection of background chloride content samples to be obtained at 64 and 76 mm (2.5 and 3.0 inches). The average background chloride ion content in kg/m^3 of concrete was determined to be 0.051 with a standard deviation of 0.004.

Figure 112 presents the corrected results for these tests. The removal of the background chloride content from each sample caused some of the samples to seem to exhibit negative chloride ion contents. The AASHTO specification indicates that these results should be rounded up to zero. Overall, the chloride ion content in the UHPC for all of the curing regimes is extremely low. There is some trend toward higher chloride ion contents near the ponded surface; however, the amount of chlorides that migrated into the concrete over 90 days is still extremely small.

1 kg/m3 = 1.686 lb/yd³, 1 mm = 0.039 inch

Figure 112. Graph. Chloride ion content results after 90 days of ponding.

An additional benefit of this set of tests is that the behavior of the surface of this steel fiber-reinforced UHPC can be qualitatively observed. Figure 113 shows a tempered steam-treated cylinder just before the 90 days of ponding began and 1 day after it concluded. This specimen is representative of all 12 tests that were completed because minor corrosion of steel fibers on and very close to the surface occurred. This corrosion would probably more aptly be described as surface staining caused by exposed fibers. There was no indication that the corrosion of the fibers was progressing into the interior of the UHPC.

(a)   (b)

Figure 113. Photos. (a) Cylinder before and (b) after 90 days of chloride ponding.

3.13.3 Scaling Resistance

The UHPC scaling resistance to deicing chemicals was evaluated through the use of the ASTM C672 standard test method.[60] In this test method, a solution of calcium chloride is ponded on the

125

surface of the concrete. The concrete specimen is then placed in a −18 ºC (−0.4 ºF) freezing environment for 18 hours followed by a 23 ºC (73.4 ºF) thawing environment for 6 hours. This cycle is repeated daily, while ensuring periodically that the surface of the specimen remains covered in the ponding solution.

The ASTM C672 testing included two slabs from each curing regime. Each slab was cast in a 356-mm by 356-mm (14-inch by 14-inch) square steel mold that was 76 mm (3 inches) deep. The cast surface on the bottom of the slab became the surface to be ponded after demolding. The curing treatments were applied to the slabs, and then the dams were epoxied to the ponding surface. The dams were composed of steam-treated UHPC. A rapid-setting, two-part epoxy was used as the bonding agent slab and the dam. Figure 114 shows one of the slabs before testing was initiated. The total exposed ponding area on the surface of each slab was approximately 0.065 m^2 (100 inches^2).

The testing of these slabs commenced in two phases. In the first phase, a walk-in freezer was used to generate the freezing condition, while the standard laboratory environment generated the thawing environment. The capabilities of this freezer were such that a consistent temperature could not be maintained. Over the course of 4 months, 70 cycles were completed. Up through cycle 50, the temperature in the freezer was usually below −9 ºC (15.8 ºF). For the next 20 cycles, the temperature was usually in between −8 and −3 ºC (17.6 and 26.6 ºF). Due to the inability of this freezer to maintain a sufficiently cold temperature, this phase of the testing was halted. At the cessation of these tests, no scaling was observed on the surface of any of the slabs.

Figure 114. Photo. Scaling slab before initiating ASTM C672 testing.

The second phase of the ASTM C672 testing used an environmental chamber to carefully control the freezing and thawing portions of each cycle to within ±1.67 ºC (±3 ºF) of the prescribed values. A total of 145 additional cycles were completed on all eight slabs. Every few cycles, the slabs were checked for leaking of the dams and for the proper solution level on the ponded surface. The slabs were also drained, flushed, inspected, and refilled after cycles 20 and 50. No

126

scaling was observed. After cycle 145, the slabs were drained through a #30 sieve to capture any small scaling particles that might have been present. Each slab produced less than 0.5 grams (0.02 ounces) of material, which included small bits of concrete, pieces of epoxy, and other small detritus that had made its way onto the slabs over the course of 95 cycles.

A final inspection of the ponded surface indicated that no scaling had occurred, thus an ASTM C672 surface condition rating of 0 was warranted. No differences were observed between the slabs from any of the four curing regimes. The surfaces did tend to show a slightly rougher texture after testing, with many more of the small air bubbles visible just under the ponded surface. Figure 115 shows the same slab that was pictured in figure 114 after having undergone the 70-plus-145 cycles of scaling as described above.
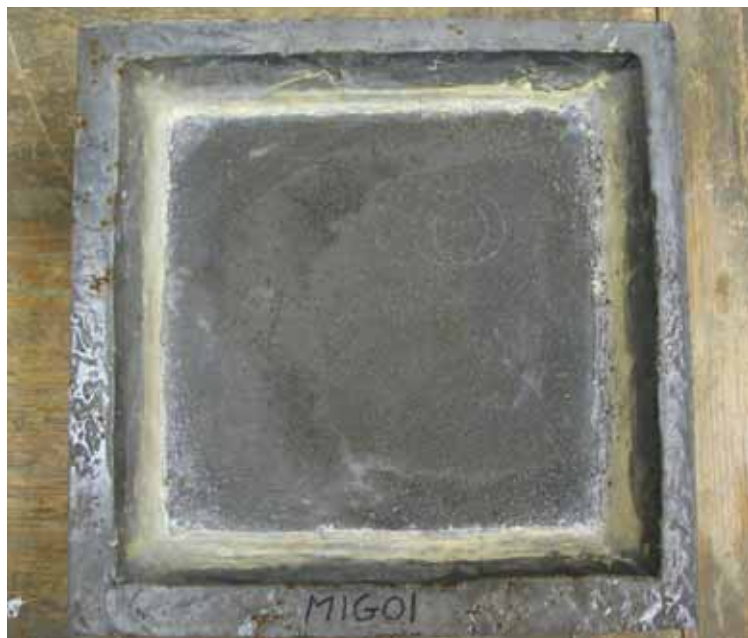
Figure 115. Photo. Scaling slab after ASTM C672 testing.

Figure 116 shows a byproduct of the ASTM C672 scaling tests. Some of the dams on top of the slabs did not seal properly with the slab surface. At the joint, the calcium chloride solution slowly leaked out and ran down the side of the slab. This leak allowed for an extremely aggressive environment on the vertical surfaces of these slabs. Even after the 70-plus-145 cycles of freezing and thawing in this environment, these vertical surfaces only showed minor surface deterioration of the type shown in the figure. The corrosion of the fibers did not seem to penetrate into the slabs, and no scaling, spalling, or chipping of the concrete surface was apparent.

Figure 116. Photo. Surface deterioration of a vertical surface after 70-plus-145 cycles of wetting/drying with a chloride solution in a freezing/thawing environment.

3.13.4 Abrasion Resistance

The abrasion resistance of UHPC was measured through the standard test method described in ASTM C944.[15] This test determines abrasion resistance by measuring the amount of concrete abraded off a surface by a rotating cutter in a given time period. The cutter consists of a series of dressing wheels mounted on a rod that is attached to a drill press. Figure 117 shows a picture of the cutter head bearing on a specimen. The drill press is used to apply a constant force through the cutter into the specimen and to rotate the cutter at 200 revolutions per minute.

The test procedure specifies that the force exerted by the cutter on the specimen surface should be 98 N (22 lb) unless the test is conducted on concrete that is particularly abrasion-resistant. Preliminary testing on UHPC indicated that doubling the load to 196 N (44 lb) as recommended by the standard would provide better results, thus this load level was used for the testing.

Cylinders with a 152-mm (6-inch) diameter were cast for these tests. The specimens were cast following normal procedures except that steel molds were used, and the molds were only filled approximately 76 mm (3 inches) full. Three cylinders were cast for each curing regime.

The abrasion resistance of a concrete surface will vary depending on the finish of its surface. For this reason, the ASTM C944 test was completed on the finishes of three different concrete surfaces for each of the four curing regimes. The surface finishes included a steel cast surface, a sandblasted surface, and a ground surface. In the test program, the 12 cylinders were all tested in the steel cast surface state. The cylinders were then sandblasted, after which they were tested again. Finally, the cylinders were ground and tested a third time.

Figure 117. Photo. ASTM C944 abrasion test setup.
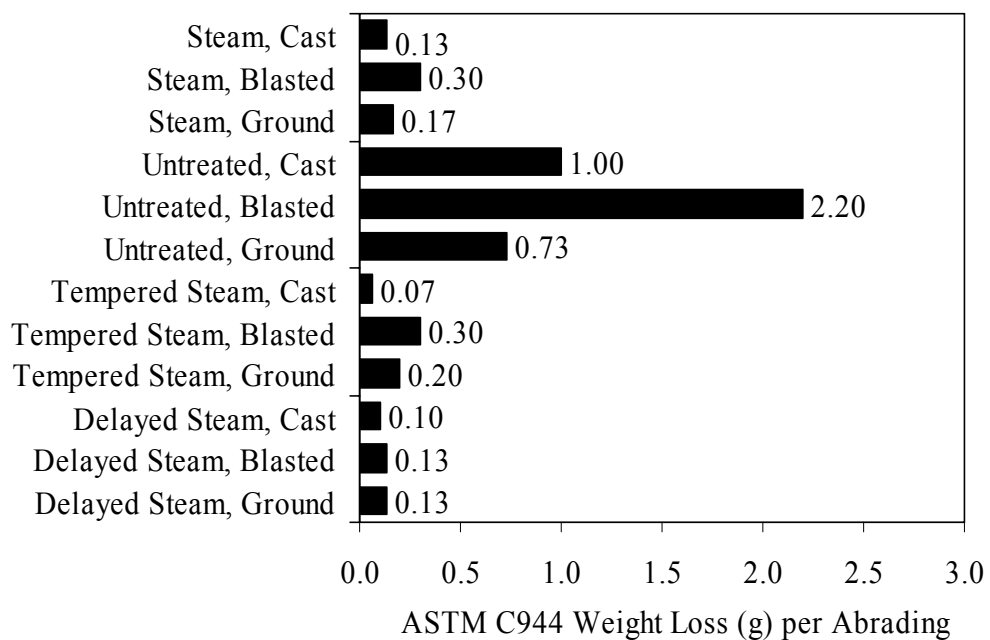
The ASTM test procedure indicates that the testing should include abrading the surface with the rotating cutter for 2 minutes. At the conclusion of the 2 minutes, the amount of concrete that has been abraded away is reported. In this test program, a modification was made to the test procedure in which the surface abrasion was repeated so that a total of between three and five abrasion sequences, with a duration of 2 minutes each, were applied to each specimen. The number of abrasion sequences varied depending on the abrasion depth capacity of the cutter and the resistance of the specimen.

Figure 118 shows two of the steel cast surface specimens after abrasion testing. The untreated cylinder on the left underwent four abrasion sequences that lasted 2 minutes each. The steam-treated cylinder on the right underwent five abrasion sequences that also lasted 2 minutes each. The photo clearly shows that the steel cast surface of steam-treated UHPC is much more abrasion-resistant than the untreated UHPC. The rotating cutter had difficulty breaking into the surface on the steam-treated cylinder and tended to skid, with only slight abrasion occurring near the center of rotation.

The results for the ASTM C944 abrasion testing are presented in figures 119 through 121. Throughout these figures, the results for each curing regime and surface condition set are the averages of the results for the three cylinders tested. Figure 119 presents the ASTM C944 abrasion weight loss as defined in the test specification. As detailed above, this result only includes the first 2 minutes of abrading for each specimen. The other two figures present the results from the entire sequence of tests completed on each specimen. Figure 120 presents the average amount of concrete per abrading over the sequence of abradings. Figure 121 presents the least-squares linear approximation of the weight loss per abrading.
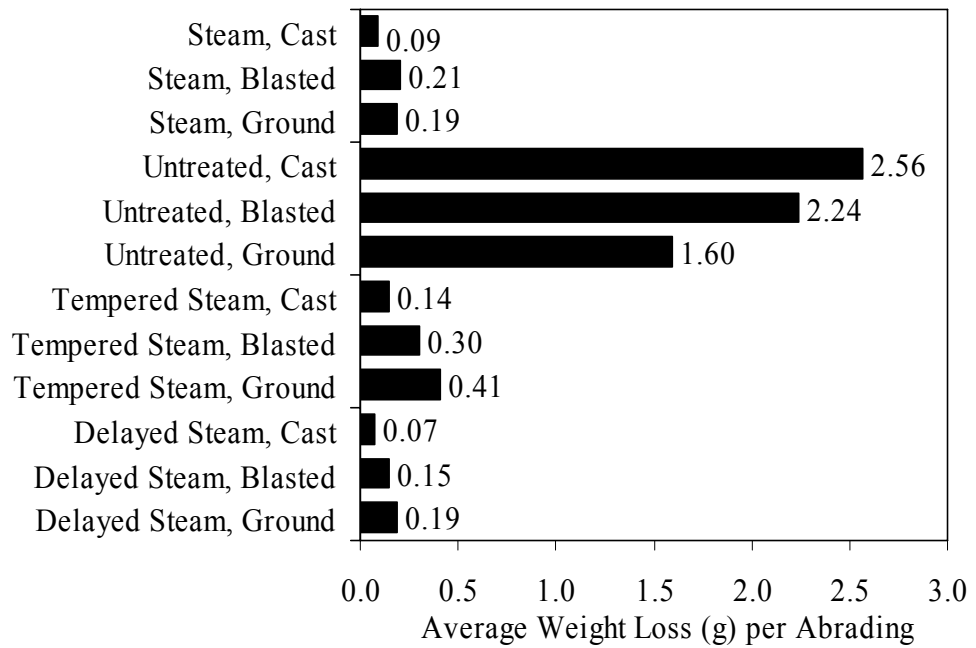
Figure 118. Photo. Steel cast surface untreated and steam-treated abrasion specimens after 8 and 10 minutes of abrading, respectively.
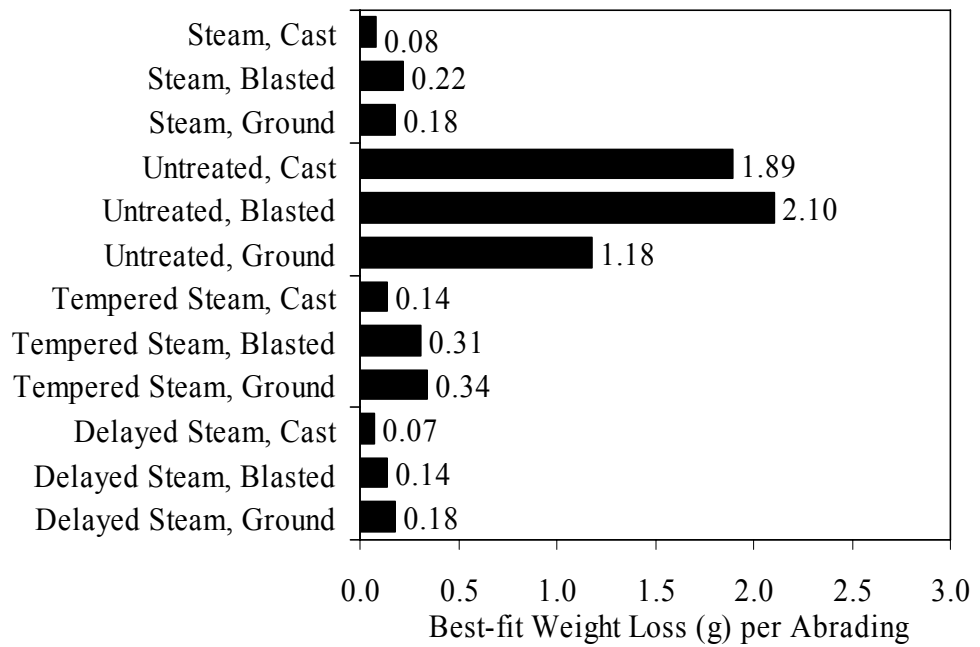
1 gram (g) = 0.035 ounces (oz)

Figure 119. Chart. ASTM C944 weight loss (grams) per abrading.

130

Figure 120. Chart. Average weight loss (grams) per abrading.

1 gram (g) = 0.035 ounces (oz)

Figure 121. Chart. Linear best-fit weight loss (grams) per abrading.

1 gram (g) = 0.035 ounces (oz)

These results show that a steam-based curing treatment of any kind has a significant impact on the abrasion resistance of UHPC. In general, the untreated cylinders lost approximately an order of magnitude more concrete per abrading than did any of the other cylinders. Quantitatively, the steam-based treated cylinders usually lost between 0.1 and 0.3 grams (0.0035 and 0.01 ounces) per abrading, while the untreated cylinders usually lost between 1 and 3 grams (0.035 and 0.1 ounce) per abrading. Also, as would be expected given its smoother texture, the steel cast surface performed the best compared with the sandblasted and ground surfaces.

These results can be compared to the results from Horszczaruk[14] presented in section 2.4.4. The testing of 83- to 100-MPa (12- to 14.5-ksi) steel fiber-reinforced concretes produced results ranging from 0.14 grams to 0.25 grams (0.005 to 0.009 ounces) of mass loss per abrading for the more abrasion-resistant concretes. (These results are presented in a form comparable to the UHPC results presented in figure 121.) However, these results are based on ASTM C944 with the standard 98-N (22-lb) load, as opposed to the double load used in the present research program. The UHPC mass loss would have been significantly lower with the decreased abrasive normal force on the cutter head. Also, note that Horszczaruk's research indicated that higher-strength concretes exhibited constant abrasion resistance, from test initiation until conclusion. This seems not to be the case with UHPC, which displayed increased abrasion resistance prior to the breaching of the smooth cast surface.

3.13.5 Freeze-Thaw Resistance

The resistance of UHPC to freezing and thawing degradation was quantified through the use of the ASTM C666 (Procedure A) standard test method.[61] In this test, concrete prisms are subjected to freezing and thawing while submerged in a water bath. The aggressive environment created in this accelerated durability test helps to determine if the concrete has a microstructure that can resist the thermal expansion and contraction effects of water. The concrete could achieve this resistance by either resisting the initial water penetration or by allowing the thermal expansion of any penetrated water to occur within a voided microstructure.

The specified lower and upper temperature value targets for the freezing and thawing environments are −18 ºC and 4.4 ºC (0 and 40 ºF), respectively. The automated equipment used in this test program allowed for five cycles of freezing and thawing to be completed per day. In this test method, each prism is housed in a water-filled container that is only slightly larger than the prism itself. The containers are placed in an environmental chamber that freezes the prisms and their surrounding water layer using cold air, and then thaws the prisms using water.

The 76- by 102- by 406-mm (3- by 4- by 16-inch) UHPC prisms produced for this test were cast following normal procedures. Three prisms were cast for each curing regime. After casting, any curing treatments were applied. The freeze/thaw testing began between 5 and 6 weeks after casting, following 2 days in which the prisms were submerged in 4.4 ºC (39.92 ºF) water to prepare them for the initial test measurement. In total, 690 cycles of freezing and thawing were conducted over the course of 9 months. During stoppages in testing, the prisms were stored in a frozen state in a walk-in freezer. In a few instances, however, machine malfunctions did allow the prisms to soak in room temperature water for up to a few days until the malfunction was corrected.

Periodically, the freeze/thaw cycling was halted, and the prisms were measured. The data collection included mass determination and capture of the fundamental transverse frequency of each prism. Figure 122 is a photograph showing the setup used to determine the fundamental or resonant frequency. In this test, a transducer records the vibrations induced in a prism supported on two wires by an instrumented hammer. The capture and determination of this frequency response was completed according to ASTM C215.

Figure 122. Photo. Resonant frequency testing of a freeze/thaw prism.

Figure 123 presents pictures of an untreated prism both before and near the end of testing. The second photograph shows that the prism experienced some deterioration of fibers that were exposed on the surface. Also, the surface of the prism tended to become slightly pitted as the cycling progressed. Overall, this pitting was very minor and was much more prevalent on the Untreated prisms than on any of the steam-treated regimes.

(a) (b)
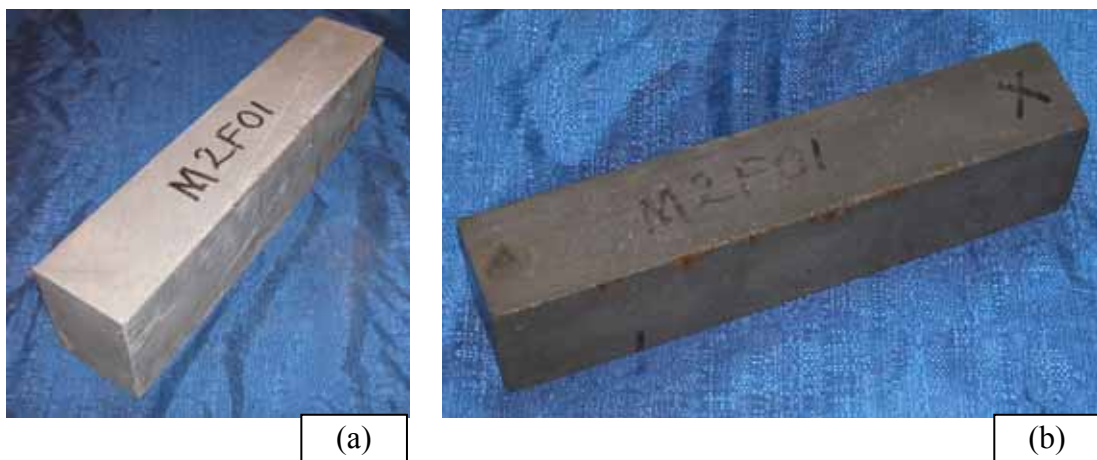
Figure 123. Photos. Freeze-thaw prism (a) before testing and (b) after 564 cycles.

The resonant frequency results from this test program are presented in figure 124. These results are the average values from the three prisms that were tested for each curing regime. Note the clear difference between the initial resonant frequency results from each curing regime. All prisms in each regime resonated within 16 Hz of one another, indicating a tight band of results.
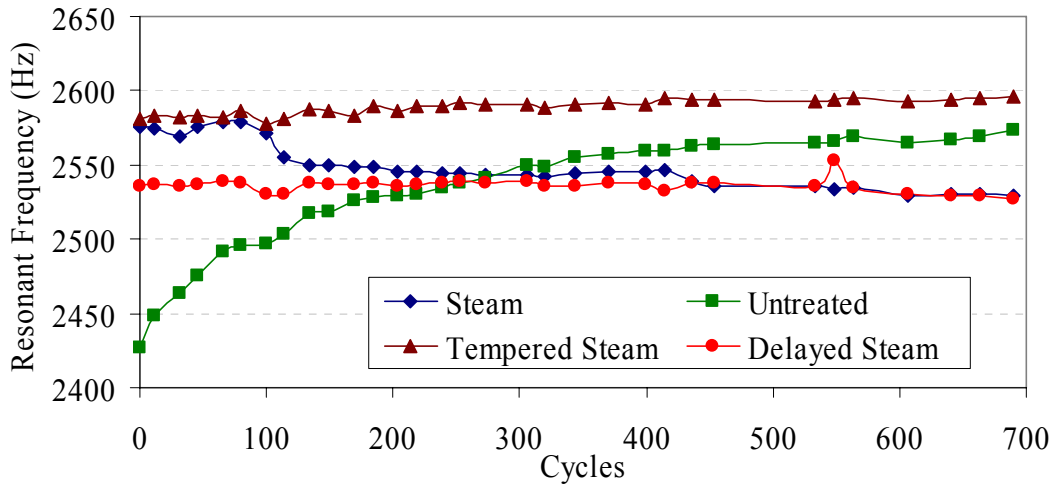
Figure 124. Graph. Resonant frequency of freeze/thaw prisms.

The relative dynamic modulus (RDM) is a value defined in the ASTM C666 test method as the percent difference in the squares of the frequency at any cycle compared with the initial frequency before freeze/thaw cycling. This calculation normalizes the results for ease of comparison to other tests. Figure 125 shows these results. In general, this test method assumes that freeze-thaw cycling will cause the RDM to decrease as the concrete deteriorates. This RDM decrease would occur due to the resonant frequency decreasing as the prism develops internal microcracking. The figure shows that the RDM changed very little in the tempered steam and delayed steam regimes, decreased slightly in the steam-treated regime, and increased significantly in the untreated regime. Overall, these results confirm that UHPC is very resistant to deterioration caused by freezing and thawing. However, it is premature to conclude that the untreated UHPC exhibits the best freeze-thaw resistance, because these RDM values are being influenced by other factors beyond those intended in the test.

One indicator that an additional unintended behavior was occurring during the freeze-thaw cycling was the mass change exhibited by the prisms. Figure 126 presents the mass change results. All the regimes exhibited mass increase throughout the testing, with the untreated prisms averaging a 0.2 percent increase by 125 cycles. In a normal freeze-thaw test, a prism will lose mass as it deteriorates. As mentioned previously, these prisms showed very little deterioration throughout the test. However, it seems that instead of deteriorating during the cycling, these prisms were taking on water and possibly even hydrating.
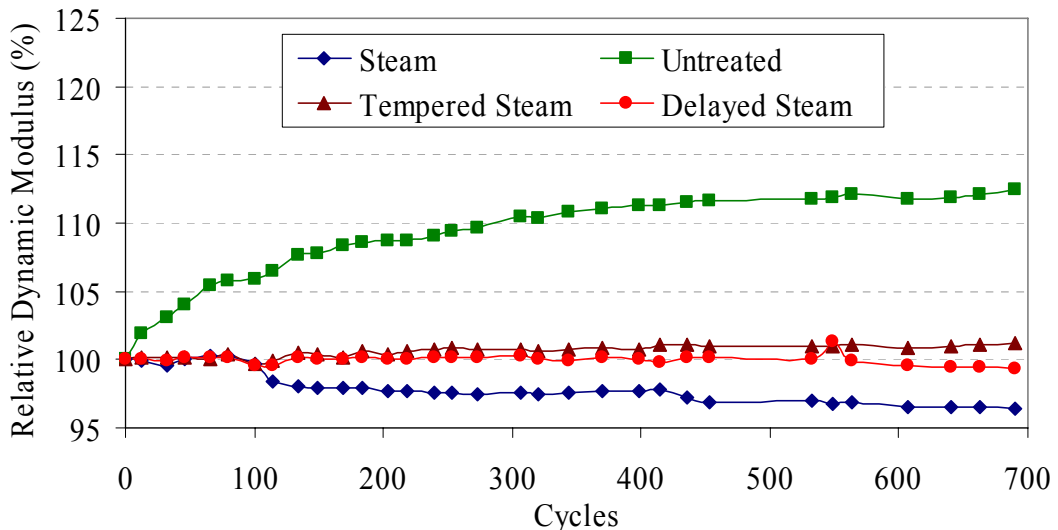
Figure 125. Graph. Relative dynamic modulus of elasticity of freeze/thaw prisms.
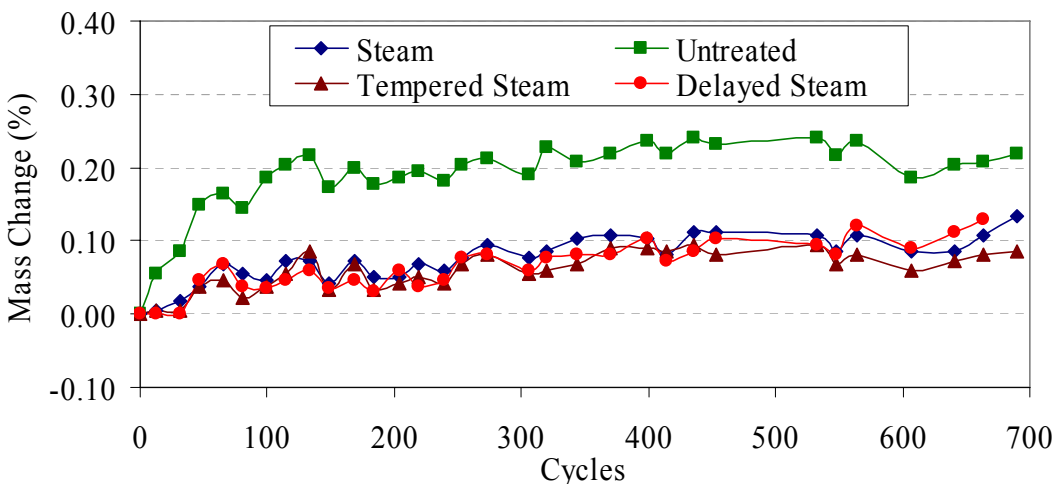
Figure 126. Graph. Mass change of prisms during freeze-thaw testing.

Further experiments were conducted to investigate the increase in RDM in the untreated prisms. To determine if the prisms were taking on water and possibly hydrating, an additional batch of eight prisms were cast. This batch included two prisms that were treated according to each curing regime. After 28 days, initial freeze-thaw measurements were completed on the prisms, and then one prism from each curing regime was placed in a water bath. The other prism from each curing regime was maintained in a laboratory environment. The prisms were kept under these conditions for 250 days, during which mass and dynamic modulus of elasticity testing was periodically completed.

The resonant frequency results from these eight prisms are presented in figure 127. The RDM results are presented in figure 128. The legend for each series indicates the curing regime and whether the prism was placed in air or water after day 28. These figures show that for the three steam-based treatment regimes, a steady increase in frequency occurred throughout the testing in the prisms maintained in the laboratory environment. The submerged prisms from these same

regimes show a more rapid increase initially followed by the same type of steady increase. The untreated prisms show different behavior, with the submerged prisms exhibiting a rapid increase in frequency response during the first 10 days and both untreated prisms showing large overall increases in frequency response. The mass change of these prisms is also instructive, with the results provided in figure 129. The masses on all of the prisms increased throughout the testing, with the untreated prisms tending to show a larger increase than their counterparts in the three steam-based treatment regimes.

One final experiment was conducted to determine if the prisms were hydrating as they were gaining water. A set of 76-mm (3-inch) diameter cylinders were cast along with the eight prisms previously discussed. These cylinders were divided into four groups, paralleling the conditions that the prisms in the untreated and steam treatment regimes underwent through day 56 after casting. An additional two sets of control cylinders were cast for testing in compression at 28 days.

Table 31 presents the results of these tests. These compression results show that placing UHPC in a water bath can increase the compressive strength. As would be expected, the strength increase is greater in the untreated UHPC than in the steam-treated UHPC. This greater increase is likely partially due to the greater permeability of the untreated UHPC.
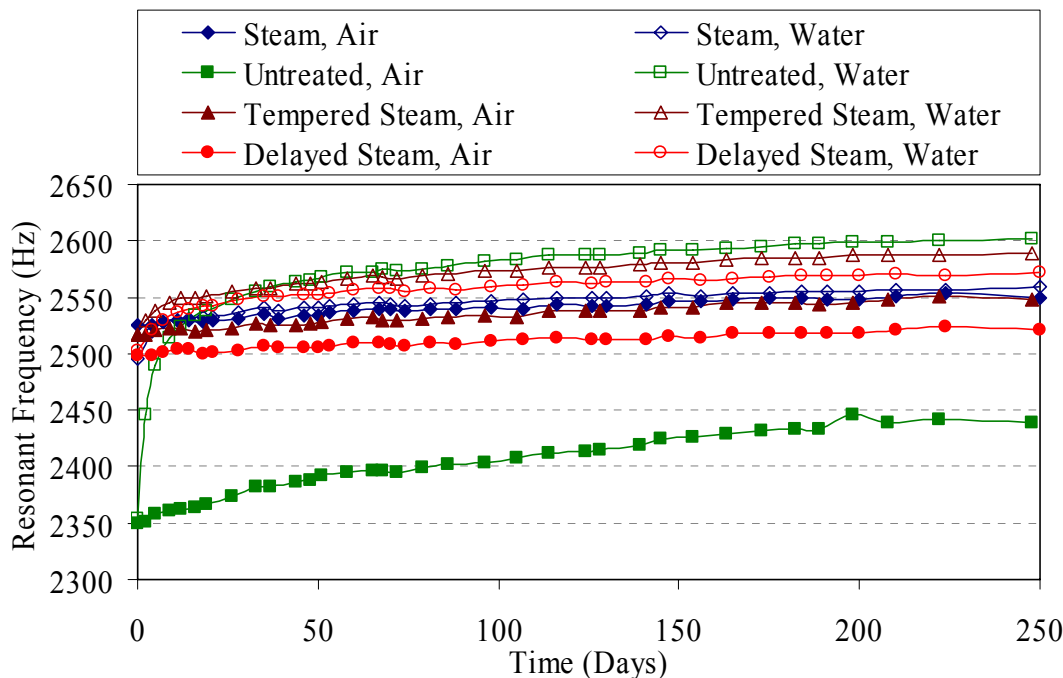
Figure 127. Graph. Resonant frequency of prisms maintained at room temperature in a laboratory environment or in a water bath.
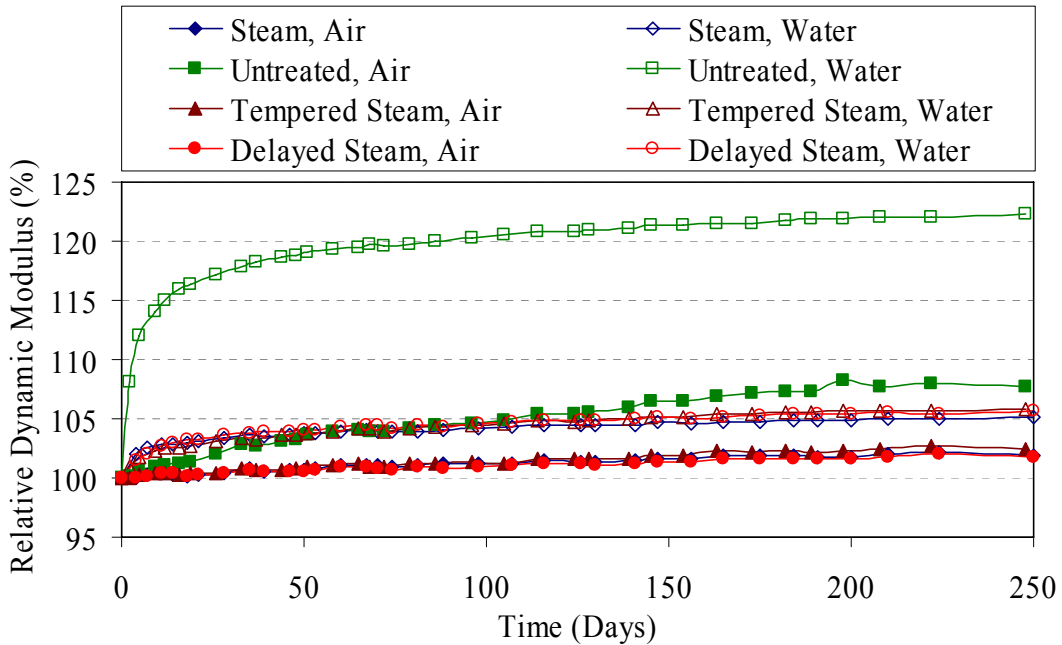
Figure 128. Graph. Relative dynamic modulus of elasticity of prisms maintained at room temperature in a laboratory environment or in a water bath.
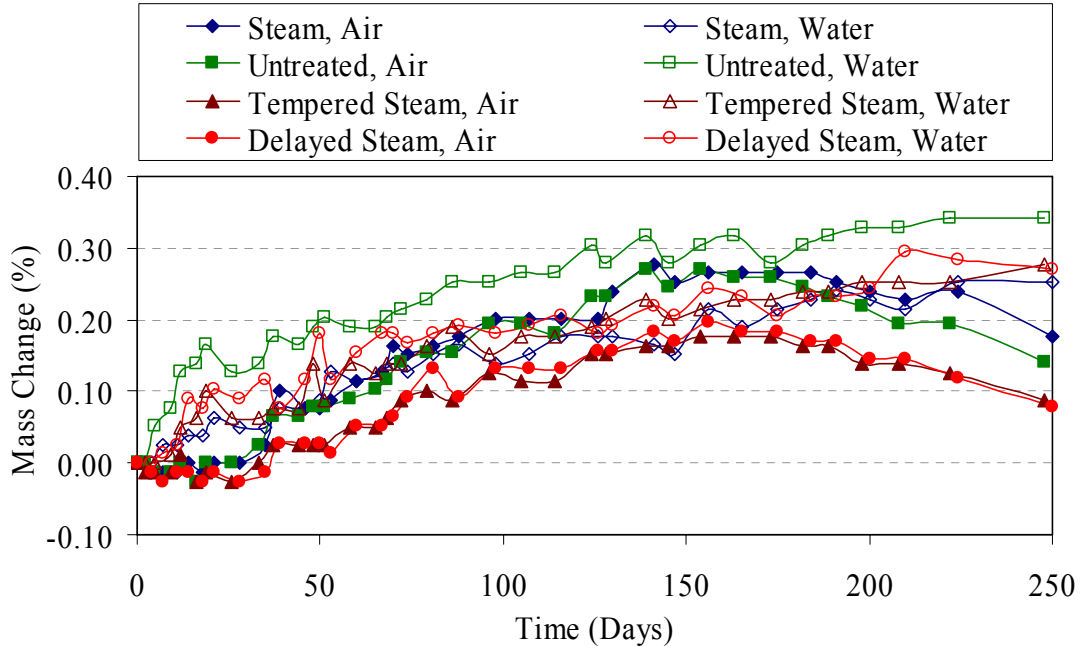
Figure 129. Graph. Mass change of prisms maintained at room temperature in a laboratory environment or in a water bath.

Table 31. Effect of a water bath on the compressive strength of steam-treated and untreated UHPC.

Curing Regime	Subsequent Environment	Age (days)	No.	Compression Strength (MPa)	
				Average	Standard Deviation
Steam	N/A	28	4	143	5.0
Steam	Air	56	5	150	4.1
Steam	Water Bath	56	5	153	8.0
Untreated	N/A	28	4	105	1.4
Untreated	Air	56	5	108	5.1
Untreated	Water Bath	56	5	120	8.1

1 MPa = 145 psi

These additional tests, which were completed following the initial freeze-thaw testing, have shown that the procedure followed for the freeze-thaw testing could lead to unintended water permeation and to additional hydration of the UHPC. This effect has been shown to be limited in the steam-based treatment curing regimes; however, it can be significant in the untreated regime. The added hydration creates the possibility of a 15 percent increase in the RDM if a prism spends 250 days in a water bath and a 10-percent increase in compressive strength if a cylinder is placed in a water bath from day 28 to 56.

3.13.6 Alkali-Silica Reaction

Alkali-silica reaction (ASR) testing was performed in accordance with ASTM C1260.[62] This accelerated test method allows for the possible detection of the deleterious effects of ASR far more rapidly that could be achieved using the standard test method, ASTM C1293.[63] The ASTM C1260 test involves submerging mortar bars in an 80 ºC (176 ºF) sodium hydroxide solution for 2 weeks, while periodically measuring the length of the bar. These tests were extended to 4 weeks.

Standard mortar bar molds were used to cast the specimens for this series of tests. Because this UHPC contains no coarse aggregate, no special preparation of the batch ingredients was necessary before casting the bars. Six mortar bars were cast for each curing condition. The mortar bars had a 25.4- by 25.4-mm (1- by 1-inch) cross section and were 280 mm (11 inches) long. The bars had gage studs cast into each end so that ASTM C490 length change measurements could be recorded throughout the testing.[49] Figure 130 shows one of the mortar bars in the length comparator for measurement.

The standard test method includes specific instructions regarding timing throughout the test. These instructions include demolding the mortar bars at 24 hours, placing the bars in an 80 ºC (176 ºF) water bath for the following 24 hours, then placing the bars in the 80 ºC (176 ºF) sodium hydroxide solution bath until test completion. Due to the curing regimes being investigated in this research program, the timetable recommended in the standard test method could not be followed. Table 32 provides the timetable for each of the five sets of specimens that were tested.

Submerging the UHPC in the 80 ºC (176 ºF) bath is somewhat similar to the steam-based curing regimes wherein the UHPC is placed in a high-heat, high-humidity environment. For this reason, it is anticipated that the test method described in ASTM C1260 may inadvertently provide additional curing to the UHPC, especially UHPC that did not undergo a steam-based curing treatment. Thus, two sets of specimens were tested in the untreated curing regime. In what is deemed the untreated (standard) set in table 32, the ASR testing was not initiated until 28 days after casting. In the untreated (modified) group, the ASR testing was initiated immediately after demolding.

Figure 130. Photo. Length comparator for ASR measurements.

Table 32. Timetable for ASTM C1260 specimens.

Curing Regime	Demold	Curing Treatment	24-hr Water Bath	NaOH Bath Start
Steam	25 hrs	26th–74th hr	98th–122nd hr	hr 122
Untreated (Standard)[†]	25 hrs	25th hr–28th day	28th–29th day	day 29
Untreated (Modified)[‡]	26 hrs	None	26th–51st hr	hr 51
Tempered Steam	26 hrs	26th–74th hr	98th–122nd hr	hr 124
Delayed Steam	26 hrs	15th–17th day	18th–19th day	day 19

[†] ASR testing initiated 28 days after casting
[‡] ASR testing initiated 26 hours after casting

Table 33 presents the results from this series of tests. The standard test method indicates that expansion values less than 0.10 percent after 14 days of testing are indicative of innocuous behavior, whereas expansion values over 0.20 percent are potentially deleterious. The UHPC expansion results are an order of magnitude below this lower threshold after 14 days and even

after 28 days of testing. Figure 131 presents the entire set of test results, including approximately 10 length readings for each curing regime throughout the 28 days of testing.

These results indicate that there should be no concern of ASR problems with the concrete after a steam-based curing regime is applied. Given the procedures used in this test method to check for ASR susceptibility, Untreated UHPC may not be as resistant to ASR as determined in these tests. However, for ASR to occur in any concrete, free water must be present. Given the low permeability of UHPC, it seems unlikely that ASR would be an issue under any curing regime.

Table 33. ASTM C1260 alkali-silica reactivity expansion results.

Curing Regime	Bars Tested	14-day Expansion (%)		28-day Expansion (%)	
		Average	Standard Deviation	Average	Standard Deviation
Steam	6	+0.013	0.008	+0.009	0.005
Untreated[†]	6	+0.011	0.002	+0.012	0.002
Untreated[‡]	6	−0.004	0.002	+0.012	0.001
Tempered Steam	6	+0.005	0.002	+0.004	0.003
Delayed Steam	6	+0.001	0.002	+0.002	0.002

[†] ASR test initiated 28 days after casting
[‡] ASR test initiated 1 day after casting
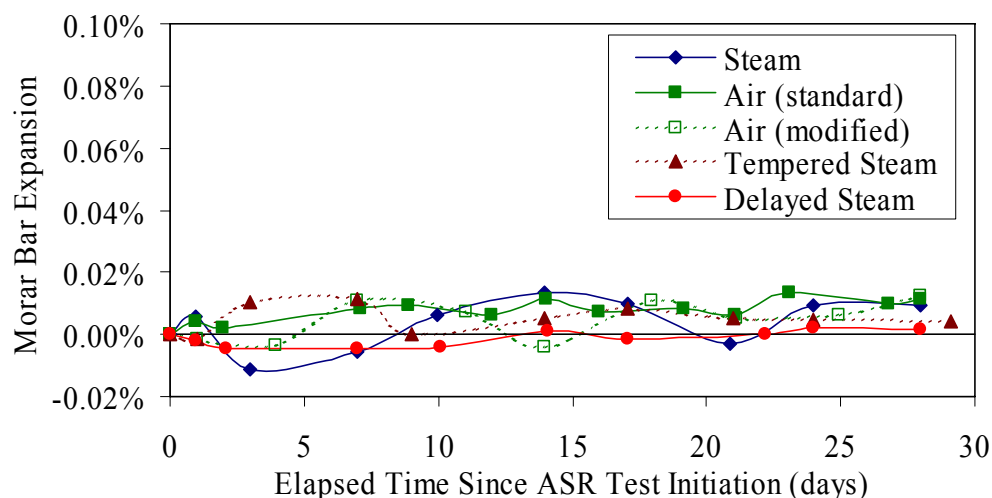
Figure 131. Graph. ASTM C1260 alkali-silica reactivity expansion results.

3.14 SPLIT-CYLINDER TENSION TESTING ON CRACKED CYLINDERS

Any material that is affected by external environmental aggressors will necessarily be more affected by those aggressors if pathways into the interior of the material are present. The durability of uncracked UHPC has been well covered by the topics discussed in section 3.13. However, in some applications cracked UHPC could be subjected to aggressive environments. The cracks could allow for ingress of contaminants and for a more rapid deterioration of the

UHPC than would be expected based on uncracked durability results. Recall the research presented in section 2.4.2 wherein Rapoport et al. indicated that the permeability of fiber-reinforced normal concrete could be increased by cracking if the cracks were larger than 0.10 mm (0.004 inch).[10]

To begin to access the durability of cracked UHPC, a series of tests were conducted to determine if the ponding of a sodium chloride solution on cracked UHPC would negatively impact the postcracking tensile strength. Although these tests are not standardized, they are a combination of the ASTM C496 split-cylinder tensile tests discussed in section 3.4.2 and the AASHTO T259 ponding tests discussed in section 3.13.2.[25,58] The split-cylinder tensile test portion of this program was conducted identically to the tests discussed earlier in the chapter, including the measurement of lateral deformation using a pair of LVDTs. The only difference was in the staging of the test wherein specimens were not necessarily loaded directly to failure (as discussed below). The ponding portion of these tests was identical to the AASHTO T259 tests described previously.

This series of tests included 30 cylinders with a 102-mm (4-inch) diameter; half of the cylinders came from batch L1R and half came from L2R. Only the steam-treated and untreated cases were investigated. The casting and curing of the specimens followed standard procedures, and the testing discussed herein was initiated on day 28 after casting.

The 15 cylinders from each batch were divided into 5 groups of 3. The first group of cylinders, the control group, was loaded to failure. The second group was loaded until cracking had occurred, then unloaded, then reloaded to failure. The third group was loaded identically to the second group, except that after unloading the cylinders were stored in a laboratory environment for 90 days. The fourth group was identical to the third group except that, during the 90-day storage, water was ponded on a cracked end of the cylinder. Finally, the fifth group was identical to the fourth group, except that a 3-percent sodium chloride solution was ponded on a cracked surface.

The cracking of each cylinder was determined by monitoring the lateral deformation behavior. The two means of determining if a crack had occurred included a clear jump in the lateral deformation or a definite reduction in stiffness of the load versus lateral deformation response. Most cylinders exhibited a clear jump in their response, but a few untreated cylinders only exhibited the stiffness change. Cylinders from the second through the fifth groups were unloaded immediately after cracking was observed.

The cracks on these specimens were then identified and measured using an optical microscope. First, alcohol was used as a volatile penetrant to highlight each crack. A crack that was made visible using this technique can be seen in figure 132. The cracks were then located using the microscope set at 350x magnification. In general, each end of each cylinder only had one crack. Once located, each crack was traced to find its largest width. The cracks were then photographed for later analysis of the crack widths. A photograph of a crack from one of the steam-treated cylinders is shown in figure 133. At this optical magnification and given the resolution of the digital photograph acquired, the crack shown in this figure is only 2 pixels wide, corresponding to a width of 0.0036 mm (0.00014 inch).
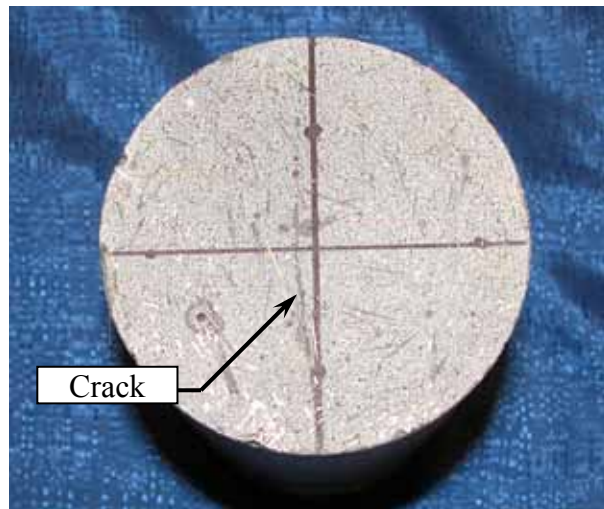
Figure 132. Photo. Crack in a split cylinder tensile specimen.
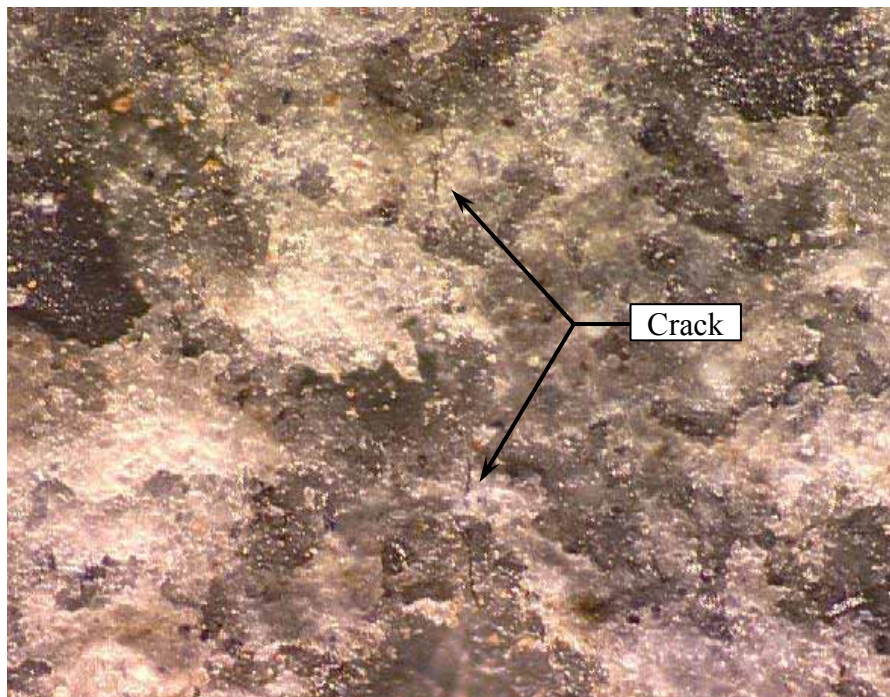
Figure 133. Photo. Crack in a split-cylinder tensile specimen under 350x magnification.
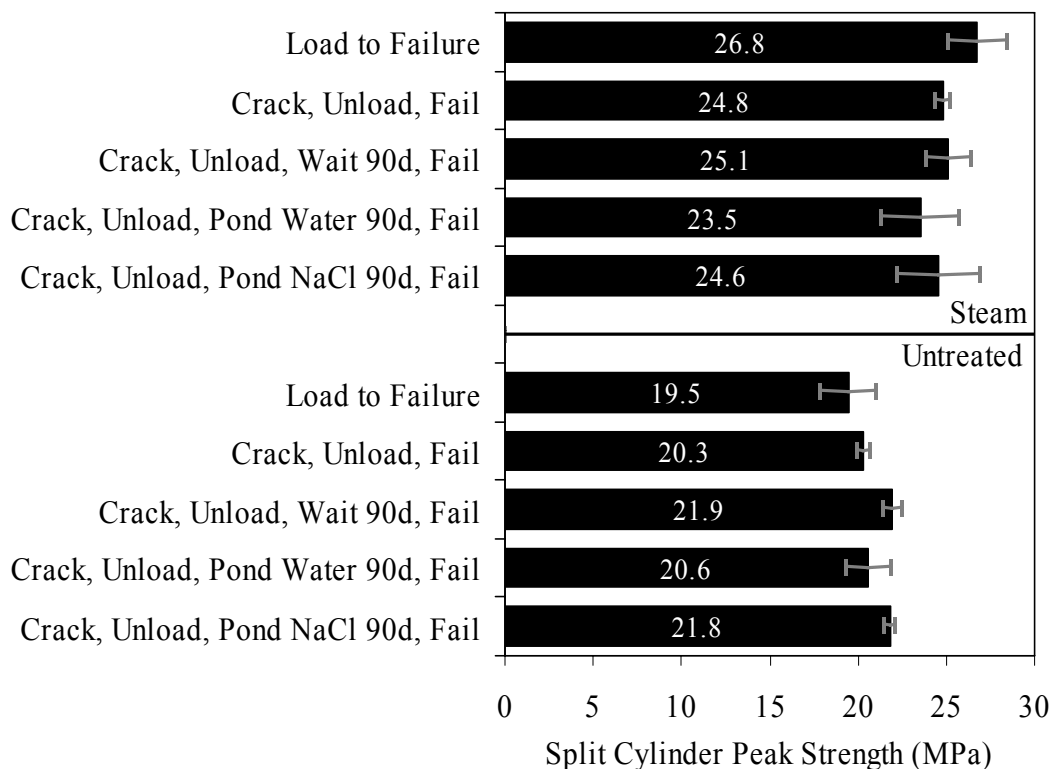
The crack widths on the ponded faces of the 12 ponded cylinders ranged from 0.0018 mm (0.00007 inch) to 0.012 mm (0.00047 inch). Ten of the 12 cylinders had crack widths between 0.0036 and 0.0069 mm (0.00014 and 0.00027 inch). Table 34 provides the crack width and split-cylinder peak strength results for the cylinders that were ponded.

Table 34. Crack width and split-cylinder peak strength results for ponded cylinders.

Curing Regime	Ponding Solution	Cylinder Number	Crack Width (mm)		Split-Cylinder Peak Strength (MPa)
			Ponded End	Nonponded End	
Steam	Water	1	0.0051	0.0036	23.4
Steam	Water	2	0.0069	0.0036	25.8
Steam	Water	3	0.0069	0.0036	21.4
Steam	NaCl	1	0.0036	0.0051	22.1
Steam	NaCl	2	0.0036	0.0018	24.7
Steam	NaCl	3	0.0036	0.0018	26.8
Untreated	Water	1	0.0119	0.0051	19.6
Untreated	Water	2	0.0069	No Crack	22.0
Untreated	Water	3	0.0051	0.0036	20.3
Untreated	NaCl	1	0.0018	No Crack	22.1
Untreated	NaCl	2	0.0051	0.0051	21.5
Untreated	NaCl	3	0.0051	0.0036	21.9

1 MPa = 145 psi, 1 mm = 0.039 inch

The results of these tests indicate that the ponding of neither the water nor the sodium chloride solution had little effect on the peak tensile load carried by the cylinders. Figure 134 provides the postcracking strength results for all five groups of cylinders for both curing regimes. The peak load carried shows no clear change, and it is clear that the ponding of the water or the sodium chloride did not have a serious detrimental effect on the fibers crossing the crack in each cylinder. However, it must also be noted that the sodium chloride solution did cause corrosion of fibers exposed on the ground end of the cylinder, similar to what was observed in the AASHTO T259 and ASTM C672 tests. Further research into the permeability of cracked UHPC is necessary to determine what crack size results in a change in the permeability characteristics of the material.

Figure 134. Chart. Split-cylinder peak strength results.

1 MPa = 145 psi

CHAPTER 4. DISCUSSION OF RESULTS

4.1 TENSILE BEHAVIOR OF UHPC

Four small-scale experimental test methods were used to study the tensile behavior of UHPC. These test methods included the ASTM C1018 prism flexure test, the ASTM C496 split-cylinder test, the AASHTO T132 mortar briquette test, and the cylinder direct tension test. Individual test results were presented in section 3.4. In this chapter, the results will be combined and compared and the test methods and their applicability and practicality for UHPC will be discussed.

4.1.1 Summary of Experimental Results

The four small-scale concrete tension testing methods used in this research provided varied bodies of results. Table 35 presents the primary quantifiable results from the four test methods. Each test provided an indication of the tensile cracking strength of UHPC. The direct tension and prism flexure tests also provided an indication of the modulus of elasticity of UHPC. Finally, the prism flexure tests provided an indication of the postcracking toughness of UHPC. For reasons discussed in section 3.4.1, the third-point loaded UHPC prism with the 305-mm (12-inch) span is taken as the standard prism flexure loading configuration, and its results are presented in this section.

The tensile cracking strength of UHPC is critical to the design of UHPC structures; however, it is difficult to determine experimentally. All of the four test methods provide realistic tensile cracking strengths that could be assumed to be accurate representations of actual tensile behavior. However, table 35 also shows that, for each curing regime, the tensile cracking strength can vary by approximately 3.4 MPa (0.5 ksi) depending on the test method used. For this reason, engineering judgment must be used to predict the true tensile cracking behavior.

Table 35 shows that the results for the cylinder direct tension and mortar briquette test cracking tensile strength were generally similar for each curing regime. This similarity is not surprising, because both test methods are based on the uniaxial application of tensile stresses. The prism flexure results, after the application of the correction factor discussed in section 3.4.1.1, are generally slightly higher than the direct tension results. Note that without the correction factor, the prism flexure results would be approximately two times the direct tension results. Finally, the split-tensile results are approximately one-third larger for all curing regimes, a result that is not unexpected when comparing split-cylinder test results with direct tension results.[27] Direct tension results are normally more highly regarded than split-cylinder results. However, direct tension tests may possibly be disproportionately impacted by local heterogeneities as compared to the larger structures that they are supposed to mimic. Therefore, lower tensile cracking strengths may be reported than what would actually be observed in practice.

Table 35. UHPC material characterization results for average tensile properties of UHPC.

Material Characteristic	Steam	Untreated	Tempered Steam	Delayed Steam	Supplemental Description
First Cracking Strength (MPa)					
Split Cylinder	11.7	9.0	11.7	11.7	ASTM C496
Prism Flexure	9.0	9.0	10.3	9.7	ASTM C1018; 305 mm span; corrected result
Mortar Briquette	8.3	6.2	9.7	6.9	AASHTO T132
Direct Tension	9.7–11.0	5.5–6.9	7.6–9.0	9.0–11.0	Axial tensile load
Combined Result, f_{ct}	9.0	6.2	9.0	9.0	Best estimate of tensile cracking strength
Modulus of Elasticity (GPa)					
Direct Tension	51.7	47.6	52.1	52.1	Axial tensile stress and strain based
Prism Flexure	58.9	49.3	56.3	55.8	Flexure and shear based; 305-mm span
Postcracking Strength (MPa)					
Mortar Briquette	9.0	6.2	9.0	6.2	AASHTO T132
Flexural Toughness					
Prism Flexure: I_{10}	14.4	12.8	13.0	13.8	ASTM C1018; 305 -mm span
Prism Flexure: I_{30}	53.0	48.3	43.1	48.3	ASTM C1018; 305-mm span
Compression Testing Results					
Compressive Strength, f_c' (MPa)	193	126	171	171	ASTM C39; 28-day strength
Modulus of Elasticity (GPa)	52.4	42.7	51.0	50.3	ASTM C469; 28-day modulus
Tension, Compression					
$f_{ct} = x \, (f_c')^{0.5}$ in MPa	0.65	0.55	0.69	0.69	
$f_{ct} = x \, (f_c')^{0.5}$ in psi	7.8	6.7	8.3	8.3	
$f_{ct} = x \, f_c'$	0.046	0.049	0.052	0.052	

1 MPa = 145 psi   1 psi = 6,895 Pa
1 GPa = 145,000 psi   1 mm = 0.039 inch

The results from these four test methods were combined together to determine the tensile cracking strength. The combining of these results takes into account the overall body of results, the number of tests, and the deviation of results from the average value. When these factors are combined, the tensile cracking strength of steam-treated UHPC is 9.0 MPa (1.3 ksi). The tensile cracking strength of untreated UHPC is 6.2 MPa (0.9 ksi). The tensile cracking strength of tempered steam and delayed steam-treated UHPC are both 9.0 MPa (1.3 ksi).

These tensile cracking strength results can be compared with the compressive strength results discussed previously in this report. The bottom of Table 35 shows that the tensile cracking strength, f_{ct}, is approximately 5 percent of the compressive strength, f_c', in all four curing regimes. Alternatively, the equation in figure 135 is frequently used to approximate a tensile strength from a given compressive strength. In this equation, the square root of the compressive strength is related to the tensile strength by a linear multiplier, x. In English units (psi), the UHPC that underwent the steam treatment has a multiplier of 7.8, the untreated UHPC has a multiplier of 6.7, and the tempered and delayed steam-treated regimes have a multiplier of 8.3.

$$f_{ct} = x\sqrt{f_c'}$$

Figure 135. Equation. Concrete tensile strength approximation.

The modulus of elasticity results obtained from the tension tests are also presented in the table. Given the limited number of direct tension tests completed, these results can be considered to be similar to the compression test modulus of elasticity results discussed in chapter 3. Although the untreated result is 11 percent higher, the remainder of the results are within 3.5 percent. However, the prism flexure modulus of elasticity results are generally between 10 and 15 percent higher than the comparable compression test results. This result indicates that the UHPC prism flexure tests tend to overestimate the modulus of elasticity as compared to the standard compression testing methods, because nearly all of the prism groups exhibit this behavior, regardless of cross section and loading configuration.

The postcracking tensile behavior is much more difficult to quantify, but this research program has resulted in a number of both general and specific findings. The mortar briquette tests provide the most direct indication of the postcracking behavior. Figures 66 through 77 show the full load-displacement curves for all of the mortar briquette tests. First and foremost, these figures indicate that UHPC tends to display postcracking strength levels similar to its precracking strength levels. The table lists the average postcracking strength values, which are all within 0.8 MPa (0.1 ksi) of the mortar briquette first tensile cracking strength levels. Note, however, that postcracking behavior is very dependent on fiber dispersion and orientation. The small-scale mortar briquettes most likely did not accurately represent the large-scale tensile members for these two factors.

Limited postcracking strength results are also available from the split-cylinder tests. These tests indicate that, under the biaxial state of stress present in this test configuration, UHPC exhibits significant postcracking load-carrying capacity. For each curing regime, the peak load carried after cracking is approximately twice the cracking load. However, the compressive forces paralleling the tensile crack in this loading configuration increase the fiber/matrix bond and thus contribute to the postcracking load-carrying capacity.

Finally, comparative results were also obtained from the prism flexure tests. The results from this standardized test can easily be compared both within this study and with normal and fiber-reinforced concretes tested by other researchers. Comparisons with the standard toughness levels set in ASTM C1018 and with the results from other researchers indicate that UHPC exhibits very high postcracking toughness values. Specifically, all the UHPC curing regimes were at or above the stated fiber-reinforced concrete toughness upper limit for the values of I_5, I_{10}, and I_{20}. Also, these tests indicate that a relatively uniform level of toughness will be achieved throughout the curing regimes. However, these results do not mean that all UHPC display identical postcracking load-carrying behavior, because the ASTM C1018 toughness measure relates postcracking to precracking behaviors and thus is biased by the precracking strength.

4.1.2 Summary of Experimental Test Methods

Sections 4.1.1 and 3.4 describe the small-scale tension tests employed in this research program and the relevant results from each test. This section builds on those presentations to present and to compare the test methods. Test capabilities and the difficulties associated with completing each test will be discussed.

The split-cylinder test is the simplest UHPC tension test to complete successfully. This test program has shown that consistent UHPC tensile cracking strength results can be obtained by following the ASTM C496 test procedure. The only addition to the test is the inclusion of a cylinder lateral expansion measurement and recording device. Thus, a measure of the tensile cracking strength of UHPC can be obtained using a standard hydraulic compression testing machine, a simple data acquisition system, and a pair of displacement transducers. Alternatively, an evaluation technique capable of detecting a crack in UHPC, such as ultrasonic inspection, could be used to note cracking in steam-based treated UHPC, thus eliminating the need for data acquisition and full-range transducers. Test results presented in section 4.1.1 indicated that conversion of the split-tensile cracking strength result to the overall tensile cracking strength result could be obtained by multiplying the split-cylinder result by a factor of 0.75. Unfortunately, the unknown postcracking stress distribution in the cylinder does not allow for the quantitative determination of any postcracking tensile behaviors.

A slightly more advanced loading setup is required for completing the AASHTO T132 mortar briquette test. The test performed in this research program required a test machine capable of loading under crosshead displacement control and a data acquisition system capable of recording load and displacement readings throughout the test. The primary benefit of this test over the split-cylinder test is that it directly measures uniaxial tensile properties of UHPC. This benefit allows for a more accurate rendering of the UHPC tensile cracking strength. Also, this test method can provide some indication of the postcracking tensile strength of UHPC; however, the difficulties inherent in the casting of these small briquette specimens decrease the confidence in any postcracking strength results. As such, the benefits of this test over the split-cylinder test are marginal unless a qualitative verification of postcracking load-carrying capacity is desired.

The ASTM C1018 prism flexure test is significantly more intensive with regard to testing equipment than either of the previous two test methods. To successfully complete this test, a test machine capable of loading under an external displacement transducer control is necessary, along with a data acquisition system to record load and displacement. Additionally, an electronic

averaging circuit to combine the deflection results from the specimen can provide more consistent, uniform loading. The benefit of the prism flexure test is that it provides an indication of the tensile cracking strength, the modulus of elasticity, and an arbitrarily defined but widely used measure of the postcracking tensile toughness. Because a cross comparison between different fiber-reinforced concretes or concretes cast in different laboratories is important, this test can provide needed results that are unavailable through simpler test setups. However, as discussed in section 3.4.1.1, tensile cracking strength results from this test method must be corrected using an empirical relationship. The acquisition of pure tensile cracking behaviors from this test method is not possible.

The final test method, the direct tension test, is the most difficult test to implement and also provides the most complete body of results. This method requires a test machine capable of loading under external displacement control, an electronic averaging circuit for at least three displacement transducers, and a data acquisition system to record the load and displacements. Additionally, a means of gripping the tensile specimen, such as the high-strength, high-modulus epoxy used in the research, is necessary. Finally, great care must be taken in the fabrication of the small-scale specimens to ensure that they replicate the regions in large-scale structures that are subjected to tensile stresses. If all these requirements are met, this test has the possibility of capturing the full tensile stress-strain or stress-crack opening behavior. These results would include the tensile cracking strength, the modulus of elasticity, the postcracking tensile strength, and the load-carrying capacity from tensile cracking through fiber pullout. The test program discussed in this report did not achieve the goal of successfully completing direct tension tests, and thus was not able to determine the full tensile stress-strain response of UHPC from small-scale tension tests.

The selection of a particular tension test for UHPC must be predicated on the results desired. The tests discussed in this section could be used to meet certain needs, but other tests or modifications of these tests could also be used. For example, it is likely that UHPC used in structures will require a minimum level of tensile strength. As a quality control issue, a hydraulically operated test machine under load control could be used to ensure that the minimum level of tensile strength is achieved. This could be accomplished by an experienced quality control professional performing a mortar briquette or split cylinder test wherein the UHPC was required to hold a sustained stress level prior to the audible indication of tensile cracking.

4.2 LOCAL AND GLOBAL MECHANICAL FAILURE MODES OF UHPC

UHPC exhibits a number of macrostructural mechanical failure modes. These failure modes can be categorized into three specific types: compressive, tensile cracking, and tensile fiber pullout. A fourth failure mode, the high-cycle fatigue failure of crack-bridging steel fibers, has been observed under special loading conditions but will not be discussed in this report.

The compressive failure of UHPC can be considered to be similar to the compressive failure of any fiber-reinforced concrete. In general terms, UHPC fails under axial compressive load through lateral tensile expansion. This lateral expansion is partially restrained by the internal steel fiber reinforcement, thus allowing for a more ductile failure than may be expected. As with any concrete, higher-strength UHPC tends to fail in a more brittle manner than lower-strength UHPC.

Compression failures in hundreds of UHPC cylinders were observed while performing the ASTM C39 compression test. The failure of any cylinder that underwent steam-based treatment was brittle, with a rapid load decrease occurring immediately after the peak load was achieved. Even as such, these cylinders remained largely intact with relatively few small fragments leaving the cylinder. The failure of the cylinders in the untreated regime occurred in a much more ductile manner. Some of these cylinders, particularly the ones with strengths above the average of 126 MPa (18.3 ksi), did exhibit brittle behavior. However, most of these cylinders failed through a continuous, nonabrupt decrease in load after reaching the peak. The failures of these lower-strength (and less cured) cylinders were significantly more ductile and exhibited quantifiable post-peak behavior that was not achievable on a hydraulically-actuated load testing machine with the higher-strength cylinders. Finally, the compression testing of a 76-mm (3-inch) diameter steam-treated UHPC cylinder that did not contain any fiber reinforcement resulted in an extremely brittle failure with significant fragmentation of the UHPC.

The tensile behavior of UHPC allows for continuing tensile load-carrying capacity across a cracked plane. The design of the structure will determine whether the tensile cracking of UHPC is a failure mode. Regardless, for the purposes of this discussion the UHPC behavior at this critical junction will be described.

Similar to the compression failures described above, the tensile cracking of UHPC can be either brittle or ductile. Although these differences in behaviors were observed in all small-scale tensile tests, the differences were most clearly observed in the split-cylinder tensile tests. In these tests, the cylinders that had been subjected to steam-based treatments tended to exhibit a clear aural indication of first cracking and displayed discontinuous load-displacement behavior as the crack abruptly formed, then was arrested by the bridging fibers. Conversely, the untreated cylinders did not exhibit an aural indication of first cracking and sometimes displayed continuous load-displacement behavior at cracking. Also, the crack width at crack arrest tended to be larger in the cylinders that underwent the steam-based treatment, which was likely due to the higher tensile strengths at which cracking occurred.

Final tensile failure of UHPC generally occurs when the steel fiber reinforcement begins to debond from and to pull out of the UHPC matrix. Because fibers are randomly distributed and oriented in the UHPC, individual fiber loads vary at any particular global load level. Mechanically, pullout occurs when the load carried by an individual fiber overcomes the ability of the UHPC to grip the fiber. Pullout by any fibers increases the load that other nearby fibers have to carry. Multiple pullouts in a specific location that require gross load redistribution through alternate load paths can be defined as fiber pullout failure.

Fiber pullout across a plane perpendicular to the principal tensile stresses was the failure mechanism that concluded all small-scale tension tests. The fibers protruding from each failure surface tended to align perpendicular to the surface, likely due to the inelastic bending of each fiber at its exit point from the UHPC matrix as the crack widened and pulled the fiber straight across the crack.

4.3 EFFECT OF CURING PROCEDURE ON UHPC PROPERTIES

One of the primary focuses of this research program was to determine the effect that the application of a curing treatment had on the behaviors exhibited by UHPC. To quantify this effect, the majority of the research completed within the material characterization portion of this study included four different curing regimes. The curing regimes included the manufacturer-recommended steam treatment, a delayed version of the same treatment, a reduced temperature version of the same treatment, and an untreated case in which the UHPC remained in a laboratory air environment until testing.

Table 36 presents a compilation of results from the material characterization study. The results provided in the table are average values that were summarized for ease of discussion. A full discussion of each portion of this test program is provided in chapter 3.

The application of a curing treatment clearly impacts UHPC behavior. A comparison of the steam-treated and untreated regime results indicates that the application of the recommended steam treatment has a significant effect on some properties. In terms of mechanical properties, steam treatment will increase the compressive strength, tensile cracking strength, and elastic modulus. In terms of long-term stability, steam treatment will decrease creep and speed the realization of the asymptotic shrinkage, virtually eliminating any shrinkage after the treatment is complete. In terms of durability, steam treatment seems to decrease the permeability of UHPC, thus increasing its resistance to chloride penetration. A more durable mechanical matrix that is better able to resist abrasive forces is also created.

The application of intermediate curing treatments, such as in the tempered steam and delayed steam regimes, also has a significant—although generally slightly reduced—impact on the UHPC behavior. While the compressive strength and elastic modulus are increased by these treatments, they both fall short of the level achieved with the full steam treatment. Interestingly, tensile cracking behavior enhancements seem to be similar regardless of the type of steam treatment applied. Note that the creep behavior is significantly enhanced by the delayed steam treatment, while it is only slightly enhanced by the tempered steam treatment. In terms of durability, the chloride ion penetrability is extremely low regardless of the steam treatment applied.

Table 36. Average UHPC material properties presented according to curing treatment.

Material Characteristic	Steam	Untreated	Tempered Steam	Delayed Steam	Supplemental Description
Compressive Strength (MPa)	193	126	171	171	ASTM C39; 28-day strength
Modulus of Elasticity (GPa)	52.4	42.7	51.0	50.3	ASTM C469; 28-day modulus
Split Cylinder Cracking Strength (MPa)	11.7	9.0	11.7	11.7	ASTM C496
Prism Flexure Cracking Strength (MPa)	9.0	9.0	10.3	9.7	ASTM C1018; 305-mm span; corrected
Mortar Briquette Cracking Strength (MPa)	8.3	6.2	9.7	6.9	AASHTO T132
Direct Tension Cracking Strength (MPa)	9.7–11.0	5.5–6.9	7.6–9.0	9.0–11.0	Axial tensile load
Prism Flexural Tensile Toughness (I_{30})	53.0	48.3	43.1	48.3	ASTM C1018; 305-mm span
Long-Term Creep (C_{cu})	0.29	0.78	0.66	0.31	ASTM C512; 77-MPa sustained load
Long-Term Shrinkage (microstrain)	766	555	620	657	ASTM C157; initial reading after set
Total Shrinkage (microstrain)	850	790	–	–	Embedded vibrating wire gage
Coeff. of Thermal Exp. ($\times 10^{-6}$ mm/mm/°C)	15.6	14.7	15.4	15.2	AASHTO TP60-00
Chloride Ion Penetrability (coulombs)	18	360	39	18.00	ASTM C1202; 28-day test
Chloride Ion Permeability (kg/m^3)	< 0.06	< 0.06	< 0.06	< 0.06	AASHTO T259; 12.7-mm depth
Scaling Resistance	No Scaling	No Scaling	No Scaling	No Scaling	ASTM C672
Abrasion Resistance (grams lost)	0.17	0.73	0.20	0.13	ASTM C944 2x weight; ground surface
Freeze-Thaw Resistance (RDM)	96%	112%	100%	99%	ASTM C666A; 600 cycles
Alkali-Silica Reaction	Innocuous	Innocuous	Innocuous	Innocuous	ASTM C1260; tested for 28 days

1 MPa = 145 psi
1 GPa = 145,000 psi
1 psi = 6,895 Pa
1 mm = 0.039 inch
1 mm/mm/°C = 1.8 inches/inches/°F
1 kg/m^3 = 1.69 lb/yd^3
1 g = 0.035 oz

Another curing treatment procedure, illuminated during this test program, is slightly outside of the clearly defined boundaries of the curing regimes. In section 3.3.5, the effect of demolding cylinders in terms of their early age setting and strength gain was discussed in terms of compressive strength. These tests showed that demolding UHPC, and thus exposing it to a low humidity environment prior to sufficient setting and strength gain, could have a significant impact on the 28-day compressive strength. It is extremely important to wait until a sufficient strength level has been achieved before demolding UHPC and to keep UHPC in a moist environment during the continued strength gain. This procedure was not always followed within this material characterization study and, as discussed in chapter 3, some of the observed behaviors were reduced as a result.

The overriding result of the entire UHPC curing treatment comparison is that, regardless of the curing treatment applied, UHPC exhibits significantly enhanced properties compared with standard normal strength and HPCs. The application of the steam treatment is clearly beneficial; however, this procedure is also not always necessary as long as the user is willing to accept decreases in strength, long-term stability, and durability.

4.4 EARLY AGE STRENGTH GAIN OF UHPC

The compressive strength gain behavior of UHPC is an important characteristic of the concrete. Results detailed in chapter 3 indicated that UHPC does not have any compressive strength for nearly 1 day after casting. Then, once initial set occurs, UHPC rapidly gains strength over the course of the next few days until over 69 MPa (10 ksi) of strength is achieved. At that point, the rate of strength gain decreases, but the strength gain continues until over 124 MPa (18 ksi) of compressive strength is achieved by 28 days.

Figure 136 presents a compilation of the compressive strength data for the untreated cylinders tested between 1 and 56 days (the results are discussed in section 3.3.2). These results include both cylinders in the untreated group and cylinders in the other treatment groups that had not yet undergone their own steam treatment. Also, recall from section 3.6 that initial set tended to occur at approximately 15 hours, and final set occurred 2 hours later.

A regression analysis was completed to fit a transition function to the data presented in figure 136. The delayed then rapid early age strength gain behavior of UHPC results in a somewhat complex approximating function. The Weibull Cumulative function, provided as the equation in figure 137 and plotted in figure 136, accurately describes the strength gain behavior for any time after 0.9 days following casting. This equation includes the time in days after casting, t, and the 28-day compressive strength in MPa, f_c', with the result being the compressive strength at time t in MPa. The initial and final set times of UHPC can vary depending on the age of the premix and the environmental conditions, thus this equation may not be applicable to UHPC exhibiting different setting behaviors.

1 MPa = 145 psi
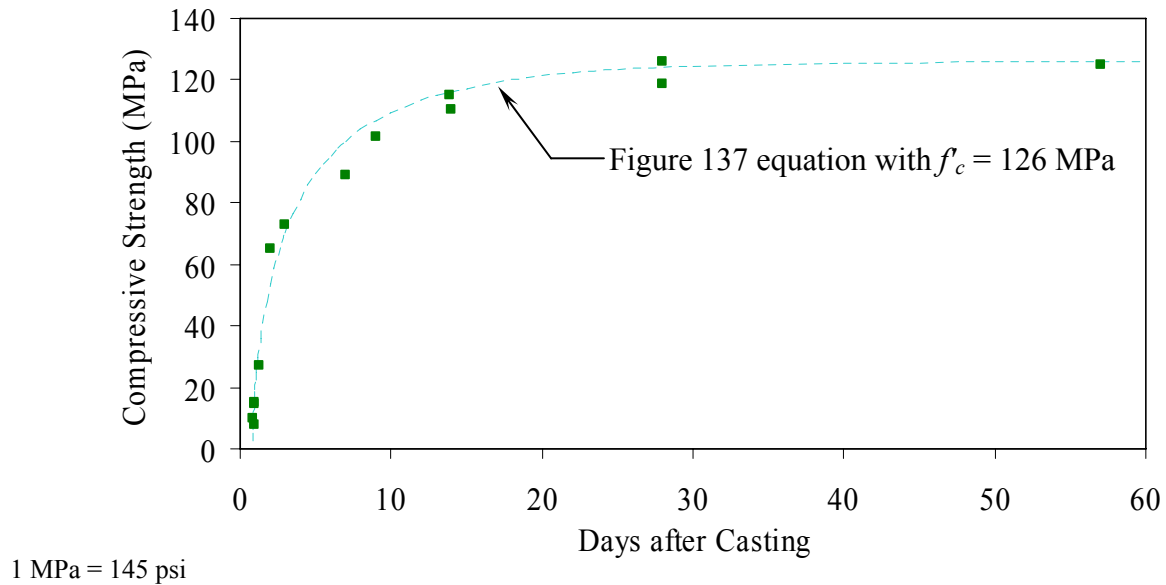
Figure 136. Graph. Compressive strength gain as a function of time after casting.

$$f'_{c,t} = f'_c\left[1 - \exp\left(-\left(\frac{t - 0.9}{3}\right)^{0.6}\right)\right]$$

Figure 137. Equation. Compressive strength at any age after casting.

4.5 COMPARISON OF CYLINDER AND CUBE COMPRESSION STRENGTH RESULTS

The cylinder is the standard concrete compression test specimen geometry used in the United States. This is understandable, because cylinder molds are inexpensive and the casting of concrete cylinders is relatively easy. However, as opposed to traditional concrete, UHPC cylinders cannot easily be prepared for testing. In any concrete compression test, the even and parallel loading of the ends of the cylinder is critical to achieving accurate test results. The high compressive strength of UHPC eliminates the possible use of end capping materials and predicates grinding or milling to ensure plane, parallel loading surfaces. Unfortunately, the equipment necessary to perform this end preparation on UHPC cylinders is not yet locally available to all quality control and testing departments.

One method of eliminating the need for cylinder end preparation is to use cubes as the standard means to measure the compressive strength of UHPC. Cubes are cast with two pairs of plane, parallel faces, thus greatly simplifying the specimen preparation process. The primary drawbacks to the use of cubes are the expense of the molds, the unfamiliarity with the test methods, and the indirect nature of the results obtained from the test. In general, cube compression test results are higher than cylinder compression test results on the same concrete due to the aspect ratio of the specimens and the confining effect of the machine platens. To account for these differences, a

154

strength reduction factor normally needs to be applied to a cube compression test result. This factor can vary significantly depending on many concrete properties, but has been reported to be in the vicinity of 0.82 for ordinary concrete and increases toward 1.0 as the concrete strength increases.[64]

Section 3.3.4 presented the results from a series of cube and cylinder compression tests. Recall that the 51-, 76-, and 102-mm (2-, 3-, and 4-inch) diameter cylinders, as well as the 51-mm (2-inch) and 100-mm (4-inch) cubes were tested and that the series of tests were repeated three times on different batches of UHPC. If the 76-mm (3-inch) diameter cylinder is considered to be the control specimen, the results showed that the compressive strength exhibited by the 100-mm (4-inch) cube specimens ranged from 1.2 percent below to 8.0 percent above the control specimen strength. The strength of the 51-mm (2-inch) cube ranged from 4.6 to 6.1 percent above. These increases of less than 10 percent are sufficiently small; therefore, cube tests should be able to be used as a direct substitute for cylinder compression tests in some applications. Although most owners will probably require cylinder compression tests as the standard strength test result reported for the foreseeable future, the UHPC component fabricator internal quality control testing using the cube specimens would not be precluded.

One additional finding from the results presented in section 3.3.4 relates to the size of the compression specimen (for either the cylinder or the cube). The results indicate that smaller specimens, particularly the 51-mm (2-inch) diameter cylinders and the 51-mm (2-inch) cubes, tended to exhibit larger standard deviations. The casting-based heterogeneities (i.e., entrapped air voids) in the UHPC that are proportionally larger in smaller specimens are likely behind these results. For this reason, the use of compression specimens that have a minimum dimension smaller than 76 mm (3 inches) is not recommended.

4.6 SHRINKAGE BEHAVIOR OF UHPC

A significant portion of this research program has focused on the tensile behaviors of UHPC and the applicability of those tensile behaviors to structural engineering. Assurance of those tensile properties in a completed structural member is a factor of many things, including both casting/placing techniques and curing treatments. Another important factor is the formwork and its ability to restrain shrinkage forces.

The test results presented in section 3.7 indicate that UHPC exhibits shrinkage behaviors that are somewhat different than those exhibited by normal concrete. Overall long-term shrinkage of UHPC is somewhat large, with an asymptotic value nearing 850 microstrain. More importantly, the results indicate that UHPC shrinks very rapidly in the 24 hours after the initiation of setting behaviors. This rapid shrinkage can include up to 400 microstrain of shrinkage during this time frame with a shrinkage rate of up to 60 microstrain per hour. The shrinkage continues at an increased rate as compared to normal concrete with 95 percent of its ultimate shrinkage occurring by 2 months after casting.

These early age shrinkage behaviors are important to the successful casting of UHPC structural members, because UHPC will crack at tensile strains significantly below these shrinkage strains. Thus, the casting of UHPC must mitigate or eliminate shrinkage restraints on the cast member. For highway bridges, standard I-shaped girders are not particularly susceptible to restrained

shrinkage cracking. However, in the casting of a member with restrained areas, such as a double-tee section or a box section, special care must be taken to allow for monitoring and the release of shrinkage strains.

4.7 LONG-TERM STABILITY OF UHPC

The basic premise behind the application of prestressing forces into concrete girders is that the application of an eccentric compressive axial force onto a beam will delay inelastic behaviors and increase the ultimate capacity. To achieve these goals, the prestressing forces must be maintained indefinitely. Time-dependent concrete behaviors such as creep and shrinkage can both negatively impact the maintenance of the prestressing force, thus reducing the enhancement provided by the prestress. This section addresses the general long-term stability of UHPC, including the creep and shrinkage behaviors that can be expected and the possible methods to alleviate those behaviors.

In large-scale, prestressed concrete girder fabrication facilities, the time required to fabricate a girder from initial form setup to cutting of strands and removing the girder from the form is critical. This amount of time determines the turnover for the casting bed and directly influences the cost of each girder. In general, precasters want to create a rapid turnover, thus they are interested in stressing the girder as soon as possible after casting. The results of this method, for any concrete, are that the expected creep and shrinkage values will be larger and the prestress losses will be greater.

The shrinkage behavior of UHPC has been discussed in sections 3.7 and 4.6. UHPC can be expected to undergo nearly half (400 microstrain) of its long-term shrinkage (850 microstrain) during the first 24 hours after setting. Also, steam treatment will hasten the achievement of the ultimate shrinkage value and will effectively stabilize the UHPC against further shrinkage indefinitely. For these reasons, delaying the stressing of the girder is clearly beneficial.

The creep behavior is also influenced by the concrete strength at girder stressing. The long-term creep results from section 3.8 indicate that creep coefficients between 0.3 and 0.8 can be expected for UHPC that is treated according to one of the curing regimes. However, the prestress would likely be applied before any of these treatments are completed in a production environment. For this reason, the creep behavior at earlier ages, and thus at lower compressive strengths, is important. The early age creep testing presented in section 3.8.2 focuses on this behavior for UHPC that is still of relatively low strength. Creep at two compressive strength levels was investigated, namely 62 and 86 MPa (9 and 12.5 ksi). These results indicate that significantly less creep will occur after moderate increases in strength; however, the creep strains observed only 30 minutes after loading a 84 MPa (12.25 ksi) cylinder to 70 MPa (10.15 ksi) were still over 50 percent of the elastic strains from the initial loading. This 30-minute effective creep coefficient of 0.52 is quite high considering that the long-term final creep coefficient for a 114-MPa (16.5-ksi) UHPC loaded after 28 days of curing is only 0.78.

Similar to the shrinkage results discussed above, the creep results indicate that delaying the stressing of the girder until higher strengths are achieved can be beneficial in terms of long-term prestressed girder behavior. These higher strengths and the better resistance to creep can come

either from purely delaying the stressing as in the untreated regime or from steam treating the UHPC prior to application of the prestress.

4.8 MODULUS OF ELASTICITY OF UHPC

Because compression testing of cylinders is a frequently used quality control method for structural concrete, engineers often attempt to relate other characteristics of concrete's behavior to the compression test results. Many researchers have performed work that focuses on the relationship between the compressive strength of concrete and its elastic modulus. This section compares the strength and modulus results of this test program with the results from predictor equations developed elsewhere. Note that this discussion is presented primarily in English units, as these correlation relationships are widely known in the United States in this format, and a conversion to metric units would lessen the relevance of the results.

Recall that the modulus of elasticity testing was completed on compression cylinders according to the ASTM C469 test method. The results from these tests were presented in section 3.3. Table 37 summarizes the overall 28-day results from these tests for each curing regime along with the compressive strength values.

Table 37. Compressive strength and modulus of elasticity results.

Curing	28-Day Compressive Strength (MPa (ksi))	Modulus of Elasticity (GPa (ksi))
Steam	193 (28.0)	52.7 (7,650)
Untreated	126 (18.3)	42.7 (6,200)
Tempered Steam	171 (24.8)	51.0 (7,400)
Delayed Steam	171 (24.8)	50.3 (7,300)

The American Concrete Institute's Building Code and Commentary (ACI 318) provides two relationships for the modulus of elasticity.[65] The equation in figure 138 shows the first relationship wherein the square root of the compressive strength of concrete is related to the modulus of elasticity through a scalar factor. In this equation, both the compressive strength, f_c', and the modulus of elasticity, E, are in psi. This equation was derived from, and is most relevant to, normal strength and normal weight concrete.

$$E = 57000\sqrt{f_c'}$$

Figure 138. Equation. ACI 318 approximation of modulus of elasticity.

ACI 318 provides a second relationship for the modulus of elasticity wherein the unit weight of the concrete is included. This modification allows for estimation of the modulus of elasticity for concrete with a unit weight between 1,440 and 2,480 kg/m^3 (90 and 155 lb/ft^3). This modification of the estimation equation is important, because both the weight of the concrete and the modulus of elasticity are normally heavily dependent on the type of aggregate used. The equation in figure 139 presents this relationship in English units, with ρ as the unit weight of concrete in lb/ft^3. Recall that the unit weight of UHPC is approximately 2,480 kg/m^3 (155 lb/ft^3).

157

Using this unit weight, this equation would transform into an equation similar to the one in figure 138 with a scalar of 63,700. Note that the equation shown in figure 139 is also the relationship provided in the AASHTO Load and Resistance Factor Design (LRFD) Bridge Design Specification.[66]

$$E = 33\rho^{1.5}\sqrt{f_c'}$$

Figure 139. Equation. ACI 318 approximation of modulus of elasticity including density.

The Comité Européen du Beton has presented a different relationship between the compressive strength and the modulus of elasticity.[20] This relationship is shown in figure 140 for metric units and in figure 141 after being converted into English units (psi).

$$E = 9.5(f_c' + 8)^{0.33}$$

Figure 140. Equation. Comité Européen du Beton approximation for modulus of elasticity (metric units).

$$E = 266600(f_c' + 1160)^{0.33}$$

Figure 141. Equation. Comité Européen du Beton approximation for modulus of elasticity (English units).

Another relationship between the compressive strength and the modulus of elasticity was developed by Kakizaki et al.[67] This research focused on high-strength concretes (83 to 138 MPa (12 to 20 ksi)). After an algebraic manipulation into English units (psi), the equation can be expressed as shown in figure 142.

$$E = 43960\sqrt{f_c'}$$

Figure 142. Equation. Kakizaki approximation for modulus of elasticity.

ACI 363 presents a relationship between the compressive strength and the modulus of elasticity that was developed specifically for high strength concretes.[68] In particular, this relationship was developed for concretes up to 83 MPa (12 ksi). It is shown in figure 143.

$$E = 40000\sqrt{f_c'} + 1000000$$

Figure 143. Equation. ACI 363 approximation for modulus of elasticity.

Finally, Ma et al. developed an equation based on experimental results from another UHPC containing no coarse aggregates.[69] The relationship is shown in figure 144.

$$E = 525000\sqrt[3]{\frac{f_c'}{10}}$$

Figure 144. Equation. Ma approximation for modulus of elasticity.

A comparison of these published relationships to the data obtained in this study indicates that some relationships are more applicable than others. Figure 145 plots the equations presented in figures 138, 141, 142, 143, 144, and 146, as well as the data presented in table 37. Additional data from untreated cylinders less than 28 days old is not shown in this figure, but was included in the analysis and is shown in the more detailed figure 147. It is clear that the ACI 318 and the Comité Européen du Beton equations overestimate the modulus of elasticity in this strength range; however, it must be stated that this strength range is well outside the typical applicability of these equations. The Kakizaki equation underestimates the results with a reasonable level of accuracy. The ACI 363 and Ma equations provide the best approximations of any published equations, as will be discussed below.
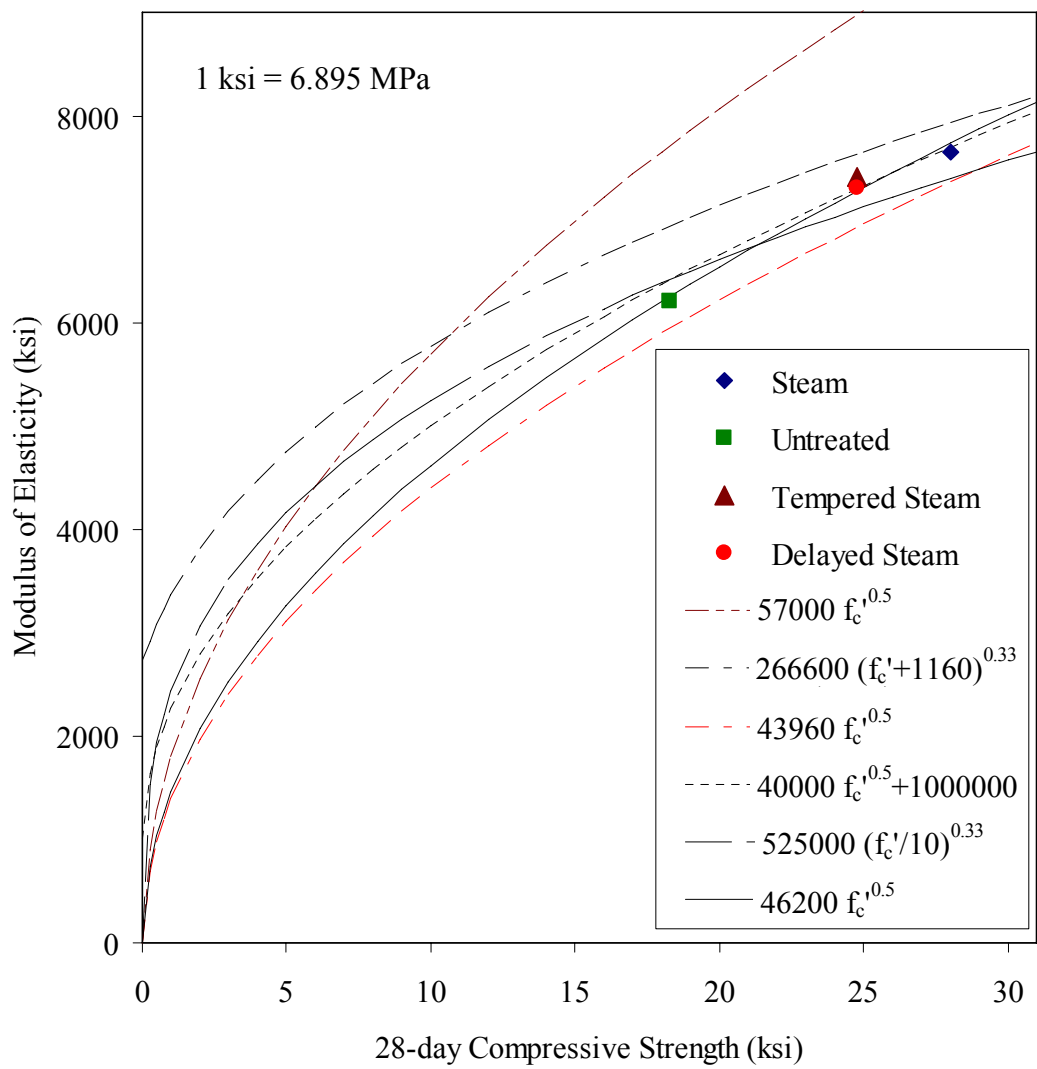
Figure 145. Graph. Modulus of elasticity as a function of 28-day compressive strength.

$$E = 46200\sqrt{f_c'}$$

Figure 146. Equation. Approximation for UHPC modulus of elasticity (in psi).

All of these equations have a similar form, some differing only by the scalar factor. The UHPC modulus of elasticity results were reevaluated to determine what type of relationship and what scalar factor would provide the best fit to the observed results. It was determined that the form of the ACI 318 equation accurately represented the shape of the UHPC relationship and only a modification of the scalar factor was required. The result of this analysis is the equation shown in figure 146 which has an R-squared value of 0.967 for the UHPC experimental results with compressive strengths above 25 MPa (3.6 ksi). This relationship is also shown in figures 145 and 147.

Figure 147 presents the most relevant equations along with the data that was used in this analysis. The figure also included the data from compressive strengths below 25 MPa (3.6 ksi) which was excluded from this analysis. The figure shows that the equation in figure 146 is applicable to UHPC over a wide range of strengths, not just to the final strength values between 124 and 193 MPa (18 and 28 ksi). Therefore, this equation is considered applicable over the compressive strength range of 28 to 193 MPa (4 to 28 ksi). Note that the ACI 363 and Ma equations displayed lower R-squared values (0.957 and 0.881, respectively), and they both overestimate the observed modulus of elasticity results at a large margin at lower compressive strengths.
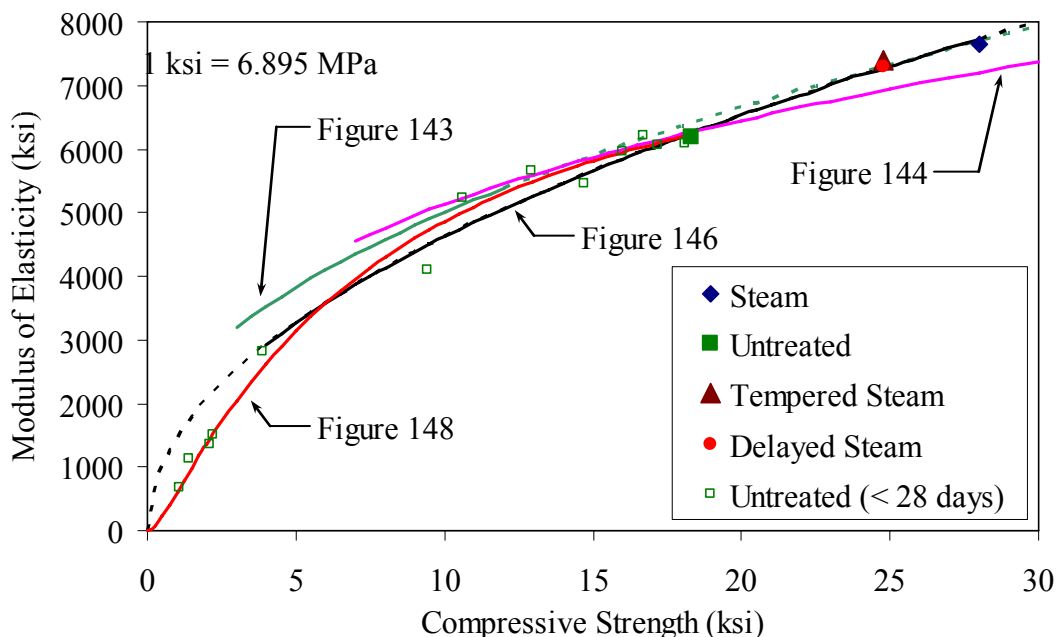
Figure 147. Graph. Modulus of elasticity as a function of compressive strength.

160

The equation in figure 146 does not accurately estimate the modulus of elasticity for UHPC with a compressive strength in the 7 to 21 MPa (1 to 3 ksi) range. The equation can overestimate the modulus of elasticity by as much as 50 percent. To rectify this lapse in the applicability of the equation, a more sophisticated equation was used to approximate the untreated curing regime data shown in figure 147. A best-fit regression analysis was applied to these data to determine a function that accurately represented the behavior. The simplest function to meet the requirements was the Log Normal function as presented in figure 148. In this equation, f_c' is the compressive strength of the concrete at a particular age and E is the corresponding modulus of elasticity, both in psi. This equation can be used to approximate the modulus of elasticity for compressive strengths as large as 131 MPa (19 ksi).

$$E = 7100000 \exp\left[-\frac{1}{2}\left(\frac{\ln\left(\frac{f_c'}{44000}\right)}{1.7} \right)^2 \right]$$

Figure 148. Equation. UHPC modulus of elasticity approximation (in psi) for compressive strengths up to 131 MPa (19 ksi).

4.9 COMPRESSIVE STRESS-STRAIN BEHAVIOR OF UHPC

The compressive stress-strain behavior of UHPC has been discussed extensively in this report, including the material property characterization results presented in section 3.3 and a further analysis of those results presented in section 4.8. The current section presents an analysis wherein an equation is determined that represents the ascending branch of the compressive stress-strain response for each of the four curing regimes. This analysis is based on the experimental results presented in section 3.3.3.
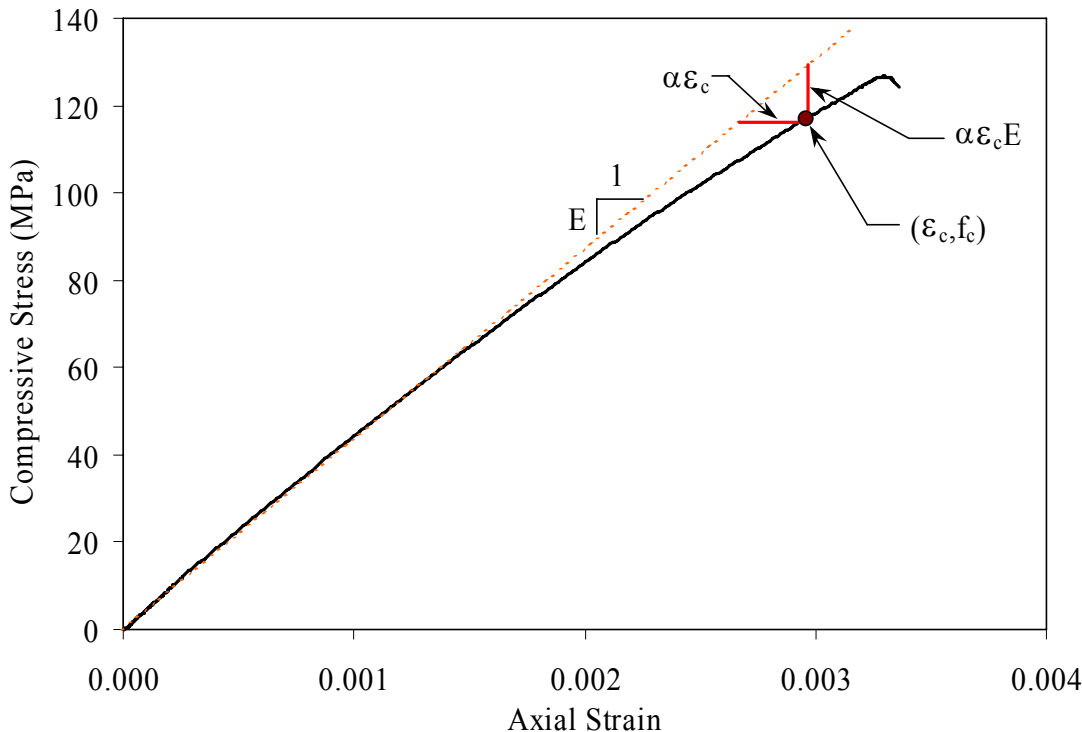
The compressive stress-strain responses of different concretes vary because concrete is a heterogeneous material without standardized mix designs. Many researchers have presented analytical approximations for the ascending branch of the compressive stress-strain behavior, all of which have been based on specific sets of experimental data. However, this body of research has resulted in minimal consensus on the equation's formulation or results.[20]

From an experimental standpoint, gathering consistent, accurate data from the full range of compressive behavior response is very difficult. This fact is primarily due to the increasingly nonlinear behaviors that concrete tends to exhibit as the strain at the compressive strength is reached and surpassed. Even if the descending branch of the behavior is ignored as the compressive strength is approached, the observed straining behavior of the concrete becomes very dependent on the experimental loading and strain measurement techniques that have been used.

The preceding discussion leads to the conclusion that any strength values and strain values from earlier in the concrete response are likely more accurate than strain values from later in the concrete response. The concrete compressive strength, f_c', and the concrete modulus of elasticity,

E, can both be considered to be relatively accurate based on experimental results. However, the concrete strain at the compressive strength and the associated secant modulus are both based on strain measurements that are more difficult to capture accurately and are thus less accurately known. This fact points to a weakness of many other models of concrete compressive stress-strain behavior, because they are based on an accurate knowledge of the compressive strain at the peak strength.

Recall from section 3.3 that a number of specific parameters were quantified within the compressive stress-strain responses of the UHPC. Intermediate stress and strain level benchmarks were identified in addition to the standard strength and stiffness measures. These benchmarks were defined by the decrease in observed stress compared with a theoretical linear elastic response at a particular strain. Average results for the 1, 3, and 5 percent decrease levels were presented in table 11. For this analysis, additional benchmarks were defined at the 10 percent decrease level and at the cessation of the continuous, steady increase in stress-strain response. Figure 149 illustrates the stress decrease factor compared with the linear elastic behavior, α, on a sample untreated UHPC compressive stress-strain curve. Sample actual stress, f_c, and strain, ε_c, values are shown along with the stress and strain differences from the linear elastic response.

Figure 149. Graph. Compressive stress-strain behavior compared with linear elastic response.

1 MPa = 0.145 ksi

These benchmarks were used to define the behavior of each compressive specimen. The results were then normalized based on the compressive strength and modulus of each specimen. Note that although the compressive stress normalization is based on the experimentally obtained compressive strength, the strain normalization is based on the theoretical linear elastic strain at the compressive strength. This normalization technique minimizes the inaccuracies discussed above by avoiding the use of the actual strain at the compressive strength. Finally, the results from each curing regime were compiled into individual data sets.

Figure 150 presents the normalized stress-strain response benchmark data points for the steam-treated UHPC cylinders discussed in section 3.3. This figure shows the general shape that the approximation must match to accurately represent the UHPC behavior. However, it does not allow for easy differentiation between potential curves that fit the data. A more accurate representation of the overall behavior can be obtained by focusing on the deviation of the actual behavior of the concrete compared with the theoretical linear elastic response. Figure 151 presents the same benchmarks in terms of the decrease from the linear elastic response compared with the normalized strain. This presentation highlights the behaviors that must be captured in the model.

163
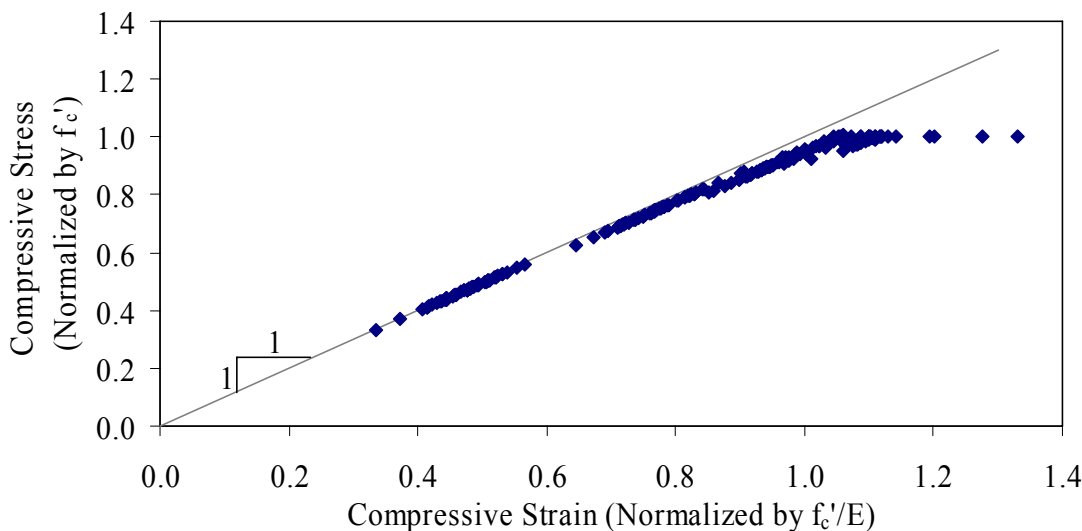
Figure 150. Graph. Normalized compressive stress-strain results for steam-treated UHPC.

Figures similar to figure 151 were created for the other three curing regimes as well. In all cases, the figures indicate that the UHPC remains close to the theoretical linear elastic response through much of its behavior. Approximation curves were fit to each of these data sets. The simplest equation that fits the data moderately well was an exponential function with two constants as provided in figure 152. These constants, *a* and *b*, help fit the equation to the data, and their values for each curing regime are provided in table 38. The approximation curve for the steam-treated UHPC is shown in figure 151.

The analysis discussed above leads to a simple means of defining the ascending branch of the compressive stress-strain response of UHPC. Figure 153 presents the equation for the standard linear elastic relationship between stress and strain with the inclusion of a modifying factor. This factor, specifically *(1-α)*, determines the extent to which the actual curve deviates from the linear elastic response. Recall that α is defined by the equation in figure 152. Dividing the equation in figure 153 by the compressive strength normalizes the equation and allows for the direct inclusion of the equation in figure 152 and therefore a single equation defining the normalized compressive stress in terms of the normalized compressive strain. Recall that this equation was derived to be applicable only for the ascending branch of the curve.

These relationships were used to create general stress-strain responses for the four curing regimes. These responses were based on the compressive strength and modulus of elasticity results presented in chapter 3. The curves are shown in figure 154.
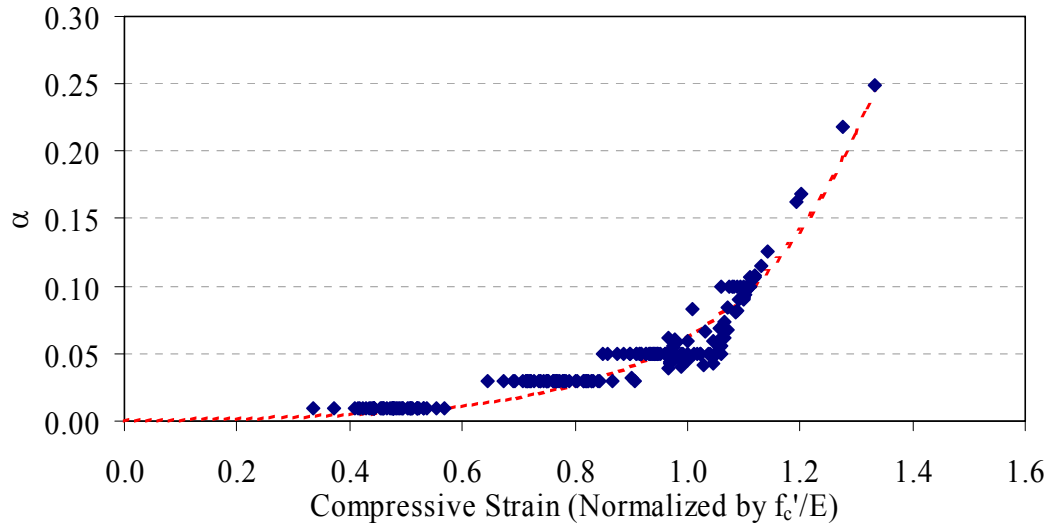
Figure 151. Graph. Deviation from linear elastic compressive behavior for steam-treated UHPC.

$$\alpha = ae^{\frac{\varepsilon_c E}{bf_c'}} - a$$
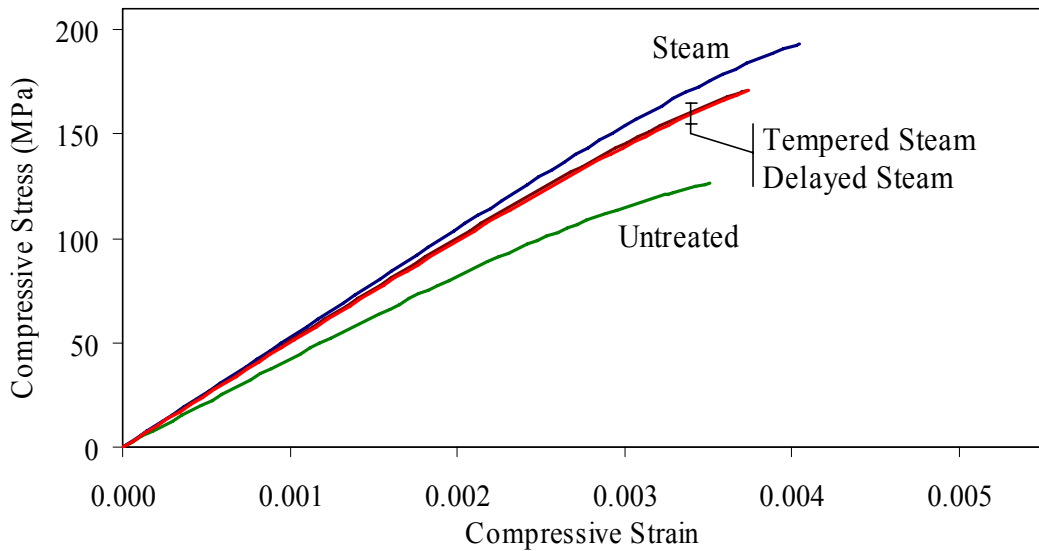
Figure 152. Equation. Deviation of compressive stress-strain response from linear elastic behavior.

Table 38. Constants for equation in figure 152.

Curing Regime	A	b
Steam	0.0010	0.243
Untreated	0.0114	0.440
Tempered Steam	0.0041	0.341
Delayed Steam	0.0044	0.358

$$f_c = \varepsilon_c E(1 - \alpha)$$

Figure 153. Equation. Compressive stress-strain behavior defined as a function of the deviation from linear elastic behavior.

1 MPa = 145 psi

Figure 154. Graph. Compressive stress-strain response approximations.

CHAPTER 5. CONCLUSIONS AND FUTURE RESEARCH

5.1 INTRODUCTION

UHPC is a new type of concrete that exhibits properties of enhanced strength, durability, and long-term stability. The objective of this research was to evaluate the material characteristics of UHPC for potential use in highway bridge applications.

The experimental phase of this research focused on determining the mechanical and durability behaviors of UHPC. More than 1,000 individual specimens were tested to determine the material characteristics of UHPC. The tests determined the compressive and tensile behaviors, the long-term stability, and the durability of UHPC. The analytical phase of this research combined, analyzed, and elaborated on the results from the experimental phase. This phase included developing predictor equations for some basic properties of UHPC.

The conclusions of this study are presented in section 5.2. A brief discussion of ongoing and potential future research topics follows in section 5.3.

5.2 CONCLUSIONS

The following conclusions are based on the research presented in this report.

1. UHPC displays significantly enhanced material properties compared with normal and HPC.

2. Steam-based treatment of UHPC tends to significantly enhance its material properties. Three steam-based treatments—steam, delayed steam, and tempered steam—were investigated and compared with UHPC that was not subjected to a curing treatment after casting. In general terms, steam treatment increases UHPC's compressive strength by 53 percent to 193 MPa (28 ksi), increases its modulus of elasticity by 23 percent to 52.4 GPa (7,600 ksi), decreases its creep coefficient from 0.78 to 0.29, and virtually eliminates long-term shrinkage. Steam treatment also decreases chloride ion penetrability to a negligible level and significantly enhances abrasion resistance. The enhancements of material properties affected by the delayed steam and tempered steam treatments are similar to those of the steam treatment but of a slightly lesser magnitude.

3. UHPC exhibits very high compressive strengths, regardless of the curing treatment applied. The average 28-day compressive strengths of steam, delayed steam, tempered steam, and untreated UHPC were found to be 193, 171, 171, and 126 MPa (28.0, 24.8, 24.8, and 18.3 ksi). The compressive strength of steam-treated UHPC was found to have stabilized by the completion of the curing treatment. Thus, steam-treated UHPC can reach its full compressive strength within 4 days after casting.

4. The mixing time and rheological properties of fresh UHPC are influenced by the concrete mixer design, the ambient environmental conditions in the mixer, and the elapsed time since blending of the premix. A 1934 vintage pan mixer was used

successfully to mix the UHPC; however, the inability of this mixer to impart significant energy into the mix resulted in extended mixing times. Low humidity within the mixer and in the mix room can result in stiffer UHPC. Older UHPC premix requires more mixing to achieve the correct rheological properties, likely due to the agglomeration of fine particles in the premix during storage.

5. The set time of UHPC is significantly delayed compared with normal concrete; final set does not occur until 12 to 24 hours after casting. This time to set could also be longer depending on the admixtures and on other constituents in the mix.

6. Once setting has initiated, UHPC gains compressive strength very rapidly. If maintained at normal laboratory temperatures, UHPC compressive strength will increase to over 70 MPa (10 ksi) by 2 days after setting. Subsequently, the rate of strength gain will decrease; 97 MPa (14 ksi) will be reached by 10 days after setting.

7. The compressive strength of UHPC is not affected by the specimen geometry used to determine the result. Cylinders with 51-, 76-, and 102-mm (2-, 3-, and 4-inch) diameters were tested according to ASTM C39, and 51-mm (2-inch) and 100-mm (4-inch) cubes were tested according to ASTM C109. The testing was conducted for two batches of steam-treated UHPC and for one batch of untreated UHPC. In all cases, the compressive strength results did not vary by more than 8 percent from the 76-mm (3-inch) cylinder control result. However, the 51-mm (2-inch) cubes and cylinders did tend to exhibit a larger standard deviation. The minimal preparation requirements for a cube specimen and the similarity of results mentioned above make the 100-mm (4-inch) cube a viable specimen geometry for UHPC compressive strength determination.

8. The curing conditions present during and just after the setting of UHPC can significantly affect the final properties of the concrete. In the untreated case, concrete cylinders that were stripped as final set was being reached exhibited 25 percent lower 28-day compressive strengths compared with those stripped 1 day after setting was complete. A 30-percent difference was observed in the steam-treated case. These strength differences are likely due to the relatively more permeable nature of UHPC at earlier ages combined with the very low moisture content in the UHPC. This low moisture content results in a loss of water to the surrounding atmosphere and thus reduced hydration of the concrete.

9. The tensile strength of UHPC, both before and after tensile cracking, is significantly higher than the strength that occurs in normal concrete. Four test methods were implemented to capture the tensile strength of UHPC. The combined results of these tests indicate that the tensile cracking strength of UHPC is approximately 9.0 MPa (1.3 ksi) after the steam-based curing treatment and approximately 6.2 MPa (0.9 ksi) without any treatment. Qualitatively, UHPC was observed to exhibit similar levels of tensile strength after cracking; however, in general, these tests were unable to indicate specific postcracking strengths.

10. The ASTM C496 split-cylinder tension test, modified to capture first cracking, provides the clearest indication of the tensile cracking strength of UHPC. Through the use of a hydraulically controlled test machine and minimal instrumentation, the tensile cracking strength of UHPC can be obtained. Other tensile tests require more extensive instrumentation, specialization of specimen geometry, and more sophisticated loading equipment. Unfortunately, the split-cylinder test is not useful for determining the postcracking tensile stress capacity, because the biaxial state of stress applied to the cylinder does not accurately mimic the conditions that are normally associated with tensile regions in a structural member.

11. The modulus of rupture defined by the ASTM C1018 prism flexure test overestimates the tensile cracking strength of UHPC by approximately 60 percent. This result was confirmed through the completion of this test on 51-mm (2-inch) square cross sections with 152-, 229-, 305-, and 381-mm (6-, 9-, 12-, and 15-inch) spans, and on 76- by 102-mm (3- by 4-inch) cross sections with a 305-mm (12-inch) span.

12. The ASTM C1018 prism flexure test provides a clear means of comparing the postcracking tensile behavior of various fiber-reinforced concretes. UHPC, regardless of curing treatment, performed exceptionally well according to the toughness indices defined by this test. For example, the I_{20} toughness index normally ranges from 1 to 25 for fiber-reinforced concretes. In UHPC, the I_{20} results ranged from 28 to 32. Although these results cannot be directly reinterpreted to apply to full-scale structural members, they do indicate that UHPC can continue to carry significant tensile loads after cracking.

13. UHPC displays durability properties that are significantly beyond those normally associated with concrete. Regardless of the curing treatment, the ASTM C666 relative dynamic modulus was at least 95 percent of the original value after more than 600 freeze-thaw cycles. UHPC exhibited no scaling under the ASTM C672 test, even after undergoing approximately 200 cycles. The chloride ion penetrability as measured by ASTM C1202 was below 50 coulombs for UHPC that had undergone the steam-based treatment, and was 360 coulombs for untreated UHPC 28 days after casting. The untreated UHPC results dropped to 76 coulombs by 56 days after casting. UHPC was found to be innocuous to alkali-silica reaction.

14. Exposing cracked UHPC split cylinders to an aggressive environment did not result in any noticeable decrease in the peak tensile load-carrying capacity. Tight cracks, as might be observed in a highly stressed tensile flexural region of an I-girder, were created by loading cylinders in a split-cylinder configuration. These cracks were on the order of 0.005 mm (0.0002 inch) wide. A cracked face of the cylinder was then ponded with a sodium chloride solution as specified in AASHTO T259. After 90 days of ponding, the cylinders were tested for peak split-cylinder tensile strength. The peak load-carrying capacity of either steam-treated or untreated UHPC did not have a discernable decrease after cracking, thus indicating that the sodium chloride solution did not enter the cracks and did not cause the fiber reinforcement to deteriorate.

15. UHPC exhibits shrinkage behaviors that are somewhat different from those of normal concrete. In total, UHPC tends to exhibit approximately 800 microstrain of shrinkage as measured from casting through 1 year. However, shrinkage initiation is affected by the delayed set times associated with UHPC, and the majority of the shrinkage occurs in a short time frame just after the concrete has set. Unrestrained shrinkage rates of over 60 microstrain per hour were observed during the period of rapid strength gain just after setting. Without any curing treatment, UHPC will continue to shrink at an ever-decreasing rate. Steam treatment accelerates the shrinkage to such an extent that the entirety of the shrinkage occurs during the 2-day treatment, and the UHPC is then stabilized against further shrinkage. Also, the total shrinkage in steam-treated UHPC tends to be slightly higher than the asymptotic shrinkage approached by untreated UHPC.

16. Large compressive stresses on relatively low-strength UHPC can cause significant short-term creep. This situation is akin to the stressing of prestressed girders. Eight to 13 ksi compressive strength UHPC was loaded to compressive stresses between 60 percent and 90 percent of the strength. During the 30 minutes following the load application, the UHPC exhibited 30-minute creep coefficients between 0.32 and 0.85. UHPC loaded to over 90 percent of its compressive strength failed under the sustained load. The creep that occurred over this short load duration indicates that the total long-term creep of UHPC loaded at this compressive strength would be much higher than that observed in the long-term creep testing.

5.3 ONGOING AND FUTURE RESEARCH

The findings from this report suggest a number of potential topics for future research:

1. Develop optimized bridge girders that take advantage of the material properties of UHPC. These bridge girders should use the tensile and compressive capacities of UHPC, while also enhancing the design life of the bridge as a whole by eliminating many of the less durable components of a normal bridge.

2. Fabricate full-scale, optimized UHPC bridge girders to resolve problems associated with casting slender concrete members with fiber-reinforced concrete.

3. Develop a practical test to quantitatively determine the postcracking uniaxial tensile behavior of UHPC.

The research program discussed herein has already been extended to encompass a portion of the topics listed above.

REFERENCES

1. Association Française de Génie Civil, *Ultra High Performance Fibre-Reinforced Concretes—Interim Recommendations,* Paris, France, 2002.

2. Hajar, Z., A. Simon, D. Lecointre, and J. Petitjean, "Construction of the First Road Bridges Made of Ultra-High-Performance Concrete," *Proceedings, 2003 International Symposium on High Performance Concrete*, Orlando, FL, October 2003, 18 pp.

3. Cavill, B., and G. Chirgwin, "The Worlds [sic] First RPC Road Bridge: Shepherds Gully Creek Bridge, NSW" *Proceedings of the Fifth Austroads Bridge Conference*, Hobart, Australia, May 2004.

4. Blais, P.Y., and M. Couture, "Precast, Prestressed Pedestrian Bridge—World's First Reactive Powder Concrete Structure," *PCI Journal*, Sept–Oct 1999, pp. 60–71, Chicago, IL.

5. Behloul, M., K.C. Lee, and D. Etienne, "Seonyu Ductal® Footbridge," In *Concrete Structures: The Challenge of Creativity,* FIB Symposium 2004 Proceedings, April 26–28, 2004, Avignon, France: Association Française de Génie Civil, 6 pp.

6. Semioli, W.J., "The New Concrete Technology," *Concrete International*, November 2001, pp. 75–79, American Concrete Institute, Farmington Hills, MI.

7. Acker, P., and M. Behloul, "Ductal® Technology: A Large Spectrum of Properties, A Wide Range of Applications," *Proceedings of the International Symposium on Ultra High Performance Concrete*, Kassel, Germany, September 13–15, 2004, pp. 11–23.

8. Buitelaar, P., "Heavy Reinforced Ultra High Performance Concrete," *Proceedings of the International Symposium on Ultra High Performance Concrete*, Kassel, Germany, September 13–15, 2004, pp. 25–35.

9. Stiel, T., B. Karihaloo, and E. Fehling, "Effects of Casting Direction on the Mechanical Properties of CARDIFRC®," *Proceedings of the International Symposium on Ultra High Performance Concrete*, Kassel, Germany, September 13–15, 2004, pp. 481–493.

10. Rapoport, J., C.-M. Aldea, S.P. Shah, B. Ankenman, and A. Karr, "Permeability of Cracked Steel Fiber-Reinforced Concrete," *ASCE Journal of Materials in Civil Engineering*, V. 14, No. 4, Jul–Aug 2002, pp. 355–358, American Society of Civil Engineers, Washington, DC.

11. Aldea, C., S. Shah, and A. Karr, "Permeability of Cracked Concrete," *Materials and Structures*, 1999, V. 32, No. 219, pp. 370–376, Bagneux, France.

12. Acker, P., "Why Does Ultrahigh-Performance Concrete (UHPC) Exhibit Such a Low Shrinkage and Such a Low Creep?" *Autogenous Deformation of Concrete*, ACI SP-220-10, 2004, pp. 141–154, American Concrete Institute, Farmington, MI.

13. Acker, P., "Micromechanical Analysis of Creep and Shrinkage Mechanisms," in Ulm, F.-J., Z.P. Bazant, and F.H. Wittman (eds.) "Creep, Shrinkage, and Durability Mechanics of Concrete and Other Quasi-Brittle Materials," *Proceedings of ConCreep-6@MIT*, Elsevier, London, 2001, pp. 15–25.

14. Horszczaruk, E., "Abrasion Resistance of High Strength Fiber-Reinforced Concrete," in di Prisco, M., R. Felicetti, and G.A. Plizzari, Eds., *Fiber Reinforced Concretes–BEFIB 2004, Proceedings of the Sixth International RILEM Symposium*, pp. 257–266, September 2004, Varenna, Italy.

15. ASTM C944, "Standard Test Method for Abrasion Resistance of Concrete or Mortar Surfaces by the Rotating Cutter Method," American Society for Testing and Materials Standard Practice C944, Philadelphia, PA, 1995.

16. ASTM C1437, "Standard Test Method for Flow of Hydraulic Cement Mortar," American Society for Testing and Materials Standard Practice C1437, Philadelphia, PA, 2001.

17. ASTM C39, "Standard Test Method for Compressive Strength of Cylindrical Concrete Specimens," American Society for Testing and Materials Standard Practice C39, Philadelphia, PA, 1994.

18. ASTM C109, "Standard Test Method for Compressive Strength of Hydraulic Cement Mortars (Using 2-inch or [50-mm] Cube Specimens)," American Society for Testing and Materials Standard Practice C109, Philadelphia, PA, 1998.

19. ASTM C469, "Standard Test Method for Static Modulus of Elasticity and Poisson's Ratio of Concrete in Compression," American Society for Testing and Materials Standard Practice C469, Philadelphia, PA, 1994.

20. Popovics, S., *Strength and Related Properties of Concrete: A Quantitative Approach*, John Wiley & Sons, Inc., New York, NY, 1998, 535 pp.

21. ASTM C1018, "Standard Test Method for Flexural Toughness and First-Crack Strength of Fiber-Reinforced Concrete (Using Beam With Third-Point Loading)," American Society for Testing and Materials Standard Practice C1018, Philadelphia, PA, 1997.

22. ASTM C78, "Standard Test Method for Flexural Strength of Concrete (Using Simple Beam with Third-Point Loading)," American Society for Testing and Materials Standard Practice C78, Philadelphia, PA, 1994.

23. Carpinteri, A., and B. Chiaia, "Embrittlement and Decrease of Apparent Strength in Large-Sized Concrete Structures," *Sadhana*, V. 27, No. 4, August 2002, pp. 425–448, India Academy of Sciences, Bangalore, India.

24. Chanvillard, G., and S. Rigaud, "Complete Characterization of Tensile Properties of Ductal® UHPFRC According to the French Recommendations," *Proceedings of the 4th International RILEM Workshop on High Performance Fiber Reinforced Cement Composites (HPFRCC4)*, 14 pp, Ann Arbor, MI, June 15–18, 2003.

25. ASTM C496, "Standard Test Method for Splitting Tensile Strength of Cylindrical Concrete Specimens," American Society for Testing and Materials Standard Practice C496, Philadelphia, PA, 1990.

26. Timoshenko, S., and J.N. Goodier, *Theory of Elasticity, 2nd Edition*, McGraw-Hill Book Company, New York, NY, 1951.

27. Petroski, H.J., and R.P. Ojdrovic, "The Concrete Cylinder: Stress Analysis and Failure Modes," *International Journal of Fracture*, V. 34, No. 4, 1987, pp. 263–279, Springer Netherlands.

28. Nanni, A., "Splitting-Tension Test for Fiber Reinforced Concrete," *ACI Materials Journal*, V. 85, No. 4, Jul–Aug 1988, pp. 229–233, American Concrete Institute, Farmington Hills, MI.

29. AASHTO T132, "Standard Method of Test for Tensile Strength of Hydraulic Cement Mortars," In American Association of State Highway and Transportation Officials, *Standard Specifications for Transportation Materials and Methods of Sampling and Testing*, Washington, DC, 2000.

30. Boulay, C., and A. Colson, "A Concrete Extensometer Eliminating the Influence of Transverse Strains on the Measurements of Longitudinal Strains," *Materials and Structures*, V. 14, No. 79, 1981, pp. 35–38, (in French), Bagneux, France.

31. Boulay, C., P. Rossi, and J.-L. Tailhan, "Uniaxial Tensile Test on a New Cement Composite Having a Hardening Behaviour," in di Prisco, M., R. Felicetti, and G.A. Plizzari, Eds., *Fiber Reinforced Concretes–BEFIB 2004, Proceedings of the Sixth International RILEM Symposium*, pp. 61–68, Varenna, Italy, September 2004.

32. Li, V., "Engineered Cementitious Composites (ECC)–Tailored Composites Through Micromechanical Modeling," *Fiber Reinforced Concrete: Present and Future*, Ed. N. Banthia, Canadian Society of Civil Engineers, 1997, 213 p., Montréal, QC.

33. Li, V.C., H.C. Wu, M. Maalej, and D.K. Mishra, "Tensile Behavior of Cement-Based Composites with Random Discontinuous Steel Fibers," *Journal of American Ceramic Society*, V. 79, No. 1, Jan. 1996, pp. 74–78, American Ceramic Society, Westerville, OH..

34. Li, Z., S.M. Kulkarni, and S.P. Shah, "New Test Method for Obtaining Softening Response of Unnotched Concrete Specimen Under Uniaxial Tension," *Experimental Mechanics*, V. 33, 1993, pp. 181–188, Society for Experimental Mechanics, Inc., Bethel, CT.

35. Li, Z., F. Li, T.P. Chang, and Y. Mai, "Uniaxial Tensile Behavior of Concrete Reinforced with Randomly Distributed Short Fibers," *ACI Materials Journal*, V. 95, No. 5, Sept–Oct 1998, pp. 564–574, American Concrete Institute, Farmington Hills, MI.

36. Lim, T., P. Paramasivam, and S. Lee, "Analytical Model for Tensile Behavior of Steel Fiber Concrete," *ACI Materials Journal*, V. 84, No. 4, July–Aug 1987, pp. 286–298, American Concrete Institute, Farmington Hills, MI.

37. Morris, A.D., and G.G. Garrett, "A Comparative Study of the Static and Fatigue Behaviour of Plain and Steel Fibre Reinforced Mortar in Compression and Direct Tension," *International Journal of Cement Composites and Lightweight Concrete*, V. 3, No. 2, 1981, pp. 73–91, Elsevier Science.

38. Phillips, D.C., and B.S. Zhang, "Direct Tension Tests on Notched and Unnotched Plain Concrete Specimens," *Magazine of Concrete Research*, V. 45, No. 162, 1993, pp. 25–35.

39. RILEM, TC 162-TDF, "Recommendations of RILEM TC 162-TDF: Test and Design Methods for Steel Fibre Reinforced Concrete Uni-Axial Tension Test for Steel Fibre Reinforced Concrete," *Materials and Structures*, V. 34, No. 235 Jan–Feb 2001, pp. 3–6, RILEM Publications, Bagneux, France.

40. Rossi, P., "High Performance Multimodal Fiber Reinforced Cement Composites (HPMFRCC): The LCPC Experience," *ACI Materials Journal*, V. 94, No. 6, Nov–Dec 1997, pp. 478–483, American Concrete Institute, Farmington Hills, MI.

41. Saito, M., and S. Imai, "Direct Tensile Fatigue of Concrete by the Use of Friction Grips," *ACI Journal*, V. 80, No. 5, 1983, pp. 431–438, American Concrete Institute, Farmington Hills, MI.

42. USBR 4914, *Procedure for Direct Tensile Strength, Static Modulus of Elasticity, and Poisson's Ratio of Cylindrical Concrete Specimens in Tension,* United States Department of Interior, Bureau of Reclamation, 1992, Washington, DC.

43. Wang, Y., V.C. Li, and S. Backer, "Experimental Determination of Tensile Behavior of Fiber Reinforced Concrete," *ACI Materials Journal*, V. 87, No. 5, Sept–Oct 1990, pp. 461–468, American Concrete Institute, Farmington Hills, MI.

44. Zhang, J., H. Stang, and V. Li, "Experimental Study on Crack Bridging in FRC Under Uniaxial Fatigue Tension," *Journal of Materials in Civil Engineering*, ASCE, V. 12, No. 1, Feb. 2000, pp. 66–73, Reston, VA.

45. Zheng, W., A.K.H. Kwan, and P.K.K. Lee, "Direct Tension Test of Concrete," *ACI Materials Journal*, V. 98, No. 1, Jan–Feb 2001, pp. 63–71, American Concrete Institute, Farmington Hills, MI .

46. ASTM E1820, "Standard Test Method for Measurement of Fracture Toughness," American Society for Testing and Materials Standard Practice C512, Philadelphia, PA, 2001.

47. AASHTO T197, "Time of Setting of Concrete Mixtures by Penetration Resistance," In American Association of State Highway and Transportation Officials, *Standard Specifications for Transportation Materials and Methods of Sampling and Testing*, Washington, DC, 2000.

48. ASTM C157, "Standard Test Method for Length Change of Hardened Hydraulic-Cement Mortar and Concrete," American Society for Testing and Materials Standard Practice C157, Philadelphia, PA, 1993.

49. ASTM C490, "Standard Practice for Use of Apparatus for the Determination of Length Change of Hardened Cement Paste, Mortar, and Concrete," American Society for Testing and Materials Standard Practice C157, Philadelphia, PA, 2000.

50. ACI 209R-92, "Prediction of Creep, Shrinkage, and Temperature Effects in Concrete Structures", *ACI Manual of Concrete Practice Part 1: Materials and General Properties of Concrete*, Detroit, MI, 1994, 47 pp.

51. ASTM C512, "Standard Test Method for Creep of Concrete in Compression," American Society for Testing and Materials Standard Practice C512, Philadelphia, PA, 1987.

52. Branson, D.E., *Deformation of Concrete Structures*, McGraw-Hill Book Company, New York, NY, 1977, 546 pp.

53. AASHTO TP60, "Coefficient of Thermal Expansion of Hydraulic Cement Concrete," In American Association of State Highway and Transportation Officials, *Standard Specifications for Transportation Materials and Methods of Sampling and Testing*, Washington, DC, 2000.

54. Neville, A.M., *Properties of Concrete, Fourth and Final Edition*, John Wiley & Sons, Inc., New York, NY, 1996, 844 pp.

55. ASTM C457, "Standard Test Method for Microscopical Determination of Parameters of the Air-Void System in Hardened Concrete," American Society for Testing and Materials Standard Practice C457, Philadelphia, PA, 1998.

56. ASTM C230, "Standard Specification for Flow Table for Use in Tests of Hydraulic Cement," American Society for Testing and Materials Standard Practice C230, Philadelphia, PA, 1998.

57. ASTM C1202, "Standard Test Method for Electrical Indication of Concrete's Ability to Resist Chloride Ion Penetration," American Society for Testing and Materials Standard Practice C1202, Philadelphia, PA, 1997.

58. AASHTO T259, "Standard Method of Test for Resistance of Concrete to Chloride Ion Penetration," In American Association of State Highway and Transportation Officials, *Standard Specifications for Transportation Materials and Methods of Sampling and Testing*, Washington, DC, 2000.

59. AASHTO T260, "Standard Method of Test for Sampling and Testing for Chloride Ion in Concrete Raw Materials," In American Association of State Highway and Transportation Officials, *Standard Specifications for Transportation Materials and Methods of Sampling and Testing*, Washington, DC, 2000.

60. ASTM C672, "Standard Test Method for Scaling Resistance of Concrete Surfaces Exposed to Deicing Chemicals," American Society for Testing and Materials Standard Practice C672, Philadelphia, PA, 1992.

61. ASTM C666, "Standard Test Method for Resistance of Concrete to Rapid Freezing and Thawing," American Society for Testing and Materials Standard Practice C666, Philadelphia, PA, 1997.

62. ASTM C1260, "Standard Test Method for Potential Alkali Reactivity of Aggregates (Mortar-Bar Method)," American Society for Testing and Materials Standard Practice C1260, Philadelphia, PA, 1994.

63. ASTM C1293, "Standard Test Method for Determination of Length Change of Concrete Due to Alkali-Silica Reaction," American Society for Testing and Materials Standard Practice C1293, Philadelphia, PA, 2001.

64. De Larrard, F., A. Belloc, S. Renwez, and C. Boulay, "Is the Cube Test Suitable for High Performance Concrete?" *Materials and Structures*, V. 27, No. 174, 1994, pp. 580–583, RILEM Publications, Bagneux, France.

65. American Concrete Institute, *Building Code Requirements for Structural Concrete*, ACI 318, 2005, 430 pp, Farmington Hills, MI.

66. American Association of State Highway and Transportation Officials, *AASHTO LRFD Bridge Design Specifications,* 2nd Edition, Washington, DC.

67. Kakizaki, M., *Effect of Mixing Method on Mechanical Properties and Pore Structure of Ultra High-Strength Concrete*, Katri Report No. 90, Kajima Corporation, Tokyo, 1992, 19 pp.

68. ACI 363R-92, "State of the Art Report on High Strength Concrete," American Concrete Institute, 1992.

69. Ma, J., F. Dehn, N.V. Tue, M. Orgass, and D. Schmidt, "Comparative Investigations on Ultra-High Performance Concrete with and without Coarse Aggregates," *Proceedings, International Symposium on Ultra-High Performance Concrete*, Kassel, Germany, September 2004, pp. 205–212.